DEVELOPMENT OF A PROSTHETIC HEART VALVE WITH INBUILT SENSING TECHNOLOGY, TO AID IN CONTINOUS MONITORING OF FUNCTION UNDER VARIOUS STENOTIC CONDITIONS

By

Caleb Gambrah MSc

A thesis submitted in accordance with the regulations governing the award of the Degree of Doctor of Philosophy in Biomedical Engineering

Biomedical Engineering Department

University of Strathclyde Glasgow

United Kingdom

June, 2020

DECLARATION OF AUTHENTICITY AND AUTHOR'S RIGHTS

'This thesis is the result of the author's original research. It has been composed by the author and has not been previously submitted for examination which has led to the award of a degree'.

Signed: Caleb Gambrah

Date: 22nd June, 2020

ACKNOWLEDGEMENTS

I would like to first of all give thanks to God for giving me the strength, resilience and wisdom to preserve throughout my PhD journey. I wouldn't be where I am without my faith in God.

Secondly I would like to thanks my parents for all the sacrifices they made in order for me to get to this stage of my academic career. Their words of encouragements and prayers have really helped me through some very low times in my journey. They have been my rock and a massive appreciation goes out to them.

To my supervisor, Prof Terry Gourlay, thank you for being a mentor and guiding me through throughout my PhD research. Your wise counsel has led to the successful completion of this work. I would be remiss if I didn't acknowledge the members of the Cardiovascular Devices research group, especially Dr Monica Kerr who spent countless amounts of hours in the lab with me and assisted me in the development and hydrodynamic testing of the polyurethane heart valves.

Finally, I would like to say a massive thank you to the members of my local church, who have been my second family since I moved to Glasgow. Their words of encouragement support and great camaraderie have in many cases served as a constant source of light and a breath of fresh air during some dark and tumultuous times.

ABSTRACT

In spite of technological advances in the design of prosthetic heart valves, they are still often subject to complications after implantation. One of the common complications is valve stenosis, which involves the obstruction of the valve orifice caused by biological processes. The greatest challenge in diagnosing the development of valve failure and complications is related to the fact that the valve is implanted and isolated. To continuously monitor the state of the valve and its performance would be of great benefit but practically can only be achieved by instrumenting the implanted valve. In this thesis, we explore the development of a prosthetic valve with inbuilt sensing technology to aid in continuous monitoring of valve function under various stenotic conditions. 22mm polyurethane valves were manufactured via dipcoating. A custom made mock circulatory system was designed and hydrodynamic testing of the polyurethane valves under different flow rates were performed with Effective orifice area (EOA) and Transvalvular Pressure Gradient (TVPG) being the parameters of interest. Valves were subjected to varying levels of obstruction to investigate the effect obstruction has on the pressure gradient across the valves. Similar tests were performed on a Carpentier Edwards SAV 2650 model bioprosthetic valve for comparison. Polyurethane valves were then instrumented with strain gauges to measure peak to peak strain difference, in response to varying levels of obstructions. All the polyurethane valves exhibited good hydrodynamic performance with EOA (>1cm^2) under baseline physiological conditions. It was also discovered that pressure difference across the valves was directly proportional to the flow rate. The pressure difference also demonstrated a slow increase during the initial stages of simulated stenosis and a sudden increase as the obstruction became severe. This provides further evidence to support the ideal that stenosis is a slow progressive disease which may not present symptoms until severe. The peak to peak strain differences also tend to decrease as

the severity of the obstruction was increased. The peak to peak strain difference is indicative of the pressures within the valve (intravalvular pressure). The results suggest that directly monitoring the pressures within the valve could be a useful diagnostic tool for detecting valve stenosis. Future works involves miniaturisation of the sensors and also the incorporation of telemetry into the sensor design.

CONTENT page no

LIST OF FIGURES

LIST OF TABLES

CHAPTER 1. ANATOMY OF THE HEART, HEART VALVES AND HEART VALVE DISEASES

1.1THE HEART

The human heart is essentially a pump, that circulates blood around the body. It's a muscular organ about the size of a fist. It consists of 4 chambers, **the left and the right atria** being the top 2 chambers and below them, the **left and right ventricles**. Separating the atria and the ventricles are 2 valves known as the **atrioventricular (AV)** valves. These valves control the direction of blood flow between the atria and ventricles. The AV valve located between the left atrium and ventricle is known as the **bicuspid or mitral valve**, and the **tricuspid valve** is located between the right atrium and ventricle. In addition to these two AV valves, there are two others, known as the **semilunar valves**. One of the semi lunar valves is known as the **aortic valve** and is located between the left ventricle and a major blood vessel known as the **aorta**. The aorta serves as the outflow tract of the left ventricle. The other semi lunar valve is known as the **pulmonary valve** and is located between the right ventricle and its outflow tract known as the pulmonary trunk, which branches of into **pulmonary arteries**. Blood enters the right atrium through two major vessels known as the **inferior and superior vena cavae.** Blood enters the left atrium through a quartet of vessels known as the **pulmonary veins** (Waite and Fine, 2007a; Calvert and Lefer, 2012; Klabunde, 2012a; Pappano and Wier, 2013b; Martini, Nath and Bartholomew, 2018).

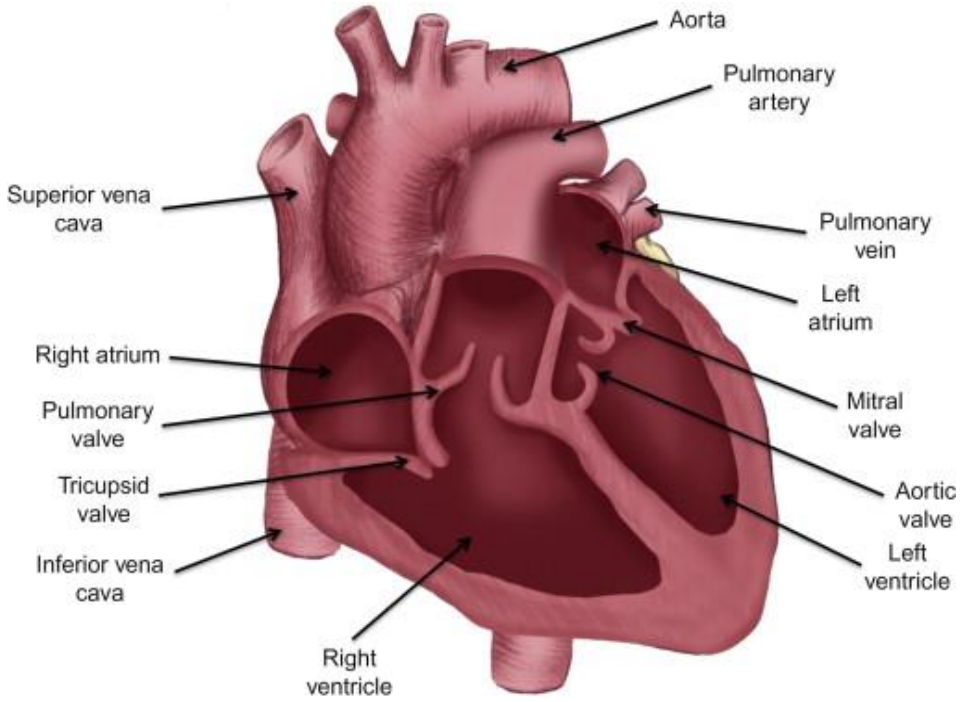

Figure 1.1Cross sectional view of the heart. “Image taken from (Calvert and Lefer, 2012)”

1.1.1. Blood flow in the heart

Flow of blood in the heart occurs in two pathways, ie the pulmonary circuit and the systemic circuit and these occur at the right and left side of the heart respectively. These two pathways occur simultaneously.

1.1.1.1 The pulmonary circuit

In the pulmonary circuit, deoxygenated blood from the upper and lower regions of the body flow into the superior and inferior vena cava respectively. Blood from both these vessels, pool into the right atrium. Blood enters the right atrium at low pressures (0-4mmHg), thus the right atrium tends to have highly distended capabilities in order to accommodate this venous return. The tricuspid valve then opens up and the blood flows into the right ventricle. During contraction of the right ventricle, the pulmonary valve, which separates the right ventricle from its outflow tract, opens up and the blood flows actively through the pulmonary trunk.

The pulmonary trunk branches into the left and right pulmonary arteries leading to the left and right lung respectively were gaseous exchange, aided by the capillaries, occurs (Klabunde, 2012a).

1.1.1.2. The systemic circulation

Oxygenated blood from the lungs enters the left atrium via a quartet of vessels known as the pulmonary veins. The blood then flows into the left ventricle via the opening of the mitral valve. During ventricular contraction, the aortic valve, which separates the left ventricle from the aorta, opens up and blood is pushed from the left ventricle through to the aortic arch. From there, a network of smaller arteries transports the oxygen rich blood to all other parts of the body. This whole process of transporting oxygenated blood from the heart to the rest of the body is termed as systemic circulation (Blanchard, 2005).

As explained, pulmonary and systemic circulation are handled by the right and left side of the heart respectively. Both the right and left atria have similar functions and that is to transport blood to the ventricles. As a result, both atria are anatomically similar. There are however, some major differences in the ventricles . The right ventricle drives blood to the lungs during contraction. The lungs are in close proximity to the heart as a result, the right ventricle does not need to pump blood over a long distance. The left ventricle however, pumps blood throughout the whole body and as a result, needs to work a lot harder. To meet the arduous demands of the systemic circulation, the left ventricle has thicker walls relative to the right ventricle, thus allowing blood to be pumped at a greater pressure throughout the body (Martini, Nath and Bartholomew, 2018).

1.1.2 Mechanical Events In The Cardiac Cycle

Electrical conduction through the heart generates a series of mechanical events, per cardiac cycle. This series of mechanical events and their relation to the electrical events are described

below. This would help gain a better understanding of how cardiac function is regulated and controlled.

The mechanical events in the cardiac cycle can generally be grouped into two parts. These are the systole, i.e. the contraction of the heart chambers, and the diastole i.e. the relaxation of the heart chambers. The direction of blood flow is regulated by the four heart valves which open and close as a result of pressured differences in the heart (Waite and Fine, 2007a). However, within these two phases also exists some more specific events. Some literature describes the total cardiac cycle in four simple phases, i.e atrial systole, atrial diastole, ventricular systole and diastole (Waite and Fine, 2007a), other literature further breaks down the systole and diastole events into a total of seven (Klabunde, 2012a) or eight phases (Martini, Nath and Bartholomew, 2018). To gain a better understanding of the cardiac cycle, we will be discussing the cardiac cycle using the convention employed by Martini et al.

Phase 1. The genesis of atrial systole

This phase marks the start of the atria contraction. At this stage, the ventricles are already partially filled due to the events of the final stage (which is discussed later).

Phase 2. Atrial ejection

As the pressure builds up in the atria and becomes higher relative to the ventricles, blood is ejected into the ventricle. During this phase, no more blood enters the atria as the atria pressure exceeds that in the veins leading into the atria. At the end of the end of this phase, the ventricles are fully filled and the volume in the ventricles at the end of this phase is known as the End Diastolic Volume of the ventricle and this is approximately 130ml.

The phase 1 and 2 comprises of the atrial systole and last approximately 100msecs. The atrial systole is represented by the P wave on the ECG.

Phase 3. End of atrial systole

This stage comprises the end of the atrial systole. Pressure starts to build up in the ventricle and as the ventricular pressure becomes greater than the atrial pressure, the atrioventricular valves close.

Phase 4. Isovolumetric contraction of the ventricles

This is the early stage of ventricular systole. In this stage, even though the ventricles are starting to contract, the pressure build up is not enough to cause the semi lunar valves to open, thus all the 4 valves in the heart remain closed at this point. It's called isovolumetric contraction because the volume of the ventricles are still the same at this point and there's no flow of blood occurring.

Phase 5. Ventricular Ejection

Once the pressure in the ventricles continue to build up, the semilunar valves open up, and the ventricles eject blood into the pulmonary an aortic trunks for pulmonary and systemic circulation respectively. The amount of blood that is ejected during this phase is known as the Stroke Volume (SV). This value is approximately 70-80ml and is approximately 60% of the End diastolic volume (Martini, Nath and Bartholomew, 2018). After peak systole, the ventricular pressure starts to fall.

Phase 6. Closing of the semi lunar valves

As the ventricular systole comes to its conclusion, the ventricles experience a sharp decrease in pressure. Blood begins to flow back into the low pressure ventricular chamber. The backflow pushes against the semi lunar valves thus forcing them to close. The walls of the

aorta, which houses the aortic valve, are elastic and as such recoil when the valve closes. This creates a small and transient pressure rise in the aorta known as the dicrotic notch. Pressure in the aorta and pulmonary trunk do not drop as rapidly as the ventricles do due to the elastic nature of the aorta and pulmonary trunk which allows potential energy to be stored, and also impedance to blood flow (Klabunde, 2012a). The End Systolic Volume is the amount of blood left in the ventricles after contraction, thus EDV-ESV= stroke volume. Another terminology used to assess the ejection function of the ventricle is called Ejection fraction which is the Stroke Volume/End Diastolic Volume. In a healthy ventricle, the ejection fraction is expected to be greater than 55% (Klabunde, 2012a).

Now it should be mentioned that atrial relaxation occurs simultaneously with the ventricular contraction. Phases 3-6 comprises of the ventricular systolic phase and last for approximately 270msecs.

Phase 7. Isovolumetric relaxation

At this phase, the ventricles start relaxing. Since the pressure in the ventricles are still higher than those in the atria, the AV valves still remain closed thus all the 4 valves remain closed and there is no flow occurring. However over this phase the ventricles return to their resting state dimensions.

Phase 8. Passive ventricular filling

The ventricular pressure continues to drop rapidly and once these pressures cross the threshold of the atrial pressures, the AV valves open and the ventricle start to fill up and expand, as the ventricles experience an increase in volume, their pressures still decrease, even

below the major veins as a result, blood flows from those veins, into the atria which are already in diastole, and continuously fill the ventricles thought the open AV valves. As a result of this, the ventricle is already about 70% filled even before atrial systole starts (Martini, Nath and Bartholomew, 2018)

Phases 7 and 8 represents the ventricular diastole and occurs till the end of the atrial systole. Ventricular diastole takes approximately 530msecs (Martini, Nath and Bartholomew, 2018).

In a complete cardiac cycle of a heart at rest diastole takes a longer time relative to systole, approximately 37.5% in systole and the remaining 62.5% is spent in diastole. A longer diastolic time is to aid in maximum filing of the ventricles prior to contraction (Blanchard, 2005).

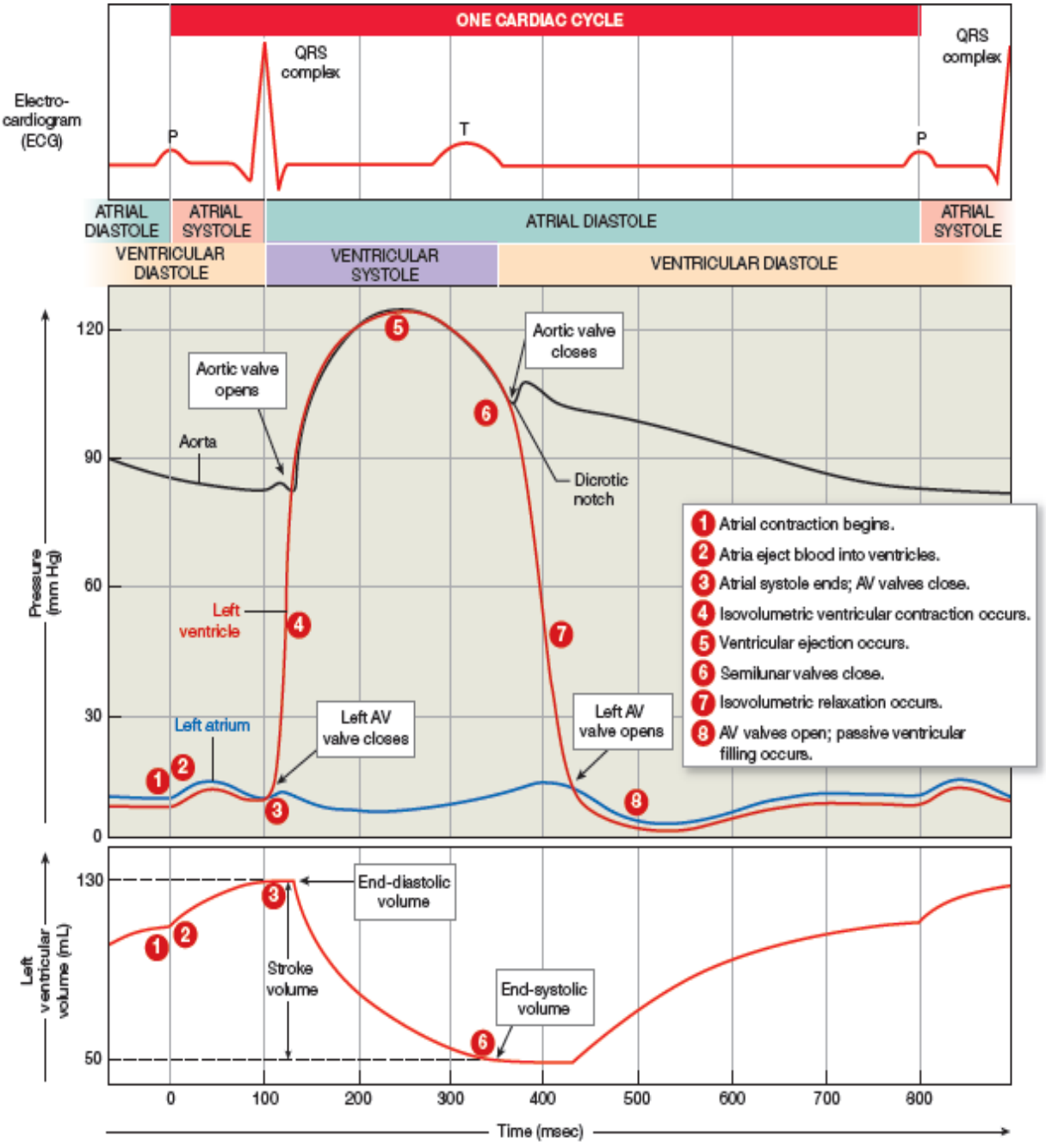

Figure 1.2. ECG, pressure and volume relationships of the left side of the heart in a single cardiac cycle. Numbers circled in red represents the phases of the cardiac cycle. Image taken from Martini et al. 2018 in Fundamentals of Anatomy and Physiology

The beating of the heart is accompanied by some audible sounds known as auscultations, commonly detected through a stethoscope. These sounds are characterised in an onamotapaeic manner, as lub dub sounds. There are 4 heart sounds, however 2 of those are very pronounced. The 4 heart sounds are labelled s1, s2, s3 and s4. The s1 and s2 represents the lub and dub sound respectively. The lub sound is produced as the atrioventricular valves close during the commencement of ventricular systole. The dub sound is produced as a result the closure of the semi lunar valves during the commencement of ventricular diastole. In a normal healthy heart, only the s1 and s2 sounds should be heard. The s3 sounds is associated with murmurs during turbulent blood flow into the ventricles. The s3 sound may be heard in children and other highly active people such as athletes and may not be a cause for concern. The last sound s4 is associated with contraction of the atria. The presence of s3 (at a later stage of life) and s4 may be used by clinicians to diagnose heart diseases (Kusko and Maselli, 2015).

1.1.3 Cardiac output

Cardiac output is a major indicator of cardiac function over time and determines peripheral tissue perfusion In order to gain a deeper understanding of cardiac function, it is imperative that a fair understanding of cardiac output and factors that affect it be explored.

Cardiac output can be defined as the amount of blood pumped by the left ventricle per minute. It is expressed mathematically as Stroke Volume x Heart Rate.

For a resting adult male healthy heart , cardiac output values are approximated differently in different literature with values such as 4.9L/min, with a resting stroke volume of 70ml and resting heart rate of 70bpm (Siddiqui, 2011) and 5.01 L/min (McClelland *et al.*, 2005);

Calvert & Lefer 2012). Calvert & Lefer approximates resting stroke volume at 70ml and resting heart rate at 72bpm. It can also be express as a range of 5-6L/min ((Klabunde, 2012a).

Cardiac output is affected by the stroke volume and heart rate, however the stroke volume is also determined by 3 major factors namely the preload, the afterload and contractility. Thus the resulting major determinants of cardiac output are heart rate, preload, afterload and contractility. Although all these factors are interrelated, we will consider then in isolation and independent of each other, for the purpose of this explanation. In this section, we define the aforementioned parameters and explain how they affect cardiac output.

i. Preload

The ventricles relax and stretch during diastole in order to accumulate the blood from the atria. The stretching of the ventricles is caused by the ventricular myocytes. The preload can be thought of as the amount of stretch in the ventricular myocytes prior to contraction or the degree of tension of the ventricular wall at the end of diastole (Lilly, 1998). With all other conditions being constant, a larger preload means a larger end diastolic volume which then leads to more blood being pumped out, i.e. a larger stroke volume. This particular phenomenon describing the direct relationship between preload and stroke volume is known as "**the frank starling law**, which states that " the larger the diastolic volume of the heart,(within physiological limits) the greater its energy of contraction." (Starling and Visscher, 1927). The larger the preload, the greater the cardiac output, if all other things remain constant.

ii. Afterload

During ventricular contraction, the ventricles need to generate pressure greater than that of the aorta, in order to open up the aortic valve for the ventricular ejection to occur. The amount of resistance or load, that the ventricles needs to overcome in order for ventricular ejection to occur is referred to as the afterload (Lilly, 1998). An increase in aortic pressure and resistance of vessels to blood flow will ultimately mean the ventricles will have to generate a much greater force in order to overcome the load. In terms of its effect on stroke volume, a higher after load means the ventricles will have to spend more time in isovolumentric contraction which means less time in ventricular ejection. This will then result in a large end systolic volume (ESV). Since SV =EDV-ESV, if EDV is constant, a large ESV will then lead to a low SV(Martini, Nath and Bartholomew, 2018). The larger the afterload, the smaller the cardiac output, if all other things remain constant.

iii. Contractility

Contractility of the cardiac myocytes refers to their intrinsic ability to contract. With all other things being constant, a high contractility of the left ventricular myocytes will lead to a larger force generating which then causes a larger volume of blood to be expelled during ventricular ejection. As a result, a greater magnitude of contractility will result in a larger stroke volume and a larger cardiac output if all other things remain constant (Vincent, 2008).

iv. Heart Rate

The 4th determinant of cardiac output is heart rate. For a normal healthy male adult, the heart rate at rest tends to be between 60-100bpm (Siddiqui, 2011; Solan, 2016; MacGill, 2017). The heart rate is generated in the sinoatrial SA node. This SA node is innervated with sympathetic and parasympathetic nerves of the autonomous nervous system which increase or decrease the heart rate respectively. With all other things being constant, as per the cardiac output formula, an increase in heart rate will cause an increase in cardiac output. This can be

observed during exercises and heightened emotional activities where the physiological demands for oxygen and other nutrients are increased (Calvert and Lefer, 2012).

1.1.4 Blood Pressure

In systemic circulation, the blood is pumped from the heart through the aorta and then to the arteries. The blood pressure serves as the driving force of the blood throughout that arterial network. When the blood pressure is low, tissue perfusion is compromised. On the other hand , a high blood pressure could come with a host of issues ranging from weak and enlarged heart, due to excessive workload on the heart, to other cardiovascular diseases (Lapum *et al.*, 2018).

In the clinical setting, blood pressure is measured at the arterial level and is expressed as arterial blood pressure. Essentially, this is the pressure exerted on the walls of the arterial during the cardiac cycle. Blood pressure is expressed as systolic over diastolic, with the systolic arterial blood pressure being the maximum pressure of the blood being ejected into the arteries during left ventricular contraction and the diastole being the residual pressure of the blood in the arteries , during left ventricular relaxation. The difference between the systolic and diastolic pressures is referred to as pulse pressure. Blood pressure is measured in mmHg. The American Heart Association, recommends blood pressure ranges of (90-120mmHg) systolic and (60-90mmHg) diastolic, as normotensive for a healthy adult (Klabunde 2012b;Madell & Cherney 2018).

Arterial blood pressure may sometimes also be expressed as a singular value known as the Mean Arterial Pressure (MAP), which is calculated as the Diastolic pressure +1/3 of the pulse pressure. (Klabunde, 2012c).

Arterial blood pressure is affected by some physiological factors which are described below

i. Cardiac output

As earlier explained, (see section 1.1.3) cardiac output is the amount of blood pumped out by the left ventricle per minute and it's a function of stroke volume and heart rate. Blood flows from a region of high pressure to low pressure. Considering laminar flow through a horizontal tube, the change in pressure is a product of flow and resistance. This is analogous to ohms law in electrical circuits V=IR In relation to physiological terms, this pressure can be represented as the MAP, flow can be represented by the cardiac output and the resistance is represent by the total peripheral resistance , which is the sum of the resistances of the network of vessels involved in systemic circulation.

MAP=CO X TPR (Mayet and Hughes, 2003)

As a result of this , it can clearly be seen that any factor that determines cardiac output(see section 1.1.5) will have a directly proportional effect on the pressure. In simple terms, high flow denotes high pressure and vice versa, assuming the peripheral resistance is constant.

ii. Blood volume

The volume of blood circulating through the body will also understandable have an impact on the blood pressure. If there's a high volume of blood in the artery, that volume will push against the walls of the artery thus causing high pressures to be experienced in the walls of the arteries. The inverse is true (Lapum *et al.*, 2018).

iii. Resistance

Resistance to blood flow in the blood vessels, has a major effect on arterial blood pressure. The higher the resistance, the more pressure is required to overcome this in order to maintain constant flow.

Resistance is also affected by 3 main components i.e. blood viscosity, vessel length and vessel diameter Mathematically, resistance can be expressed by Poiseulle;s equation

$$R \propto \frac{n.L}{r^4}$$

Where n is the viscosity, L is the length of the vessel and r is the radius of the vessel (Klabunde, 2012c). From this equation, it can be clearly seen that an increase in viscosity of the blood and or the length of the blood vessel will cause an increase in resistance thus pressure and vice versa. Similarly, an increase in vessel diameter decreases resistance and as a result blood pressure. A decrease in vessel diameter will cause an increase in resistance and subsequently, blood pressure. A practical clinical manifestation of this is in artherosclerosis where plaque builds up in the arteries thus narrowing the cross sectional area and causing hypertension (Wu *et al.*, 2017).

iv. Compliance

Compliance of a vessel is its ability to expand to accommodate increase in its content. A practical example is that of a balloon. When air or fluid is introduced into a balloon, it expands, and then relaxes once the fluid is let out. Similarly, the arteries have the capability to expand temporally during systole to accumulate blood, which is then slowly release in diastole. The arteries ability to expand during the pressure surge in systole helps to reduce the resistance in the vessel which in turn, helps reduce the pressure. A stiffer vessel would cause a higher resistance which would then lead to high pressures needed to overcome this resistance to maintain adequate perfusion (Lapum *et al.*, 2018). The arteries generally tend to become stiffer with age, thus blood pressure tends to increase with increasing age (Harvey, Montezano and Touyz, 2015).

A combination of compliance and resistance in the large arteries are the major contributors to the slow decline of blood pressure during the diastolic phase observed on a typical arterial pressure tracing (Pappano and Wier, 2013a). This is necessary for constant perfusion

1.2. ANATOMY OF HEART VALVES

In describing the anatomy of the heart, , we made references to the 4 valves that open and close at specific stages of the cardiac cycle, in order to control the direction of blood flow in the heart. These valves are namely the atrioventricular valve (bicuspid and tricuspid valves) and the semi lunar valves (aortic and pulmonary valves). In this section, we describe a bit further in detail, the anatomy of these valves and how these anatomical features aid in their function.

1.2.1 The mitral valve

The mitral valve is located between the left atrium and ventricle. It has 2 leaflets (posterior and anterior leaflets) and as a result is sometimes referred to as the bicuspid valve. The leaflets are connected by a fibrous D shaped ring known as the mitral valve annulus, which is attached to the aortic root, the ventricle and atrial wall. The annulus has the capability to change size during various stages of the cardiac cycle. Special chords known as the chordinae tendae, connects to the free edges of the valve leaflets and are anchored to the ventricles via the papillary muscles. During ventricular diastole, the chordinae tendae is in a slacked and relaxed state and the valve leaflets are open, however during systole, tension exerted on the chordinae tendae pulls on the leaflets causing them to close. This anchoring support provided by the chordina tendae, prevents the mitral valve from collapsing into the atrium during ventricular systole. The 2 leaflets acts to cover the valve orifice during closure, however there are 2 other small indentations in the leaflets, known as commisures, that allows for adequate coaptation of the leaflets during closure. (Yoganathan et al. 2004;Bateman et al. 2013; Kanjanauthai & Sharma 2015)

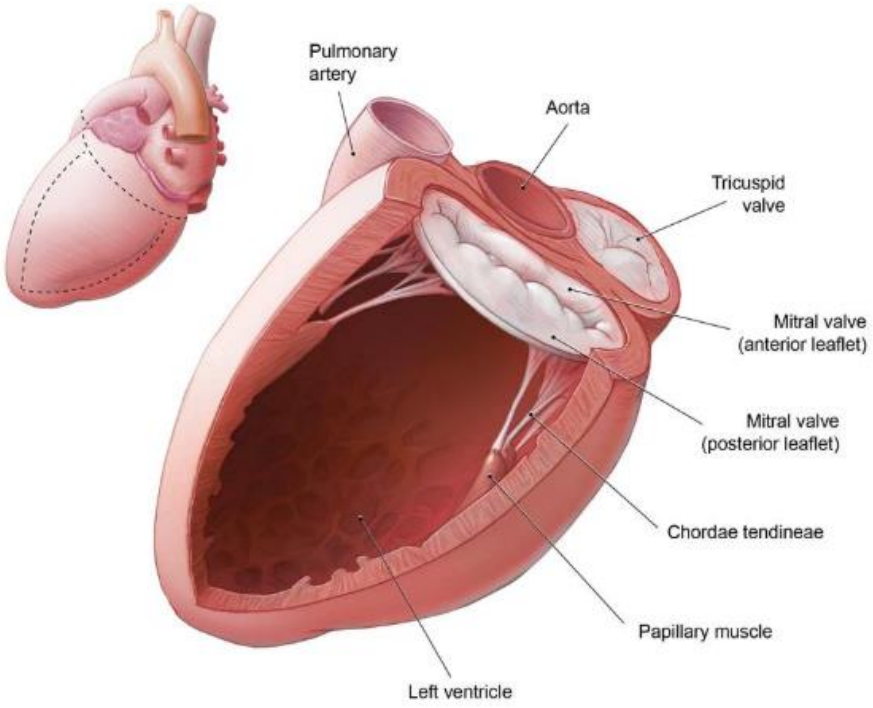

Figure 1.3. Structure of the mitral valve. Image taken from (Kanjanauthai and Sharma, 2015)

1.2.2. The tricuspid valve

The tricuspid valve is the other atrioventricular valve, located between the right atrium and ventricle. Structurally, the tricuspid and mitral valve are similar. It has leaflets, annulus, chordinae tendae and papillary muscles. The major difference is that the tricuspid valve has a 3rd leaflet known as the septal leaflet and also has a variable number of commisures. The tricuspid valve also tends to be larger with more chordinae tendae attached to various portions of the valve leaflet (Yoganathan, He and Casey Jones, 2004).

1.2.3. The aortic valve

Situated between the ventricles and their outflow tracts are the semi lunar valves. The aortic valve is situated between the left ventricle and the aorta. Located in the aortic root, the aortic

valve has 3 leaflets which are connected to the walls of the aortic root via 3 bulges known as the sinuses. Two of these sinuses contain the origins of the coronary arteries which serve as blood supply to the cardiac muscles. The sinuses are connected to the ascending aorta at a junction known as the sinotubular junction (Rozeik, Wheatley and Gourlay, 2014b) The base of the leaflets are connected by a fibrous ring known as the annulus ring. During valve closure, the 3 leaflets comes together in a tripod like fashion forming the coaptation region. This region tends to have overlapping tissue from each valve known as the lunula, thus ensuring that the valve is properly sealed off. The aortic valve is considered to be arguably the most important valve since it directly aids systemic circulation (Waite and Fine, 2007b; Bateman *et al.*, 2013)

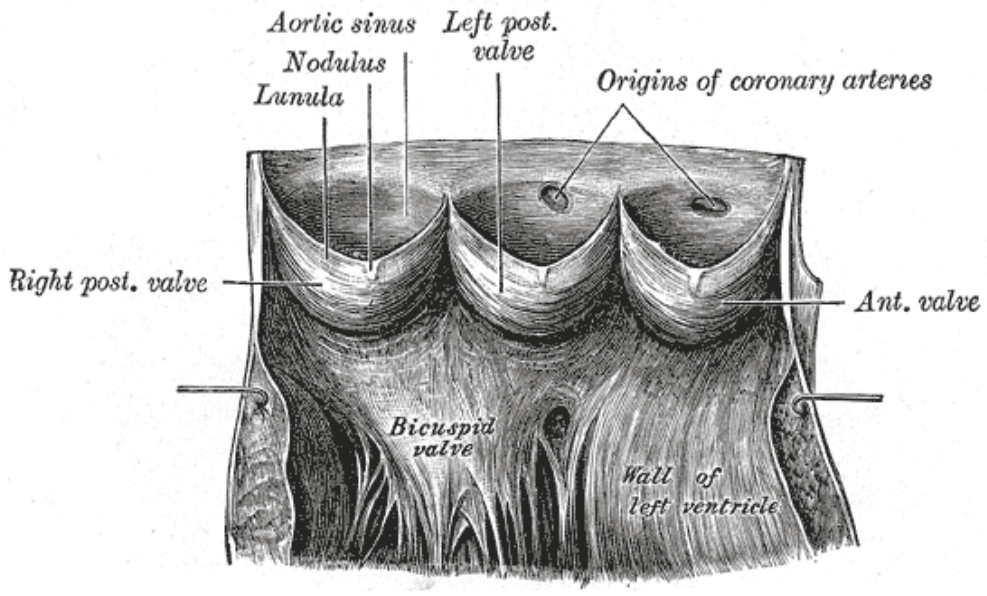

Figure 1.4. A cut open aortic root showing the 3 aortic valve leaflets, the sinus and origin of coronary arteries. Digitized image taken from Henry Gray in Anatomy of the Human Body, 1918 https://www.bartleby.com/107/illus497.html

1.2.4 The pulmonary valve

The pulmonary valve has a similar structure to that of the aortic valve however the pulmonary valves tend to be larger according a study conducted by Westaby et al. in 1984 on 169 cadaver specimens, which showed mean aortic valve and pulmonary valve diameters of 23.2 ± 3.3mm and 24.3 ± 3mm respectively. The sinuses also tend to be smaller in the pulmonary valve and are also void of coronary artery origins. Another difference is in the leaflet thickness, with the pulmonary leaflets being generally thinner than that of the aortic valve (Yoganathan, Lemmon and Ellis, 2000).

Semi lunar valves derive their name from the half-moon shape of their leaflets. Due to their location in the heart, semi lunar valves are more stable and thus do not require chordinae tendae to facilitate their function. The semi lunar valves open due to a positive pressure gradient as ventricular pressure rises in systole, and close during diastole, as the backflow of blood pushes against the leaflets.

Heart valves undergo a lot of stress during cyclic loading and unloading. The pulmonary and tricuspid valves withstand pressures of around 30mmhg when closed, and the bicuspid and aortic valve withstands pressures up to 150mmhg and 100mmhg respectively. Due to these constant stresses, the valves may get diseased over time, with left heart valve diseases being more prevalent (Yoganathan, Lemmon and Ellis, 2000).

1.3. VALVULAR HEART DISEASES

Valvular heart disease is a very common cardiovascular disease, leading to significant mortality and morbidity especially among elderly people (LaHaye, Lincoln and Garg, 2014). Valvular disorders may be caused either congenital abnormalities or by a variety of acquired diseases. Some of these are displayed below.

1.3.1. Causes of valvular heart diseases

i. Rheumatic fever

Rheumatic fever is an inflammatory condition that usually occurs after a severe case of throat infection (strep throat) caused by the bacteria streptococcus pyogenes. This condition may cause scarring of the heart valves, which may result in valvular fibrosis and result in valve stenosis and/or regurgitation. Rheumatic fever tends to be more prevalent in children between 5-15years of age (Bender, 1992). It's after effects, known as rheumatic heart diseases, may lead to chronic valve complications, especially of the mitral valve (Roberts and Ko, 2009). Advancements in medicine have made rheumatic fever a rarity in developed countries. In developing countries however, rheumatic fever tends to be the main cause of heart valve disorders. (Bender 1992; Padmavati 1978; Carapetis 2007; Burke 2013).

ii. Calcific degeneration

This condition is most common in aortic valves and tends to be more prevalent in adults 35 and over. Calcific degeneration arises from the accumulation of calcium deposits on the valve. This causes the stiffening of the valve leaflets and narrowing of the valve opening.

iii. Myxomatous degeneration

This is a process which causes the tissues of the heart valves to lose their elasticity. This leads to the valve leaflets becoming soft and flabby. Myxomatous degeneration also may even cause the weakening and eventual rupture of the chordinae tendae , which is responsible for controlling the opening and closing of the atrioventricular valve leaflets, thus leading to backflow/ leakage of blood. Myxomatous degeneration may be due to factors such as accumulation of glycosaminoglycans, collagen alterations, and also the non proper regulation of the degradation and regeneration process of the leaflet support matrix (Wang and Bashore,

2009). The exact mechanism by which myoxamatous degeneration is triggered, is however not very defined (Rippe *et al.*, 1980; Trochu *et al.*, 2000). Myxomatous degeneration is known to affect mainly the mitral valve and is considered to be the primary cause of mitral valve prolapse (Henein, 2009).

iv. Infective endocarditis

This is an inflammatory condition is characterised by the proliferation of bacteria, fungi and other micro-organisms on the endocardium of the valves, resulting in infection. It is majorly caused by 2 bacteria species, streptococci and staphylococci (Bender, 1992). These clump of microorganisms growing on the surface of the valve wall, referred to as vegetations, tend to cause holes in the valve wall, damaging the structure of the valve thus causing valve dysfunction (Cabell, Abrutyn and Karchmer, 2003). Consequently, these clusters of micro-organisms could migrate through the blood stream and block a blood vessel, leading to embolism. Infective endocarditis is mostly, as a result of a prior untreated infection and it tends to affect valves that have prior history of ailment. Antibiotics given to patients before they undergo any procedure which may trigger the release of bacteria into the bloodstream may help prevent infective endocarditis (Bender, 1992).

1.3.2. Types of native valve diseases

Dysfunction of native heart valves presents in two forms. The valve may fail to open completely, which is known as stenosis, or fail to close completely, causing regurgitation. Congenital abnormalities could also be as a result of both stenosis and regurgitation. In this section we explore further the two forms of valvular dysfunction

1.3.2.1. Aortic Stenosis(AS)

With the exclusion of systemic hypertension, Aortic Stenosis (AS), is considered to be the 2nd most common and fatal heart disease, following coronary heart disease (Wang and Bashore, 2009). Epidemiological studies show that 12.5% of people over the age of 75 has

moderate to severe AS (Nkomo *et al.*, 2006). According to the Euro Heart Survey of patients with single valve disease, 43.1% was as a result of aortic stenosis, making it the most common native heart valve disease (Iung *et al.*, 2007). It is further estimated that by the year 2020, 3.5 million people residing in England will have aortic stenosis (Ramaraj and Sorrell, 2008). Aortic stenosis is caused by 3 main factors; calcific degeneration, rheumatic fever or congenital abnormalities such as bicuspid aortic valve, where 2 of the 3 aortic leaflets are fused. Regardless of the cause, most cases of AS, has the aortic valve covered with calcific deposits and also narrowed valve orifice. Stenosis causes obstruction of blood flow from the left ventricle, thus causing the heart to work excessively to maintain cardiac output. This causes the heart to weaken over time causing the heart to fail. Patients with AS tend to be asymptomatic for many years till the situation becomes severe due to ventricular compensatory mechanisms (Bender, 1992).

Figure 1.5. Operatively excised stenosed aortic valve leaflets with calcific deposits. “Image taken from Roberts and Ko in Valvular Heart Disease, 2009”

1.3.2.2. Aortic Regurgitation (AR)

In general, valve regurgitation may also be referred to as valvular insufficiency. Aortic Regurgitation (AR), is the failure of the aortic valve to close completely. This causes backflow of blood from the aorta to the left ventricle during the diastolic phase. AR may be caused by congenital abnormalities such as bicuspid aortic valve, or acquired diseases such as infective endocarditis, rheumatic fever and degenerative aortic valve diseases. Dilation of the aortic root could also lead to the improper closing of of the aortic valve, leading to regurgitation.

AR may be either chronic or acute, although their causes tend to overlap. Acute AR is mostly as a result of infective endocarditis or trauma (Stout and Verrier, 2009),and that of chronic AR are commonly due to rheumatic fever and abnormalities with ascending aorta. As with aortic stenosis, patients may be asymptomatic until the situation becomes severe. The constant backflow of blood into the ventricles causes an increase in left ventricle end diastolic pressure, which with time travels through the pulmonary circuit, leading to pulmonary edema and hypertension (Bender, 1992; Wang, 2014).

1.3.2.3. Mitral stenosis

Mitral Stenosis (MS), is the narrowing or obstruction of the mitral valve orifice. MS is caused most commonly by rheumatic fever. The mitral valve is located between the left atrium and ventricle, thus obstruction to blood flow in the mitral valve causing an excessive pressure build up in the atrium. This blood and fluid build up may transfer to the lungs and blood vessels leading to pulmonary hypertension and edema which consequently could lead to heart failure and death. Patients with MS tend to be asymptomatic for a long time, with initial signs appearing decades after rheumatic fever episode (Dima, 2014).

1.3.2.4. Mitral regurgitation (MR)

Mitral regurgitation is the reversal flow of blood from the left ventricle to the left atrium during ventricular systole, as a result of improper closure of mitral valve during ventricular

systole. Like mitral stenosis, rheumatic heart diseases tend to be a major culprit in MR and patients may remain asymptomatic until situation is severe. Rheumatic heart diseases tend to cause degeneration of the muscle controlling the closure of the mitral valve. Another common cause of MR is myxomatous degeneration, which creates soft and flabby leaflets in a condition known as **mitral valve prolapse (MVP).** MVP is usually benign but may lead to regurgitation in severe cases (Price & Gibson 2010; Thakkar 2014).

1.3.2.5. Tricuspid valve stenosis and regurgitation

These account for just about 5% of valvular disorders and mostly occur in conjunction with other valvular disorders of the mitral and or aortic valve. The major cause of tricuspid valve disorders is rheumatic fever, although it may also be caused by congenital abnormalities. Tricuspid valvular disorders tend to take years to fully manifest (Bender, 1992).

1.3.2.6. Pulmonary valve stenosis and regurgitation

Diseases of the pulmonary valve are also very rare and are commonly due to congenital defects. Congenital pulmonary stenosis causes obstruction to the right ventricle outflow. Pulmonary regurgitation may also be caused by pulmonary hypertension (Wang and Bashore, 2009).

1.4.TREATMENT OF HEART VALVE DISEASES

There exist various treatment methods for native heart valve diseases. The choice of treatment is dependents on various factors which include mainly the age, cause, general health of the patient and also the severity of the heart valve disease.

1.4.1. Medication

The initial treatment for non severe native heart valve disease includes provision of medication to treat the symptoms and or conditions that may exacerbate the heart valve

disease progression. These include medications to treat or control high blood pressure and cholesterol, irregular heartbeats, also known as arrthymia, coronary heart disease and heart failure. Patients suffering from heart valve disease may also be encouraged to live a healthier lifestyle (Parikh and O'Gara, 2009).

1.4.2. Valve Repair

In more severe situations, surgical intervention may be necessary to repair the valve. Valvuloplasty is one of the methods used to repair the valve. Originally valvuloplasty was done by inserting a finger, with or without a knife attached into an obstructed valve to manually clear the obstruction. This method, known as finger fracture valvuloplasty was performed without the aid of imaging techniques. Further to that the displacement of calcium during this procedure could also lead to stroke. Finger fracture valvuloplasty as a valve repair protocol was ceased in the early 1970s and replaced with balloon valvuloplasty.

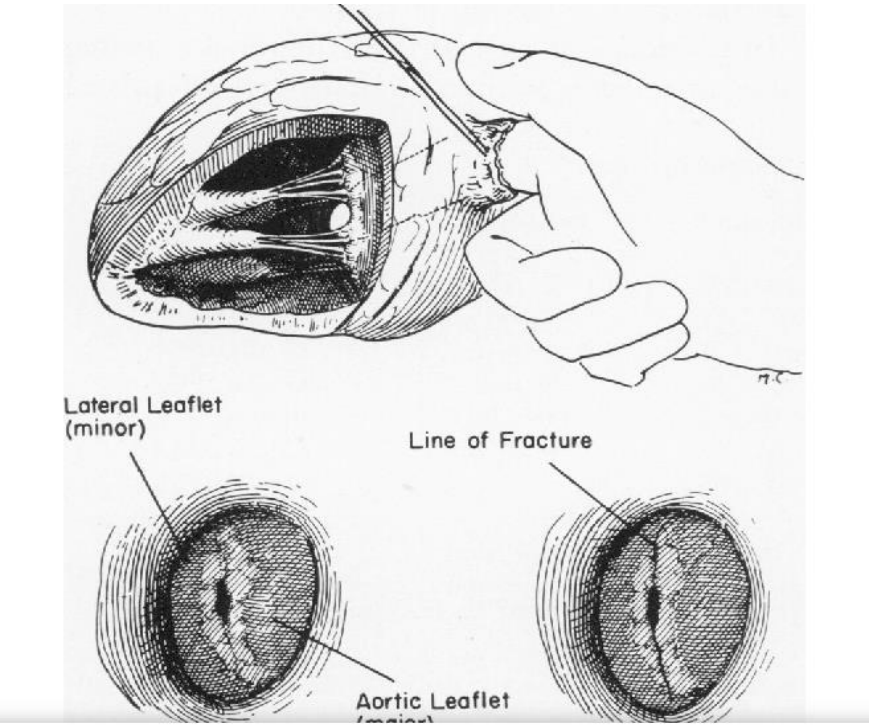

Figure 1.6. Finger fracture valvuloplasty. Image taken from Edward F Bland in Circulation (1952), Vol 52, pp 290-299.

Balloon valvuloplasty is a minimally invasive process aided by imaging modalities, where a deflated balloon is inserted into the tip of a catheter and threaded through the blood vessel to the opening of the valve and then inflated, thus allowing the valve to open up properly. Annuloplasty is another surgical technique used to treat valve regurgitation. This technique involves implanting a ring around the valve annulus, which then forces the leaflets together, ensuring tighter coaptation during valve closure. This is most commonly used on mitral valves. Commisurotomy may also be used to treat valve stenosis. Commisurotomy involves making an incision in the commissures of the valve in order to provide relief of obstruction (Peltz, 2013). It should hover be mentioned that surgical treatment of stenosis may also lead to regurgitation (Mezilis, Salame and Oakley, 1999; Hill *et al.*, 2016). Resection and suturing may also be done to repair a leaflet.

1.4.3. Valve replacement

Medication and valve repair may delay the progression of heart valve disease, however they do not provide a long term solution. In the case of severe and chronic native valve disease, a replacement of the native valves may be the ultimate and only solution.. The advancement of technology has made possible for diseased valves to be replaced with devices known as artificial/prosthetic heart valves. These valves are discussed in further details in chapter 2.

CHAPTER 2. ARTIFICIAL HEART VALVES

Since the introduction of prosthetic valve replacement surgery in 1960s, over 80 models of heart valves have been developed. Approximately 280,000 valve replacement surgeries are performed worldwide on a yearly basis (Pibarot and Dumesnil, 2009). In the UK alone, over 6000 valve replacement procedures are performed yearly (Bloomfield, 2002) Commercially available prosthetic valves tend to be either mechanical or bioprosthetic .

2.1 Mechanical heart valves

These valves are mostly made out of metal and carbon alloys and are classified according to their structure. There are 3 kinds of mechanical valves namely, the ball and cage valve, disc valves and bileaflet valves.

2.1.1Ball and cage valve

The ball and cage valve are the earliest prosthetic valves designed and implanted in the descending aorta of dogs by Charles Hufnagel in 1952. This valve consisted of a ball placed inside a tube. Increase in pressure during systole, pushes the ball upwards towards the tube, allowing blood to flow. Decrease in pressure causes the ball to drop back to the base of the valve, forming a seal. This valve was not implanted directly into the heart and as a result could not fully replace the heart valve (DeWall et al. 2000;Bloomfield 2002;Pibarot & Dumesnil 2009).

To allow implanting directly into the heart, Dr Albert Starr, a cardiovascular surgeon, teamed up with engineer Mr Lowell Edwards and together they reengineered Hufnagels initial design, which led to the first heart valve to be implanted in a human heart, in 1960. The valve consisted of a silastic ball and was surrounded by metal arches which created the cage. The movement of the ball due to pressure changes, caused the opening and closing of the valve, similar to Hufnagels design. This valve is commonly referred to as the " **Starr-**

Edwards valve" . Over the years there's been different modifications of the Starr-Edwards valve, but the design and principle of operation remains similar to the original. Although ball and cage valves are no longer being used, several 1000s of patients still have them already implanted (Matthews, 1998; Starr, 2007; Pibarot and Dumesnil, 2009).

2.1.2. Disc valves

Due to abundance of problems that affected ball cage valves mainly thrombogenicity, other types of valves were developed. One of these were the disc valves, developed in the late 1960's. One of the first disc valves developed were the caged disc valve. The **caged disc valve**, is similar to caged ball valve, however the ball is replaced by a flat disc instead. This disc is held in place by metal struts creating the cage. Common examples of caged disc valves are the Cooley -Cutter and Kay-Shiley valve. These valves however, did not demonstrate a significant improvement over the ball valves.

Tilting disc valves were then introduced. These valves consist of a single disc that tilts at an angle to occlude or open the valve. The disc is held together by metal struts and had a tilting angle between 60 and 70 degrees. The materials used for disc were initially Delrin and later replaced by pyrolitic carbon. Common models of tilting disc valves include the Bjork- Shiley and Hall-Kaster valve. Tilting disc valves were found to be a big improvement over caged valves in terms of improved haemodynamics and lower thrombogenicity (Chaikof, 2007; Joana and Filsoufi, 2013).

2.1.3. Bileaflet valves

To further improve on valve function and design, bileaflet valves were introduced for clinical use in 1977 by St Judes Medical (company now acquired by Abbot). These valves consist of 2 semi circular discs that pivot on the strut of the valve, allowing the valve to open and close. The opening angles range from 75 to 90 degrees. Common commercially available bileaflet valves include the St Judes Medical bileaflet valve, Cardiamed rotating bileaflet valve, On-X

bileaflet valve among others. The significant advantage of the bileaflet valves over other mechanical valves is that bileaflet valves allow a more natural flow of blood since the leaflet are able to open completely, thus providing less resistance to backflow and also lower rates of thrombosis.

Since the introduction of the bileaflet valves, they have been the most preferred and go to prosthetic valve, especially among young patients, with over 2 million of leaflet valves being implanted (Bonow *et al.*, 2006; Chikwe, Filsoufi and Carpentier, 2010; Grunkemeier *et al.*, 2015).

Mechanical prosthetic valves, although durable, do require continuous anticoagulant treatment due to the less than desired of their materials. To avoid the burden and potential hazards of this treatment, research has led to the production and commercialisation of bioprosthetic valves i.e. valves made from suitable biological materials. In the next section we talk about the kinds of bioprosthetic heart valves used in clinical practice.

2.2. Bioprosthetic valve

Depending on the source of the biological tissue, bioprosthetic valves can either be termed as autograft (from the same person), homograft/allograft(from a human donor or cadaver) or heterograft/xenograft (from another species).

2.2.1. Autograft valves

Valve replacement via the use of autograft valves were pioneered by Dr Donald Ross in 1967. This procedure, which earned the title “ross procedure”, involved replacing a patient’s diseased aortic valve, with the same patients pulmonary valve, essentially transferring a

patient's pulmonary valve into the aortic valve position. A pulmonary allograft is then used to replace the pulmonary valve that was taken out. Due to the tissue being from the same individual, these pulmonary autografts tend to have good hemodaynamic properties and low thrombogenicity. Ross procedure is mostly preferred when replacing aortic valves in young children and adolescents due to the fact that the tissue has the ability to grow with the aortic root, hence allowing the valve to grow with the young child (Hoffmann, Lutter and Cremer, 2008)

2.2.2. Homograft/allograft valves

These are valves that are taken from a human cadaver heart or from a donor. Cryogenic techniques are mostly used to keep these valves viable for implantation and they are also treated with antibiotics. The use of homograft valves is more common in the aortic position, although as explained in the Ross procedure, homograft pulmonary valves are used to replace pulmonary valves. The uses of homograft valves are usually in situations where the native or prosthetic valve is inflicted by endocarditis. Due to limited availability of donors and also the perceived difficulty of the surgical procedure involved, homograft valve use is limited. Studies conducted by Barrat-Boyes et al. in 1969, showed a lot of complications with patients with homograft valves. However, studies in later years showed massive improvements in the survival rates, thus suggesting an improvement in surgical procedures and management of homograft valve patients (Hoffmann et al. 2008; Carrel 2009).

2.2.3. Xenograft/ Heterograft valves

These are valves made from tissues from animal species. Commercially available xenograft valve are made from either porcine valves or bovine pericardium. These valves are treated with glutaraldehyde in order to strengthen the leaflets and to lessen the host immune response when implanted. Other techniques such as photo oxidation of valves have been shown to reduce calcification of these xenograft valves (Moore and Adams, 2001). Xenograft valves

are often reinforced with a stent which helps to hold the valvular tissue in their correct anatomical position and also ease the implantation process. There are also stentless bioprosthetics which due to the non rigidity, provides a larger orifice area and best haemodynamic results, however they require extremely skilled persons to perform the implantation procedure (Hoffmann, Lutter and Cremer, 2008).

2.2.4. Percutaneous Heart Valves

The aforementioned valves are implanted via open chest surgery. Open heart surgery is obviously extremely invasive and has its own plethora of associated complications. As a result, not all patients may be suitable for open heart valve replacement procedures. This has led to valves with the ability to be implanted percutaneous. Percutaneous implantation is done by 2 main access points namely retrograde and antegrade delivery.

Retrograde delivery, also known as transfermoral delivery involves access to valve implantation site through the femoral artery or vein in the groin area, although sometimes the subclavian and or carotid artery may also be used. The other access point, known as antegrade or transapical approach, involves making a small incision in the intercostal space and through which access to the valve site is gained via the apex of the ventricle (Bleiziffer *et al.*, 2013) . The first report of percutaneous valve implantation in a human was by Bonhoeffer et al in 2000. In this report, pulmonary valve replacement was done in a 12 year old boy with pulmonary valve stenosis and regurgitation (Bonhoeffer *et al.*, 2000).

Since its first report of human implantation by Cribier et al. in 2002, Transcather Aortic Valve Implantation (TAVI), has become the most common type of percutaneous valve implantation is gaining increasing acceptance as a method of treating patients with severe

aortic stenosis, who also present various contraindications for conventional open chest surgery (Walther and Kempfert, 2012).

In the TAVI process itself, a guide wire is threaded through the vascular access of choice, to the diseased native aortic valve. A catheter with a deflated balloon at the tip is threaded over the guide wire into the obstructed or stenosed valve and inflated, after which the balloon tipped catheter is withdrawn. This process is known as balloon valvuloplasty and creates room for the artificial heart valve. The TAVI valve is then crimped over a balloon tipped catheter and deployed either transfermorally or transapically to the annulus of the diseased valve. Depending on the valve type, the stent may then self expand or may be mechanically expanded by inflating the balloon. This process is aided by real time imaging modalities such as fluoroscopy (Ruparelia and Prendergast, 2016). TAVI valves are essentially stented bioprosthetic valves, however due to its unique style of implantation, its stent design tends to be different. TAVI valves stent should have the crimping and expanding abilities. The stents are designed in a thin wire mesh configuration to aid crimping and also aid delivery. Self expandable stents are made out of shape memory alloys with nitinol being the material of choice. These alloys can be deformed when cold and will resume their natural shape once it comes into contact with heat in the body after implantation. This particular feature is what makes the valves “self expandable”. Balloon expandable valve stents are mostly made from stainless steel and cobalt chromium alloys. Valve skirts, made out of polyester or pericardium, are located at the base of the stent and function to reduce leakage when implanted. (Rozeik, Wheatley and Gourlay, 2014a). The Medtronic Evolut pro+ Valve and Edwards Sapien valves are common examples of self expandable and balloon expandable TAVI valves respectively

Some of the initial drawbacks of the TAVI valves were that once its been deployed, it cannot be repositioned or retrieved. This has led to the design of repositionable and retrievable

valves such as the self-expanding Lotus Edge Valve and The Direct Flow Medical (DFM) heart valve (Rozeik, Wheatley and Gourlay, 2014a). Another emerging trend in the use of TAVI valves involves valve in valve procedures where a TAVI valve is inserted into a failed bioprosthetic valve. This is commonly done when there a need to reoperate but the patient has contraindications of surgery (Simonato and Dvir, 2019).

2.3.THE POTENTIAL OF POLYMERIC VALVES AS AN IDEAL VALVE REPLACEMENT OPTION

Some characteristics of an ideal artificial heart valve include

- Minimum mean systolic trans-valvular pressure drop (minimal resistance to forward flow)
- Minimum regurgitation (minimal closing volume and leakage volume)
- Large effective orifice area
- Low risk of calcification and thrombosis
- Long durability (>400million cycles, equivalent to 10years for mechanical valves, >200million cycles, equivalent to 5 years for bioprosthetic valves)
- Not damaging to blood elements
- Easy to implant and replace
- Easy to manufacture
- Easy to sterilize, store and transport

(Burriesci, Marincola and Zervides, 2010)

Commercially available heart valves come in two forms , either mechanical or bioprosthetic . Mechanical heart valves are known for their durability, however due to the synthetic nature of their materials, their hemodynamic and biocompatibility is mostly compromised thus making them susceptible to thromboembolic complications. Due to this, perpetual anticoagulation treatment is required for patients implanted with these valves and this has limited the pool of patients who can benefit from mechanical heart valves (Gott, Alejo and Cameron, 2003).

Bioprosthetic valves were then introduced in an effort to curb the issues with mechanical heart valves. These valves mimic the trileaflet shape of the native aortic valves and as a result, presented better hemodynamic profiles. Although successful in terms of limiting anticoagulation therapy, it presents with its own disadvantages which include structural defects and also calcification thus making them less durable (Carpentier, 1989). This has led to the conundrum of solving one problem, but replacing it with another, thus making the choice of heart valve to implant, a hot topic of debate (Choudhary, Talwar and Airan, 2016).

Over the years, there has been a lot of research into developing valves that would combine the durability of mechanical valves and also the hemodynamic and biocompatibility of bioprosthetic valve, which has led to the emergence of polymeric heart valves (Mackay et al. 1996; Daebritz et al.2003; Gallocher 2007; Ghanbari et al. 2009; Burriesci et al. 2010; Rahmani et al. 2012; Claiborne, Slepian, et al. 2013; Bezuidenhout et al. 2015; De Gaetano et al. 2015) These are valves made out of polymer and polymer composites.

The concept of polymeric valves itself is not entirely new. In the year 1958, Elliot & Callaghan reported on their experimental all plastic ventricular pump with tricuspid valves. In that same year, Ten Berge also reported on his experimental polymeric valvular prosthesis. Shortly after that, the first successful clinical implantation a polyurethane valve, as a

replacement option for the mitral valve , was reported by Braunwald et al. in 1960. From first indications, it would seem that polymeric valves were on the rise, however the success of the Star Edwards valve and also the intervention of minimally invasive mitral valve surgeries, rendered the polymeric valves an afterthought and limiting their use to artificial hearts and ventricular assist devices (Bezuidenhout, Williams and Zilla, 2015). Drawbacks of existing heart valve replacement options have however necessitated the need to revisit the potential of polymeric valves as an alternate and ideal valve replacement option.

Polymeric valves were to ideally combine the biocompatibility of bioprosthetic valves with the durability of the mechanical valves, however practically, these valves have been far from perfect and as a result, there are currently no commercially available polymeric valves for use as total heart valve replacement. These valves do however still project a promising outlook Trileaflet polymeric valves have had an unreliable history. Prior to the Braunwald et al's clinical success in 1960, researchers Roe and Moore had started implanting polymeric heart valves, however due to severe complications including embolization, the study had to be brought to a halt (Gallocher, 2007). Buoyed by the success of the first clinical implantation of polymeric valves as a total mitral valve replacement option, Braunwald et al began clinical trials in implanting patients with Teflon valves as a total aortic valve replacement option. Again complications lead to high morbidity. The high mortality rate, coupled with the emergence of mechanical and later on bioprosthetic valves, played a major role in stunting the path to commercialisation of polymeric valves (Daebritz *et al.*, 2004).

Even following the commercialisation of mechanical and bioprosthetic valves, research still continued in polymeric valves, albeit it with minimal success. In their 2013 review article (Claiborne, Slepian, *et al.*, 2013) cites some of these earlier polymeric heart valves developed and their failures. These include the Mori et al's silastic trileaflet valve in 1973, Imamura and Kaye's Polytetrafluoroethylene (PTFE) trileaflet valves which were implanted in dogs in

1977, Wisman et al's polyurethane valve in 1983 and Kiraly et al's Hexyn trileaflet polymeric valve. In 1990, Nista et al also reported on the failure of PTFE valves after implantation in sheep. In vivo durability has long being the bane of polymeric valves , with thromebogenic complications, material degradation and calcification being the most common modes of failure (Claiborne, Slepian, *et al.*, 2013).

The invivo failure of polymeric valves are thought of be as a result of their material properties, design and style of manufacture, with common earlier polymeric valve materials including silicone, polyurethane and PTFE. However, technological advancements in polymer science in terms of creating more stable biopolymers, has led to a resurgence and also promising outlook of polymeric heart valve research.

A Glasgow group, led by Wheatley, have developed a trileaflet polymeric valve made out of polyurethane, manufactured via a technique known as dipcoating. This valve was then subjected to hydrodynamic and accelerated fatigue testing invitro. The hydrodynamic performance even exceeded its mechanical and bioprosthetic valve counterparts. Further to that, all the polymeric valves testing in the accelerated fatigue tester were able to exceed the equivalence of 10yrs without fail, with 3 of the valves reaching an equivalent of 13 years. Wheatley et al, later on, implanted these valves in the mitral position of sheep, alongside some commercially available mechanical and bioprosthetic valves, for comparison. A follow up after 6 months revealed that the polyurethane valves performed better than the mechanical and bioprosthetic valves, thus highlighting the potential of biostable polyurethanes as a material of choice in polymeric valve development. (Mackay et al. 1996;Wheatley et al. 2000).

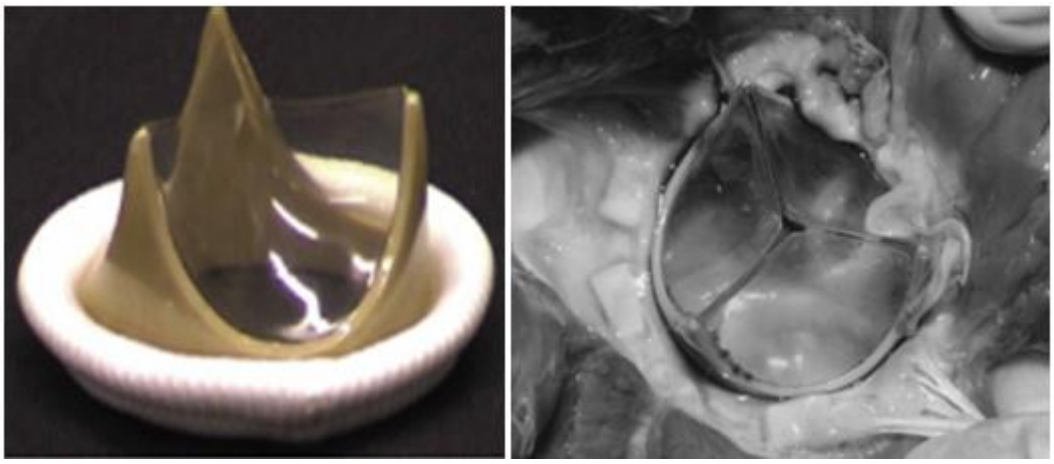

Figure 2.1 Polyurethane valve by Glasgow group. Left-Polyurethane valve developed by the Glasgow group. Image taken from (Bezuidenhout, Williams and Zilla, 2015). Right-Polyurethane valve implanted in sheep. Image taken from (Wheatley et al., 2000).

Daebritz et al have also investigated the use of Polycarbonate urethane (PCU) as materials of choice for polymeric heart valves. In their study, PCU valves, alongside commercially available bioprosthetic valves, were implanted in calves in both aortic and mitral valve positions. The results again showed superiority of PCU valves over the bioprosthetic valves invivo (Daebritz *et al.*, 2003, 2004).

In vitro hydrodynamic tests have also been conducted on polymeric valves made nanocomposite polyurethane material such as Polyhedral Oligomeric Silsesquioxane Poly(Carbonate-urea) urethane (POSS-PCU) and results show better hydrodynamic function in comparison with bioprosthetic valves, particularly in terms of transvalular pressure gradient, effective orifice area and energy loss (Rahmani *et al*.,2012, 2012).

Another polymer that has been investigated invitro is Poly(Styrene-block-IsoButylene-block-Styrene) (SIBS). This polymer has shown good oxidative stability, haemocompatibility, hydrodynamic function and durability in comparison with bioprosthetic valves and mechanical valves (Yin et al. 2005; Gallocher et al. 2006; Claiborne, Sheriff, et al. 2013; (De

Gaetano *et al.*, 2015). A 2010 in vivo study on SIBS valve with reinforced Polyethylene terephthalate (PET) fabric implanted in sheep however showed failure due to material degradation and calcification (Wang *et al.*, 2010).

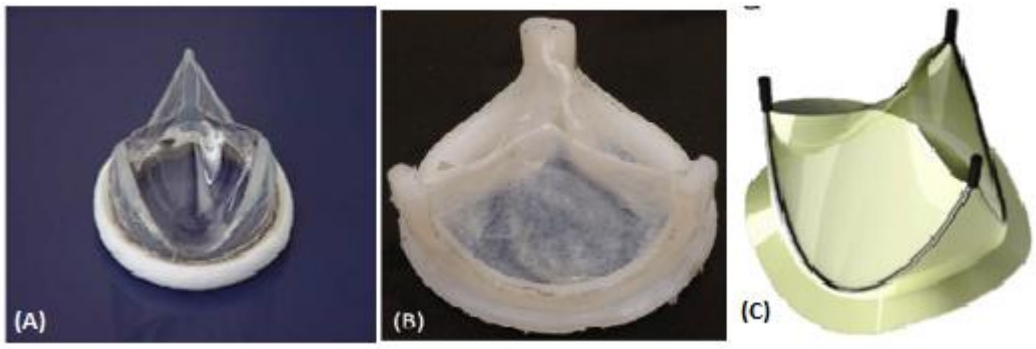

Figure 2.2. Polymeric heart valves. (A)- ADIAM PCU valve. Image taken from (Daebritz et al., 2004) (B)-xSIBS valve. Image taken from (Claiborne, Sheriff, et al., 2013a) (C)-POSS-PCU valve. Image taken from (Rahmani et al.,, 2012)

In recent years, there has been a growing interest in polymeric valves and its use as an alternative to the bovine or porcine tissue leaflets in valves used for Transcather Aortic Valve Implantation (TAVI) procedures.

Rozeik et al have conducted mechanical testing on thin carbon nanotube polyurethane composites, as a replacement option for the existing thicker TAVI leaflets, which due to their increased size, may lead to some vascular complications during delivery. The results of their tests suggest there's a potential for carbon nanotubes polyurethane composites as an option for TAVI valves susceptible to high strains rates during function (Rozeik, Wheatley and Gourlay, 2017).

Rotman et al describes their TAVI valve with leaflets made from xSIBS, which is a cross linked version of clinically used SIBS. These valves have been subjected to invitro hydrodynamic and hemodynamic testing, with a commercially available bioprosthetc and

TAVI valve for comparison. Their results showed comparable hydrodynamic function and superior hemodynamic function of the polymeric TAVI valve in comparison with the commercial valves. The valves also exceeded 400million cycles (equivalent to 10years) during durability testing (Rotman, Kovarovic, Bianchi, *et al.*, 2019; Rotman, Kovarovic, Chiu, *et al.*, 2019).

TAVI valves with leaflets made from polyethyleneglycole diacrylate (PEGDA) hydrogel and non woven polyethylene terephthalate (PET)/polyamide6 (PA-6) , with self expandable nitinol stent have been reported by Guo et al. Mechanical testing revealed these polymeric leaflets possessed mechanical properties comparable to the native aortic valve leaflet. Further to that, invitro hemodynamic tests showed superb hemodynamic function and low platelet adhesion (Guo *et al.*, 2019)

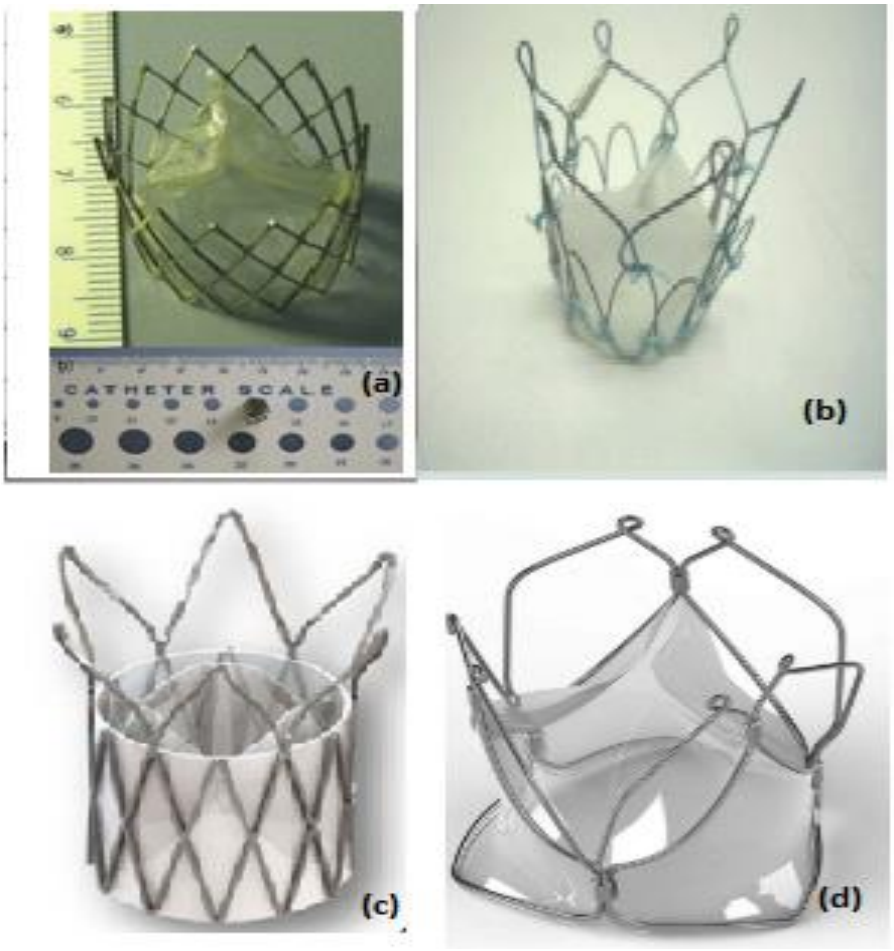

Figure 2.3. Polymeric TAVI valves (a)-Mecora PU valve with nitinol stent. Image taken from (Attmann *et al.*, 2006) (b)- Clairboirne SIBS valve with nitinol stent. Image taken from (Claiborne, Slepian, *et al.*, 2013). (c)- PolyNova xSIBS valve with nitinol stent . Image taken from (Rotman, Kovarovic, Chiu, *et al.*, 2019), (d)- Triskele POSS-PCU valve with nitinol stent. Image taken from (Bezuidenhout, Williams and Zilla, 2015)

So far , advances in polymer science has aided in new materials that have shown potential as valve replacement options. This is a step in the right direction to the ultimate realisation and commercialisation of polymeric heart valves. Further invivo tests are however necessary in order to make this a possibility.

2.4. HEART VALVE MANUFACTURING PROCESS

Prosthetic heart valves, due to their invasive nature and its interaction with the cardiovascular system, are classified as class 3 medical devices, i.e high risk medical devices. As a result, they undergo very stringent manufacturing and testing protocols before going into the market. Manufacturing technique depends on the type of valve and also the company producing said valve.

In this section, we are going to be exploring the manufacturing process of mechanical and bioprosthetic (tissue) valves. Mechanical valves will focus on the bileaflet valve design as these are the most common mechanical valves currently being produced and implanted (Grunkemeier *et al.*, 2015).

i. Bileaflet valves

All valves, implanted via open heart surgery, consists of three major components, the support structure, sometimes referred to as the stent, the leaflets, ie the movable parts of the valve and then the sewing cuff used to attach the valve to the native valve annulus during implantation. The bileaflet valve consists of 2 semi-circular discs that are connected via hinges in the support structure and open and close in a butterfly wing like manner. The intricate details of the manufacturing process differ from company to company. Below is a generalised description of the manufacturing process.

Common raw materials used for making the valve structure /housing include titanium and graphite. The support structure is machined with high resolution machining and laser cutting equipment, after which they are coated with pyrolitic carbon to improve upon the durability, wear resistivity ,biocompatibility and thromboresistivity of the valve (Lankford, 1999). Surface polishing then takes place to remove any debris and give a smooth finish.

The valve leaflets are also machined from graphite bars and then coated with pyrolitic carbon. To aid in adequate viewing of leaflet motion via radiation based imaging techniques, some models of valves have tungsten incorporated into the leaflets. Components then move to a contamination free room, also known as a clean room, where the leaflets are attached to the internal portion of the strut via hinges. Valves are then tested in a mock circulatory system. Sewing ring, made commonly out of double velour polyester material or PTFE is then prepared, and mounted unto the support structure. Sewing cuff is held in place using lock rings commonly made out of titanium. The valve is then mounted unto a special valve holder that will aid the surgeon in implantation after which the valve moves to the sterilization process.

Valves are packaged in transparent double barrier containers and sterilised via steam sterilization, labelled and shipped out (SJM Mechanical Valve Manufacturing 2011).

The manufacturing process of bioprosthetic valves are very different from those of mechanical valves. Further to that, porcine and pericardium valves tend to also differ in terms of their manufacturing process. In this section, we will be discussing the manufacturing process of some of the current most commonly implanted xenograft valves. Major bioprosthetic valve manufacturing companies include Abbot, Edwards lifesciences and Medtronic.

ii. Stented porcine bioprosthetic valves.

The aortic root is cut out from a pig's heart. A longitudinal dissection of the aortic root is done to expose the 3 leaflets of the aortic valve. The 3 leaflets are then cut and trimmed. To ensure best quality leaflet tissue, most manufacturing companies select the best leaflet per aortic root. The leaflets then go into the tissue preparing stage. As part of the tissue preparation process, leaflets are treated with glutaraldehyde to help eliminate antigenicity

when implanted into the human body. Although this process does tremendously reduce antigenicity, several researchers (Kim et al. 1999; Vesely 2003; Manji et al. 2006) have shown that the process promotes calcification of leaflets after implantation.

The valve stent are machined from flexible polymer material or metal, commonly cobalt chromium alloys and titanium. The stent is then covered in polyester fabric material, with a silicon ring encapsulated in the fabric at the base of the stent thus providing the sewing ring. To aid in visualisation, some valves have a thin stainless steel wire around the outside of the stent, prior to covering with the fabric.

The leaflets are then inserted and sutured into the stent. The stent may also be covered with thin strips of treated bovine pericardium. This decrease the amount of fabric exposed to blood and also causes a tissue to tissue interface between the valve leaflets and stent during blood outflow for enhanced bio and hemocompatiblity.

Valves are then tested and mounted onto special valve holders and moved to sterilisation. Sterilization of the valve involves anti-mineralisation treatment to reduce susceptibility to calcification due to gluteraldehyde fixation. Common antimineralisation agents include alpha oleic acid and ethanol (Singhal, Luk and Butany, 2013). St Jude Medical/ Abbot uses a patented anticalcification treatment known as Linx AC, in some models of their valves, to minimise calcification (Jamieson *et al.*, 2011). Edward lifesciences also use their patented Xenologix and Thermafix treatments to reduce calcification in their bioprosthetic valves (EdwardsLifesciences, 2002)

iii. Stented pericardial valves

The manufacturing process of porcine and bovine pericardial valves do share some similarities, however there exists some very distinct differences. For both valves, the stents

are either metal/polymer covered in fabric, differences however exist in the leaflet formation. Porcine leaflets are essentially, whole aortic root leaflets from pigs heart , whereas bovine pericardial valve leaflets are made from flat sheets of bovine pericardium. This allows for more flexibility in the design and also allows the possibility of making bileaflet valve, as opposed to porcine valves, which are limited to trileaflet.

Bovine leaflets are attached in one of 2 ways. 3 independent bovine pericardial tissue are cut and sutured onto the stent. Models manufactured this way include the Perimount Valves from Edwards Lifesciences. Other companies, such as St Jude Medical (Abott), wrap a single thin strip around the 3 stent posts and then suture these leaflets unto the posts. This process is aided by mounting the stent unto a specially designed mandrel, with the shape and size of the desired final product. The St Jude trifecta bovine pericardium valves ,have their stents wrapped in thin strips of porcine pericardial tissue before leaflet attachment. They then undergo testing, sterilization and antimineralisation techniques similar to those of porcine valves.

iv. Stentless bioprsothetic valves

With stented valve tissues, it is believed that the inclusion of the stent increases the unnatural distribution of the stresses on the tissue i.e, more stresses tend to be on the portion of the leaflets near the stents. The stents also tend to inhibit the effective orifice area of the valve (Vesely 2003; Dasi et al. 2009). For these reasons stentless bioprosthetic valves were introduced. They consist of a whole intact porcine aortic root with gluteradledhyde fixation. These valves come in either the trimmed or untrimmed form. Untrimmed valves, such as the Edwards Prima Plus, have trim lines to aid the surgeon to trim the aortic root to desired shape prior to implanting. These also contain suture lines to aid proper orientation of valves.

Stentless bioprosthetic valves tend to have fabric at the base of the aortic root to aid in implantation and suturing and to also prevent leakage.

v. TAVI valves

Due to their percutaneous style of deployment, the design considerations of TAVI the design considerations are different from the other bioprosthetic valves. The leaflets are laser cut from a thin strip of porcine, bovine or equinine pericardium and stitched together. Some TAVI valves such as the Symetis Acurate TA valve, have their leaflets made out of native porcine valve leaflets, similar to stentless bioprosthetic valves. These leaflets are then attached to the stent.

Self expanding stents are made out of nitinol due to the shape memory effect, whiles balloon expandable valves are commonly made out of stainless steel and cobalt chromium alloys and in some cases, polymer. These stents are laser cut/machined in a mesh like form to aid in crimping over the catheter. At the base of the stents are the valve skirt. These skirts are to conform adequately to the native valve annulus to prevent paravalvular leakage. These are covered with either polyester fabric, mostly Dacron, or pericardium tissue(Sinning *et al.*, 2012; Bourantas and Serruys, 2014).

2.5. ARTIFICIAL HEART VALVE COMPLICATIONS

The idea of a perfect prosthetic heart valve is one that is yet to be realised. Native heart valve complications are as a result traded in for prosthetic heart valve complications The type and severity of the complications depends on factors such as the type, model, position and size of

the valve. Some of the complications of artificial heart valve may also common in native counterparts. In this section, we discuss some of the complications of artificial valves.

i. Mechanical failure

This complication is mostly common in mechanical valves. It involves the destruction of mechanical valve components such as the strut, disc occluder and sewing rings. This is a catastrophic event which could lead to heightened mortality rate in patients with such valves implanted. One of the well documented mechanical failure cases, was the outer strut fracture of the Bjorky-Shiley 60 degrees concave convex valves. This model was a tilting disc valve which was introduced into clinical use in 1976. The design was to improve durability, haemodynamic performance and to decrease thrombosis . However, in September, 1978, there was a reported incident of fracture of the strut, causing the disc occluder to migrate from its original position within the valve (Hiratzka *et al.*, 1988). From then till June 1987, there were an additional 213 reports of strut fracture out of about 83,000 implanted valves. Testing revealed that excessive outlet strut stress leading to fracture could occur during valve closure. In 1986, all distributed valves were recalled and further production of the specific model was halted (Hiratzka *et al.*, 1988). The controversy resulted in a lot of lawsuits filed against the manufacturing company. Although a lot of these valves were recalled, quite a few still remained implanted (Omar *et al.*, 2001).

Dehiscence, which presents as a gap in the opening of the sewing ring leading to regurgitation, can also be classified under mechanical failure of a valve. This is caused by technical error during valve implantation, infective endocarditis or just disintegration of the sewing ring. It is more common in valves with thin sewing rings (Chambers, 2009).

ii. Thrombosis and thromboembolism

Prosthetic heart valves are foreign bodies and as a result are all at a risk of thrombosis due to the interaction of blood and the synthetic materials. These thrombus could lodge between the opening of the heart valve, obstructing leaflet motion, blood flow and may also lead to other thromboembolitic complications. The risk of thrombosis is higher in mechanical valves than in bioprosthetic ones and also higher in the mitral position (Edmunds 1987; Vesey & Otto 2004;Zhang et al. 2012). To decrease the risk of thrombosis, patients with mechanical valves, are put on a lifetime anticoagulation therapy with warfin. Warfin is however said to be associated with foetal loss hence not recommended for women of child bearing age. Other risk factors for valve thromboembolism include atrial fibrillation, previous history of thromboembolism, left ventricular disfunction and left atrial dilation (Pibarot and Dumesnil, 2009).

iii. Device obstruction

This is the occlusion of the opening of the heart valve causing obstruction to blood flow. This is very common in mechanical valves, occurring in 0.5-4.5% of patients per year (Edmunds 1987;Deviri et al. 1991). Obviously this is a very serious complication that could lead to death if not treated promptly. Studies conducted by Deviri et al. in 1991, suggests that thrombosis (77%) , pannus formation (10.7%), or a combination of both (11.6%), are the major causes of prosthetic valve obstruction .

iv. Pannus formation

Pannus formation presents as an abnormal growth of tissue in the valve. Whilst it is very different from thrombosis, the mechanical effect on heart valve is also device obstruction.

During treatment of device obstruction, it is very necessary to determine its etiology as that could affect the intervention protocol used (Barbetseas *et al.*, 1998; Barroso Freitas-Ferraz *et al.*, 2019)

v. Stenosis

Just like their native counterparts, prosthetics heart valves can also be affected by stenosis. Over time, bioprosthetic valves may accumulate calcific deposits which may cause leaflets to stiffen and not open properly. Risk of calcification increases with age, pregnancy and position of valve, with mitral valve position being the most common. In mechanical valves, stenosis is presented as device obstruction(Vesey and Otto, 2004). Patients with prosthetic valve stenosis tend to exhibit symptoms synonymous with that of the native valves with the major exception being the presence of an audible click in the mechanical heart valves. Thus both native and prosthetic valve stenosis are diagnosed similarly (Vongpatanasin, Hillis and Lange, 1996).

vi. Haemolysis

Mechanical trauma to red blood cells may lead to haemolysis. In heart valves, this could be as a result of turbulent or unnatural flow profiles causing excessive shear forces on the walls of the red blood cells. A significant complication of haemolysis, called **haemolytic anaemia** is documented to be caused by paravulvular regurgitation of the valve. This leakage tends to occur in the small gaps in the valve between the sewing ring and the annulus of the valve. Studies conducted also show that patients with a genetic disorder of the connective tissues known as marfans syndrome are also at a high risk of paravalvular regurgitation. In bioprosthetic valves, deteriorations and tears of the tissue structure could also cause paravalvulvular leakages and unnatural flow profiles ultimately leading to haemolytic anaemia and other haemolytic complications (Maraj *et al.*, 1998).

vii. Endocarditis:

Interactions between the foreign materials of the prosthetic valve and their host tissues may cause inflammations, known as endocarditis. Another cause of endocarditis is staphylococcus, in which case is known as infective endocarditis. Early endocarditis ie occurring during the first 2 months following surgery has been known to have a high mortality rate, of about 80% (Wolff *et al.*, 1995). Late valve infective endocarditis(after 2 months) is mostly caused by secondary procedures such as dental procedures, urological procedures and other procedures that involve the use of indwelling catheters (Horstkotte *et al.*, 1995). Infective endocarditis tends to affect the sewing and may lead to abscess formation, embolitic events and regurgitation.

2.6. THE EFFECT OF AORTIC VALVE STENSOSIS ON CARDIAC FUNCTION (PATHOPHYSIOLOGY)

As earlier mentioned, aortic valve stenosis presents as an obstruction or narrowing of aortic valve orifice. Native valve and bioprosthetic valve stenosis may be caused by calcification. Stenosis in mechanical valves is presented as device obstruction commonly due to thrombosis and or pannus formation. Aortic valve stenosis, whether in the native valve or prosthetic valve, is a very dangerous condition which if not detected and managed accordingly, could lead to high mortality due to its effect on cardiac function. this effect is explained further below:

Obstruction of the aortic valve, leads to an increase in resistance to flow in the left ventricular outflow tract as per the equation

$$R \propto \frac{n.L}{r^4}$$

Where R = resistance , n=viscosity, L is the length and r is the radius.

Assuming viscosity and length remain constant, it can be seen that resistance is inversely related to the 4th power of the radius of the valve orifice. Considering the valve orifice as a circle with area $A = \pi r^2$, it can then expressed as

$$R \propto \frac{1}{A^2}$$

Thus even a small decrease in valve orifice area will then lead to a high increase in resistance, assuming all other conditions remain constant.

Pressure upstream and downstream the aortic valve, i.e. the left ventricular pressure and the aortic pressure respectively, an increase in the resistance to flow in the valve will require a higher left ventricular pressure needed to overcome this resistance in order to not compromise flow. This is mathematically expressed as

$$\frac{LVp - Aop}{R} = F$$

Where LVp= Left ventricular pressure, Aop =Aortic pressure, R is the resistance and F is the flow. This increase in LVp also leads to a higher transvalvular pressure gradient to be experienced across the valve.

Flow is also a function of velocity and area (F=VA), as a result a decrease in the valve orifice area then leads to an increase in velocity, assuming constant flow. This increase in velocity causes turbulent flow (Klabunde, 2012b)

As aortic stenosis progresses it leads to host of left heart complications. Aortic valve stenosis tends to be a slow progressive disease. Its slow progressive nature allows for the left ventricles to compensate for the increase in afterload by increasing its wall muscle thickness.

This compensatory mechanism is known as left ventricular hypertrophy and allows for the ventricles to handle the higher ventricular pressure needed to maintain adequate systolic ejection and preserve cardiac output. This compensation contributes to some patients being asymptomatic in the initial stages of the disease (Martin, 2013). Another way the heart compensates for the obstruction is by extending the ejection time of the left ventricle in order to allow for the left ventricle to fully eject its content thus not compromising on the stroke volume (Zacharias and Goldstein, 2015)

The compensation is however temporary and can only be kept up for so long. As the ventricle becomes thicker, it causes the ventricle to be less compliant, resulting in a decrease in preload and impairment in ventricular filling. A decrease in ventricular filling, will automatically mean less blood will be pumped out (Stroke volume) and as a result, cardiac output is reduced. With the inability of the ventricles to expand and fill properly, blood continues to accumulate in the left atrial chamber which also leads to an increase in the volume and pressures experienced in the left atrium (Zacharias and Goldstein, 2015).

Symptoms of aortic valve stenosis typically tend to manifest between moderate to severe stenosis. Common symptoms of severe aortic valve stenosis include exertional shortness of breath, angina (chest pains) , dizziness , syncope (fainting) and systolic murmurs . Following the onset of the symptoms, if untreated, the prognosis is very poor ie between 2 -3 years (Ramaraj & Sorrell 2008; Rozeik et al. 2014b). Severe aortic valve stenosis has no effective drug therapy and as a result surgical or catheter based intervention presents as the sole effective solution (Pibarot, Sengupta and Chandrashekhar, 2019) . Due to the high morbidity rate of aortic valve stenosis, early diagnosis is very key.

2.7. SUMMARY

Heart valve replacement is the long term solution for severe native valve malfunction. Mechanical valves and bioprosthetic valves are the two commercially available valves. Mechanical valves are heralded for their durability but require perpetual anticoagulation therapy due to the synthetic nature of the materials. Bioprosthetic valves tend to be more bio and hemocompatible but are limited in their durability. Polymeric heart valves have the potential of combining the durability of mechanical heart valves and the biocompatibility of bioprosthetic heart valves. Even though there has been a lot of promising research in the field of polymeric valves, its path to clinical implementation has been less than satisfactory. Native heart valve complications are often traded in for prosthetic valve complications after implantation. These complications may ultimately causes obstruction/stenosis of the prosthetic valves. Valve obstruction is characterised by increase in transvalvular pressure gradient, jet velocity and decrease in the effective valve orifice area (EOA).

CHAPTER 3. HEART VALVE EVALUATION AND DIAGNOSTIC TECHNIQUES

The assessment of heart valve function after implantation is necessary in order to be able to accurately diagnose any complications and intervene accordingly. Diagnosing valve complications is a challenging task and as a result, there exists a plethora of diagnostic techniques used either as standalone or in combination with others. In this chapter, we discuss the diagnostic techniques and procedures used in the clinical setting for the evaluation of heart valves.

3.1. Echocardiography

Echocardiography is the gold standard method used for assessing both native and prosthetic heart valve function (Wilkins *et al.*, 1986; Baumgartner, 2009; Parnell and Swanevelder, 2009; Zoghbi *et al.*, 2009; Saikrishnan *et al.*, 2014; Lancellotti *et al.*, 2016) It is a non-invasive imaging technique pioneered by Inge Elder and Hellmurt Hertz in 1953. Elder and Hertz were able to use ultrasonic techniques to obtain time varying images of the heart for diagnosis of mitral valve disease (Harvey, 1996; Edler and Lindström, 2004; Singh and Goyal, 2007; Maleki and Esmaeilzadeh, 2012). The success of Elder and Hellmurt, led to the acceptance of echocardiography as the imaging modality of choice for valvular diseases.

Echocardiography diagnostic techniques tend to be similar for both native and prosthetic valve complications and different echocardiography modalities may be used depending on the type of the valve, position of the valve, severity and type of valve disease. It should however be noted that the use of echocardiography for prosthetic valve presents a higher challenge than their native counterparts (Lancellotti *et al.*, 2016). There are different types of echocardiography and these are explained below.

i. 2D Transthoracic Echocardiography (TTE)

The European Association of Cardiovascular Imaging recommends 2D Transthoracic Echocardiography (TTE), as the initial imaging modality for the assessment of prosthetic valve function (Zoghbi *et al.*, 2009; Lancellotti *et al.*, 2016). In 2D Transthoracic Echocardiography (TTE), the ultrasound probe is placed over the chest area of the patient and multiple planes of views are captured in order to get an overall image of the heart. 2D TTE helps to provide information such as the sizes of the heart chambers, left ventricular function, movement of valve leaflets or occluders and also presence of calcification (Zoghbi *et al.*, 2009). Although 2D TTE tends to be quick, it may not provide sufficient accurate visual information on the structure of the valve required for a thorough assessment (Maganti *et al.*, 2010).

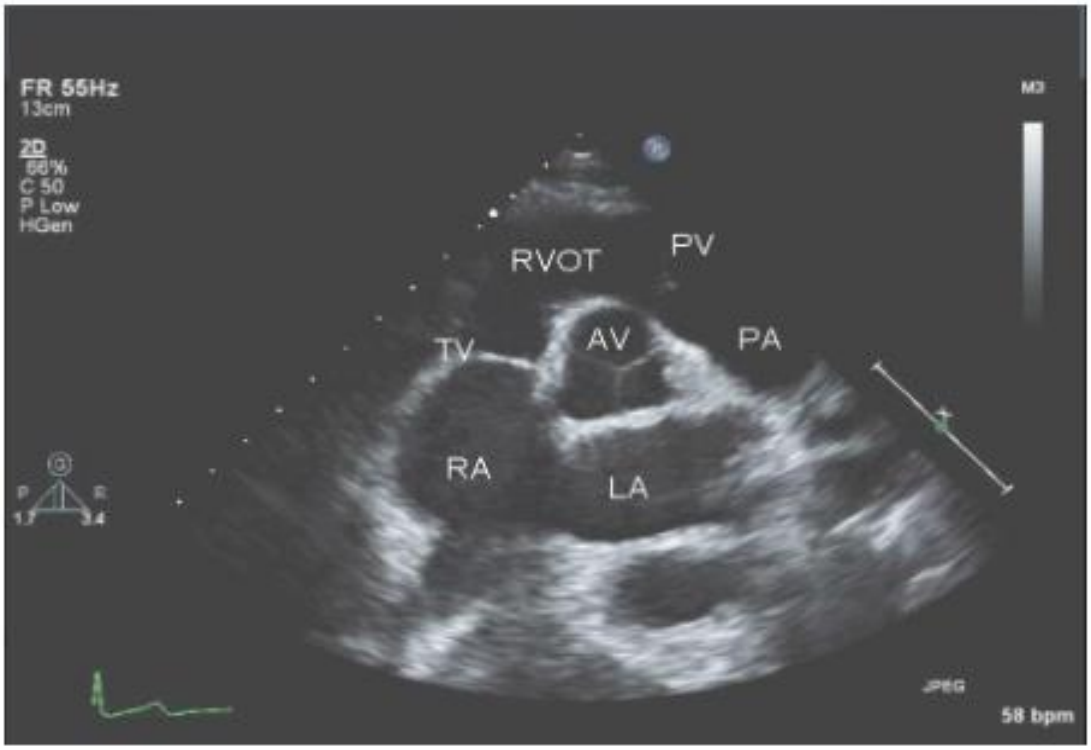

Figure 3.1. Image of the 2 atria, 3 valves and right ventricle outflow tract captured by 2D TTE. TV-tricuspid valve, RA-right atrium, LA- left atrium, AV- aortic valve, PV-pulmunary

valve, PA-Pulmunary artery, RVOT- right ventricular outflow tract. Image source (https://www.echocardiographer.org/Old%20html%20files/TTE.html)

ii. 2D Transoesophageal Echoicardiography (TOE)

2D Transoesophageal echocardiography (TOE) is also an alternative way of assessing valve morphology and its commonly used when 2D TTE results are inconclusive or when prosthetic heart valve complications are suspected (Vahanian *et al.*, 2007). A special ultrasound probe is inserted through the oesophagus of the patient and images are captured from behind the heart. 2D TOE allows for clearer images and better visualisation of the posterior part of the aortic valve and also the atrial side of the mitral valve due to the close proximity of the oesophagus to the heart. Similar to 2D TTE, careful angulation of the probe is necessary to view valve leaflet motion (Lancellotti *et al.*, 2016). TOE tends to be however be a more complex procedure relative to TTE. In general, 2D TTE and TOE are necessary in terms of visualising the structure of the heart valve which then aids in assessing and or diagnosing complications of either the native or prosthetic heart valve.

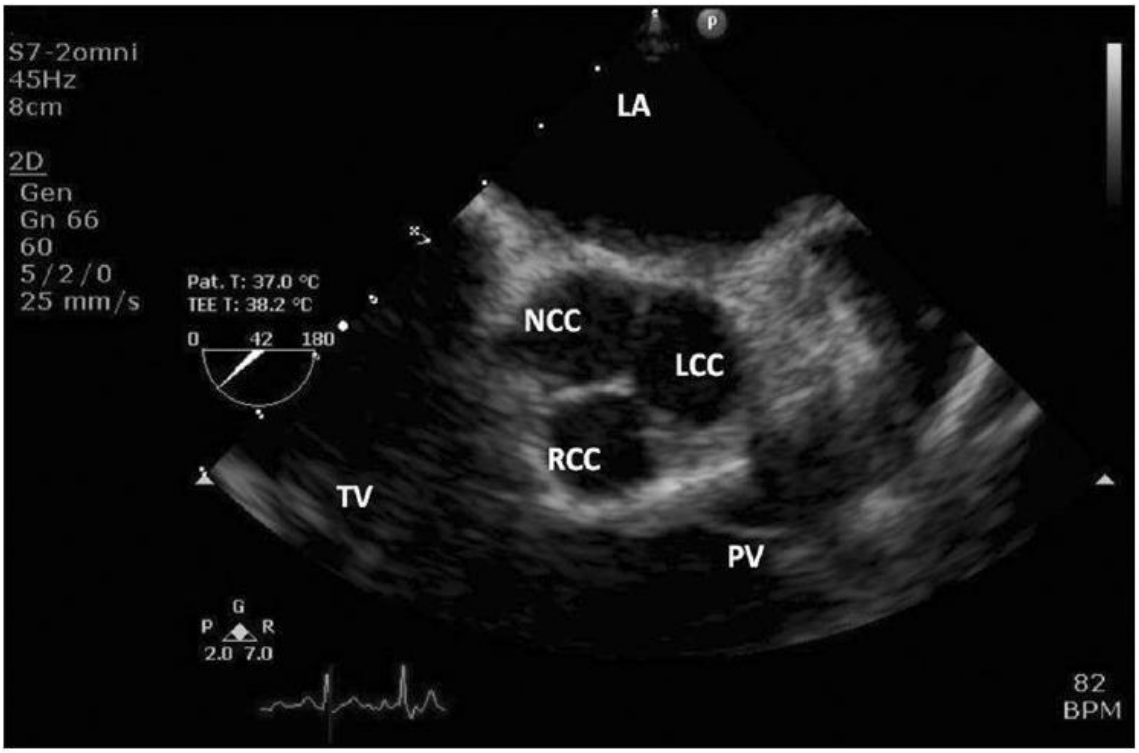

Figure 3.2. Image of the native aortic valve taken via 2D TOE. LA- left atrium, TV- tricuspid valve, PV- pulmonary valve, NCC-non coronary cusp, LCC- left coronary cusp, RCC –right coronary cusp. Image taken from (Prabhu, Raju and Pauli, 2012)

iii. 3D Echocardiography

Real time 3D echocardiography has also emerged as a promising echocardiography modality for assessing valve function. 3D echocardiography provides a 3 dimensional view of the valve structure thus assumptions or uncertainties of valve morphology can be eliminated (Wu and Takeuchi, 2017) which then leads to better accuracy in differentiating between complications such as thrombus and pannus formation (Liu, 2013) . 3D echocardiography also allows a surgical view of the valve and as a result, is very useful in terms of detection of valvular regurgitation especially in the mitral position (Shiota, 2014). With 3D echocardiography, accurate quantification of left ventricular chamber volume can be

achieved to assess left ventricular function as a result of valvular malfunction (Wu and Takeuchi, 2017). 3D echocardiography is relatively easy to use can be performed either transthoracic or transoesophageal (Lancellotti *et al.*, 2016).

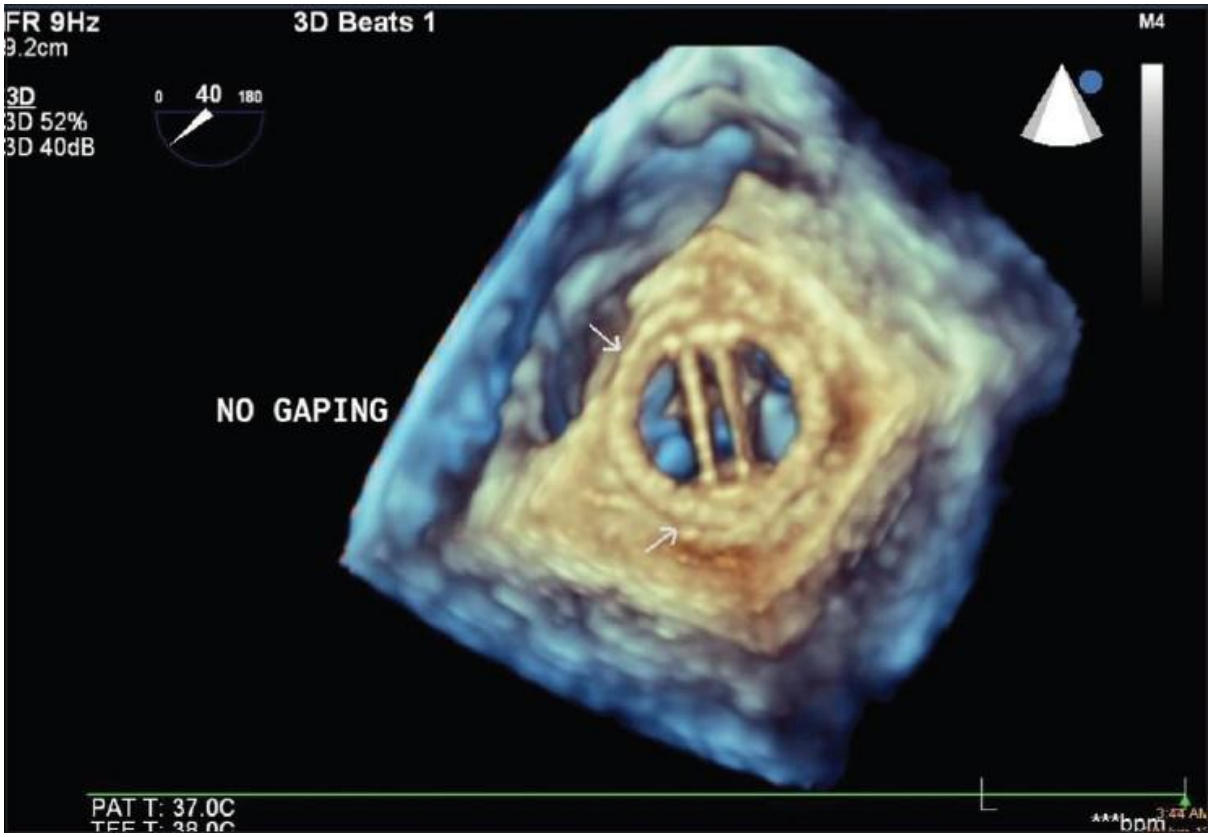

Figure 3.3. 3D Transeosophageal echocardiography of a bileaflet mechanical valve in the mitral position. Image source ((Chauhan, Hasija and Singh, 2014)

iv. Stress echocardiography

Some patients that may initially appear asymptomatic, may have haemodynamic indicators of valvular dysfunction. Such patients may be subjected to stress echocardiography. This works on the principle that during exercise, the heart works hard in order to maintain perfusion and as a result, there's a higher potential for symptoms that had hitherto been masked, to be revealed. A transthoracic echocardiography reading is first done at rest to obtain a patient specific baseline measure. The patient is then subjected to exercises in a controlled

environment such as on a treadmill or stationary bicycle, in order to put ‘stress’ on the heart. Echocardiography data is then taken after the exercise for comparison. A supine bicycle is also employed if echocardiography data is required during and not post-exercise. In situations where the performance of exercise based stress testing is not ideal, a medication known as dobutamine could also be applied in low doses in order to induce a faster heart rate thus mimicking the stress the heart would undergo during exercises (Garbi *et al.*, 2015).

v. Doppler Echocardiography

All prosthetic valves tend to possess a level of obstruction compared to their native counterparts. Assessment of blood flow in the valve is necessary to quantify the severity of this obstruction. Doppler Echocardiography is the mainstay method used. Parameters for stenosis and regurgitation evaluation include peak velocity, shape/contour of the jet velocity, peak and mean pressure gradient, Effective orifice area (EOA) and Doppler velocity index (DVI). The American Heart Association (AHA)/American College of Cardiology (ACC) recommendations classification of severe native aortic valve stenosis using Doppler echocardiography, as peak aortic jet velocity > 4.0m/s, mean transvalular pressure gradient > 40mmHg and EOA < 1.0cm2 (Pibarot and Jean G. Dumesnil, 2012). The prosthetic aortic valves, peak velocity > 4m/s, mean gradient of > 35mmHg and EOA <0.8cm2 are the cut offs for significant stenosis (Zoghbi *et al.*, 2009). However these parameters are flow dependent and as a result, should not be used in isolation.

Doppler echocardiography may use a continuous transmission and reception of ultrasound from the piezoelectric crystals in the probe. This is known as Continuous Wave (CW) Doppler. The advantage of this is that there are no limitations on velocities that can be detected and as a result accurate estimations of high velocities can be achieved. The

drawback of CW Doppler however, is that signal tends to get attenuated with increase in depth. Ultrasound signals may also be transmitted and received intermittently and this mode is known as the Pulsed Wave (PW) Doppler. Although pulsed wave echocardiography may not have the same advantage of being able to record high velocities, it has good depth acuity relative to the continuous wave Doppler. Colour flow Doppler is also a PW Doppler modality that allows flow imaging with colour maps corresponding to flow velocities to facilitate better visualization (Reeder *et al.*, 1986).

Obstruction of the aortic valve orifice leads to turbulent flow which is observed as an increase in the velocity of the antegrade flow across the aortic valve during systole. This is known as the jet velocity and is a one of the very important haemodynamic metrics used in assessing valvular obstruction in a clinical setting. Measurement of the jet velocity is best achieved with CW Doppler (Burwash *et al.*, 1993; Baumgartner *et al.*, 2016).

The transvalvular pressure gradient across an obstructed valve in the systolic phase can also be calculated indirectly from Doppler echocardiography as a function of velocity, using the modified Bernoulli's equation

$$\Delta P = P_1 - P_2 = 4(V_2^2 - V_1^2)$$

Where ΔP is the instantaneous transvalular pressure, P_1 and P_2 are the pressures proximal and distal to the valve respectively and $V_{1 \text{ and } 2}$ represents the proximal and distal velocities. Furthermore, during valve obstruction V_2 is far greater than V_1. This then further simplifies the equation to

$$\Delta P = 4(V_2^2)$$

As can be seen there's a direct correlation between the pressure difference and the velocity. However it should be noted that this change in pressure is an instantaneous one. To find the

mean pressure gradient, instantaneous pressures are collected over the ejection phase and averaged (Baumgartner *et al.*, 2016; Lancellotti *et al.*, 2016).

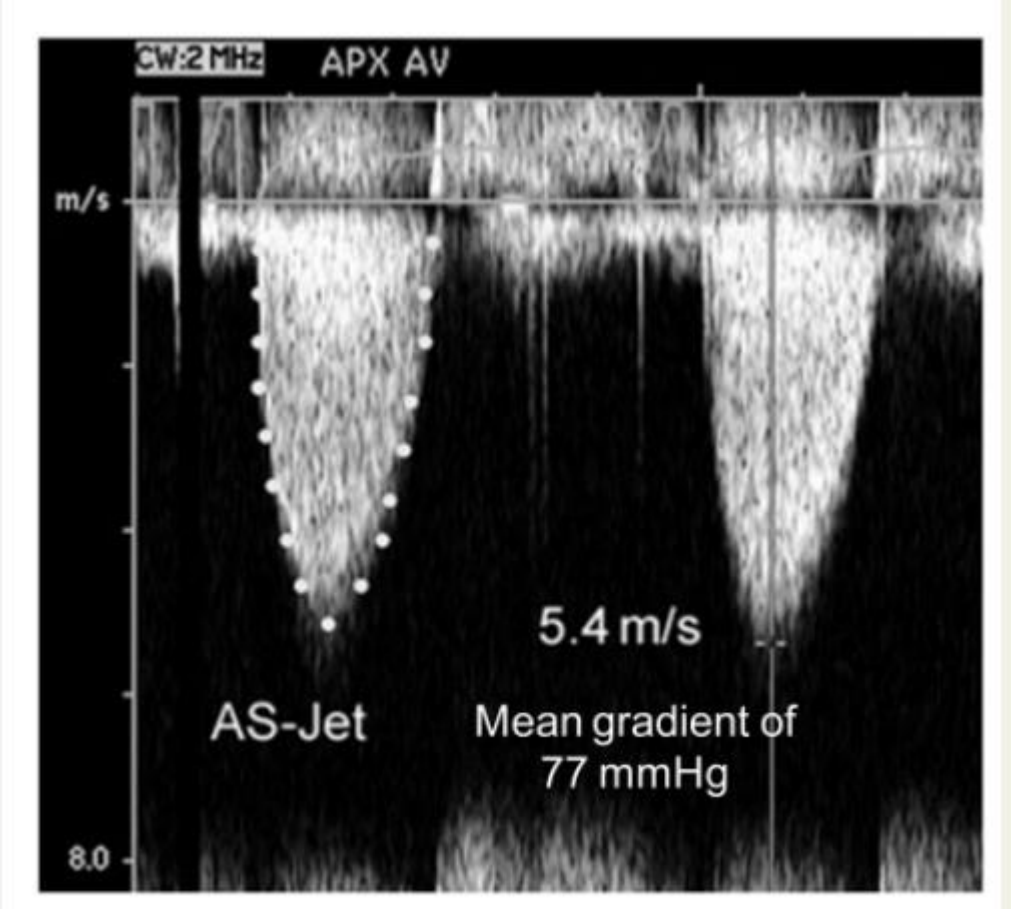

Figure 3.4. Determination of mean transvalvular pressure gradient using jet velocities measured from continous wave Doppler echocardiography. Image taken from (Baumgartner *et al.*, 2017).

Both velocity and pressure gradients are flow dependent, however the valve area of a stenosed valve is more independent on flow and is also a useful parameter used in conjunction with the other parameters to assess the stenosis severity. The effective orifice area is essentially the area of the vena contracta of the valve (Lancellotti *et al.*, 2016). This is calculated by Doppler echocardiography using the continuity equation, which assumes that

all the stroke volume flow from the left ventricle passes through the stenotic valve and as a result for an aortic valve, $Q_1=Q_2$, and since Q=VA

$$A_2 = \frac{A_1.V_1}{V_2}$$

Where A_2 and V_2 are the area and velocity at the vena contracta of the stenosed valve respectively and A_1 and V_1 are the area and velocity at the Left Ventricular Outflow Tract (LVOT). The velocity over the systolic ejection period can be determined form Doppler echocardiography by the integral of the velocity with respect to time over the systolic phase, also known as the Velocity Time integral or VTI. The cross sectional area (CSA) of the LVOT can also be determined from the diameter. As a result the EOA of the valve then becomes

$$EOA = \frac{CSA_{LVOT} \times VTI_{LVOT}}{VTI_{valve}}$$

(Baumgartner *et al.*, 2016). This formula can also be used for valves in the mitral position.

The Doppler velocity index, also known as the DVI, is a dimensionless entity that can also be used as a parameter to assess valve obstruction. This is basically the ratio of the proximal velocity to the velocity through the valve i.e. $DVI=V_{LVOT}/V_{valve}$. A DVI < 0.25 is indicative of severe prosthetic aortic valve obstruction (Zoghbi *et al.*, 2009).

3.2. Cardiac Catherisation

Cardiac catherisation is also another method employed primarily to detect valve obstruction. Pressure distal and proximal to the valve is measured by threading fluid filled or micromanometer tipped catheters into the heart via commonly the brachial, radial or femoral artery. The cardiac catheterisation process is aided by imaging techniques such as fluoroscopy. Once at the site, pressures distal and proximal to the valve are measured and

transvalvular pressure gradient calculated. The cardiac output is then calculated either by the Fick's principle or by thermodilution (Saikrishnan *et al.*, 2014).

The Fick's principle employs blood oxygen concentration and consumption rates using the formula:

$$CO = \frac{VO_2}{CaO_2 - CvO_2}$$

Where CO is the cardiac output, VO_2 is the oxygen consumption and CaO_2 and CvO_2 are the oxygen concentration of the arterial and venous blood respectively (Vachiéry and Dewachter, 2018).

Due to potential inaccuracies in estimating VO_2 via Fick's principle, the thermodilution option is mostly preferred in the clinical setting (Gawlinski, 2000; Vachiéry and Dewachter, 2018). Thermodilution involves the injection of a cold saline solution of known temperature into the right atrium via a catheter. The solution mixes with the blood thus causing a temperature change and the outflow of the blood in the pulmonary artery is detected by thermistor within the catheter. This change in temperature over time data is calculated and converted into cardiac output measure via computer algorithm (Gawlinski, 2000).

Once the transvalvular pressure gradient and cardiac output are determined, the effective valve orifice area is calculated via the Gorlin's formula (Gorlin and Gorlin, 1951). This is different from the continuity equation used in Doppler echocardiography. The Gorlin's formula is explained in section 5.1.5.

3.3. Computed Tomography (CT)

Computed Tomography (CT) is an imaging technique that uses x ray principles to create images of internal organs. CT is used to evaluate heart valve function in a clinical setting, especially when there's a strong suspicion of valvular dysfunction. It allows incremental

information on the opening and closing of the valve leaflets, valve integrity and general morphology of the valve. CT is superior to echocardiography in terms of differentiating between thrombus and pannus formation in mechanical valves (Ueda *et al.*, 2012; Salamon *et al.*, 2015). Planimetry of the anatomic orifice area allows for stenosis evaluation in bioprosthetic valves. Multidetector CTs can be used to capture multiple x ray images and then reconstructed to create a 3D image with high spatial and temporal resolution (Saikrishnan *et al.*, 2014; Lancellotti *et al.*, 2016). CT may also be timed with ECG data in order to capture the images at specific stages of the cardiac cycle for better analysis of valve function and to also diagnose complications such as endocarditis (Fagman *et al.*, 2012)

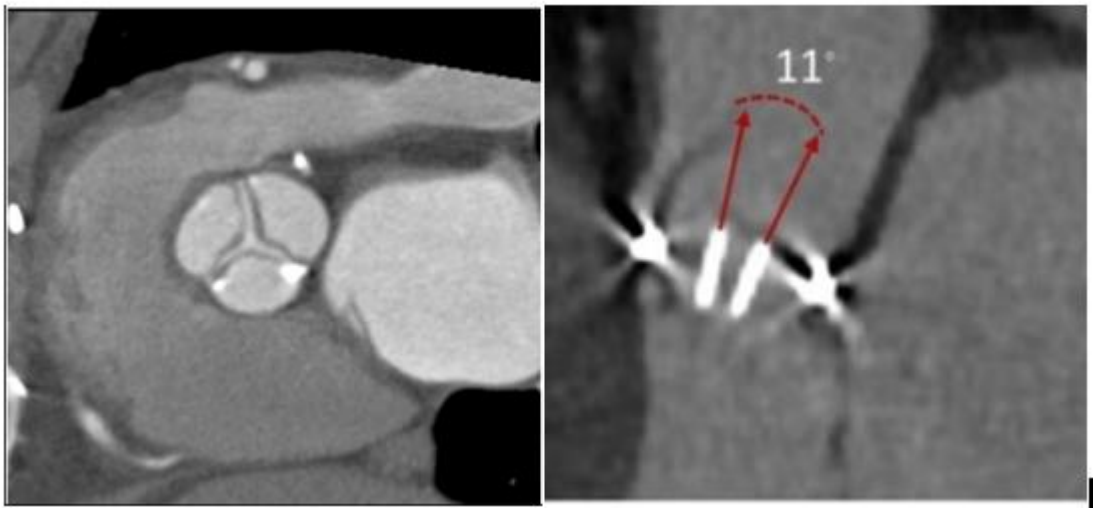

Figure 3.5. Left-Aortic valve morphology developed by reconstruction of images captured by MDCT during the systolic phase. Image taken from (Schoenhagen *et al.*, 2011). Right-Reconstructed image from MDCT showing the opening angle of a bileaflet mechanical valve. Image taken from (Ho and Desai, 2018)

3.4. Fluoroscopy

Fluoroscopy is also another imaging modality used to assess heart valve function, especially in mechanical valves (Annabi *et al.*, 2018). Fluoroscopy uses x ray techniques to produce real time images. Using multiple angles, information such as leaflet/occluder mobility, motion of

the valve sewing ring, and also mechanical failure or migration of valve components can be acquired in order to diagnose complications such as thrombosis (Montorsi *et al.*, 2000). The main viewing angles commonly utilised are the posterior –anterior and lateral valve to assess the orientating of the valve in the heart. The x ray beam may also be oriented parallel to the valve ring and the tilting axis of the valve order to assess the closing and opening angles of the valve (Lancellotti *et al.*, 2016). Fluoroscopy provides the best view of mechanical valve mobility in the aortic position, (Khouzam, 2007; Muratori *et al.*, 2013; Annabi *et al.*, 2018) and is recommended to be used in conjunction with echocardiography especially when echocardiography results are inconclusive (Muratori *et al.*, 2013).

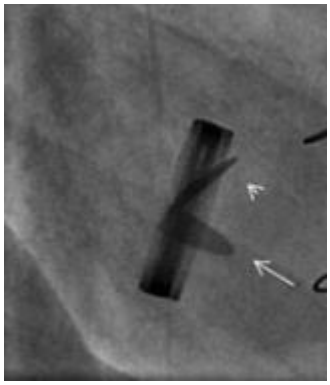

Figure 3.6. Fluoroscopy of a bileaflet prosthetic valve showing a stuck leaflet. Arrowhead points to leaflet stuck in a closed position, whereas the other leaflet (indicated by arrow), is fully open. Image taken from (Fadel *et al.*, 2014)

3.5. Magnetic Resonance Imaging

Magnetic resonance imaging (MRI) is an imaging technique that uses magnetic fields to provide images of organs. It is especially useful in viewing soft tissues and as a result, can also be used to view cardiac structures including heart valves. Cardiac MRI can be used to provide 3D real time anatomy of heart valves and also blood flow. With this information, EOA can be calculated either directly at the vena contracta, via the use of the continuity equation (Annabi *et al.*, 2018) or the Gorlin equation (Valenti *et al.*, 2015), to assess the

severity of obstruction. MRI can also be used to assess the volume of regurgitant blood flow which aids in assessing valvular regurgitation. For safety purposes, a magnetic field 1.5 or 3 Tesla is recommended when imaging heart valves (Annabi *et al.*, 2018).

3.6. Nuclear imaging

This imaging technique is used sparingly when it comes to assessing valve function (Lancellotti *et al.*, 2016). In nuclear imaging, a radiopharmaceutical is ingested and the radiation being emitted is detected by gamma cameras and images are formed based on these radiations. Single Photon Emission Computed Tomography (SPECT) and Positron Emission Tomography (PET) are the common modalities of nuclear imaging. Some studies have suggested that the use of radiopharmaceutical 18F- fluorodeoxyglucose (FDG) in combined PET and CT is able to detect infective (Pizzi *et al.*, 2016) and non infective endocarditis in artificial heart valves (Mathieu *et al.*, 2017; Scholtens *et al.*, 2018) . The use of a combined PET and CT modality with 18F- sodium fluoride is also reported to be able to detect calcification of native valve leaflets (Dweck *et al.*, 2012).

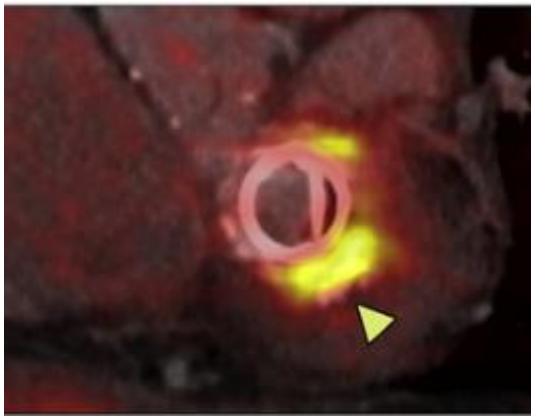

Figure 3.7. Combined PET/CT image of a mechanical mitral valve showing a large uptake of FDG suggesting the presence of infective endocarditis (this is indicated by the arrowhead). Image taken from(Pizzi *et al.*, 2016)

3.7. Other Diagnsotic techniques

All the above mentioned techniques of evaluating heart valves involves equipment and procedures that can only be performed in a clinical setting by trained professionals. With the exception of cardiac catherisation, all the techniques are imaging modalities which provide a way of visualising the valve and its function. Other techniques involving diagnosis of prosthetic valve function based on auscultations have also been explored.

A Germany based company, Cardiosignal Gmbh, has developed the Myotis 3C, which is a phonocardiogram system consisting of a display monitor, a transducer probe containing a microphone and data acquisition system to record and display valve sounds. Various studies have used this device to acquire and investigate bileaflet mechanical valve heart sounds during closure, in an effort to detect malfunctions such as thrombosis (Bagno *et al.*, 2008; Bagno, Anzil, Buselli, *et al.*, 2009; Bagno, Anzil, Tarzia, *et al.*, 2009; Susin *et al.*, 2011; Tosoni *et al.*, 2017).

To enable monitoring of valve function from the comfort of a patients home, the same company has developed a handheld device known as the Thrombocheck. The Thrombocheck uses spectral analysis of closing valve sounds to detect valve dysfunction in bileaflet mechanical valves. Clinical studies have been conducted to prove its superior accuracy in terms of early detection of valve dysfunction relative to gold standard echocardiography methods (Ben Zekry *et al.*, 2005; Fritzsche *et al.*, 2005; Fritzsche, Eitz, *et al.*, 2007; Fritzsche, Schenk, *et al.*, 2007). The use of the Myotis 3C and the Thrombocheck is however hitherto limited to bileaflet mechanical valves

3.8. Challenges and limitations of current diagnostic techniques

Early and accurate diagnosis of valve malfunction presents as a challenging task. This is even more challenging in prosthetic valves relative to their native counterparts (Baumgartner, 2009). Current diagnostic techniques do possess the limitations that further exacerbate the

task of evaluation valve function. The challenges and limitations are discussed in further detail below.

3.8.1. Echocardiography

Although echocardiography is considered to be the mainstay and go to method for evaluation of heart valves, they do come with their own challenges. In 2D echocardiography, multiple angles of view need to be captured in order to present an optimum representation of the valve morphology. These constant adjustment of viewing angles, make 2D echocardiography challenging. Furthermore, incremental rotation of the transducer probe is necessary to visualise valve leaflet motion. These technical challenges reduce the accuracy of 2D echocardiography and have been highlighted in some studies. In 2006, Muratori et al conducted a study to assess the accuracy of 2D echocardiography in terms leaflet motion detection in mechanical valves. The results showed that for valves in the mitral position, the opening and closing angles were correcting identified in 85% and 100% of mechanical valves by TTE and TOE respectively. In the aortic position however, closing angles could not be identified and the accuracy of identifying opening angles reduced to 40 and 77% in single disc valves by TTE and TOE respectively. This accuracy was even lower in bileaflet valves (13 and 35%) by TTE and TOE respectively, suggesting that although TEE functions better due to its close proximity to the heart, the general accuracy of 2D echocardiography in detecting leaflet motion is less than ideal for aortic prosthetic valves (Muratori *et al.*, 2006). Incorrect alignment of the uitrasound beam also leads underestimation of velocities and pressure gradients in Doppler echocardiography(Baumgartner *et al.*, 2017)

Secondly, since echocardiography is an imaging modality based on ultrasonic principles, 2D echocardiography is affected by motion artefact by other underlying body organs. This causes obstruction, attenuation and/ reverberation of the ultrasound signal. This is known as acoustic shadowing and reverberation and it’s more common in TTE. Acoustic shadowing can also be

caused by the prosthetic parts of the valve (especially mechanical valves). This can lead to obscuring of vegetation and regurgitant flows as a result leading to incorrect underestimation of endocarditis and valve regurgitation. The reverberations of signals can also present as an abnormal mass in echocardiography which can then lead to overestimation of obstruction (Chambers, 2009;Zoghbi *et al.*, 2009). Obstruction of mechanical prosthetic heart valves are mostly caused by pannus formation, thrombosis or both. Although they may cause similar clinical manifestations, their intervention and treatment protocols tends to be different (Nishimura *et al.*, 2017). As a result, it is very important to distinguish the etiology of the valve obstruction. The acoustic shadowing and reverberation limitations of 2D TTE makes it difficult as a diagnostic technique in this instance (Salamon *et al.*, 2015). TOE, in combination other imaging modalities, is preferred (Nishimura *et al.*, 2017), although there has been previous reports suggesting that 2D TOE is also inconclusive in differentiation between pannus and thrombus formation (Hurwitz, Waxman and Hecht, 2009).

Another challenge in Doppler echocardiography is in the interpretation of the data. Mechanical valves tends to have non quintessential velocity profiles, which could result in overestimation of velocities (Rashtian *et al.*, 1986; Baumgartner, 2009). This overestimation then ultimately leads to inaccurate estimation of pressure gradient an effective orifice area as both parameters are functions of velocity (Bech-Hanssen *et al.*, 2001). A phenomenon known as “pressure recovery”, may also cause discrepancies in transvalvular pressure gradient data acquired from both Doppler echocardiography and cardiac catheterisation (Baumgartner, Schima and Kühn, 1993; Vandervoort *et al.*, 1995; Garcia *et al.*, 2003; Bach *et al.*, 2012; Mohan *et al.*, 2017; Hameedullah *et al.*, 2018; Clavel and Pibarot, 2019). For a valve with narrowed orifice area, one would expect the lowest pressure and highest velocity to be observed at the vena contracta (smallest orifice area). As the flow passes the narrow area and flows downstream, it decelerates and part of the kinetic energy is converted back to pressure

and potential energy thus the pressure is 'recovered'. Now Doppler echocardiography measures the change in pressure between the upstream flow and the vena contracta, whereas in cardiac catheterisation, catheters are placed a couple of millimetres upstream and downstream the valve. Due to pressure recovery, the pressure difference recorded by cardiac catheterisation tends to be lower than that measured at the vena contracta by Doppler echocardiography. Pressure recovery is more prevalent in bileaflet mechanical valves (Vannan and Sarkar, 2003).

In general, prosthetic heart valves possess an inherent level of obstruction thus makes it more challenging to evaluate and interpret their data relative to their native counterparts (Zoghbi *et al.,* 2009). Due to the technical limitations and challenges in 2D echocardiography, the evaluation of valves tend to be operator dependent and is susceptible to observer variability and also poor retesting reliability (S. *et al.*, 1995; Jacobs *et al.*, 2005).

3D echocardiography provides superior visualising of heart valves relative to their 2D counterparts however they also have their limitations. The propagation of ultrasound is the same in both 2D and 3D echocardiography. The quality of images are hindered by the trade-off between spatial and temporal resolution more so in 3D echocardiography (Turton and Ender, 2017). Similarly to 2D echocardiography, acoustic shadowing and reverberations may be present in 3D echocardiography. There are however some 3D echocardiography specific limitations such as "drop outs". Drop outs are caused by the ultrasound beam hitting its target at an oblique angle thus not all the signal is reflected back into the transducer. Dropouts presents as holes in a 3D echocardiography images (Le *et al.*, 2016). Blurring is also one of the 3D echocardiography specific limitations and causes objects to appear thicker than usual. Blurring is caused by sub optimal elevation resolution axis (this is the axis responsible for creating 3rd dimension (thickness). Appearing of lines in a 3D echocardiogram, known as "stitching" is a specific limitation of 3D echocardiography. Stitching tends to happen when

multiple image slices are merged during image processing (Faletra *et al.*, 2014; Le *et al.*, 2016; Turton and Ender, 2017; Wu and Takeuchi, 2017). 3D echocardiography also provides limited visualisation of anterior cardiac structures (Lancellotti *et al.*, 2016).

3.8.2. Cardiac Catheterisation

Cardiac catheterisation, by virtue of its invasiveness, comes with various possible vascular complications. Post cardiac catheterisation, blood may leak from the vessel and cause a solid swelling of clotted blood (hematoma). Although most hematomas may be benign, continual growth could create the presence of a pseudoaneurysm causing hemodynamic instabilities (Manda and Baradhi, 2018). With transfemoral access, bleeding into the abdominal space (retroperitoneaum) may also occur. Cross flow of blood between the arteries and the veins at the access point may cause a clump known as an arteriovenous fistula which may require surgical intervention (Miller, 2012; Manda and Baradhi, 2018). Forceful or incorrect insertion of the catheter may also puncture the major blood vessels like the aorta which can progressively lead to aortic dissection (Neo, Pua and Lee, 2010; Tanasie *et al.*, 2011; Tarun, Aggarwal and Dohrmann, 2019). Although rare, thrombosis and embolism may occur mainly as a result of large diameter catheter sheaths, long catheterisation time, diabetes mellitus and also previous arterial diseases(Manda and Baradhi, 2018).

In addition to vascular complications, they are also heart valve related limitations and challenges in the use of cardiac catheterisation as a diagnostic tool. In 1987, there was an infamous legal case where a catheter got irreversibly trapped in a Bjork-Shiley valve during cardiac catheterisation. This impaired the disk movement and lead to almost instant death of the patient (Kober and Hilgermann, 1987). Due to entrapment of catheters and complications such as valve regurgitation, crossing mechanical valves with catheters is not recommended (Morris, 1979; Karuppiah *et al.*, 2015). In the case of bioprosthetic valve, passing a catheter

through a calcified degenerative valve may cause tears in the leaflet leading to regurgitation (Zoghbi *et al.*, 2009).

Issues or inaccuracies in the pressure measuring sensors at the tip of the catheters may also cause wrong estimation of transvalvular pressure gradient. Pressure recovery also tends to create controversies in accurate diagnosis of valve function via the use of cardiac catheterisation relative to standards like echocardiography. Another limitation of cardiac catheterisation as a diagnostic tool is that it only provides haemodynamic data and doesn't give any information on the valve morphology (Saikrishnan *et al.*, 2014).

3.8.3. Fluoroscopy

Fluoroscopy is known to be a quick and easy method of assessing valve function however it also has its limitations. Although fluoroscopy is said to be very good at detecting leaflet motion of mechanical valve, it is unable to visualise with good integrity, that of bioprosthetic valves (Elmasry, 2014). Another limitation of fluoroscopy is that it is unable to differentiate between thrombus or pannus as the etiology of valve obstruction (Elmasry, 2014; Lancellotti *et al.*, 2016; Annabi *et al.*, 2018). Fluoroscopy uses x ray radiations to generate images and as a result, both patients and operators risk exposure to ionizing radiation (Barakat *et al.*, 2018). In valve evaluation, provision of haemodynamic data is key. Fluoroscopy only provides visual data of the valve thus inability of heamodynamic assessment in fluoroscopy serves as a limitation (Lancellotti *et al.*, 2016).

3.8.4. Computed Tomography

Similar to fluoroscopy, Computed Tomography (CT), uses x rays to create images. The use of multiple detectors in CT helps to create multiple images which are reconstructed to create a better visual. However this exposes patients to high doses of radiation. In fact the radiation from CT is said to be equivalent to about 200 conventional chest xrays (*The surprising dangers of CT scans and X-rays*, 2015) and accounts for the majority of radiation exposure in

medical imaging (Costello *et al.*, 2013). Exposure to high doses of radiation serves as a limitation of CT as a valve evaluation tool. Contrast media injected during CT has also been associated to kidney complications which further exacerbates the risks involved in CT (Andreucci *et al.*, 2017; Hinson *et al.*, 2017; Ozkok and Ozkok, 2017). Metallic objects from prosthetic valves causes artefacts which can severely reduce the quality of images reconstructed in CT thus limiting its accuracy as an evaluation tool (Gjesteby *et al.*, 2016). Similar to fluoroscopy, CT is limited by its inability to assess the flow and haemodynamics of heart valves (Saikrishnan *et al.*, 2014; Annabi *et al.*, 2018).

3.8.5. Magnetic Resonance Imaging

Metallic artefacts are a limitation of Magnetic Resonance Imaging (MRI). This is caused from the ferromagnetic components of prosthetic valves and other implanted devices and could severely reduce the image quality. The appearance of artefacts in images could obscure some portions of the valve anatomy thus leading to confounding diagnostic results (Hargreaves *et al.*, 2011). MRI of cardiac structures is also limited by its low spatial and temporal resolution which affects the quality of the images (Lancellotti *et al.*, 2016). Specifically, low temporal resolution may lead to underestimations of peak velocity in cases where there are turbulent flows for a short period of time. The presence of eddy currents in MRI, if not compensated for, could lead to phase offset errors and miscalculations of flow quantification across the valve. Visualisation of valve regurgitation jets with MRI is limited in comparison with echocardiography (Gulsin, Singh and McCann, 2017). Flow measurements in MRI are acquired over a number of cardiac cycles. This is however very difficult to achieve in patients with irregular heartbeats and as a result presents as a challenge of MRI (Myerson, 2012).

In terms of viewing valve morphology MRI may also present some limitations. MRI image slices tend to be relatively thicker than the cardiac structures. Using thinner MRI images

slices may however lead to a higher signal to noise ratio which will affect the integrity of the captured images (Gulsin, Singh and McCann, 2017). Another drawback of MRI is that it is time consuming, expensive and due to size restrictions of the scanner, may not be suitable for very obese or claustrophobic persons (Chaothawee, 2012; Cavalcante *et al.*, 2016).

3.8.6. Nuclear Imaging

Exposure to radiation is a staple in nuclear imaging and as a result, serves as a limitation. Secondly, the use of nuclear imaging is mostly limited to diagnosis of endocarditis and no other forms of valve malfunctioning (Lancellotti *et al.*, 2016).

Generally, heart valve diagnostic methods involve bulky expensive equipment and trained personnel and as a result tests are only performed on an ad hoc basis which prevents continuous monitoring of valve function. With the exception of cardiac catheterisation, all the other valve diagnostic techniques used in the clinical setting are non-invasive and as a result, direct measurements of valve haemodynamic parameters cannot be achieved. Limitations of current techniques often imply a large change in valve function is required for detection. This limits early detection of valve malfunction.

Based on the background reading and challenges of current valve diagnostic techniques, there is a clear clinical need for direct and continuous monitoring of implanted prosthetic valves in real time.

3.9. DIRECT AND REAL TIME MONITORING OF ARTIFICIAL HEART VALVES

Direct and continuous monitoring of heart valves in real time can potentially be achieved by integrating sensors into heart valves. Technological advancements in bioMEMS allows for micro and nano sensors to be manufactured for various biomedical applications. Extensive review of literature shows there are currently no commercially available valves with inbuilt sensing technology. Research on this is also minimal. Some of them are highlighted below:

Steinberg described his patented invention of a prosthetic valve monitoring system. In his invention, Steinberg proposed two ways of monitoring valve function. In the first instance, the valve leaflets are magnetised and a voltage induced in a coil in close proximity is monitored as output representative of valve function. The second method involves incorporating the conductors within the leaflets itself. In the presence of a magnetic field, the induced voltage can be detected and monitored (Steinberg, 1988)

Another patented invention by Manuel Villafana in 1996, described a prosthetic valve integrated with a wireless sensing technology. This sensor detects valve leaflet motion and transmits such data. The transceiver inbuilt in this technology is also claimed to have the potential to produce pulses to pace the heart in cause of an arrthymia (Villafana, 1996).

Extensive review of literature hitherto, shows no further updates or information on the road to clinical realisation of both Steinberg and Villafana's inventions.

In a study by Lanning and Shandas, vibration sensors made out of piezo electric material, were constructed and attached to the housing of various commercially available bioprosthetic and mechanical valves. The aim of this study was to detect motion of valves leaflets in response to simulated thrombosis and leaflet stiffening of mechanical and bioprosthetic valves respectively. Joint frequency analysis showed sensors were able to detect changes in closing sound frequencies of the valves during thrombosis and leaflet stiffening. It should also be mentioned that these tests were conducted in vitro and on only a few selected commercially available valves. Further to that, these sensors didn't incorporate telemetry into the design (Lanning and Shandas, 2003)

Rivero et al, also conducted a study on the use of magnetic sensors to detect failure of bioprosthetic valves. In this study, thin strips of magnetic sensors were attached to the leaflets of the bioprosthetic valve and tested in an invitro system. During simulated malfunction,

these sensors were able to detect changes in valve function by analysis the motion of the leaflets (Rivero *et al.*, 2007).

A magnetic tracking system of mechanical valve leaflets was also proposed and investigated by Baldoni and Yellen. In this study, a disc shaped magnet of size similar to that of a tilting disc valve, was tracked using computational methods with success, thus also presenting a potential solution for non invasive imaging and evaluation of heart valve prosthesis (Baldoni and Yellen, 2007).

There has also been research done in development of micorsized implantable pressure sensors, which although have not been tested in prosthetic valves, they do have the potential to detect valve malfunction specifically stenosis or obstruction by monitoring changes in valvular pressure profiles.

A fully implantable wireless pressure sensor, for use in biomedical applications has been designed and tested by Chen et al. In this study, they demonstrated the ability of the sensor to track and transmit pulse pressure. In vivo studies were also carried out in mice, to detect and monitor intracranial pressure. The signal receiver however had to be in very close proximity to the sensor in order to transmit pressure data without any attenuation thus not making it very suitable for monitoring deep seated organs and tissues (Chen *et al.*, 2014). Tan et al. also designed a magneto harmonic pressure sensor consisting of an elastic pressure membrane in an airtight chamber which also contains a soft magnetic material. Upon external excitation via magnetic field, a harmonic signal is produced, which varies with varying pressure (Tan *et al.*, 2011).

Various researchers (Allen *et al.*, 2006; Fonseca *et al.*, 2006; Chiang, K. Lin and Ju, 2007; Ginggen *et al.*, 2008; Stern *et al.*, 2010; Je *et al.*, 2011; Murphy *et al.*, 2013), have designed

and demonstrated the use of wireless pressure sensors for biomedical applications, with positive results.

Although the development of implantable pressure sensors is a very active research area, their path to clinical realisation has been less than satisfactory. The Endosure Wireless AAA sensor by CardioMEMS for monitoring pressure in an aneurysm sac, the CardioMEMS HF system for pulmonary artery pressure monitoring, and the Titan Wireless Implantable Haemodynamic Monitor (ISS Inc, Ypsilanti, MI) (Hubbert *et al.*, 2017), are one of the few commercially available permanently implanted pressure sensors. Suffice to say, whilst implantable sensors do have the potential for direct, accurate and continuous monitoring, they are not devoid of challenges.

3.10. CHALLENGES FACED IN IMPLEMENTING SURGICALLY IMPLANTABLE SENSORS

i. Biocompatibility

Surgically implantable sensors are classified as class 3 or high risk medical devices. These sensors may be implanted for a short term, i.e. less than 30days or long term (chronic monitoring) i.e. more than 30days (European Commission - DG Health and Consumer, 2010). One of the major challenges facing the development of implantable sensors is biocompatibility. The in vivo environment tends to be very hostile and humid with various proteins, ions and enzymes. For accuracy, the sensing element of an implantable sensor needs

to be exposed to the environment whilst the other parts i.e. micro circuitry needs to be isolated to prevent leakage of in vivo fluids, leakage currents and potential short circuiting. Due to the foreign nature of these sensors, their interaction with the biological media may elicit some adverse reactions. Adhesion of proteins to the sensing element of the sensor, known as biofouling, is one of the more common of such reactions (Roberts *et al.*, 2012; Yu, Kim and Meng, 2014). Others include fibrosis and corrosion, which may tend to alter the sensor properties (Fonseca *et al.*, 2006). Suggested ways of mitigating bio-incompatibility include coating the sensing element with a thin film of biocompatible material such as titanium oxide (Clausen *et al.*, 2010) Packaging material also needs to be biocompatible as this will be in direct contact with the in vivo environment. Packaging considerations also include hermetic sealing and double encapsulation with biocompatible materials such as Parlyene to prevent leeching. (Voskerician *et al.*, 2003; Takahata *et al.*, 2004; Najafi, 2007; Chen *et al.*, 2008; Axisa *et al.*, 2009).

ii. Telemetry

For implantable sensors, there is the need to be able to transmit the signal outside the operating environment for monitoring and diagnostic purposes. These can be achieved either wired or wirelessly, with the latter being ideal due to patient comfort, convenience of monitoring especially in the case of chronic implantable sensors and also less risks of infections from telemetry lead wires. Wireless telemetry mostly achieved via Radio Frequency (RF) or inductive coupling (Hannan *et al.*, 2012) . Implantable sensors with active telemetry tend to have various components such as microcontrollers, amplifiers, transmitters and receivers to aid signal processions and long distance transmission. These components

needs to be supplied with power thus the name ‘active telemetry’. Power supply to the components is achieved through on board batteries strapped to the system however these tend to make the implant bulky and also due to the limited lifespan of the batteries, they become inconvenient for long term use (Yu, Kim and Meng, 2014). Further to that there is also the risk of exposing biological tissues in close proximity to excess heat produced by the active elements (Khanna, 2016). Rechargeable batteries become necessary for chronic implantable sensors using active telemetry. Wireless charging may be achieved, through some sort of RF based inductive coupling. To circumvent the challenges associated with chronic power supply via batteries, alternative means of harvesting energy to power implantable devices have been explored. Some of them include the use of optical charging via photovoltaic cells incorporated in sensor design (Murakawa *et al.*, 1999) and also ultrasonic means (Echt *et al.*, 2006), however these are plagued by low transmission and difficulty in miniaturisation. Other methods include the use of biofuel cells which convert biochemical energy into electrical energy (Olivo *et al.*, 2011; Katz, 2014), thermoelectricity, i.e. generation of electricity using the temperature differences in the body (Amar, Kouki and Cao, 2015). Harvesting energy from the moving organs such as the heart, via the use of piezoelectric materials have also been researched as an option for powering implantable devices (Li *et al.*, 2010; Dagdeviren *et al.*, 2014; Lu *et al.*, 2015). RF signals also tend to have a high degree of dissipation in biological tissues thus causing signal attenuation to and from the implanted sensor (Poon, O’driscoll and Meng, 2010).

Passive telemetry may presents as a more ideal solution due to its simplicity of circuitry, ability to manipulate size, and its suitability for long term monitoring. Since these systems do not come with active elements, issues of power supply are heavily mitigated. Sensors employing passive telemetry generally consist of an inductor coil connected to a capacitor, forming an LC tank. A change in the measurand causes a corresponding change in

capacitance, which in turns thus causes a shift in the resonance frequency of the circuit. The resonance frequency is thus the output of the sensor. Wireless powering and data transmission is achieved via a readout coil inductively coupled to the LC sensor (Fonseca *et al.*, 2006; Chen *et al.*, 2008; Ferguson and Redish, 2011; Chen *et al.*, 2014; Huang, Dong and Wang, 2016).

A major challenge in passive telemetry is inductive coupling efficiency which effectively affects the spatial range and signal attenuation of the sensor. In passive telemetric systems, increasing the size of the inductor in the sensor will generally increase the spatial range of the signal, however that inadvertently increase the size of the implanted sensor, which may not be ideal. The trade-off between sensor size and range thus making it more challenging powering and transferring data from sensors implanted in deep seated organs (Chen *et al.*, 2014; Yu, Kim and Meng, 2014; Huang, Dong and Wang, 2016). For efficient inductive coupling, proper alignment of both implanted and external coils needs to be achieved thus presenting a challenge in monitoring organs with high motion capabilities. Inductive coupling inefficiency may also affect active telemetric devices that rely on this method for wireless charging. Ways of improving coupling efficiency and reducing signal attenuation include the use of small ferrite rods in the internal and external coils (antennas) to increase the coupling integrity (Harpster *et al.*, 2002; Saidani and Gijs, 2002).

Due to the challenges involved in RF and inductive coupling telemetry, researchers have been looking at alternate ways of transmitting data from implantable systems, to the outside world. In their review article, Ferguson & Redish discuss a technique known as “intrabody communication”, as an alternative to current existing telemetric systems. This system uses the conductive properties of the body to transmit signals to the surface of the skin either through galvanic or capacitive coupling. These signals are then picked up by electrodes attached to the skin. Although this method is yet to be clinically realised, there has been varying levels of

success in cadaver testing (Lindsey *et al.*, 1998) and also in animal testing (Sun *et al.*, 2003). High signal attenuation and difficulty in miniaturisation also presents as a drawback of this technique (Ferguson and Redish, 2011).

iii. Drift

Accuracy and stability over time in implantable pressure sensors is very important, especially in chronic monitoring. In an ideal situation, change in sensor output should be due solely to a change in the measurand. Any deviation from this could be classified as drift (Yu, Kim and Meng, 2014). Recalibration of the sensor is necessary to solve issues with sensor drift. Now this presents more of a challenge for implantable sensors as standard recalibration techniques requires surgical interventions which is not ideal. Due to general material aging and fatigue of the sensing element, over a long period of time, drift will be inevitable. Other factors may exacerbate this process in vivo. These are discussed below.

Interaction between the sensor and the hostile in vivo environment may cause adverse reactions which may alter the sensor properties and cause drift. Improper packaging of pressure sensors may cause leeching of in vivo fluids into the sensor. This may also alter the sensor element properties and cause a shift in the reference or baseline pressure. This is known as baseline shift (Kim, Powell and Ziaie, 2016). Fonseca et al. reported on issues with baseline shift in implantable sensors. In their study, a micro pressure sensor was implanted to monitor abdominal aortic aneurysm. A mean baseline pressure shift of 28.2mmHg over just 6 days of testing was detected thus highlighting the role drift can play in either over or underestimating pressure if adequate compensation is not accounted for (Fonseca *et al.*, 2006). Biofouling, corrosion of sensor element and fibrous tissue encapsulation of the sensor, have been known to cause sensor drifts (Patrick *et al.*, 2017). Temperature variations of the in

vivo environment may also cause drift of implantable piezoresistive pressure sensors over time (Gibari *et al.*, 2017).

Packaging of sensors itself could also lead to drift in sensors (Jiang, 2010) thus it is important that appropriate material and encapsulation means are employed. Encapsulation of the sensors in Parlyene, tends to be a common method employed by researchers (Takahata et al. 2004; Najafi, 2007; Chen et al. 2008; Chen et al. 2014; Huang et al. 2016; Shapero & Tai 2018). Encapsulation of sensor in a silicone filled medical grade polyurethane balloon has also been reported as means of significantly reducing drift effects (Kim, Powell and Ziaie, 2016). Additional modifications to the microcircuitry of the sensors can also be implemented to compensate for baseline and temperature associated drifts in implantable pressure sensors (Gibari *et al.*, 2017).

3.11. SUMMARY

Echocardiography is the gold standard method of diagnosing or evaluating the function of prosthetic valves. Cardiac catheterisation, fluoroscopy, MRI, CT and nuclear imaging are also other techniques useful in the evaluation of heart valves. Current diagnostic techniques are hampered by issues such as acoustic shadowing and reverberation, low spatial/temporal resolution and exposure to ionizing radiation. Furthermore these methods are performed on an adhoc level and doesn't allow for continuous monitoring of valves. These limitations often lead to late and inaccurate diagnosis of heart valve complications. Instrumentation of heart valves with sensors could aid in continuous and direct monitoring of heart valves in real time. Hitherto there are no commercially available prosthetic valves with inbuilt sensing technology. Potential issues in implementing implantable sensors include biocompatibility, sensor drift and telemetry.

CHAPTER 4 RESEARCH AIMS AND OBJECTIVES

4.1 RESEARCH AIMS AND OBJECTIVES

The aim of this study is to determine whether instrumentation of artificial valves with sensors, present as a usable diagnostic tool to detect valve obstruction. To achieve this aim, we need to go through some specific objectives.

The specific objectives of this study are:

- To develop and manufacture polymeric valves
- To develop a hydrodynamic testing rig, with which the fabricated polymeric can be tested
- To perform pulsatile flow hydrodynamic testing of manufactured valves
- To investigate the effect of obstruction on transvalvular pressure
- To instrument valve with sensors and investigate their capability to detect pressure changes during simulated obstruction.

4.2 PROPOSED METHODOLOGY

Polymeric valves will be fabricated using the dip coating technique. The hydrodynamic tester to simulate the left side of the heart will then be designed and manufactured. Following that, the fabricated polymeric valves will be subjected to pulsatile flow hydrodynamic testing under ISO 5840 standards. A commercially available bioprosthetic valve will also be subjected to the same tests for comparison. Transvalvular pressure gradient and effective orifice area will be calculated as indicators of valve function assessment. Valvular obstruction will then be simulated and the corresponding change in transvalvular pressure gradient in both the polymeric and bioprosthetic valves will be recorded and assessed. Finally the polymeric valves will be instrumented with pressure sensors and subjected to obstruction simulation tests to determine the ability of the sensors to detect pressure changes during obstruction.

4.3 HYPOTHESIS

We hypothesis that instrumenting valves with pressure sensors will provide adequate and accurate information relating to pressure changes in obstructed valves.

CHAPTER 5. MATERIALS AND METHODS

5.1. DESIGN AND FABRICATION OF POLYMERIC VALVES

5.1.1. INTRODUCTION

One of the aims of this study is to fabricate polymeric valves. These valves will undergo comparative valve testing and will ultimately be instrumented with sensors to determine whether these can be used as a stenosis diagnostic tool. As explained earlier, polymeric valves have the potential to be the ideal prosthetic heart as they can potentially combine the durability of mechanical heart valves with the biocompatibility of bioprosthetic valves (Bezuidenhout, Williams and Zilla, 2015). Polymeric valves were chosen due to their relative simplicity in manufacturing, and also the low cost involved. In addition, as the cardiovascular devices research group in the department of biomedical engineering at Strathclyde University, have a lot of experience in the manufacture of polymeric valves , the learning curve in this critical element of the study should be reduced.

This section describes the design and fabrication process of trileaflet polymeric heart valves used in our study. These valves are designed for use in the aortic position.

5.1.2. STENT DESIGN

Valve stents were designed using CREO 3D modelling software. These stents have internal diameter, external diameter and height of 22mm, 25 mm, and 15.5mm respectively. The stent also has three half ellipto-hyperbolic cut outs, which ultimately defines the shape of the valve leaflets. These stents were manufactured from Delrin rods by Brightwake Ltd (Nottinghamshire, UK) using our design.

Figure 5.1. CAD model of the valve stent

5.1.3. FABRICATION PROCESS

Polymeric valves manufactured for this study are all trileaflets and fabricated through a technique known as dipcasting/dipcoating. In this technique, a specially designed cylindrical mandrel of 23mm diameter, with three ellipto-hyperbolic indentations at the tip, (moulded to fit the similar shape of the valve stent) is repeatedly dipped into a polymer solution and left to dry, forming the valve leaflets. Manufacturing via dipcasting is a popular technique, highlighted in various previous studies (Mackay *et al.*, 1996; Daebritz *et al.*, 2003; Ghanbari *et al.*, 2009; Burriesci, Marincola and Zervides, 2010) mainly due to its simplicity and consistency of valves manufactured under controlled conditions.

For this study, a polyurethane solution was synthesised by dissolving pellets of Carbothane PC-3585A (Lubrizol, Ohio) in Dimethylacetamide (DMAC) (Sigma-Aldrich, Dorset, England) solvent in a fume cupboard. Carbothane is a medical grade thermoplastic Polycarbonate Urethane, also referred to as PCU. PCUs are used in a wide variety of medical implants due to their good mechanical, bio stability and biocompatibility properties (Zhu *et al.*, 2016; Elsner and McKeon, 2017). Due to their excellent properties, they are ideal for long term implantation and also considered ideal material to produce the valve leaflets for this study.

5.1.3.1. Fabrication of the valve

The stainless steel mandrel was initially wiped down with 70% alcohol solution, placed on a hot plate under moderate heat for approximately 5 minutes and then left to cool down. This is to ensure the mandrel is properly dry as absorption of water by the polymeric solution may negatively affect its mechanical behaviour (Altaf, Ashcroft and Hague, 2011; Aguirre-chagala *et al.*, 2017) The valve stent is then placed over the tip of the mandrel and dipped into the polymer solution, allowing it to coat the whole stent. The coated mandrel was then clamped upside down in the fume cupboard for the polymer to dry off for approximately 45-60 minutes. After the solution had stopped dripping, the mandrel was placed in its upright position on a hot plate under moderate heat for approximately 20-30minutes. This aids in accelerating the evaporation process of the polymer solution. A thin film of polymer is left on the mandrel, forming the leaflets, as the solution dries. This forms the first dipping and drying cycle. The process is then repeated until desired leaflet thickness is achieved.

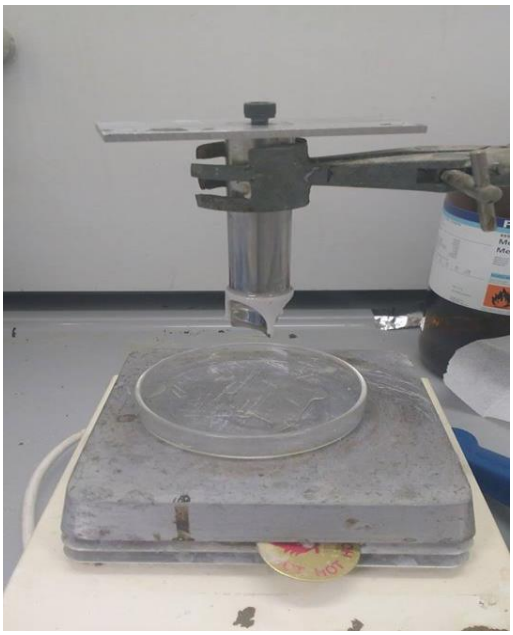

Figure 5.2. The dip coating process. Dip coated mandrel suspended upside down to dry.

To remove the valve, the mandrel was submerged in water overnight to loosen the bond between the valve and the mandrel. The stent with the polymeric leaflets was carefully pried

from the mandrel. A pair of scissors was then used to cut the free edges of the valve, separating the leaflets and also disposing of the thick ridge of dried polymer accumulated during the inverted drying process. Valves were then physically inspected for defects.

Best results with regards to uniform thickness distribution and minimal physical defects depend on a number of factors mainly the concentration of the polymeric solution, the number of successive dips and also the drying process. We initially started out with a moderate concentration of 20% w/v of polymeric solution with between 4-5 successive dipping and drying cycles. It was however noticed that multiple dipping tends to cause inconsistencies such as bubble generation, especially at the commissures of the valve. It also caused non uniform thickness distribution. Also multiple dipping tend to cause very low reproducibility due to the inevitable human inconsistencies that arises during the dipping process. This issue was also experienced by Mackay et al, 1996, who suggested a way to reduce human inconsistencies during dipping, by using thicker solution and fewer dipping cycles to achieve desired thickness.

With this in mind, the concentration of our polyurethane solution was varied from 20 to 35%w/v. The number of successive dipping and drying cycles were also reduced from between four and five dips, down to two. This seemed to create a more consistent and reproducible method. It was also noticed during subsequent testing, that the valve tends to tear at the commissures very early in the testing. This was found to be due to the weak bonding between the leaflets and the interior portion of the stent. This was mitigated by coating the interior part of the stent with a film of the dipping solution before fitting the stent over the mandrel for the dipping process

The suture ring was created by wrapping 2 layers of rubber band material around the base of the stent, secured with cyanoacrylate adhesive. A picture of the final product is displayed below.

Figure 5.3. 22mm polymeric heart valve fabricated via dip coating.

5.2. DEVELOPMENT OF THE HYDROYNAMIC TESTING RIG

5.2.1. INTRODUCTION

In vitro artificial valve evaluation is conducted in pulse duplicators, also known as hydrodynamic testers or mock circulatory loops. These bench top setups are hydraulic circuits capable of simulating the physiological environment and pressure profiles of the heart (most commonly the left side of the heart) (De Paulis et al. 2005; Claiborne et al. 2013; Hildebrand 2003; Lanzarone et al. 2009; Fisher et al. 1986; Bazan & Ortiz 2011; Gregory 2009; Taylor & Miller 2012; Maleki et al. 2014; Walker 2006; De Gaetano et al. 2015; Mouneimne et al. 2010).

The ultimate aim of this research project is to determine whether instrumenting valves with sensors can provide diagnostic information with regards to the onset of aortic valve stenosis. In order to achieve this aim, polymeric valves were developed. These valves are subjected to hydrodynamic testing in the simulated aortic position, in order to assess the valve performance against gold standard ISO 5840 requirements. Further to that obstruction simulation tests will be conducted before and after sensor instrumentation. All these tests are conducted in an invitro system that simulates the natural heart valve environment.

In this section, we outline the process of designing and developing the custom hydrodynamic tester apparatus. This apparatus is designed to simulate the physiological environment of the left side of the heart. We begin with describing our preliminary setup, the pump calibration process and limitations of the preliminary setup. Based on these limitations, we describe some improvements we made to improve the hydrodynamic system in order to generate a more physiological environment under the test conditions.

5.2.2. PRELIMINARY SETUP DESCRIPTION

For our preliminary setup, we employed an existing custom made hydro –pneumatic system used in a previous study in the University of Strathclyde Bioengineering department (Edwards *et al.*, 2015) in which the influence of MRI magnetic field on valve performance was assessed

The system is a simple circuit which consists of a piston pump connected to an electric motor (Parvalux, Wallisdown, Bournemouth, UK), a reservoir representing the left atrium and the prosthetic valve housing chamber with inlet and outlet pressure ports to measure upstream (ventricular) and downstream(aortic pressure) across the valve . These components are all connected to each other via PVC clear braided hose. The test fluid (water), is sucked from the reservoir via the piston pump, and is pushed through the hose, to the inlet of the valve chamber (ventricle) through the valve, then through the valve chamber outlet (aorta) back to

the reservoir tank. SS13L pressure transducers (Biopac Systems, Goleta, GA) were used to detect and record aortic and ventricular pressure recordings. Data acquisition and data display software system (Acknowledge 4.1) are all purchased from Biopac Systems Inc. To hold the valve in place in the midsection of the chamber, ring like valve holders were designed using CREO 3.0 software and 3D printed.

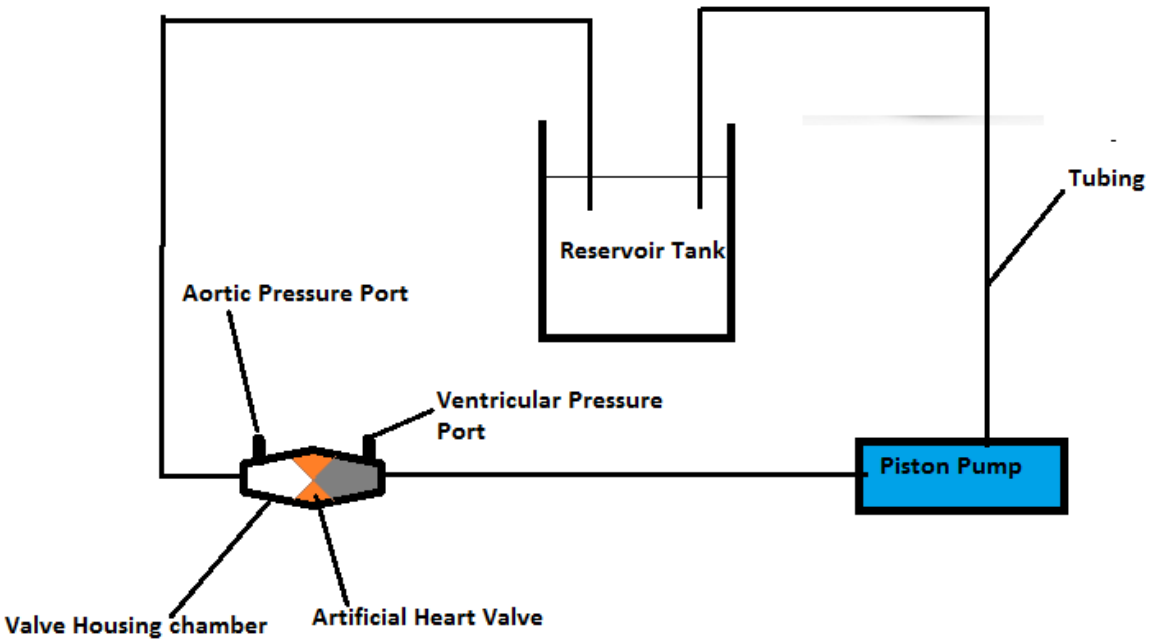

Figure 5.4. Schematic diagram of the preliminary setup

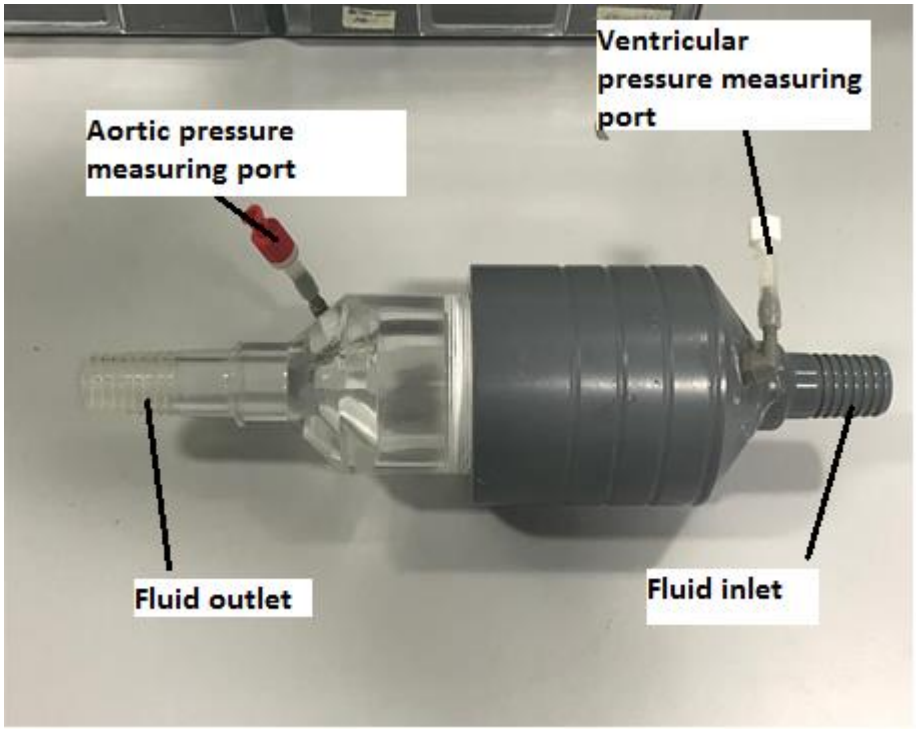

Figure 5.5. A labelled diagram of the valve housing chamber

5.2.3. PUMP CALIBRATION

The pump essentially represents the function of the left ventricle of the heart and is the most important component of the hydrodynamic tester. Hydrodynamic valve testing is done at various flow rates. These flow rates are a representation of the range of cardiac output. Mathematically,

Cardiac output= Stroke Volume x Heart Rate.

Before testing can be done, it is thus important that our pump system be calibrated so we are able to accurately adjust pump settings to achieve desired flow output. As earlier mentioned, the pump employed is a piston pump. It consists of a stainless steel hollow cylindrical chamber which houses the fluid to be pumped. The tip of the chamber has an inlet and outlet, with valves to control flow direction. The arm of the piston is connected via a screw to the drive wheel which rotates via the geared motor in a rocker arm like mechanism. The drive wheel has 10 holes drilled into it in an arc-like pattern. Moving the piston arm to selected

hole regulates the displacement of the piston head, reducing or lengthening the piston stroke thus regulating the amount of fluid displaced (stroke volume). The motor is connected to an external speed regulator . Pump speed is controlled by a dial with speed setting numbered from 1 -10, with 1 being the lowest speed, 10 being the highest. The pump was calibrated with the preliminary setup configuration and a fabricated polymeric valve inserted in the valve chamber.

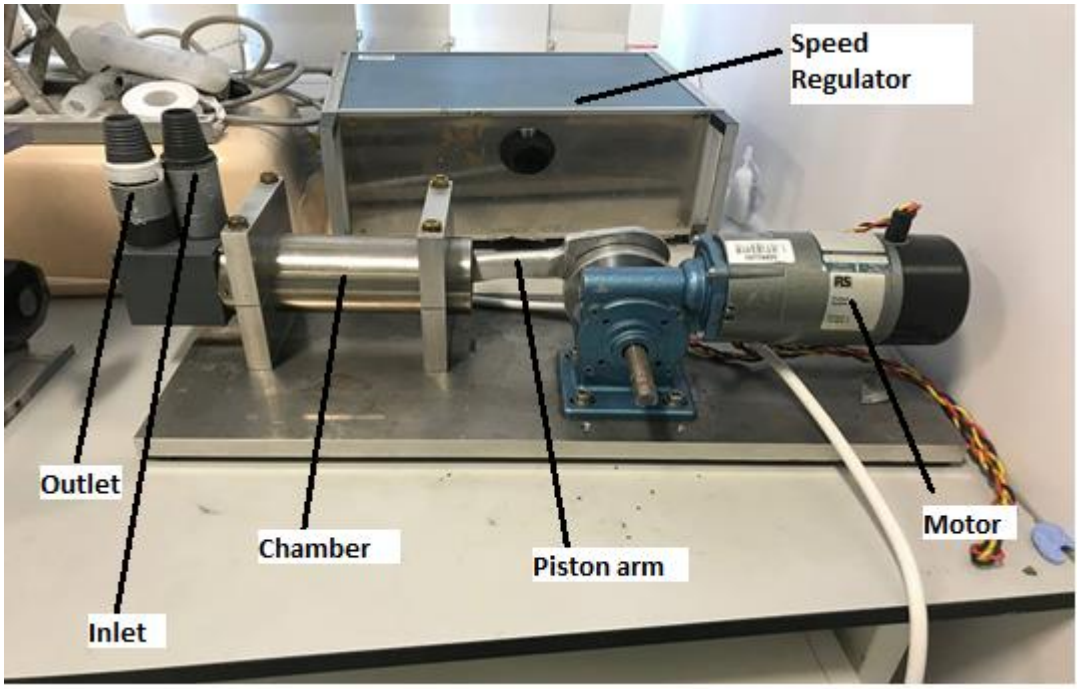

Figure 5.6. The piston pump used in the hydrodynamic tester design

5.2.3.1 Pump frequency/speed calibration

Pressure against time data for each setting was collected over a number of cycles (n>10) and heart rate was calibrated for each setting as follows:

Heart rate (beats per minute) or Pump speed (cycles per minute) = 60/((T2-T1)/N)

Where T2= end diastolic time of last cycle

T1=end diastolic time of first cycle

N= number of cycles between T1 and T2.

End diastolic time was detected via visual inspection as the time corresponding to the largest downward deflection in the pressure data per cycle.

As an example, for a pressure data set with selected block of 14 cycles, and T1 and T2 being 7.75 and 19 seconds respectively, the period /time length per cycle would be calculated as

$Period = \frac{19-7.75}{14} = 0.804$seconds

0.804 seconds =1 cycle

60 seconds =60/0.804 = 74.63, approximately 75 cycles or beats per minute.

For each speed setting from 1 through to 10, the process was repeated 3 times and an average was found. Figure 5.7 shows the calibrated settings of the pump.

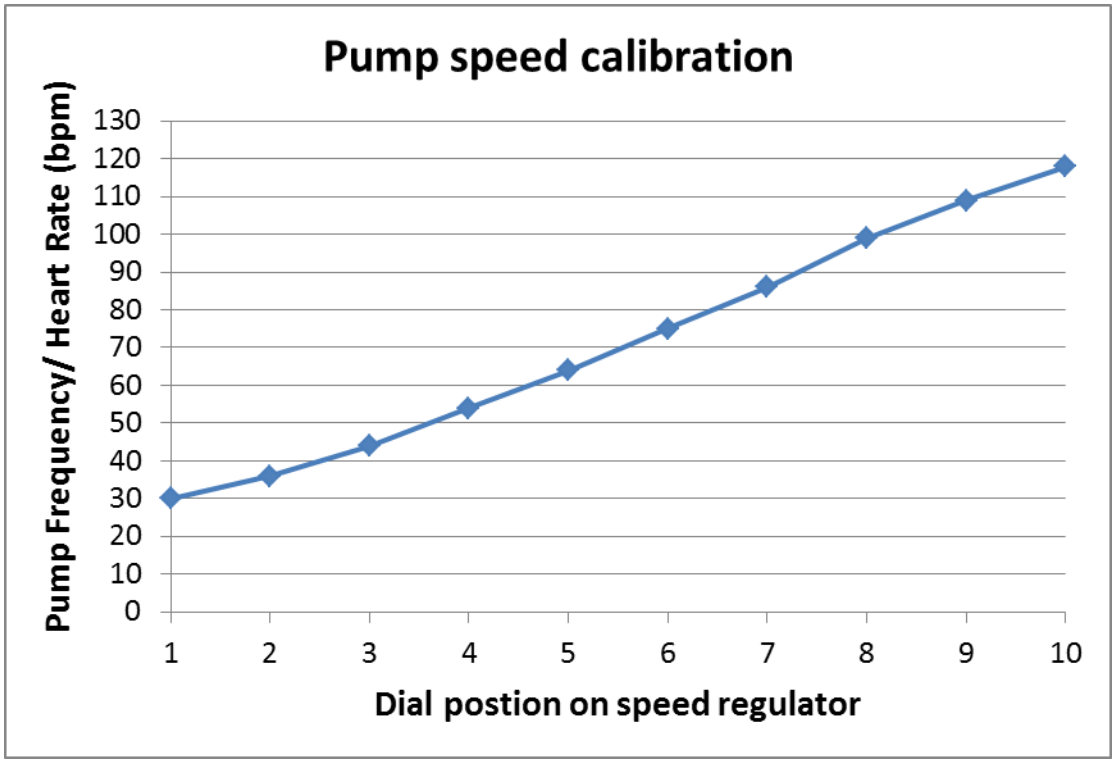

Figure 5.7. Pump speed settings

5.2.3.2 Stroke volume calibration

In the physiological terms, stroke volume is the volume of blood pumped out by the left ventricle per beat. This is calculated as the End diastolic volume (EDV) – End systolic volume (ESV). EDV is the volume in the ventricle after maximum filling and ESV is the volume remaining after the maximum fluid has been pumped out (Martini, Nath and Bartholomew, 2018). Relating this to our piston pump, the fluid chamber represents the left ventricle. During systole the piston moves deeper into the chamber thus increasing the pressure which causes the forward flow of the fluid. During diastole, the reverse happens. Thus by measuring the volume of the fluid chamber and the displacement of the piston during the forward and backwards phase of the pumping cycle, the EDV and ESV can be calculated.

Firstly it was necessary to determine the volume of the fluid chamber. The fluid chamber is a stainless steel cylinder with volume computed as

$V_{chamber} = \pi r^2 h$ ……(1),

Where r is the radius of the cylinder, h is the length of the cylinder. Pump speed was then set to the lowest speed ie 1 on the dial setting. And the piston arm was adjusted to the first hole on the drive wheel. Just at the end of the forward phase of the pump, i.e. when the piston has experienced maximum displacement, the pump was stopped and a ruler was inserted into the chamber to measure the piston displacement ($d_{systolic}$). The pump was turned back on and at the end of the backwards/filling phase, when the piston arm had experienced minimum displacement, the pump was again turned off and displacement was measured ($d_{diastolic}$) . Thus

$ESV = \pi r^2\left(h - d_{systolic}\right)$ …… (2)

$EDV = \pi r^2(h - d_{systolic})$ …… (3)

$Stroke\ Volume\ (SV) = EDV - ESV$……(4).

For each hole on the drive wheel, numbered from 1 -10, equations 1 -4 were used to calculate the stroke volume. All stroke volume calibration was done at the lowest pump speed as this helps us to stop the pump at the accurate time in order to measure the displacement of the piston. Figure 5.8 shows the calibrated stroke volume.

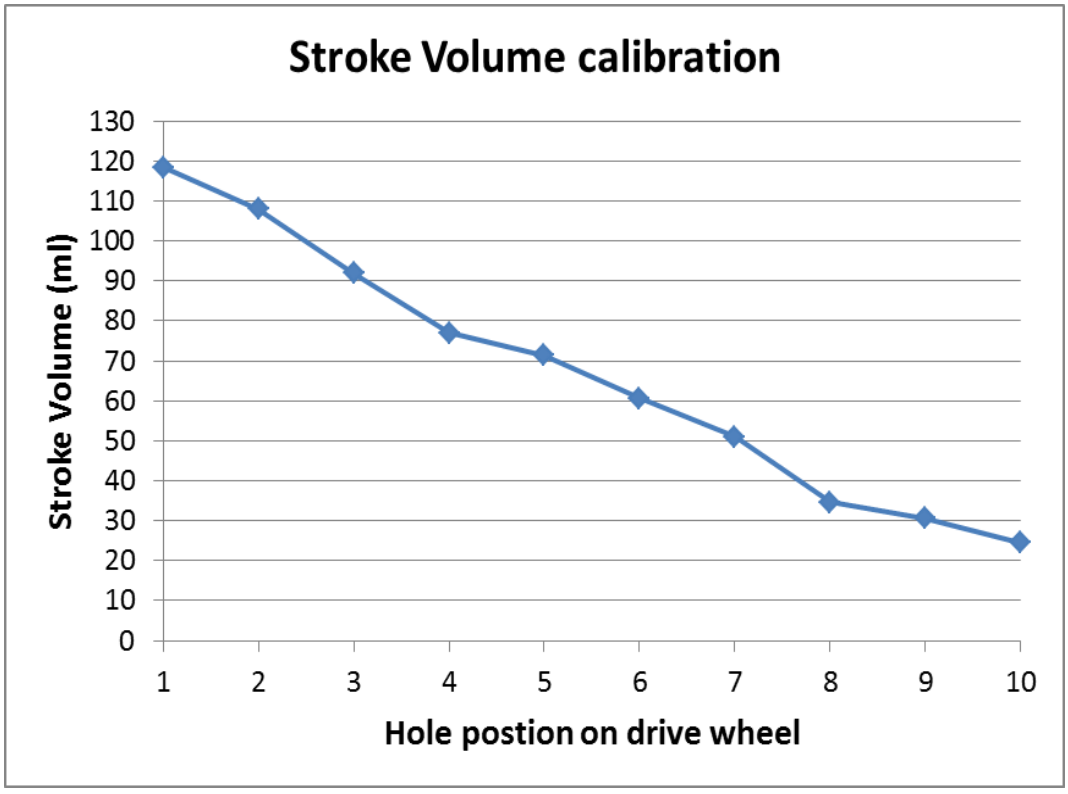

Figure 5.8. Pump stroke volume calibration

5.2.4. RESULTS AND OBSERTVATIONS FROM THE PRELIMINARY HYDRODNAMIC TESTER SETUP

The aim of the hydrodynamic tester design is to create a system that would be able to replicate physiological pressure waveforms under normal cardiac output. The average healthy heart rate of an adult at rest is approximately 75 beats per minute and the corresponding cardiac output is approximately, 5Litres/min. In our tester, the closest to this ideal cardiac output was 5.3L/min, which was achieved keeping the speed dial at 6, corresponding to 75bpm and the drive wheel hole position at 5, corresponding to 71.4 ml (see figures 5.7 and 5.8 respectively). The product of the SV and HR (pump speed) in these positions leads to the value of 5.3L/min which is close to normal resting cardiac output.. At this cardiac output, we aim for the ideal physiological systolic pressures of (100-130mmHg) for both aortic and ventricular systolic pressure, with the ventricular pressure slightly higher.. Ideal diastolic pressures for the aortic and ventricular pressure were (70-80)mmHg and (0-20)mmHg respectively. A visual representation of ideal physiological pressure waveforms, known as the "Wiggers" diagram, is shown in figure 5.9 below

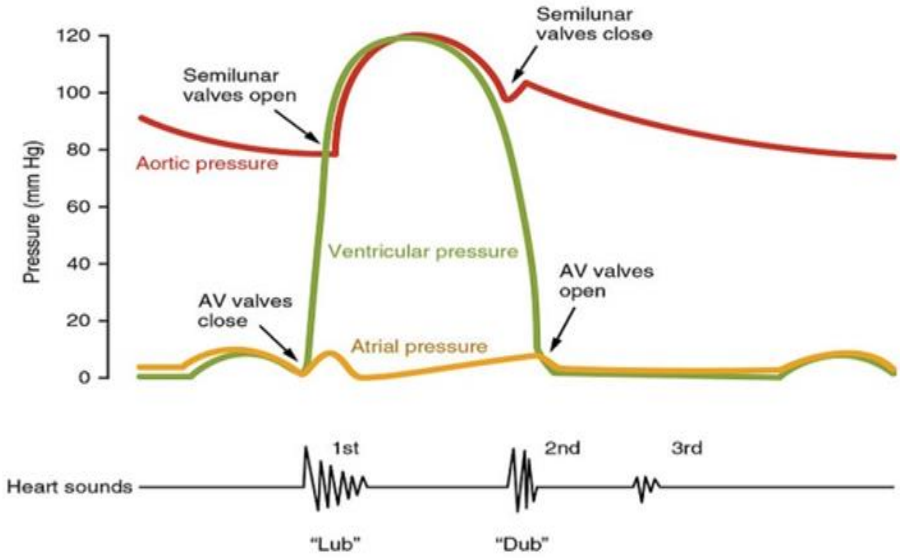

Figure 5.9. The wiggers diagram showing the ideal pressure waveforms and amplitudes

Source (http://learnwise.co/wiggers-diagram-labeled/)

In order to get a better understanding of our preliminary setup and its ability or inability to create physiological pressure waveforms, we experimented with varying the pressure head between the 3 main components, ie the pump, the valve chamber and the reservoir. The idea was that varying the pressure heads will help determine the best configuration to achieve our target pressures. Pressure heads were achieved by placing a component on a bench top of height 0.89m relative to the other components. The different configurations of the components are shown in the figure below.

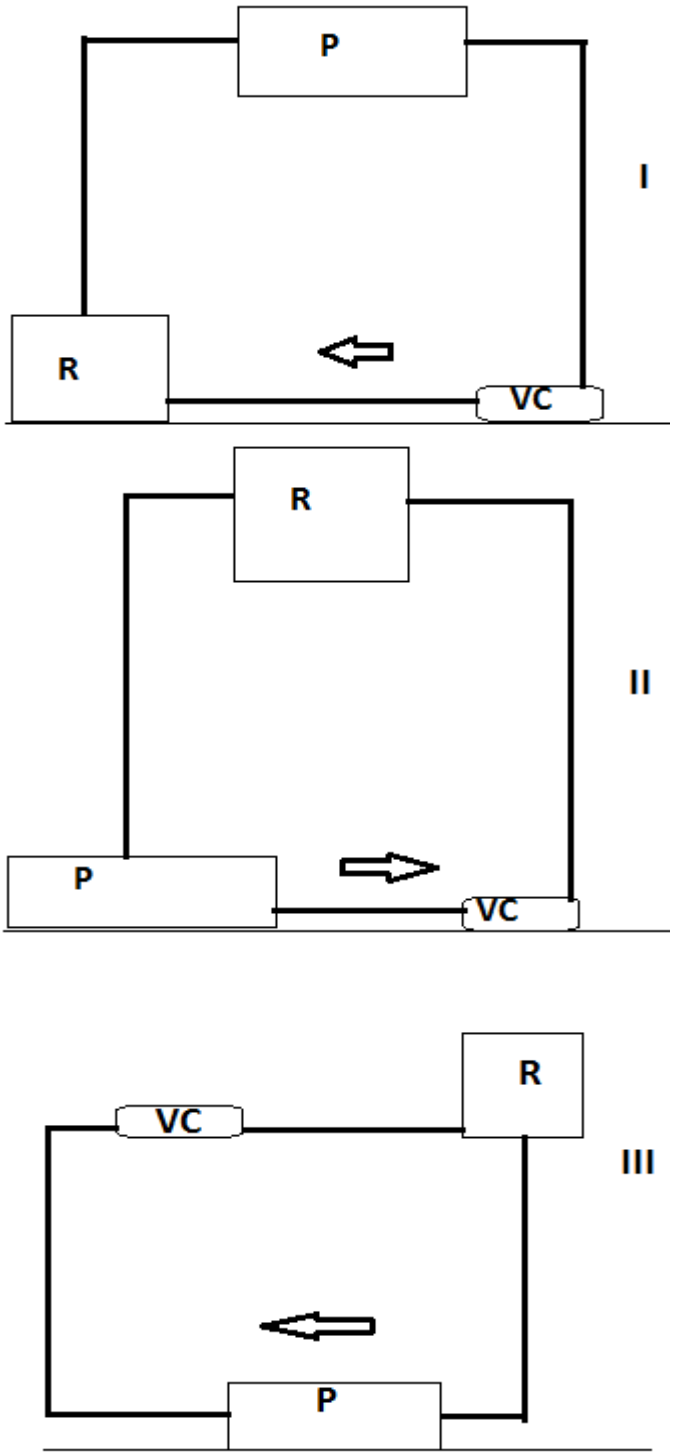

Figure 5.10. Pressure head variations between the pump, valve chamber and reservoir. R=reservoir,VC= valve chamber, P=pump. Arrow represents the flow of fluid. Height between bench and floor is 0.89m. The 3 different component arrangements are labelled I, II and III.

5.2.4.1 PRELIMINARY RESULTS

The preliminary results at a cardiac output of 5.3L/min are presented below

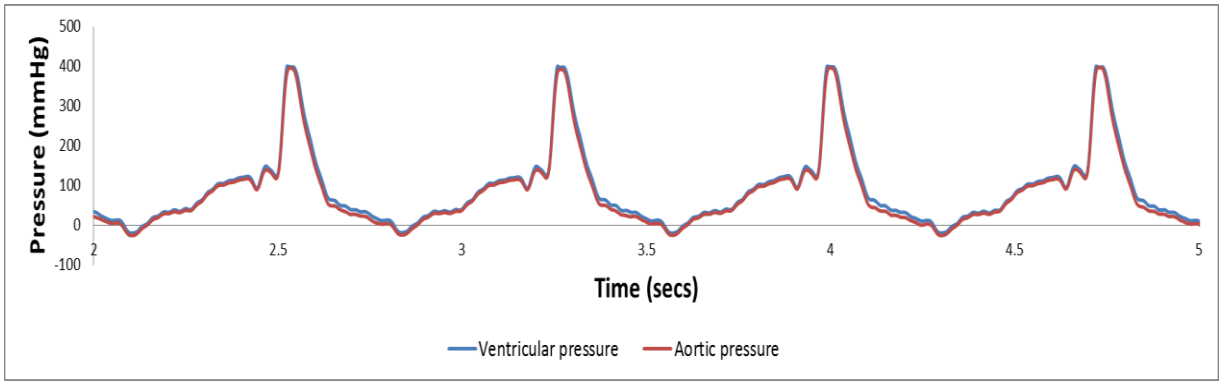

Figure 5.11. Valve pressure profile at 5.3lmin cardiac output. Pressure head variation I ie Pump on table, valve chamber and reservoir on floor. Mean peak systolic ventricular pressure=400mmHg, mean peak systolic aortic pressure=395mmHg

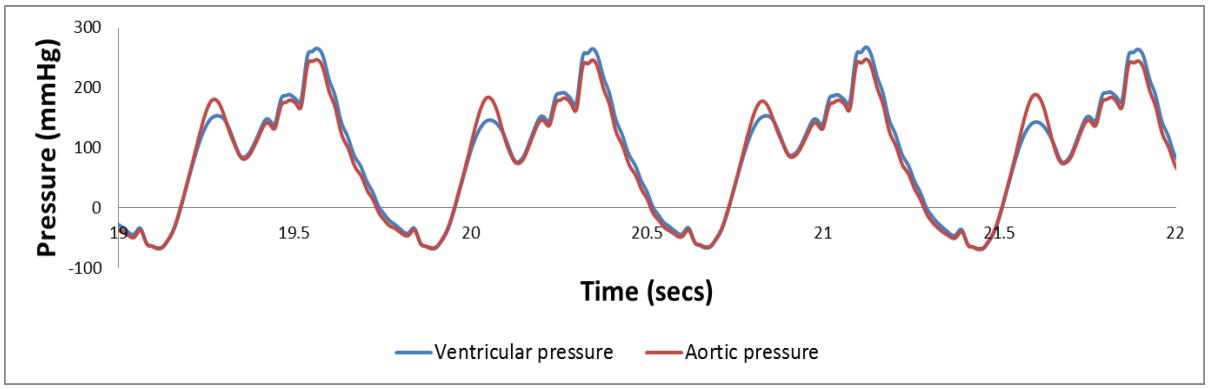

Figure 5.12. Valve pressure profile at 5.3lmin cardiac output. Pressure head variation II ie Valve chamber and pump on the floor with the reservoir placed on the table. Mean peak ventricular pressure=277mmHg, Mean peak aortic pressure=260mmHg

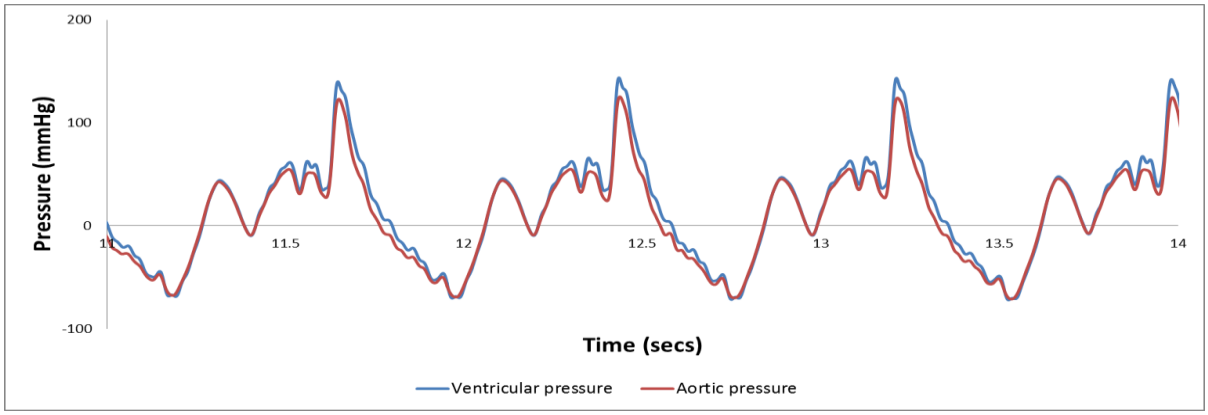

Figure 5.13. Valve pressure profile at 5.3lmin cardiac output. Pressure head variation III ie valve chamber and reservoir on the table with the pump placed on the floor. Systolic ventricular pressure =140mmHg, systolic aortic pressure=120mmHg.

5.2.4.2. OBSERVATIONS

The following were some observations made from the results of the preliminary setup of the hydrodynamic tester.

5.2.4.2.1 Non Physiological Waveform Patterns And Amplitudes

Comparing the figures from our preliminary setup (see figures 5.11-5.13) to the Wiggers diagram in figure 5.9, it can immediately be observed that the pressure profiles generated by our systems are far from physiological. They are very erratic with various oscillations and spikes in the waveforms as opposed to the smooth waveform in the ideal scenario in the Wiggers diagram, thus suggesting the turbulent nature of flow in the setup.

Placing the valve chamber and the pump at a lower height relative to the reservoir (II) generates mean systolic aortic and ventricular pressures of approximately 260 and 277mmHg respectively, which is outwith the normal physiological range described in the wiggers diagram. The pump also created a high suction during the diastolic phase , as seen in the large negative deflection in the waveform approximately (-50mmHg) as seen in figure 5.12.

Placing the pump at a lower height relative to the valve chamber and the reservoir (III) generates mean systolic aortic and ventricular pressures of 120 mmHg and 140mmHg respectively. Whilst these values were closest to our target pressures, there were still some very erratic oscillations in the waveform (see figure 5.13). Furthermore, reducing the pump height did not seem to have any significant effect on the negative pressures experienced in diastole. In an effort to eliminate the high negative values we decided to create a positive pressure head relative to the valve chamber and the reservoir by placing the pump higher (I). Although this reduces the negative pressure profiles to approximately -10mmHg, and also relatively reduces the oscillations, it causes a large spike in peak systolic waveform values to pressures between 350 to 400mmHg (see figure 5.11), again outwith the normal physiological range

5.2.4.2.2. Identical Aortic And Ventricular Pressure Waveforms

Looking at the Wiggers diagram (figure 5.9), the ventricular pressures rises up quickly during the systolic phase. Once the pressure exceeds that of the aortic pressure, the aortic valve opens and the aortic pressure also rises in tandem with that of the ventricular pressure. Once the ventricular pressure falls below its peak and the pressure in the ventricle becomes slightly lower than that of the aortic pressure, the pressure difference causes the aortic valve to close. The mitral valve opens thus allowing the ventricles to fill up rapidly thus causing a sharp decrease in ventricular pressure i.e. the diastolic phase. The shape of the ventricle waveform is thus synonymous to a half sine wave. The aortic pressure waveform however, during diastole, does not experience a sharp decrease as that of the ventricular pressure. It actually experiences a slow decay similar to an exponential decay curve.

However looking at figures 5.11-5.13, it can be observed that the aortic and ventricular pressure waveforms, rose and fell in similar fashion even in the diastolic phase of the pump cycle. This was further proof that this system was unable to simulate the normal

physiological pressure environment. During the initial valve testing, it was also observed that the polymeric valve was unable to close at any time during the filling phase of the pump cycle, due to the imbalance in pressure differences.

5.2.5. LIMITATIONS OF THE PRELIMINARY SETUP

As stated earlier, the preliminary setup consists of the pump, valve chamber , with the polymeric valve inserted, and the reservoir tank representing the left atrium. All of these components are connected via PVC clear braided hose. From observing the results, it was clear our system had some limitations, which are outlined below.

5.2.5.1 Lack of compliance

Blood vessels exhibit compliance which allows for the vessels to dilate in response to increase in pressure. Mathematically,

$C = \frac{\Delta V}{\Delta P}$, where V and P is the volume and pressure respectively.

Compliance is essentially a measure of how elastic the blood vessel is and this has a massive effect on the pressure waveform. During systole, the aorta dilates as the pressure is increased. This causes the aorta to store blood temporarily. During the diastolic phase of the cardiac cycle, i.e. as the left ventricle fills, the stored blood and thus pressure in the aorta is released slowly. This phenomenon ensures blood flow and perfusion all times even during the diastolic phase of the cardiac cycle. The compliance of the aorta ensures elevation of diastolic pressures, reduction in peak systolic pressures and also a decrease in pulse pressure (systolic –diastolic pressure) (Nobari *et al.*, 2012 ; Pappano and Wier, 2013a).

Relating this to our hydrodynamic setup, the valve chamber, which houses the polymeric valve and also contains the manometer lines for aortic and ventricular pressure measurements, is made out of hard plastic material, thus not exhibiting the compliant nature

of the aorta. The clear braided PVC hoses used for connecting the components and also as fluid conduits (analogous to blood vessels), also exhibit very minimal compliance. The general lack of compliance is likely to be a cause of the high systolic and low diastolic pressures experienced in the aortic pressure waveforms generated by our preliminary hydrodynamic tester setup.

5.2.5.2 Rigidity of the left ventricular chamber

The left ventricle is an elastic muscle which contracts during systole and expands to during diastole, thus accounting for the smooth rapid rise and fall in pressure, as seen in the ventricular pressure waveform of the Wiggers diagram. The ventricle exhibits a degree of compliance, albeit minimal relative to the aorta. In the hydrodynamic setup, the left ventricle is represented by the piston pump fluid chamber. This is made primarily out of stainless steel, which is very rigid and does not possess any elastic properties. The rigidity of the pump chamber is suspected to be a major cause of the turbulence generated by our system.

5.2.6. IMPROVEMENTS TO PULSE DUPLICATOR SETUP

As earlier mentioned, compliance of the vessels has a magnificent effect on the blood pressure wavefrom patterns. Another factor that affect pressure and blood flow in the arterial tree is the resistance of the arteries to blood flow, called peripheral resistance. The peripheral resistance of blood vessels is determined by 3 major factors which are the length of the vessel, the radius of the vessel and finally the viscosity of the blood. Mathematically it is expressed as $R \propto \frac{n.L}{r^4}$,

where n is the viscosity, L is the length and r is the radius of the vessel (Klabunde, 2012c).

From the equation above, it can be seen that there is a direct relationship between the resistance and vessel length, thus the longer the vessel, a higher resistance to flow will be experienced. Again looking at the equation, it can be seen that there is an inverse relationship

between resistance and the radius of the vessel. The higher order (exponent 4) of the radius component denotes that a small change in vessel radius causes an exponentially large change in resistance. During systole, the arteries dilate (vasodilation), as they are filled with fluid. This causes an increase in the vessel radius thus reducing resistance to flow which ultimately leads to adequate perfusion of organs. The opposite occurs during vasoconstriction, ie when the blood vessels constrict during diastole (Siddiqui, 2011)

5.2.6.1. INTRODUCTION TO WINDKESSEL MODELS

Most mock circulatory designs (Westerhof, Elzinga and Sipkema, 1971; Wright, 1988; Gourlay, 1997; Felipini, 2005; Walker, 2006; Lanzarone, Vismara and Fiore, 2009; Bazan and Ortiz, 2011; Leopaldi *et al.*, 2012; Taylor and Miller, 2012) employ a lumped parameter model known as the "Windkessel model" to simulate the flow and pressure mechanics in the aorta. This model incorporates primarily the compliance and resistance of the aorta and small arteries respectively.

Renowned German physiologist, Otto Frank, is mostly accredited for having formulated and popularised the Windkessel model as a way of describing fluid flow and pressure dynamics in the aorta. In his model, Frank describes the systemic circulation (left side of the heart) as a closed loop hydraulic system. This system contained a water pump connected to the reservoir, with the reservoir having a volume of air entrapped in it. As the reservoir gets filled with water via the pumping action of the pump, the water compresses against the air pocket above. The air pocket in turn exerts an opposite force on the water in the reservoir. This force pushes the water out of the reservoir (Catanho, Sinha and Vijayan, 2012).

The resulting output of Frank's Windkessel model is that there is constant non intermittent flow of water out of the spout of the tube, even during the backward/ suction phase of the pump cycle. Relating this to physiological terms, this means that regardless of the stage of the cardiac cycle, perfusion is not compromised. In the Windkessel model, the pump represents

the heart, the reservoir simulates the compliant nature of the aorta and the peripheral resistance is intrinsically generated via the length and radius of the tube and also the viscosity of the fluid (Westerhof, Lankhaar and Westerhof, 2009).

The earliest Windkessel model, considered just 2 major parameters i.e. compliance, “C” and resistance ,”R” thus is referred to as a 2 element windkessel model.

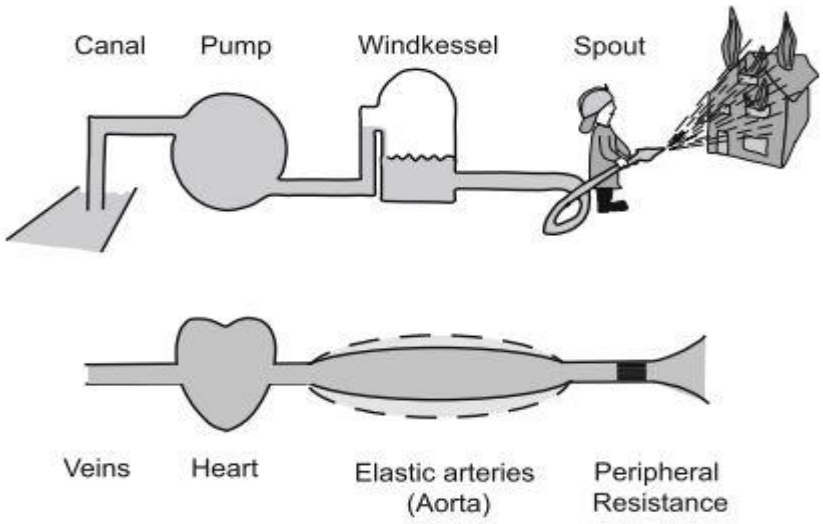

Figure 5.14. The Windkessel concept (top shows the hydraulic representation, bottom shows the physiological representation) (from Westerhof et al, 2009)

The Windkessel model can also be represented in an electrical form, for mathematical and electrical simulations. In its electrical circuit equivalent, the compliance is represented by a capacitor in the sense that a capacitor stores charge and then slowly releases said charge. Similarly, the compliance causes the aorta to dilate and store blood during the systolic phase and slowly release it during the diastolic phase (Waite and Fine, 2007a). The resistance is represented by an electrical resistor. In the electrical circuit model of the windkessel, the capacitor and resistor are placed in parallel, with a power supply connected across the system. This power supply produces a time varying voltage, which is the hydraulic and physiological representation of the pressures generated by the pump and left ventricle respectively.

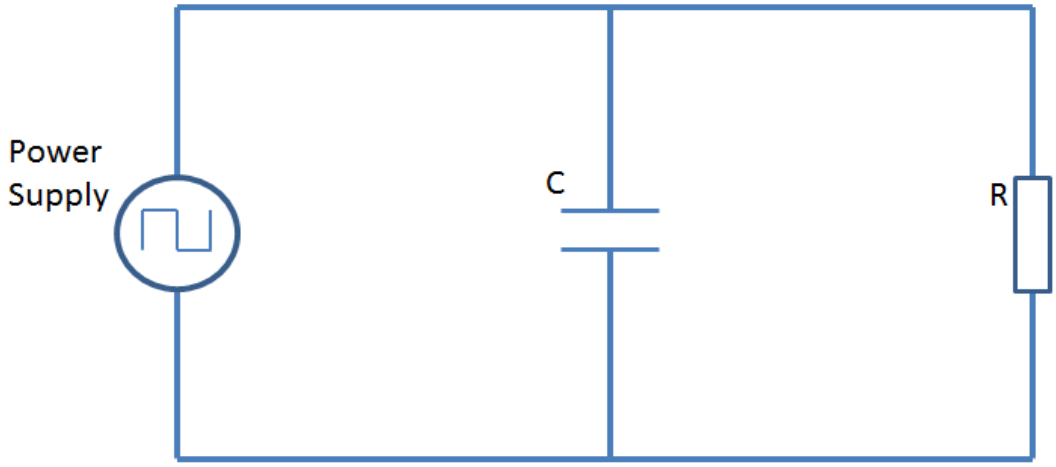

Figure 5.15. The electrical circuit equivalent of a 2 element Windkessel model

As earlier mentioned, the initial setup of our hydrodynamic tester generates non physiological pressure waveforms for both the aortic and ventricular pressure wavefroms. In order to generate more physiological aortic pressure waveforms, we employed a 2 element windkessel in our hydrodynamic testing rig. We discuss the design , fabrication and implementation of compliance and resistance below.

5.2.6.2. SYSTEMIC COMPLIANCE DESIGN

5.2.6.2.1. The use of balloons

To simulate compliance of our hydrodynamic system, we initially employed the use of long neck balloons. We cut off the neck of these balloons and connected one side to the aortic side of the valve chamber, and the other side to the tube leading to the ventricular chamber. We varied compliance by reducing or increasing the number of balloons utilised. By doing so, we were able to increase or decrease the layers of balloon material which thus had an effect on the rigidity and thus compliance.

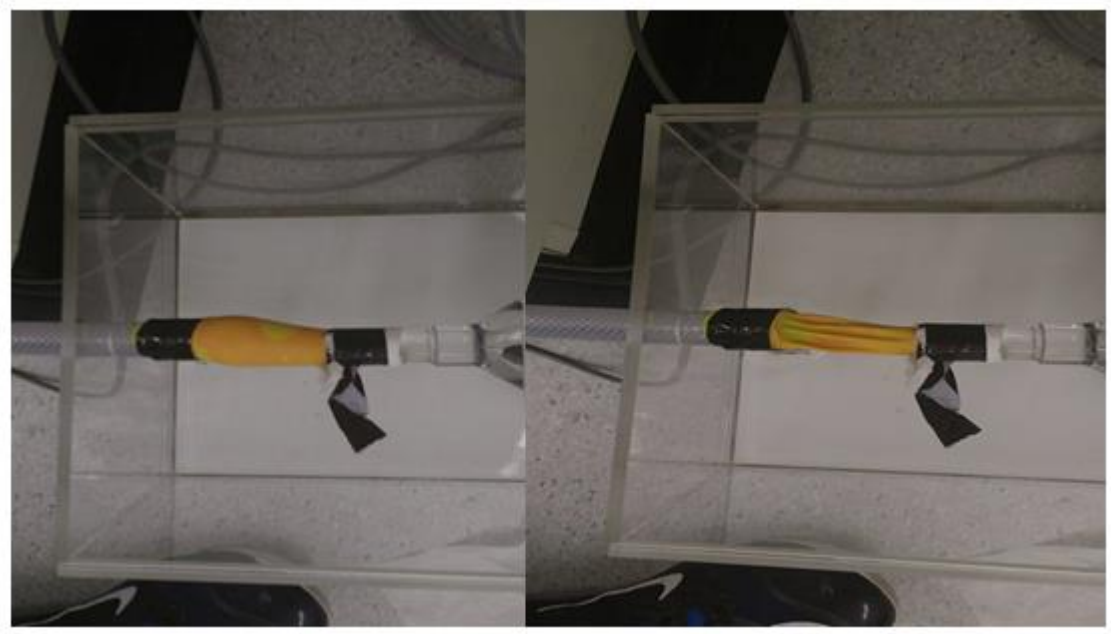

Figure 5.16. Three layers of balloon compliance (left shows system in systole, right shows system in diastole)

Low number of balloon layers equals more compliance and the inverse is also true. We however experienced some limitations. First of all attaching mutlilayered balloon necks proved to be very difficult. In many instances, we experienced kinking of the innermost layer of balloon which led to fluid accumulation in the balloon thus causing “aneurysm” which eventually would burst under constant cyclical loading. Secondly, in order to vary the

compliance, the entire system had to be stopped and drained, the balloons had to be disconnected from the system. We then had to insert or take off layers of balloon material, reconnect this back to the system after which the system had to be primed before further testing could be done. All this made this compliance simulation method very complicated and non-reproducible. It also made real time control of compliance, which is necessary to fine tune the hydrodynamic system, impossible to achieve.

5.2.6.2.2. Variable compliance

In order to create a more variable compliance system to aid real time compliance control, we employed a slightly modified version of the quintessential windkessel pneumatic only compliance chamber. This modified version is known as a membrane based compliance chamber and has been suggested as a more physiological option for simulating compliance and fine tuning hydrodynamic testers in order to produce more physiological aortic/arterial pressure waveforms (Walker, 2006; Gregory, 2009; Taylor and Miller, 2012).

The compliance system consists of 2 acrylic cylindrical chambers. The top chamber is of height 55mm, diameter of 100mm, with a 5mm wall thickness and is referred to as the pneumatic chamber. The bottom chamber is also of height 75mm, diameter of 100mm with a 5mm wall thickness and contains the test fluid. A latex material of thickness 0.25mm separates the hydraulic and pneumatic chambers. Introducing air into the pneumatic chamber, creates a high pressure in the pneumatic chamber, relative to the hydraulic chamber thus causes the elastic membrane to deflect downwards into the hydraulic component. This causes an increased volume of air in the pneumatic chamber, relative to the volume of fluid in the hydraulic chamber. During systole, the pressure in the hydraulic chamber increases thus exerts a force on the membrane pushing the membrane upwards . As the pressure in the hydraulic chamber reduces during the diastolic stage, the stored energy in the elastic membrane, pushes back on the fluid in an attempt to return back to its deflected state and this

force pushes fluid out of the hydraulic chamber, thus simulating the elastic nature of the blood vessels. The volume of air in the pneumatic chamber is directly proportional to the amount of compliance of the system.

A hole is made in the centre of the top of the pneumatic chamber and a small tube is fitted in the hole. A 2 way female-male luer lock stopcock valve (Cole Palmer, UK), which was then fixed to the tip of the tube and was connected via another small tube, to a mini air brush compressor (Sealey,UK). The stopcock valve serves as both to introduce and bleed air of out the pneumatic chamber. Another hole was drilled in the pneumatic chamber and fitted with a threaded female luer component to measure pressure in the pneumatic chamber if necessary.

The hydraulic chamber also consists of a hole with a luer fitting to measure the fluid pressure. Two tapered barbell fittings are located at the base of the hydraulic chamber as fluid inlet and outlet.

The entire compliance system is mounted on a rectangular slab of acrylic material, with 4 holes at the corners of the slab. Threaded steel rods were inserted into the holes essentially creating a cage around the compliance system. Two thin rods with metal washers, were slipped horizontally, over the top of the rods till they made contact across the top of the compliance chamber. These thin rods were held in placed and secured with stainless steel nuts thus creating a clamping system to ensure additional hermetic sealing at the membrane chamber interface. Figure 5.17 shows the complete compliance chamber design.

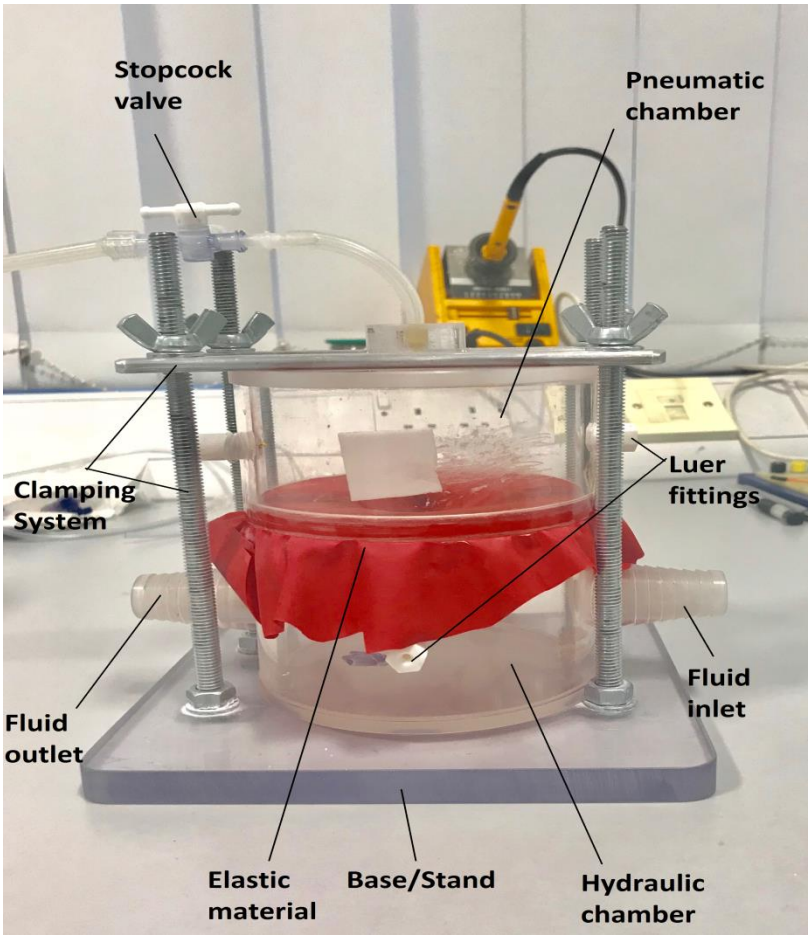

Figure 5.17. A labelled diagram showing membrane based compliance chamber

Figure 5.18. The mini air brush compressor used to introduce air into the pneumatic chamber

5.2.6.3. PERIPHERAL RESISTANCE

For the simulation of resistance, it was important we had a system to allow real time control of the resistance. Resistance was simulated by via the use of a G clamp. This was slipped over the tube connecting the compliance chamber to the reservoir tank. The G clamp was placed close to the compliance chamber. Tightening the clamp increases the resistance and loosening the clamp reduces the resistance. The use of the clamp , although very rudimentary, did provide a real time control of the resistance, which is ideal for fine tuning the pressure waveforms of our system.

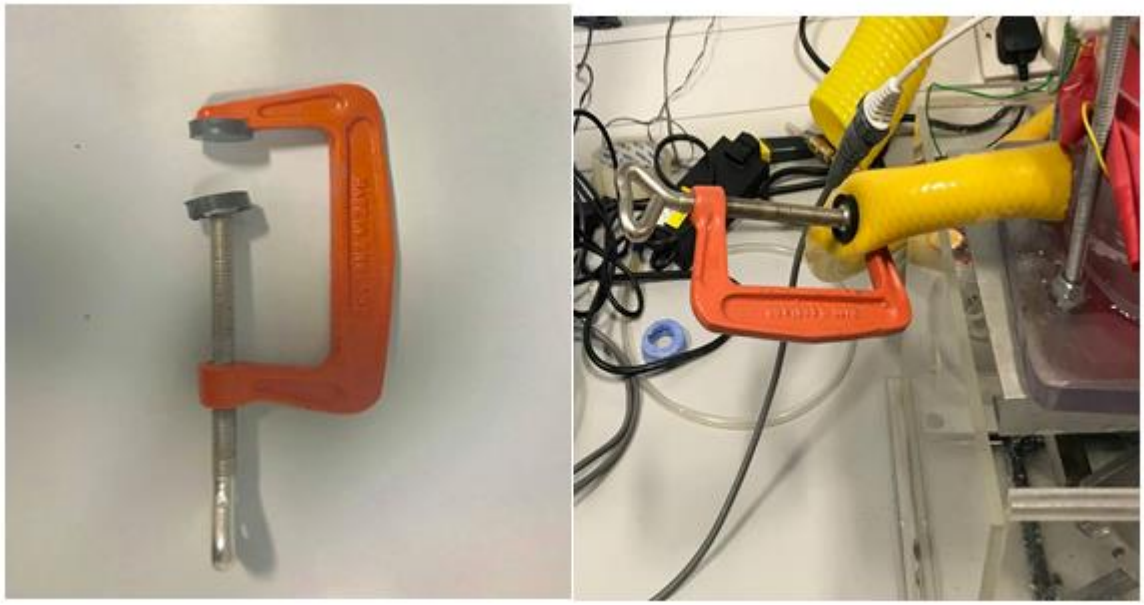

Figure 5.19. Peripheral resistance. Right shows the G clamp used to simulate the peripheral resistance. Left shows the G clamp connected to the hydrodynamic setup

5.2.6.4. VENTRICULAR CHAMBER

As earlier mentioned in the initial setup, the rigid piston chamber is essentially representing our ventricular chamber and doesn't take into account the elastic nature of the ventricles. To remedy that, we manufactured an elastic ventricular chamber. The design of this chamber was based on that of our variable compliance chamber. This consists of 2 cylindrical chambers separated by a latex membrane of 0.25mm thickness. Both top and bottom

chambers are of equal dimensions, i.e. 100mm diameter and 85mm height with a 5mm wall thickness.

Unlike the compliance chamber however, the top chamber has 2 tapered barbell fittings (one on each side) situated at different heights relative to each other. One of them is situated at a height 25mm from the top of the chamber and the other, about 55mm from the top of the chamber. The barbell fitting furthest away from the top chamber connects to the outlet of the pump and ensures adequate distension of the membrane into the bottom chamber is achieved. Connecting the fitting closer to the top of the chamber to the pump inlet ensures the membrane itself doesn't get sucked into the pump during diastole. A hole is drilled in the centre of the ceiling of the top chamber and fitted with a stopcock valve. Another hole is drilled about 42.5 cm height from the top of the chamber and also fitted with a stopcock valve.

The bottom chamber has 2 tapered barbell fittings, one on each side, of equidistant height of 25cm from the base of the bottom chamber. A hole is drilled at a height of 42.5mm measured from the base of the chamber, and fitted with a stopcock valve.To ensure the system is secured and clamped adequately, a clamping system, similar to that used for the variable compliance system, was employed.

The entire ventricular chamber system is laid horizontally. The top chamber is connected to the pump. The outlet of the pump is connected to the barbell fitting located closer to the latex membrane and the inlet of the pump is connected to the other barbell fitting on the top chamber. The top chamber is filled with water. This is referred to as the "**service fluid"**. The 2 ends of the bottom chamber are connected to the other components of the hydrodynamic system and will be filled with test fluid from the atrial reservoir. A 15mm ball check valve,

serving as a mitral valve,is connected between the atrial reservoir and the bottom chamber of the system.

During the diastolic phase of the pump, the service fluid is sucked from the top chamber which causes the latex membrane to distend into the top chamber thus increasing the volume and decreasing the pressure in the bottom chamber (test fluid chamber). This allows the check valve to open and the test fluid flows passively from the atrial reservoir into the bottom chamber. The atrial reservoir located at a higher height relative to the other components of the hydrodynamic system (30cm) which creates a positive pressure head and aids passive filling of the bottom chamber (ventricular chamber). During systole, the pump pushes the service fluid into the top chamber thus increasing the pressure in the top chamber. This pressure pushes against the elastic membrane which in turn pushes the test fluid in the bottom chamber throughout the system. The increase in pressure in the test fluid chamber causes the check valve to shut thus preventing the back flow of the test fluid.

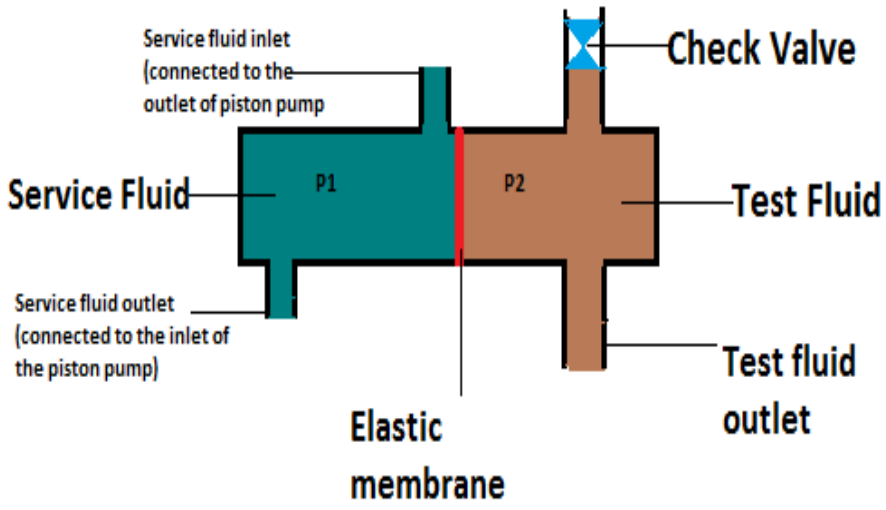

Figure 5.20. The plan view of the ventricular chamber at rest when pressure in the service fluid chamber (P1) is equal to the pressure in the test fluid chamber (P2). The elastic membrance stays in a neutral postion.

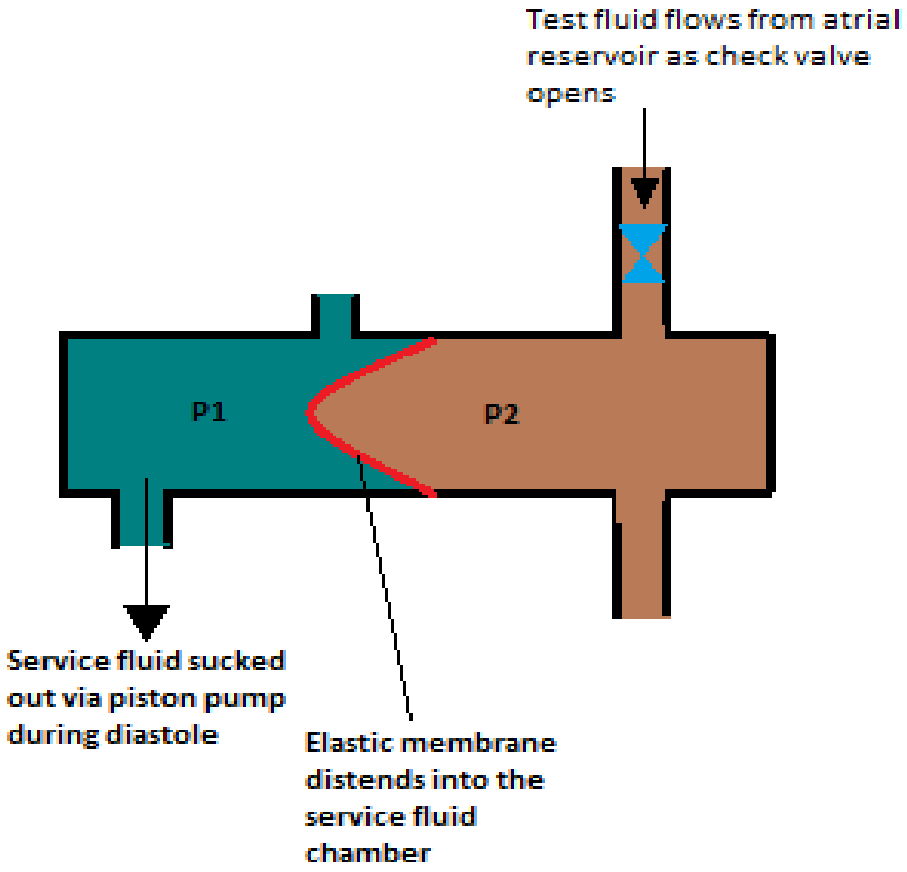

Figure 5.21. Diastolic phase of the ventricular chamber cycle. P1 decreases as fluid is sucked out from the service fluid chamber. Elastic membrance deflects into the service fluid chamber, thus increasing the volume and also decreasing the pressure (P2) in the test fluid chamber. Check valve opens up allowing filling of the test fluid chamber.

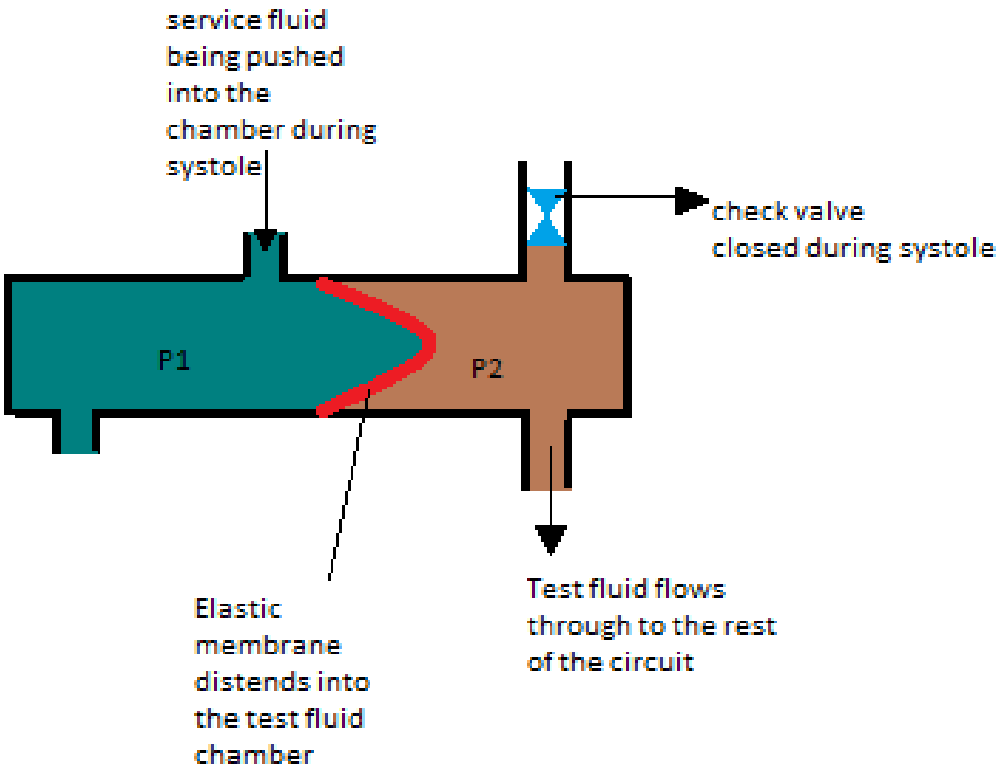

Figure 5.22.Systolic phase of the cycle. As pump pushes fluid into the service fluid chamber, P1 increases which causes the elastic membrane to distend into the test fluid chamber and pushes test fluid out of the chamber. The increase in P2 causes the check valve to close preventing back flow.

In summary, the service fluid controls the movement of the elastic membrane which in turn controls the flow and pressure in the bottom chamber. The cyclical deflections of the elastic membrane in the bottom chamber, creates an elastic and deformable ventricular chamber, which is a more physiological representation of the left ventricle. Figures 5.23 and 5.24 are diagrams of the ventricular chamber

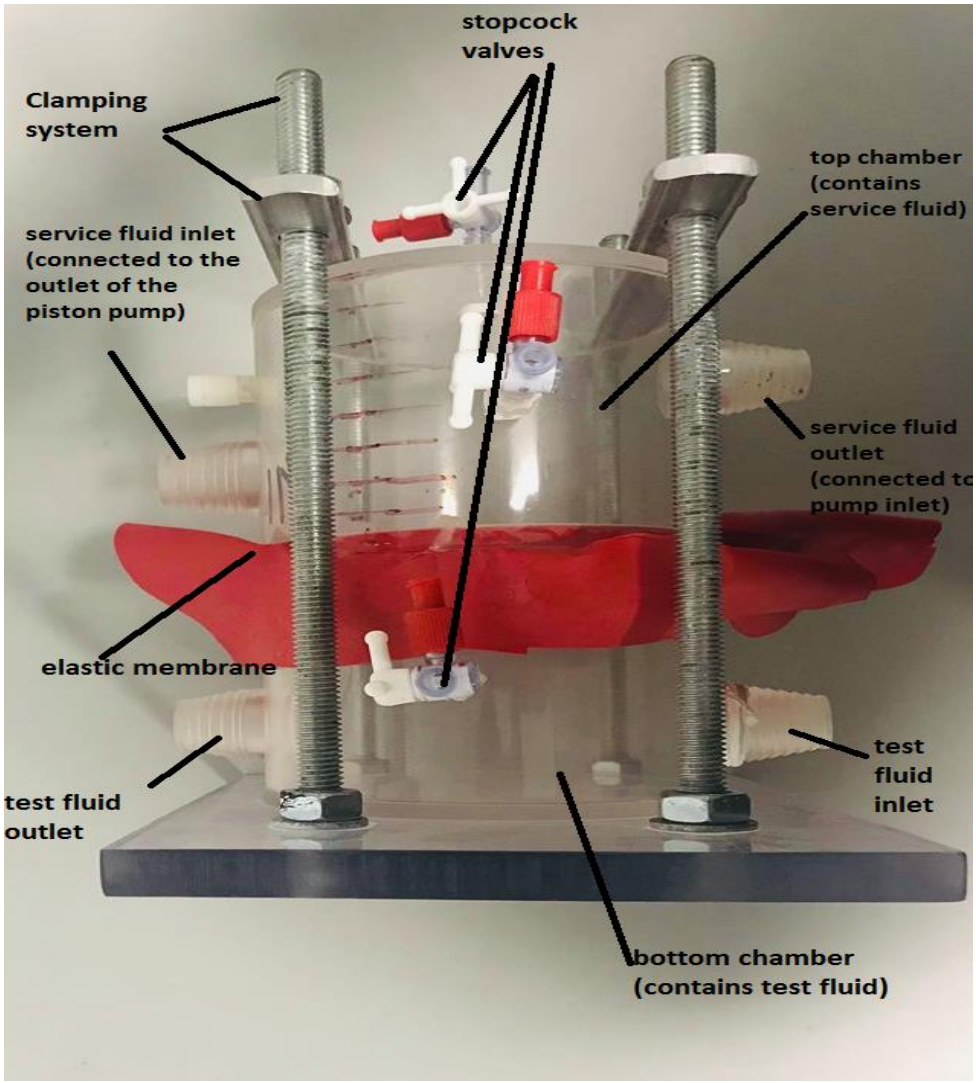

Figure 5.23. A labelled diagram showing the completed ventricular chamber design

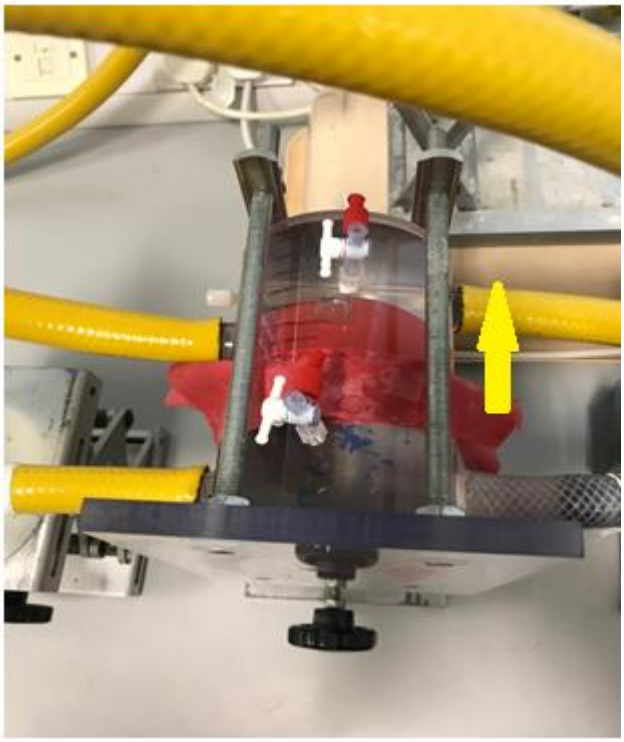

Figure 5.24. The ventricular chamber system in action (membrane extending upwards into the top chamber (shown by yellow arrow) suggests the pump in diastole mode.

5.2.6.5. SMOOTHENING CHAMBER

Initial data gathered from the hydrodynamic setup with the already discussed modifications, still suggested a bit of turbulence in the ventricular pressure waveform. In order to minimise this, we introduced another element which we term as the "**smoothening chamber**". This was connected between the outlet of the elastic ventricular chamber and the inlet of the test valve housing chamber.

The smoothening chamber is essentially a pneumatic only windkessel chamber with the air pocket fully eliminated (the chamber is fully filled with the test fluid). The expansion and relaxation of the walls of the chamber during the systolic and diastolic stage of the pump cycle respectively, provides extra ventricular compliance which aids in smoothening the fluid waveform.

To design the smoothening chamber, we then employed a wide mouth low density polyethylene (LDPE) bottle with an airtight lid. We drilled a hole in the lid and inserted a tube with a stop cock valve fitted at the tip of the tube. The purpose of this valve is to bleed out air. Another hole was drilled a couple of centimetres from the base of the bottle and was fitted with a female to female luer 3 way stopcock valve. This valve has several functions which include introducing or bleeding out fluid and also if necessary, can be fitted with a pressure sensor to monitor fluid pressure. In order to connect this system to the rest of the hydraulic system, tapered barbed ends were designed in CREO 3D and 3D printed. These tube fittings were inserted in holes drilled in the lateral sides of the bottle and were secured with cyanoacrylate glue.

The smoothening chamber was initially exposed to atmosphere to aid rapid filling with the test fluid. Once the chamber was filled to the brim with the test fluid, it was covered with the airtight lid. Any air pockets trapped in the chamber were released via the bleed valve located at the top of the lid. Figures 5.25 and 5.26 show the smoothening chamber in better detail

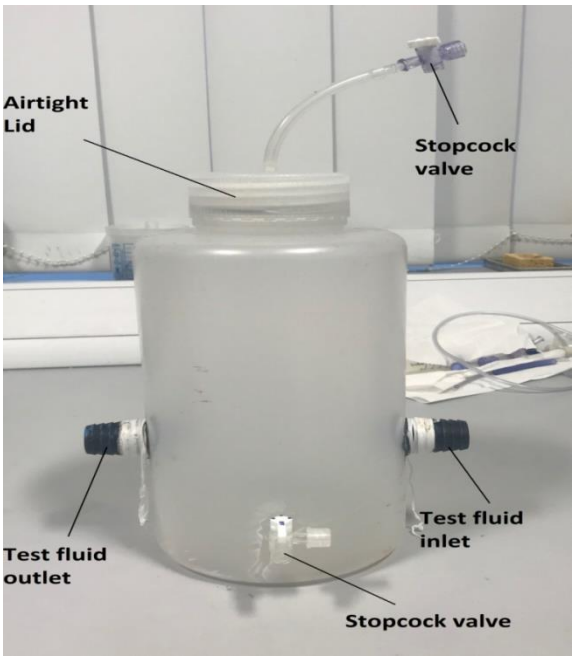

Figure 5.25. A labelled diagram of the smoothening chamber

Figure 5.26. The smoothening chamber between the ventricular chamber and the valve housing chamber

5.2.6.6. ATRIAL RESERVOIR

The atrial reservoir, contains the test fluid that circulates through the hydrodynamic testing rig. This is a plastic cylindrical beaker opened to atmosphere. The atrial reservoir is raised to a height 30cm relative to the other components of the hydrodynamic setup. A hole is made near to the bottom of the reservoir and a 3d printed tapered nozzle fitting is inserted and secured into the hole via cyanoacrylate glue. It is further made watertight by wrapping a bit of thread seal around the hole-nozzle junction and serves as the fluid outlet. A tube is connected from the nozzle fitting, to the inlet of the ventricular chamber. Fluid flows passively from the atrial reservoir into the deformable ventricular chamber via gravity. The check valve fitted in the tube connection also prevents backflow of fluid.

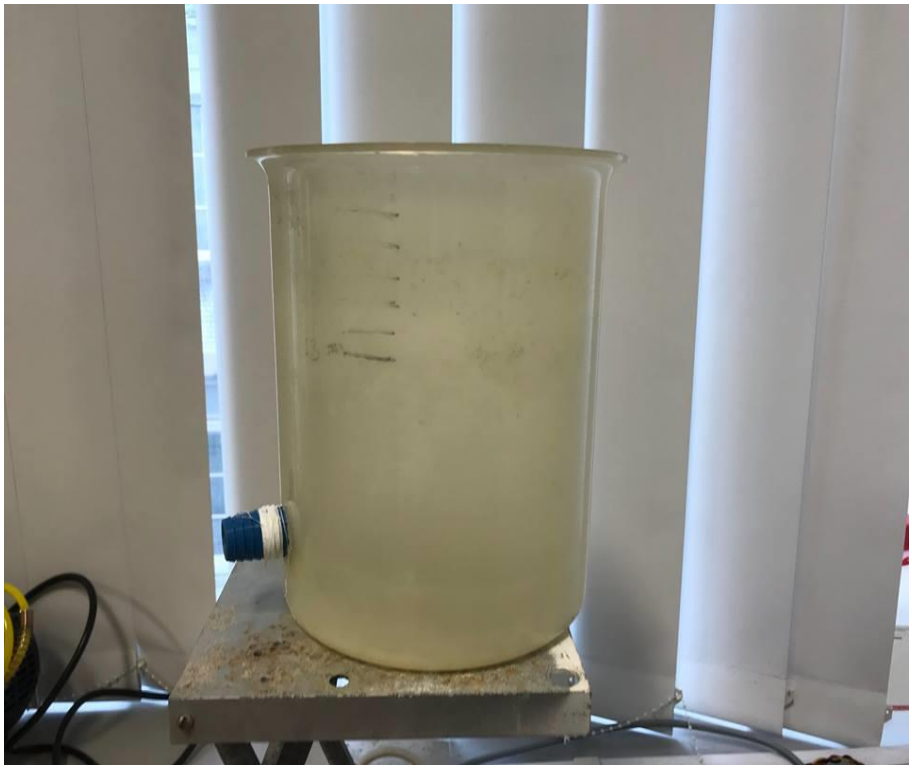

Figure 5.27. The atrial reservoir mounted on a stand

5.2.7. OVERALL DESCRIPTION OF COMPLETED SETUP

The completed hydrodynamic testing rig is to simulate the left side of the heart . The test fluid is housed in the atrial reservoir elevated to a height of 30cm relative to the other components of the setup. The positive pressure head allows fluid to flow under the influence of gravity The test fluid is always kept at the 3litre mark on the reservoir. Fluid flows passively from the atrial reservoir to the bottom part of the deformable ventricular chamber system, which a 15mm brass check valve (ScrewFix, UK) inserted in the tube, close to the ventricular chamber. This check valve represents and functions as a mitral valve. The top part of the ventricular chamber is connected to the pump and is filled with the service fluid. The pumping action controls the movement of an elastic diaphragm in the ventricular chamber system, which in turn controls the movement of test fluid in the bottom part of the ventricular chamber.

Figure 5.28. 15mm check valve(mitral valve). source (https://www.screwfix.com/p/single-check-valve-15mm/38236

Fluid then flows from the ventricular chamber into the smoothening chamber and then moved into the aortic valve housing chamber. The aortic valve housing chamber contains the test artificial valve and contains 2 pressure ports to measure the aortic and ventricular pressure. From there the fluid passes through the systemic compliance chamber and peripheral resistance and then finally back into the atrial reservoir, where the cycle begins again.

Figure 5.29 completed hydrodynamic setup in better detail

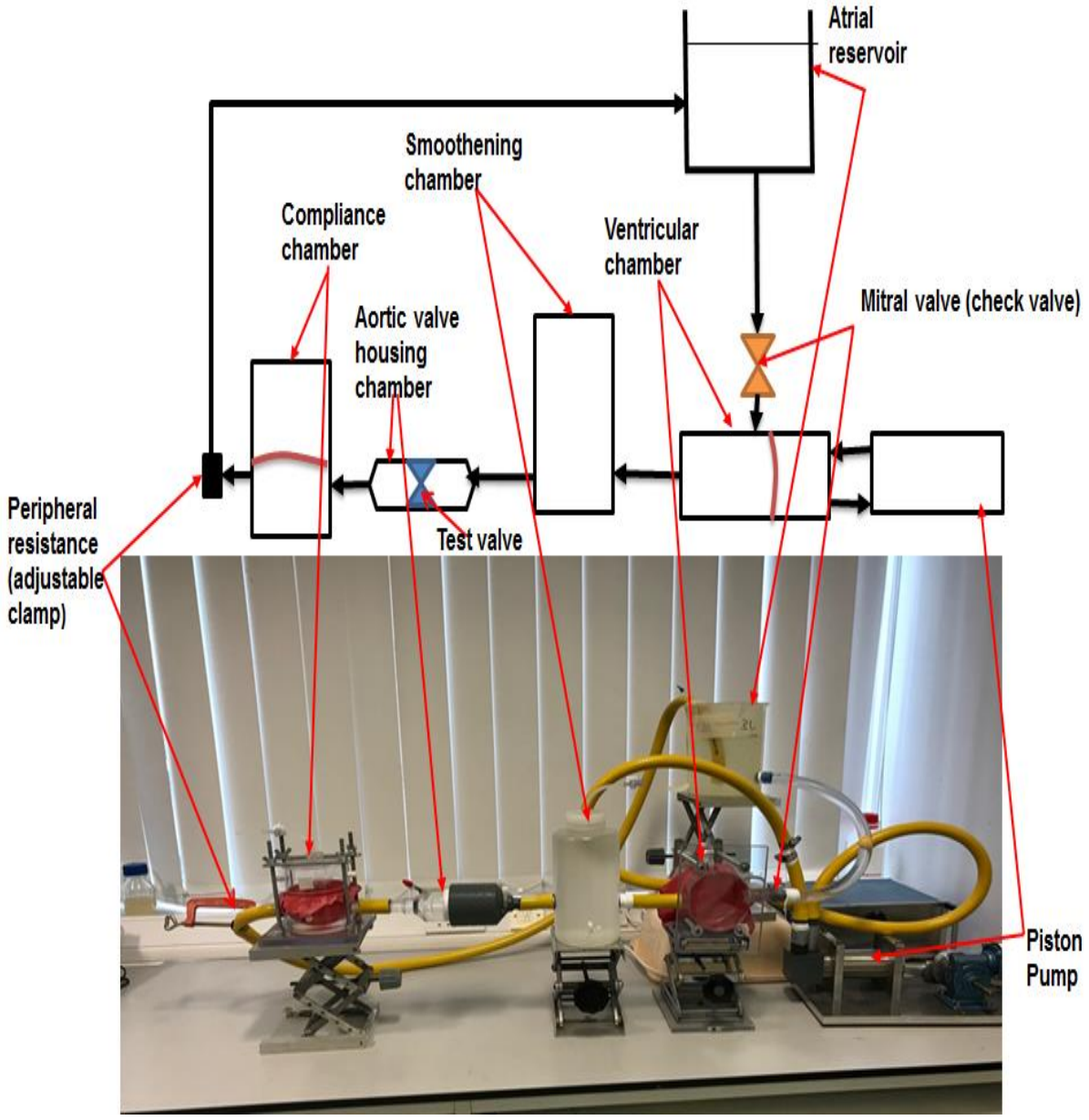

Figure 5.29. Complete setup of the hydrodynamic system. Top shows the schematic diagram and the bottom is an image of the actual system. The black arrows in the schematic diagram shows the direction of fluid flow.

5.3. PULSATILE FLOW HYDRODYNAMIC TESTING OF POLYMERIC AND BIOPROSTHETIC VALVES

5.3.1 INTRODUCTION

En route to market, prosthetic heart valves undergo a series of tests to make sure they meet the standard minimum requirements in accordance with the ISO 5480 standards. One of the tests, performed at the early stage of valve testing, is the pulsatile flow hydrodynamic test. The pulsatile flow test is an invitro test conducted in a simulated physiological environment. This environment is simulated through the use of a pulse duplicator, which is also sometimes referred to as a mock circulatory loop or a hydrodynamic tester. The major aim of this test is to assess and evaluate the fluid mechanic properties of these valves under various physiological and non-physiological conditions. This serves to predict how these valves will perform in vivo. Common parameters assessed during pulsatile flow hydrodynamic testing include the transvalvular pressure gradient, effective orifice area (EOA), regurgitation (back flow) and also the opening and closing times of the valves (Kelley, Marquez and Popelar, 2013).

Our valves are subjected to pulsatile flow hydrodynamic testing in the aortic position. With polymeric valves being a relatively new area of research, it is important to determine whether they are able to meet the minimum required standards other heart valve substitutes such as mechanical and bioprosthetic valves are subjected to. This could further throw light on the potential of polymeric valves as an ideal valve replacement option. Since these valves will also be instrumented with sensors, we need to make sure that the integration of sensors themselves does not cause a change in hydrodynamic function. Performing the pulsatile flow testing prior to instrumenting the valves with the sensors will help us determine that.

This section describes the pulsatile flow hydrodynamic testing of our fabricated polymeric aortic valves. These tests are conducted in our custom made hydrodynamic testing rig which has been explained in detail in section 5.2. of our thesis. Parameters of interest in this study are transvalvular pressure gradient (TVP) and effective orifice area (EOA). Similar tests are conducted on a 27mm Carpenter Edwards SAV model 2650 bioprosthetic valve for comparison.

5.3.2. CALIBRATION OF THE HYDROYNAMIC TESTER

The aortic and ventricular waveform patterns in the pulse duplicator are heavily influenced by the compliance and also resistance. In order to create an ideal physiological pressure environment for testing, adjustments of compliance and resistance is necessary prior to testing. Calibration was performed using the Carpenter Edwards bioprosthetic valve.

A valve holder of height, internal and external diameter of 16mm, 50mm and 40mm respectively, was designed for the bioprosthetic valve. The internal portion of the valve holder has a protrusion which serves as a seat for the valve. The interior of the valve holder is threaded which allows for another threaded male component to be inserted and thus screw the valve tight around the suture ring. This is seen in figure 5.31.

Figure 5.30. The valve holder for the bioprosthetic valve. Top left: Top view of bioprosthetic valve holder. Top right: Side view of the valve holder. Bottom left: Side view of the valve holder with threaded plasic male insert. Bottom right: Bioprosthetic valve inserted in the valve holder.

The valve was then inserted in the valve holder and placed in the valve chamber of the hydrodynamic tester. A 20% glycerol-water solution, similar to the viscosity of blood was employed as perfusate for the hydrodynamic tester. The pump was then switched on to allow perfusate to completely fill the valve chamber. At a pulsatile flow rate of 5.3lmin, compliance

and resistance values were adjusted in real time by varying the volume of air in the top part of the compliance chamber, and also the tightness of the clamp respectively. This was done till aortic pressure waveforms fell within ideal pressure values of (100-130mmHg) systolic pressure and (60-80mmHg) diastolic pressures. Once this was achieved, the air valve in the compliance chamber was shut thus maintaining the air volume and consequently the compliance. The tightness of the clamp, representing resistance, was also maintained once the target pressures had been achieved. The calibration process was repeated prior to testing a new polymeric valve.

5.3.3. DESCRIPTION OF THE PULSATILE FLOW HDRODYNAMIC TESTING PROTOCOL

For the polymeric valve to fit adequately into the valve chamber of the hydrodynamic tester, a valve holder was designed in CREO 3.0 and 3D printed. A clay mould of the interior portion of the valve holder was also made and fitted around the suture ring of the valve prior to inserting the valve into the 3d printed valve holder. This is to ensure a secure fit of the polymeric valve in the valve holder during testing. A picture of the polymeric valve holder and the clay mould and the polymeric valve in the holder, are all shown below.

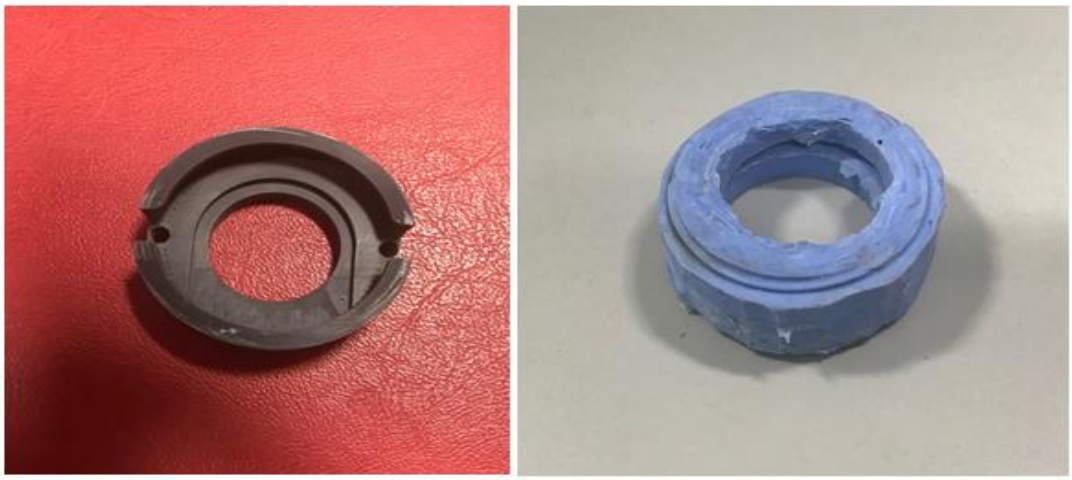

Figure 5.31. Left: 3D printed polymeric valve holder. Right: Clay mould

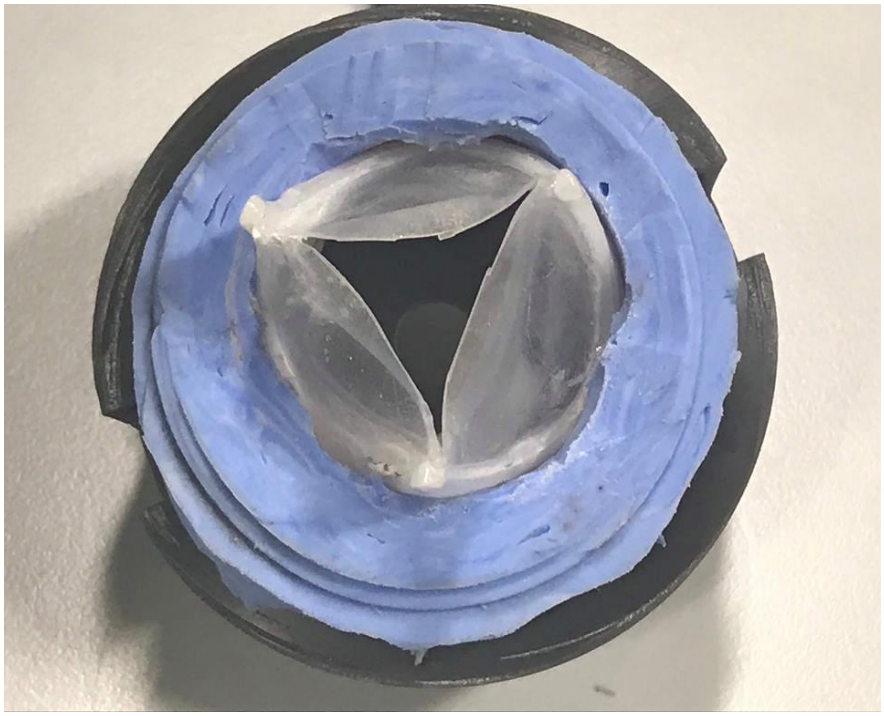

Figure 5.32. Polymeric valve inserted in valve holder.

According to the ISO 5840, pulsatile flow testing should be conducted at 4 different flow rates between 2-7L/min under normal heart rate of an adult at rest. As a result, our study was also conducted at 4 different flow rates ie 2.3, 3.8, 5.3 and 6.9L/min respectively. This was achieved by varying the stroke volume of the pump whilst keeping the pump frequency at a constant 75bpm.

Our 22mm polymeric valve was then fitted into the valve holder and placed in the valve chamber, which was then connected to the rest of the testing rig. Testing begins with the 5.3lmin flow rate. Prior to data collection, the system was allowed to run continuously for approximately 1-2minutes. This allows the test fluid to adequately circulate through the system and also to prime the system to eliminate bubbles.

Data was then collected for approximately one minute after which the pump was stopped , flow rate was adjusted to 3.8L/min and the testing cycle was repeated for 2.3L/min and 6.9L/min in that order. It should also be mentioned that after each flow rate adjustment, the

system is allowed to run continuously for 1-2 minutes to stabilise before pressure data is captured and recorded.

SS13L pressure transducers (Biopac Systems, Goleta, GA) connected upstream and downstream the valve chamber, where used to collected left ventricular and aortic pressure data respectively. These pressure transducers are connected to a Biopac data acquisition module and displayed using the (Acknowledge 4.1) software from Biopac Systems. Pressure data was sampled at 1000 samples per second.

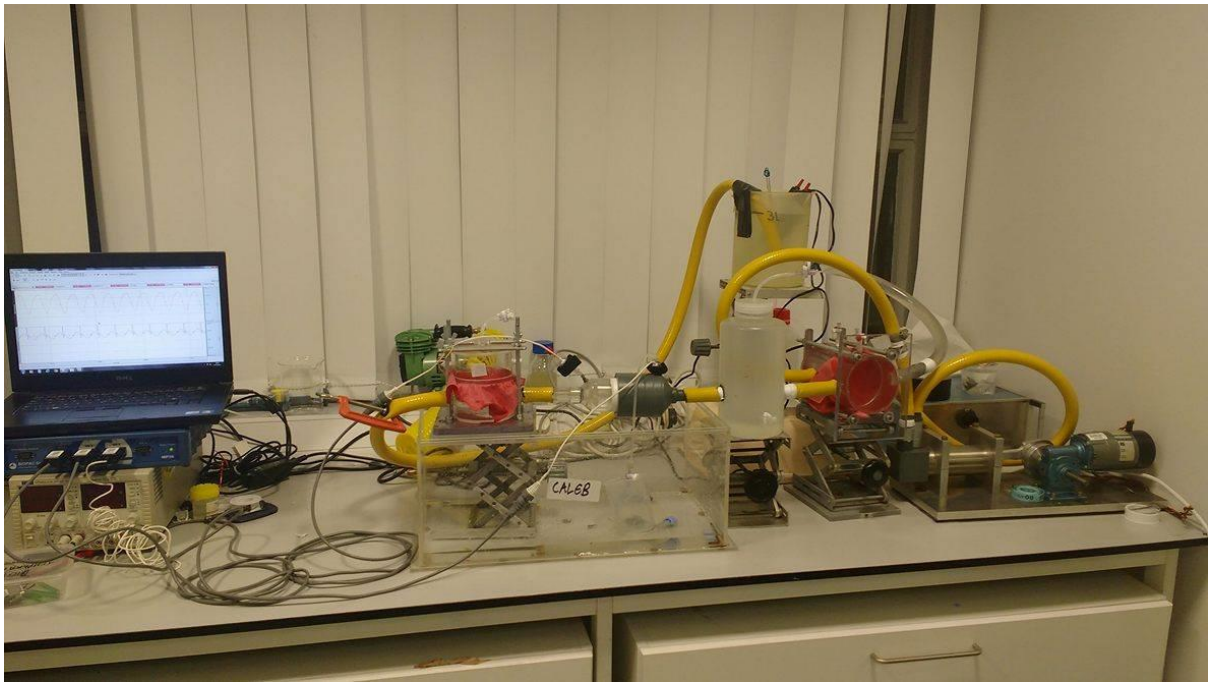

Figure 5.33. Pulsatile Hydroynamic testing in progress. Watertight transparent plastic basin labelled ‘Caleb’ was used to collect fluid spillage which occurred when valve had to be taken out of and or inserted in the hydrodynamic testing rig.

A total of 4 polymeric aortic valves were tested under pulsatile flow hydrodynamic testing. The test fluid was maintained at a temperature off approximately 34-37℃ by fish tank water heaters inserted into the reservoir tank of the hydrodynamic testing rig.

5.3.4. CALCULATION OF THE TRANSVALVULAR PRESSURE GRADIENT

Transvalvular pressure difference, as the name implies, is the difference in the pressure profile across the heart valve. This parameter is very important when evaluating the hydrodynamic performance of the valve as it may be indicative of obstruction to flow due to stenosis (Awtry and Davidoff, 2011).

The transvalular pressure difference for this study, is thus calculated as the mean of the pressure difference between the upstream (Ventricular pressure) and the downstream (Aortic pressure) during the systolic phase and is expressed as the Mean Systolic Pressure Difference (MSPD).

MSPD=$\frac{\sum_{i=1}^{n} \Delta p}{n}$ ..... eq 5.1, where n is the number of data points in the systolic phase and Δp is the pressure difference.

5.3.5 CALCULATION OF EFFECTIVE ORIFICE AREA

The effective orifice area (EOA) is one of the parameters used in particular to assess the severity of valve stenosis. It is a measure of the degree towhich the valve stenosis obstructs flow. This is based on the calculation of the orifice area of the valve via the use of hydraulic principles.

In invitro hydrodynamic assessments of cardiac valves, a common way of calculating EOA is via the use of a formula proposed by Dr Richard Gorlin (Gorlin and Gorlin, 1951). Popularly referred to as "The Gorlin formula", this formula was derived from a combination of bernoulis equation and the flow continuity equation .This section of the our study looks to recap the Gorlin formula, address a very common misconception and also explain some modifications made to the formula in order to preserve its accuracy in recent times. Finally,

we present the complete Gorlin formula employed in our study to calculate the effective orifice area.

According to Gorlin & Gorlin 1990, the generalised formula is as follows

$$EOA(cm^2) = \frac{forward\ flow\ rate\ (Q)}{C \times \sqrt{2\Delta P/\rho}} \ldots\ldots \text{eq 5.2}$$

Where EOA = effective orifice area

Q = forward flow rate

C =discharge coefficient

Δp =pressure difference

ρ=density

The derivation is as follows:

Consider flow through a conduit at 2 points, 1 and 2, with 2 being the point of minimal cross sectional area (vena contracta), which in our case can be represented as stenosis. For conservation of energy, bernouli states that

$$P_1 + \frac{1}{2}\rho v_1^2 + \rho g h_1 = P_2 + \frac{1}{2}\rho v_2^2 + \rho g h_2 \ldots\ldots\ldots\ldots\ldots\ldots \text{eq.5.3}$$

Where P=Pressure, g=acceleration due to gravity, h= height, v= velocity,

Rearranging eq 1 gives

$$P_2 - P_1 = \frac{1}{2}\rho(v_1^2 - v_2^2) + \rho g h_1 - \rho g h_2 \ldots\ldots\ldots\ldots\ldots\ldots \text{eq 5.4}$$

Density and gravity are constant throughout the fluid, and also considering the horizontal nature of the flow conduit, h_1 and h_2 are also equal thus,

$\Delta P = \frac{1}{2}\rho(v_1^2 - v_2^2)$……eq 5.5

At the vena contracta, $v_2 \gg v_1$ assuming constant flow rate, thus

$\Delta P = \frac{1}{2}\rho(v_2^2)$……..eq 5.6

$v_2 = c_v \frac{\sqrt{2\Delta P}}{\rho}$……eq 5.7 where c_v is the viscosity coefficient

For a given flow rate Q, the velocity is determined by the cross sectional area A by the equation

$Q = vA$ ……eq 5.8

However at the vena contracta (point 2), the flow stream contracts towards the centre of the conduit orifice, with a contraction coefficient c_c

$Q_2 = c_c v_2 A_2$…….eq 5.9

Considering flow of an incompressible fluid in a vessel at 2 different points, the continuity equation states that,

$Q_{1=} Q_2 = Q$

Thus $A_{2=} \frac{Q}{c_c v_2}$……eq 5.10

Substitiuting eq 5.7 into 5.10 gives rise to the equation,

$$\boldsymbol{A_2 = \frac{Q}{c_c c_v \times \sqrt{\frac{2\Delta P}{\rho}}}}$$……..eq 5.11.

Where A_2 is the Effective Orifice Area (EOA) expressed in cm^2

$Q = cm^3/s \ \ , \Delta P = g/cm \cdot s^2 \ , \rho = g/cm^3$

Now if this derivation is done properly, then obviously the units should correspond to cm^2. Substituting the units into eq 5.11 gives

$$EOA\ units = \frac{cm^3}{s} \div [\frac{g}{cm \cdot s^2} \times \frac{cm^3}{g}]$$

$$EOA\ units = \frac{cm^3}{s} \div [\frac{cm^2}{s^2}]$$

Since the expression in the $[\frac{cm^2}{s^2}]$ is a perfect square, we can take the square root of it, thus

$$EOA\ units = \frac{cm^3}{s} \times \frac{s}{cm} = \boldsymbol{cm^2}$$

The forward flow Q is the phase of the cardiac cycle at which the valve is in an open state. For the aortic and pulmonary valve, this would be in the systolic phase only, whilst forward flow in mitral and tricuspid valve occurs during the diastolic phase

$$Q(\frac{cm^3}{s}) = \frac{Cardiac\ output(\frac{ml}{\min})}{Heart\ Rate\ (\frac{beats}{\min}) \times SEP\ or\ DFP(secs)} \text{.....eq 5.12}$$

SEP and DFP are the systolic ejection period and the diastolic filling period respectively.

In literature, the constant C in the Gorlin formula ,(see equation 5.2) ,referred to either as the contraction coefficient or the discharge coefficient and is not uncommon to see them being used interchangeably as their numerical values are very similar (Garcia and Kadem, 2006) ie approximately 1 for aortic valves and 0.85 for mitral valves (initially 0.7) (Cohen and Gorlin, 1972).

5.3.5.1 CONTROVERSIES AND POTENTIAL SOURCES OF ERROR WITH THE GORLIN FORMULA

Perhaps in an effort to simplify the formula, the Gorlin formula is presented without the density component in a lot of literature as the density of the fluid is approximated as $1\frac{g}{cm^3}$ (Garcia & Kadem 2006 ; Hakki et al. 1981; Cannon et al. 1992; Bashore 2009). Now whilst this may not necessarily have an adverse influence on the numerical value of EOA, it does causes some confusion as without the density factor, the unit of EOA cannot be mathematically derived as cm^2.

Another hot topic of controversy when it comes to the use of the Gorlin formula is a second constant introduced into the equation. Some researchers quote the Gorlin formula with a second constant 44.3 ie

$EOA(cm^2) = \frac{forward\ flow\ rate\ (Q)}{C \times 44.3 \times \sqrt{\Delta P\ (mmHg)}}, C \sim 1$ (Cannon *et al.*, 1992; Bashore, 2009), whilst others tend to use the constant "44.5" (Hakki *et al.*, 1981), "50" (Blais et al. 2001; Garcia & Kadem 2006) or "51.6 " (De Gaetano et al. 2015; Hui et al. 2018).

Hakki et al. actually further goes on further simplify the Gorlin formula based on their experimental observation that the product of Systolic Ejection Period (SEP), Heart Rate (HR) and the constant 44.5 is approximately 1000 thus simplifying the Gorlin equation down to $\frac{Cardiac\ Output\ (\frac{L}{\min})}{\sqrt{\Delta p(mmHg)}}$.

This is referred to as the Hakki equation and has been used in some literature for EOA calculations (Puymirat *et al.*, 2010; Valenti *et al.*, 2015). Suffice to say, discrepancies in the constant, tend to lead to inaccuracies in the EOA calculation, which has caused the need to investigate the origin and the correct numerical value of the constant.

Revisiting the general Gorlin formula,

$$EOA(cm^2) = \frac{forward\ flow\ rate\ (Q)}{C \times \sqrt{2\Delta P/\rho}}$$

$P = \rho gh, where\ p = density\ (\frac{g}{cm^{3)}}, g\ is\ gravity\ \left(\frac{980cm}{sec^2}\right)$,

Thus $\sqrt{\frac{2\Delta P}{\rho}} = \sqrt{2gh,}\ where\ h\ is\ unity$ (1), thus $\sqrt{2 \times 980}$=44.27~44.3.

This is where the constant "44.3" is introduced. However it should be noted that in their paper, Gorlin & Gorlin specifically mention that the unit of pressure used is cmH_2O. The constant is just a units conversion factor that arises from measuring pressure in **cmH_2O** (Brown, 2018). In standard clinical practice, the unit of pressure used is **mmHg** , thus if Gorlins formula is to be used , it's imperative a unit conversion from cmH_2O to mmHg is done.

1mmHg =1.36cmH_2O, thus

$\sqrt{\frac{2\Delta P}{\rho}} = \sqrt{2gh,}\ where\ h\ is\ unity$ (1), = $\sqrt{2 \times 980 \times 1.36}$=51.6.

This explains the apparent confusion in the constant, if pressure is to be measured in mmHg, then the constant used should be "**51.6"**, not 44.3 as used in the Hakki equation and other cited literature.

The revised and accepted formula for use by ISO 5840 standards for calculating EOA of aortic valves thus becomes,

$EOA(cm^2) = \frac{forward\ flow\ rate\ (Q)}{51.6 \times \sqrt{\Delta P/\rho}}$……eq 5.13

5.3.5.2 COMPLETE FORMULA FOR EOA AS USED FOR THE HYDRODYNAMIC ASSESSMENT IN THIS STUDY

In our study, the flow rate Q, was calculated using the formula in equation 12. The final formula used for the EOA calculations in our study then becomes

$$EOA(cm^2) = \frac{CO}{HR \times SEP \times 51.6C \times \sqrt{\Delta P/\rho}} \text{.....eq 5.14}$$

- CO= Cardiac output (ml/min)
- HR= Heart Rate (beats per min) : 75bpm
- SEP= Systolic Ejection Period (s) : 0.37 s
- C=Discharge coefficient : 1
- ΔP= Mean Systolic Pressure Difference (mmHg)
- ρ=density (g/cm^3). At 20% glycerol –water solution, ρ ~1.04

5.4. INVESTIGATING THE EFFECTS OF VALVE STENOSIS ON TRANSVALVULAR PRESSURE

5.4.1 INTRODUCTION

Stenosis is defined as the narrowing or obstruction of the valve opening (Bender, 1992). One of the variables used in clinical settings to diagnose stenosis is the transvalvular pressure gradient. When the aortic valve is obstructed over time, the ventricle is forced to work harder to pump blood through the obstructed valve resulting in an elevated ventricular pressure relative to the aortic pressure, thus causing a higher transvalvular pressure gradient. Valvular stenosis is however said to be a slow progressive disease with patients being asymptomatic until the disease becomes severe (Maganti *et al.*, 2010) With this being said, it is difficult to diagnose early the onset of valvular stenosis.

Investigating the effects of stenosis on transvalvular pressure gradient in an invitro setup may provide initial information as to the mechanics and also the progressive nature of stenotic valves. Furthermore, since our valves will ultimately be instrumented with sensors, data from this study will be used to validate the sensor output.

In this study, we investigate the effect valvular stenosis has on transvalvular pressure gradient, in our bespoke hydrodynamic testing rig.

5.4.2 SIMULATION OF STENOSIS

Stenosis was simulated as obstruction to the valve opening at the base of the valve. It should be noted that simulation of stenosis in this study is not meant to mimic the biological nature of which stenosis occurs , but rather the mechanical and pathophysiological effect of flow obstruction on the valves.

Four varying degrees of obstruction were simulated via the use of obstruction discs with varying internal diameters. The values of the internal diameters of these obstruction discs were calculated as percentages of the valve annulus diameter for both the polymeric valve and the Carpenter Edwards bioprosthetic valve. Levels of valve obstruction were varied in 25% increments, i.e. from no obstruction (0%) to 75% obstruction.

Obstruction discs for the polymeric valve were designed in CREO 3D and 3d printed. Slits designed in the polymeric valve holder, allows for these discs to be fitted snugly in the valve holder, thus effectively reducing the internal diameter of the valve exposed to flow, once the valve is inserted in the holder. Obstruction discs for the bioprosthetic valve were machined from polyoxymethalene (POM) rods.

The dimensions of the internal diameters of the obstruction discs for both polymeric and bioprosthetic valves are shown below.

Obstruction (%)	Bioprosthetic valve (mm)	Polymeric valve (mm)
0	27	22
25	20.25	16.50
50	13.50	11
75	6.75	5.50

Table 5.1. Internal diameter dimensions of the polymeric and bioprosthetic valve obstruction discs.

Figure 5.34.Obstruction discs used to simulate the 4 various degrees of valve stenosis/obstruction, from 0%-75% obstruction, from left to right respectvely. Top: Polymeric valve. Bottom: Bioprosthetic valve

5.4.3 DESCRIPTION OF THE EXPERIMENTS

Obstruction tests were conducted in our hydrodynamic testing rig. The testing rig was calibrated prior to the testing. This calibration process has already been described in section 5.2.3.

After calibration, the polymeric valve was then inserted into the valve holder with the 0% obstruction disc in place. This was then placed into the valve holder. The pump was then set to 5.3L/min flow rate and allowed to run continuously for approximately 2 minutes, thus allowing test fluid to fully fill the valve chamber. After this process, the actual testing then begins. This is described below

At the 5.3L/min cardiac output, aortic and ventricular pressure data was collected for over a minute after which the pump was stopped. The flow rate was then reduced to 3.8L/min after system was allowed to run for about another 2 minutes to allow system to acclimatise to the new flow rate. Pressure data was then recorded at the new flow rate for over a minute. The cycle was then repeated for 2.3L/min and 6.9Lmin respectively. The polymeric valve was then taken out of the holder and visually inspected for defects. Subject to passing the visual inspection test, the valve was then put back in the holder, this time with the 25% obstruction disc, and the testing cycle repeated again. The same process was repeated for the 50% and the 75% obstruction conditions respectively.

	0% Obstruction
1	Flow rate adjusted to 5.3L/min
2	2 minute system run
3	Data recorded at 5.3 L/min (>1min)
4	Pump stopped
5	Flow rate adjusted to 3.8L/min
6	2 minute system run
7	Data recorded at 3.8L/min (>1min)
8	Pump stopped
9	Flow rate adjusted to 2.3L/min
10	2 minute system run
11	Data recorded at 2.3L/min (>1min)
12	Pump stopped
13	Flow rate adjusted to 6.9L/min
14	2 minute system run
15	Data recorded at 6.9L/min (>1min)
16	Pump stopped
17	Valve taken out, inspected for defects, obstruction disc inserted
18	Valve with new obstruction disc inserted back into the hydrodynamic system

Table 5.2. Sequence of events in the obstruction testing experiment under the 0% obstruction condition. These sequence of events where repeated for the 25%, 50% and 75% obstruction conditions respectively.

A total of 4 polymeric valves underwent the obstruction test. The same test was also conducted on the Carpernter Edwards SAV 2650 bioprosthetic valve for comparison. Pressure data was analysed over the best 15 continuous cycles per recording. The description of the test fluid and equipment used for data recording are already described in section 5.3.3.

5.5. INSTRUMENTATION OF POLYMERIC VALVES

5.5.1. INTRODUCTION

The main aim of our study was to investigate whether instrumenting valves with sensors capable of detecting pressure changes could provide useful diagnostic information in terms of

detecting the onset of valve stenosis. In order to achieve this, it is imperative that the right sensor be acquired. It is also important that we explore the best way to fit the sensors in order to get the best results and not to interfere with the valve function. In this section, we describe ideal sensor characteristics for instrumenting these valves. We also describe the procedure for instrumenting the valves and finally the experiments conducted in order to acquire data from the sensors indicative of pressure changes as a result of valve stenosis.

5.5.2. THE IDEAL SENSOR CHARACTERISTICS

Hitherto, the variable of interest in our study on stenosis had been transvalvular pressure. This had been achieved by attaching two SS13L pressure transducers on the manometer ports in our valve chamber. These ports, situated distal and proximal to the heart valve had allowed us to detect upstream and downstream valve pressure with good fidelity. Armed with this information, the difference in pressure i.e. the transvalvular pressure had been determined.

It should however be mentioned that if the sensors are to be physically attached or intergrated into the valve it will be practically impossible to detect pressure across the valve ie TRASVALVULAR pressure gradient as this will require attaching sensors proximal and distal to the valve.

Faced with this challenge, it was decided that a better solution would be to insert the sensors inside the valve i.e. in the interior portion of the valve stent. Changes in the sensor readings would then be monitored as stenosis is simulated. As a result, the variable of interest for the instrumented sensors would be INTRAVALVULAR pressure i.e. pressure in the valve annulus. With the location of the sensor placement now resolved, the next task was to determine the required characteristics of the sensor.

It should be noted that sensors to be employed in this work were going to be either readily made commercially available ones , or custom made by a third party. It was never the aim to

design these sensors ourselves. With that being said, we had to identify the ideal sensor specifications.

SIZE: One of the more important sensor considerations was the size of the sensor itself. Given that the sensor would be attached to the interior of the stent, it is important that the sensor be small enough to fit the surface of the stent. Having too big a sensor would make the entire system bulky non-functional and has the potential to interfere with the valve function. Further to that, having a large sensor attached to the interior portion of the stent, where it will be exposed to flow, would in itself introduce an element of obstruction to flow. Since the entire purpose of the study is to determine if the sensor would be able aid in diagnosis of valve stenosis, a larger than ideal sensor may impact on the factor it is designed to measure, which will ultimately influence the quality of the data acquired.

The surface of the interior portion of the stent is in triangular in shape with a surface area of approximately 122mm^2. The sensor will be placed at the centre of this surface with dimensions 7mm by 7mm and radius of curvature of approximately 60mm. These dimensions helped to set the limits of our ideal sensor size. Thus the preferred dimensions of the sensor were selected as being ≤ 7mm length by 7mm width. The sensor should also be very thin so it doesn't protrude and interfere with the flow mechanics within the valve ideally <3mm.

OPERATING PRESSURE AND TEMPERATURE RANGE: The polymeric valves are tested in a hydrodynamic testing rig which simulates in vivo conditions including blood pressure and temperature. These sensors will be attached to the valves and subjected to the flow, pressure and temperature conditions of the testing rig. As a result, it is imperative that the operating pressure and temperature range of the sensor fall in the range of blood pressure and temperature generated by the hydrodynamic testing rig, in order to not compromise the accuracy and reliability of the sensor output.

The hydrodynamic testing rig employed for this project focuses on simulating the left side of the heart thus pressure ranges of interests are the aortic and ventricular pressures. Previous tests have already been performed on polymeric heart valves under different flow rates and stenotic conditions, which generated a range of aortic and ventricular pressures. It was discovered that the hydrodynamic testing rig generates systolic aortic pressures from 50mmHg to 170mmHg, with aortic diastolic pressures also ranging from 20-85mmHg. Systolic ventricular pressure ranged from 60-240mmHg. Ventricular diastolic pressure had values in the negative range due to the intrinsic high suction properties of the pump employed for the hydrodynamic testing rig, i.e. between (-20 to -100mmHg). The aforementioned pressure values are dependent on the flow rate and the degree of stenosis. Since the instrumented valves will be subjected to the same testing conditions, the sensors should be able to detect pressures within these specified ranges.

In the hydrodynamic testing rig, the temperature of the test fluid in the atrial reservoir is kept between 34-37℃ by two Hidom Pro Heat Quartz Glass Heater (Hidom Electric Co Ltd, Shenzhen). This was monitored by a glass thermometer. It should however be noted that as the fluid circulates through the system, some heat will be dissipated. Factoring heat loss and allowance for flexibility of sensor choice, we estimated an operational temperature range of the ideal sensor to be between 20-40℃.

OPERATING MEDIUM: The instrumented valve would be fully submerged in the test fluid during testing, thus the ideal sensor should be fluid compatible.

BIOTELEMETRY: At this stage of the project, the aim is to determine whether sensors would be able to provide diagnostic information regarding prosthetic valve stensosis. The ultimate and ideal end goal would be to implant these valves in vivo. Being able to transmit data wirelessly is a hallmark of a good implantable sensor. In this invitro testing stage of the

project, having a sensor with inbuilt telemetry capabilities, will eliminate the needs for wires allow for easy instrumentation and will provide a more accurate representation of how the sensor could work with the valve invivo, thus reducing the learning curve from invitro to ultimate in vivo application.

A summary of the ideal sensor specifications, complete with tolerance, are summarised in the table below

SIZE	<7mm length by 7mm width by 3mm height
OPERATING TEMPERATURE	20-40℃
OPERATING PRESSURE RANGE	-100 to 240 mmHg (-0.13332 to 0.32 bar)
OPERATING MEDIUM	Fluid
BIOTELEMETRY	Yes

Table 5.3. Ideal sensor specifications

CHALLENGES FACED WITH ACQUIRING IDEAL SENSOR

During the initial search for an ideal pressure, a sensor developed by a Stanford university based research group, led by Zenan Bao, became of interest. These are ultra-miniature passive sensors, with sizes as small as $1mm^2$ surface area, with a 0.1mm thickness. Telemetry is incorporated via inductive coupling. These sensor have been tested on the radial artery to validate wireless pulse pressure monitoring, have undergone invivo testing in mice and have shown the capability to detect pressures up to 500mmHg (Chen *et al.*, 2014). These sensors are believed to have been ideal for our application as they meet all our requirements. However upon further research, it was discovered that these sensors were hitherto, not

commercialised thus were unavailable for purchase and a collaborative agreement with the PI couldn't be established in time.

During our search, some commercially available pressure sensors did catch our attention. Although some sensors did meet our required specifications, none of them meet all the requirements. Some of these sensors are summarised below.

The ESCP2 M6 is a capacitive wireless pressure sensor (European Sensor Systems, Greece). This sensor is cylindrical in shape and has Bluetooth wireless capability over a 100m with a lithium battery power supply. This sensor can also be used in harsh fluid environments which would have been ideal for our application. However its large dimensions i.e. (26mm diameter and 90mm height) and high operational pressure range (>1bar) made it unsuitable for our intended application.

The ME 790 and ME 75X series (Mettalux, Switzerland), are cylindrical piezoresistive pressure sensors with operational pressures ranging from as low as between 0-0.15bar to 0-400bar depending on the model. This initially caught our attention due to the low operational pressure range. Although they are considered small, their sizes exceeds the size requirements for the ideal sensor (18mm diameter, 7.35mm height for ME 790, 18mm diameter, 15mm height for the ME 75X).

Other sensors /transducers considered were miniature sized pressure sensors such as EPIH, EPB, EPL and the XPR46 series (TE Connectivity, Switzerland). From a physical size stand point, these sensors were closest to our required dimensions of the sensing element and could detect low pressures such as 0-0.35bar. All the sensors came with connecting lead wires and couldn't incorporate wireless telemetry. The EPIH sensors were however fluid media incompatible.

These examples of sensors are by no means an exhaustive . They simply highlight examples of commercially available sensors that were of interest with respect to our application.

It was discovered during the search for pressure sensors that it was going to be very difficult to find a sensor that met all our specifications. In order to be able to find a sensor for this intended project, it was necessary to go back to the drawing board and take a second look at possibly redefining the specifications of the sensors. Below presents some compromises made to the sensor specifications.

BIOTELEMETRY: Being able to transmit sensor data wireless would be very ideal for remote invivo valvular pressure monitoring, which is the ultimate end goal of the project. It should however be mentioned that for the scope of this project, the sensors would be attached to the valves and tested IN VITRO in response to simulated stenosis. At this stage of the project, wireless transmission of sensor data is not necessarily a requirement for successful experiments. Sensor data could be transferred via insulated wired lead connections and then connected to a data acquisition and display system in close proximity to the hydrodynamic setup.

OPERATING PRESSURE RANGE: We previously stated the operating pressure range to be between -100 to 240mmHg, based on previous experiments conducted in our bespoke hydrodynamic testing rig. During the search for the ideal sensor, it was discovered that ultra-miniature pressure transducers capable of detecting low pressures, are designed to only detect pressure in the positive ranges, which is understandable since in vivo blood pressures are also in the positive pressure ranges. Our hydrodynamic setup did generate non physiological negative pressures during the ventricular diastole phase. With the limitations of commercial ultra miniature pressure sensors in terms of detecting negative pressures, and also the non physiological nature of negative pressures, we decided to redefine our operational pressure

range to eliminate negative pressures. Thus the new practical operating pressure range was set to (0-240mmHg).

Specifications on size, operating temperature range and operating medium could not be compromised without affecting our ability to conduct the experiments. Furthermore, operating temperature range was not an issue as most pressure sensors did meet that requirement.

Armed with this information, we were able to narrow our choices to the EPB and EPL sensor series. At this point, it was necessary to consider another pressing limitation, which is cost. According to information given by suppliers (Strainsense, UK), these sensors range from (£862 to £939) each. Conducting an experiment of this nature would include multiple testing and familiarisation with the sensors. It is obvious that multiple sensors would be required which would further increase the costs significantly. As a result we needed to consider other low cost options of achieving the desired effect.

5.5.3. MAKING THE CASE FOR STRAIN GAUGES

Strain gauges are sensors used to measure displacement or strain. They consist of either a thin conductor in the form of a wire, or a metal foil. Its principle of operation is as follows; when a force is applied on the gauge, it causes a change to the cross sectional area and also the length of the wire thus causing a change in the electrical resistance. Mathematically,

$R = \rho \frac{L}{A}$ Where L= length, A=cross sectional area and p is the resistivity of the wire of foil material. A force that causes the strain gauge to go in tension, will increase the length and also reduce the cross sectional area thus causing an increase in resistance. A contraction force will cause the opposite effect (Neuman, 2000). The strain gauge is then connected to a wheatstone bridge which generates a voltage output proportional to the change in resistance. This voltage output is representative of the strain or displacement of the gauge.

Strain gauges are used in various applications such as load cells to detect forces. A force applied on the gauge causes the tension or compressive strain of the gauge, thus force can be detected by measuring the strain or the displacement of the strain gauge. Strain gauges also form the basis of a wide range pressure transducers. Pressure transducers consist of a diaphragm which deforms as the pressure is introduced. In pressure transducers incorporating strain gauges, a strain gauge is attached to the diaphragm thus detecting the strain. The change in strain is then represented as a change in pressure (Mootanah and Bader, 2006).

In our application, we require a sensor that is very small, thin, low cost and also able to detect pressure thus making strain gauges an ideal candidate for this project. Although strain gauging valves in general seems to not be very common, researchers such as Lin et al, 2010 have also successfully experimented with the use of microscale strain gauges to detect strain on polyurethane valve leaflets. They achieved these by attaching the strain gauges directly to the surface of the valve leaflets themselves.

Strain gauges, although very rudimentary , actually do meet all the practical sensor characteristics already defined for this project stated above and are also low cost, thus providing a more practical option for use. These strain gauges will be attached to the interior portion of the valve stents to detect deflections as a result of pressure changes.

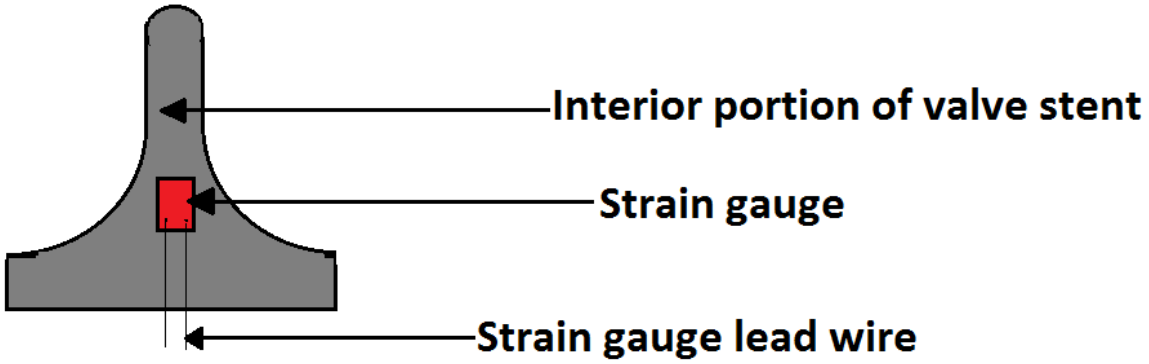

Figure 5.35. A drawing showing the strain gauge positon on valve stent

The FLA-2-11-3LJCT (Tokyo Sokki Kenkujo Co, Ltd, Tokyo) with a gauge factor and resistance of 2.14 and 120 ohms respectively was employed for this study. It has a gauge length of 2mm and 3 vinyl lead wires with length of 3m and temperature range from -20 to 80℃. A pack of 10 strain gauges cost less than £100 thus making it cost efficient.

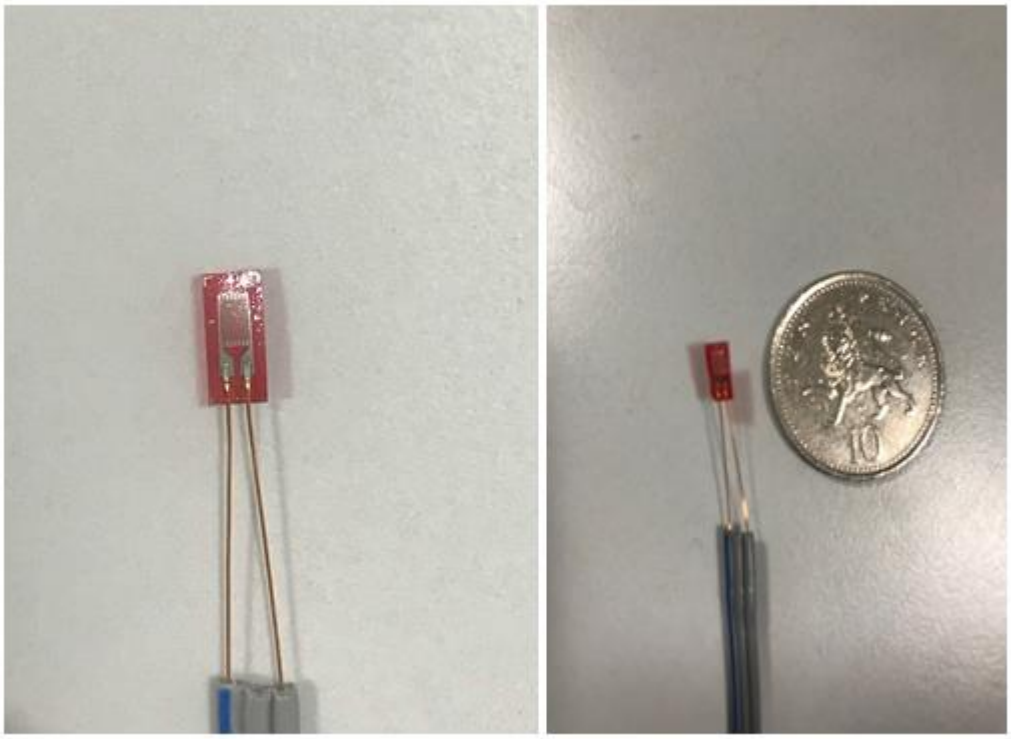

Figure 5.36. Strain gauge used to instrument polymeric valves

5.5.4. STRAIN GAUGE INSTALLATION PROCEDURE

Before the strain gauge could be bonded to the inner surface of the Delrin valve stent, the surface had to be prepared for optimised bonding of the gauge.

1. The surface was initially wiped down with 70% rubbing alcohol and gauze.
2. A few drops of M-prep conditioner A (MCA-1) was then applied unto a sandpaper and the surface was sanded down with the conditioner.
3. A few drops of M-prep neutraliser (MN5A-1) was then applied unto a piece of sandpaper and surface was sanded down with the neutraliser

4. Steps 2 and 3 were repeated 7 times
5. Surface was then exposed to UV light for approximately 30minutes

The strain gauges also needed to be prepared. The strain gauge was laid horizontally on a clean flat surface. A piece of clear Mylar tape was then stretched over the strain gauge and pressure was applied to ensure the strain gauge adhered to the tape. If done correctly, pulling the tape back will automatically lift the strain gauge off the surface thus exposing the underside of the gauge. A drop of cyanoacrylate glue is then applied to the underside of the gauge and also the surface of the stent and the 2 surfaces are brought into contact with each other. Constant pressure is applied over the Mylar tape for approximately 10-15mins. The Mylar tape is finally totally stripped away thus leaving the strain gauge bonded to the stent surface. This completes the installation procedure.

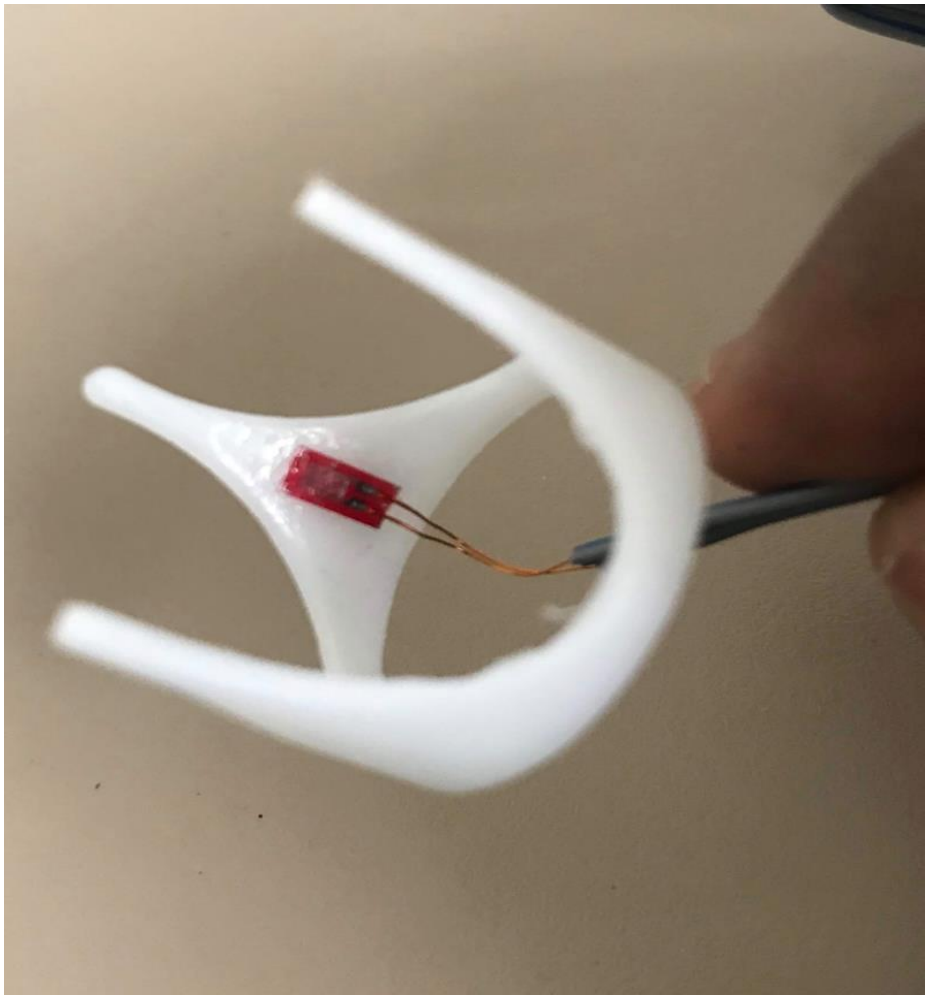

Figure 5.37. Strain gauge successfully bonded to the inner portion of the valve stent

The strain gauges where attached to the stent prior to formation of the valve leaflets via dip coating. The valve leaflet formation process has already been described in section 5.1.3, however there was one major difference in this case. Previously, the formation process had involved heating up the mandrel prior to slipping the stent over it and also exposing the mandrel setup to heat after each dip coating cycle. Since the strain gauge properties are temperature dependent and operate in a temperature range, we eliminated the process of

exposing the mandrel to heat so as to not potentially reduce the integrity and reliability of the stain gauge.

The strain gauge, in its raw form, is not fluid compatible thus the surface of the strain gauge had to be protected if its intended use is in a fluid medium. After the valves have been formed and removed from the mandrel, a thin layer of polymeric solution was then applied over the strain gauge and left to dry thus forming a thin fluid resistant protective barrier.

Figure 5.38. Polymeric heart valve instrumented with strain gauge

5.5.5. DESCRIPTION OF THE EXPERIMENTS WITH STRAIN GAUGES

The aim of this experiment is to investigate the ability of the sensors to detect intravalvular pressure changes as a result of simulated stenosis. Pressure changes will be detected by measuring the strain or deflection of the valve stent these gauges are bonded to. In the cardiac cycle, systolic phase occurs as an increase in pressure and inversely, a decrease in pressure during the diastolic phase. As a result, we hypothesize that the systolic phase will present as an increase in strain and the diastolic phase, a decrease in strain accordingly.

This experiment is conducted in the hydrodynamic testing rig already developed and described. Strain gauged valves were tested under 4 flow rates i.e. 2.3, 3.8, 5.3 and 6.9L/min and also under 4 simulated stenosis (from 0% to 75%). The details of the obstruction discs used to simulate stenosis, has already been outlined in section 5.4.2. Since the strain gauges have lead wires connected, modifications had to be made to the valve holder and also the obstruction discs to allow for the wires.

A small hole was made in the ventricular section of the valve holder and also in the obstruction discs. This is to make sure the strain gauge wires can pass though the valve holder and connected to the strain gauge recorder outside the hydrodynamic testing rig. These modifications are shown in figures 5.41 and 5.42 below.

Figure 5.39. Bottom view of the strain gauged polymeric valve in the valve holder with the 75% obstruction disc. Hole has been drilled in the obstruction disc to allow for the lead wires of the strain gauge.

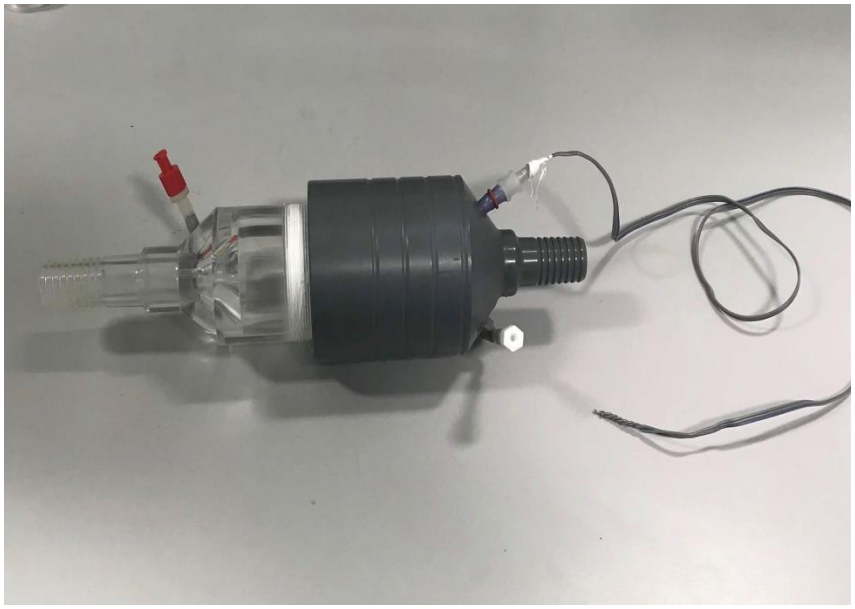

Figure 5.40. Strain gauged valve placed in valve housing chamber prior to connecting to hydrodynamic testing system and strain gauge recorder. An extra hole has been drilled into the grey section of the valve housing chamber to allow the strain gauge lead wires to be connected to the recorder

Strain gauged valves were inserted into the valve holder and connected to the hydrodynamic system. The lead wires from the strain gauge were connected to the Model P3 strain indicator and recorder (Vishay Micro measurements, North Carolina) in a quarter bridge configuration. Strain gauge data was sampled at 1 sample per second. This was the highest sampling rate that could be set on the Model Ps strain indicator

Figure 5.41.Model P3 strain gauge indicator and recorder with the 3 strain gauge lead wires connected in a quarter bridge configuration.

Valves were tested starting with the 5.3lmin flow rate, at no obstruction condition for a few cycles. Valve was then taken out, and the 25% obstruction was introduced and tested. Similar process was then repeated for the 50% and 75% obstruction state. The entire cycle was repeated for the 3.8, 6.9 and 2.3L/min respectively. It should be mentioned that the strain gauge recorder was zeroed/balanced every time a valve was disconnected from the recorder. This happened prior to testing valve under either a different flow rate or obstruction condition. Furthermore, the hydrodynamic testing rig was allowed to run continuously for approximately for 2-3 minutes prior to recording strain data. Strain data was recorded via an SD card inserted in the recorder. Aortic and ventricular pressure data was also recorded simultaneously with the Biopac pressure transducers connected to the valve chamber. The sample rate of the Biopac data acquisition system was set as equal to that of the strain gauge recorder (1 sample per second) to allow for uniformity.

We were also interested to see the long term reliability of the strain gauges, thus testing under flow rate of 5.3L/min under the no obstruction condition was performed for 10 hours continuously.

A total of 4 polymeric valves underwent testing with water kept between 34-37℃, as test fluid.

5.6 SUMMARY

In this chapter, the fabrication of the polymeric valves used in our study has been described. We then describe the design of the hydrodynamic testing system. This system is designed to simulate the left side of the heart. The initial setup and its limitations in terms of replicating the adequate physiological environment is described. Improvements were made to the system by incorporating a 2 element windkessel model to simulate systemic compliance and peripheral resistance. Hydrodynamic testing of the polymeric heart valves were performed to assess the transvalvular pressure gradient and the effective orifice area (EOA) of the valves. Another experiment was also performed to investigate the effect of valve obstruction on the transvalvular pressure. A total of 4 polymeric valves were tested under 4 different flow rates between 2-7L/min under constant pump speed. A Carpentier Edwards SAV 2650 bioprosthetic valve was used as control.

We also described the ideal sensor characteristics for instrumenting the heart valves and various limitations in sensor acquisition. Following that, we make a case for why strain gauges can provide a practical option in terms of detecting deflections of the valve stent due to pressure changes resulting from simulated stenosis. We have described the process of installing the strain gauges in the valves and also the tests conducted with the instrumented polymeric valves in the hydrodynamic testing rig. These tests were conducted under 4

different flow rates and 4 levels of simulated stenosis. Finally we also performed continuous testing for 10 hours in order to investigate the reliability of the strain gauges.

CHAPTER 6 RESULTS

6.1 VALVE MANUFACTURE

To determine leaflet thickness of the valves, another batch of 6 polymeric valves were developed consecutively using the protocol outlined in section 5.1.3. The leaflets were then

removed from the stent and an RS Pro 150mm digital calliper was used to measure the valve thickness at the free edge and also the belly of each of the 3 leaflets per valve.

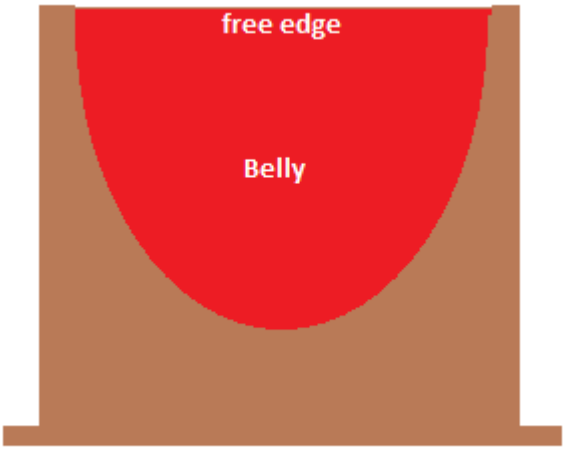

Figure 6.1. Longitudinal section of polymeric valve showing the 2 locations on the leaflets where thickness measurements were taken.

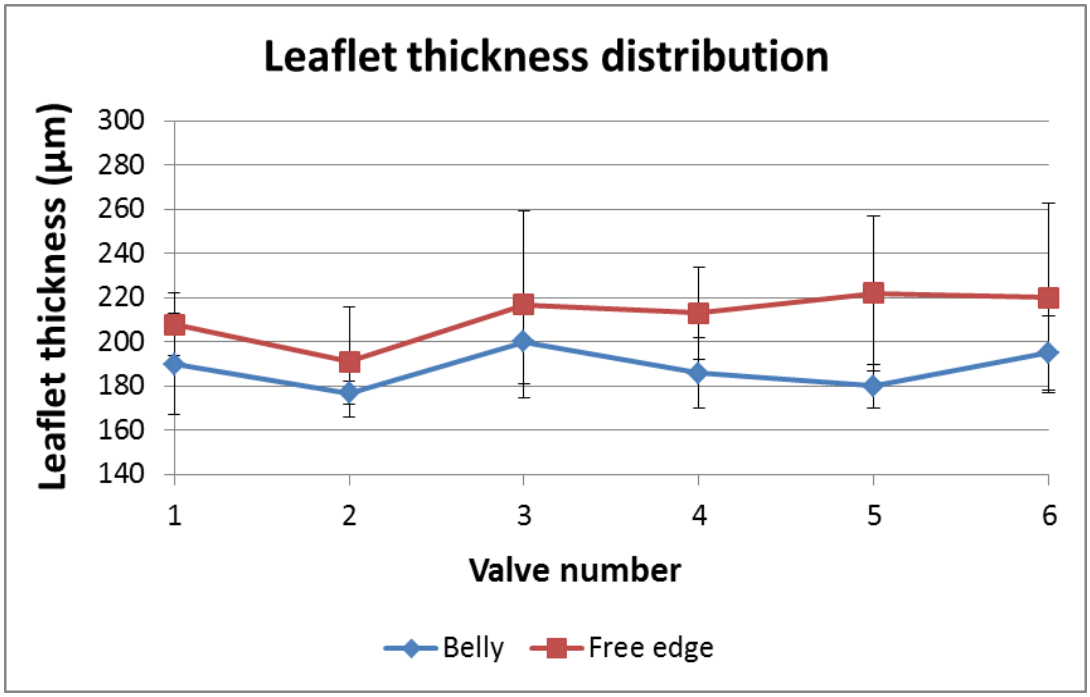

Figure 6.2. Leaflet thickness distribution of 6 polymeric valves at the belly and free edges. Data is presented as mean and standard deviation with n=3 (ie 3 leaflets per valve).

6.2 THE PULSE DUPLICATOR

The hydrodynamic tester generates flow rates between 1.8 and 8.8L/min. Physiologically, these represents the cardiac output. As explained earlier in section 5.2.3, the stroke volume and heart rate are determined my adjusting the screw position on the pump drive wheel and also the dial on the pump speed regulator respectively. The cardiac outputs were then determined by multiplying the stroke volume by the heart rate.

According to ISO 5840 standards for cardiac valve testing, cardiac outputs for pulsatile flow hydrodynamic heart valve testing should be calculated at a constant heart rate (75bpm) and then varying the stroke volume. Similarly we used the same process to determine the range of cardiac outputs being determined by the pump. ISO 5840 further states that pulsatile flow hydrodynamic testing should be conducted under 4 different cardiac outputs between 2-7L/min.

During the pump calibration stage (section 5.2.3), it was determined that setting the pump speed regulator dial to "6", generates a pump speed of 75 beats per minute. This speed position was kept constant and the stroke volume of the pump was varied to generate the cardiac outputs of the piston pump as according to the ISO 5840 requirements. The results of the cardiac output calibration is presented in table 6.1 below

Screw position on drive wheel	Stroke volume (ml)	Cardiac Output (L/min)= Stroke volume x 75bpm
1	118.4	**8.8**
2	108	**8.1**
3	92	**6.9**
4	77	**5.8**
5	71	**5.3**
6	60.6	**4.5**
7	51	**3.8**
8	34.7	**2.6**
9	30.6	**2.3**
10	24.5	**1.8**

Table 6.1. Cardiac output settings for the piston pump. The 4 highlighted rows, show the flow rates between 2-7L/min employed for heart valve testing. Cardiac output values are rounded to 1 decimal place.

We show below in figures 6.3 to 6.10, sample pressure waveforms generated in the hydrodynamic tester during the bioprosthetic valve pulsatile flow testing. These pressure waveforms were recorded and saved in a Microsoft Excel worksheet.

All the wavefroms shown below are colour coded for easy identification. The red wavefrom represents the Left Ventricular Pressure waveforms. The blue wavefrom represents the

Aortic Pressure waveforms. The green waveform is the Transvalvular Pressure Gradient (TVPG), which is determined by subtracting the Aortic Pressure from the left Ventricular Pressure waveforms

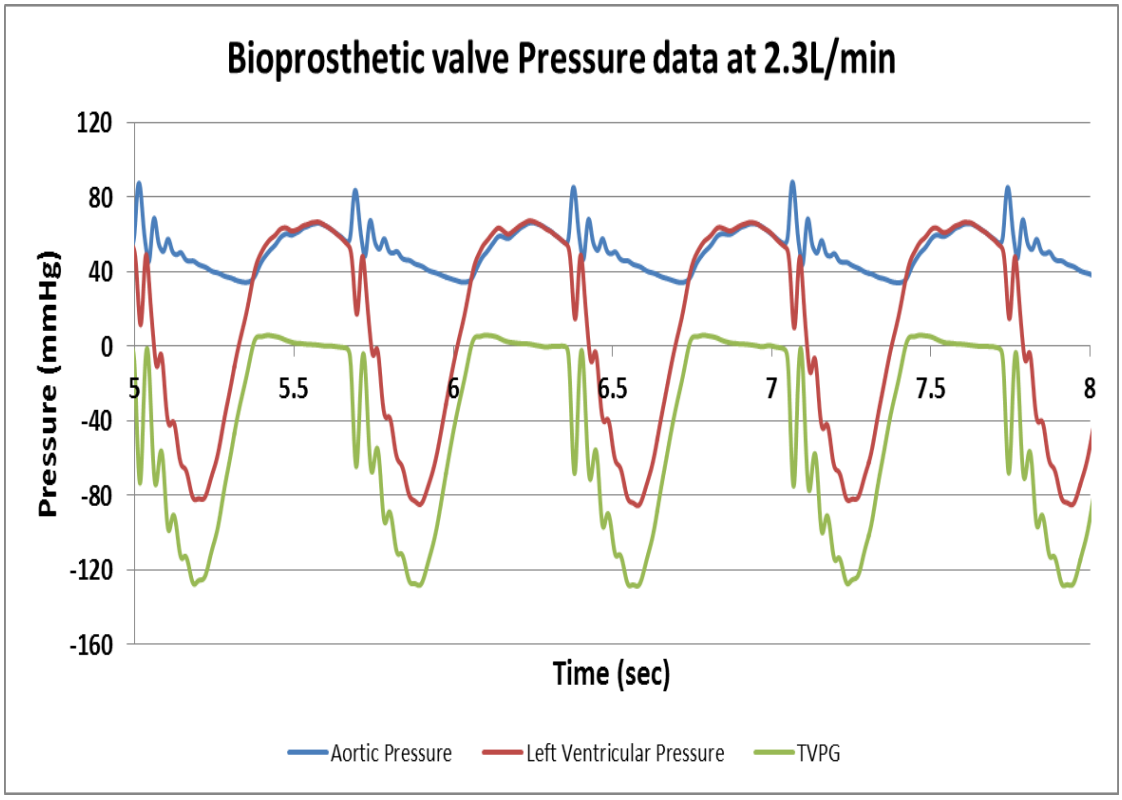

Figure 6.3. A snapshot of pressure data recorded by the SS13L pressure transducers during pulsatile flow hydrodynamic testing of the bioprosthetic valve between 5 to 8 seconds at 2.3L/min. Under this flow rate, the average systolic and diastolic aortic pressure values are 66.03mmHg and 34.10 mmHg respectively, with n>15 cycles. Large spikes in aortic pressure wavefroms represents the closure of the artificial valve, also known as the dicrotic notch.

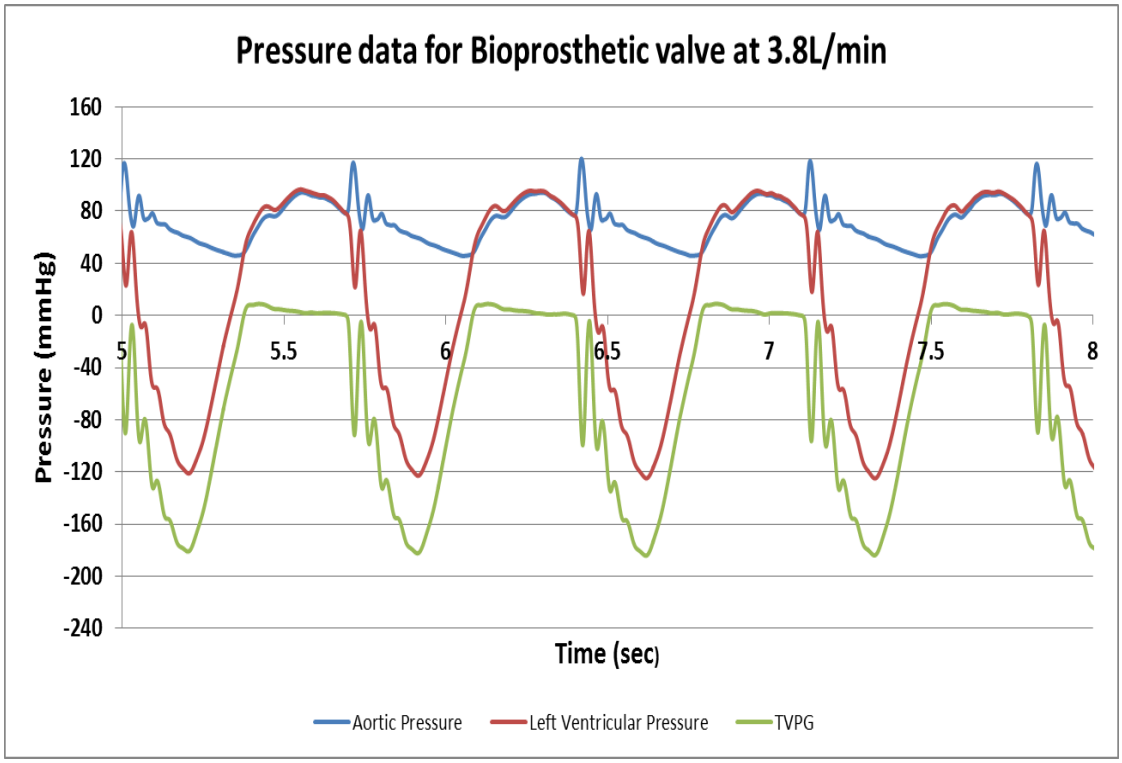

Figure 6.4. A snapshot of pressure data recorded by the SS13L pressure transducers during pulsatile flow hydrodynamic testing of the bioprosthetic valve between 5 to 8 seconds at 3.8L/min. Under this flow rate, the average systolic and diastolic aortic pressure values are 93mmHg and 45.75mmHg respectively, with n >15 cycles. Large spikes in aortic pressure wavefroms represents the dicrotic notch.

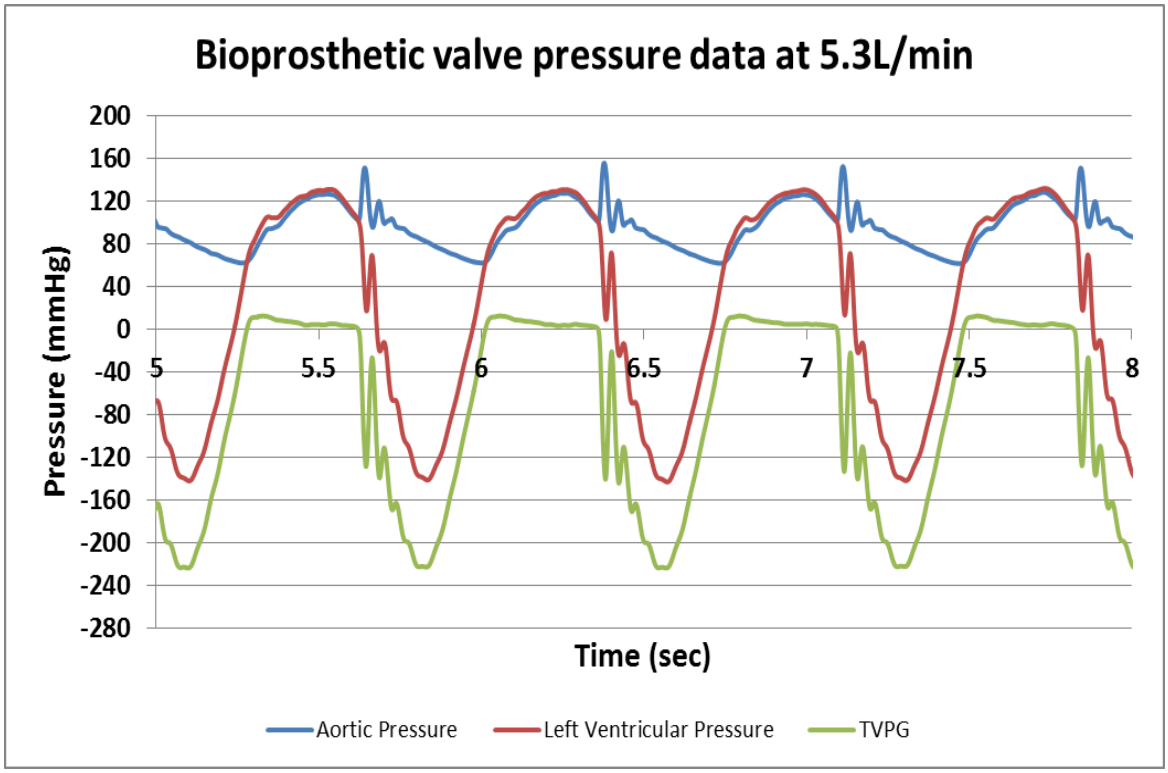

Figure 6.5. A snapshot of pressure data recorded by the SS13L pressure transducers during pulsatile flow hydrodynamic testing of the bioprosthetic valve between 5 to 8 seconds at 5.3L/min. Under this flow rate, the average systolic and diastolic aortic pressure values are 124.10 mmHg and 61.45 mmHg respectively, with n>15 cycles. Large spikes in aortic pressure wavefroms represents the dicrotic notch.

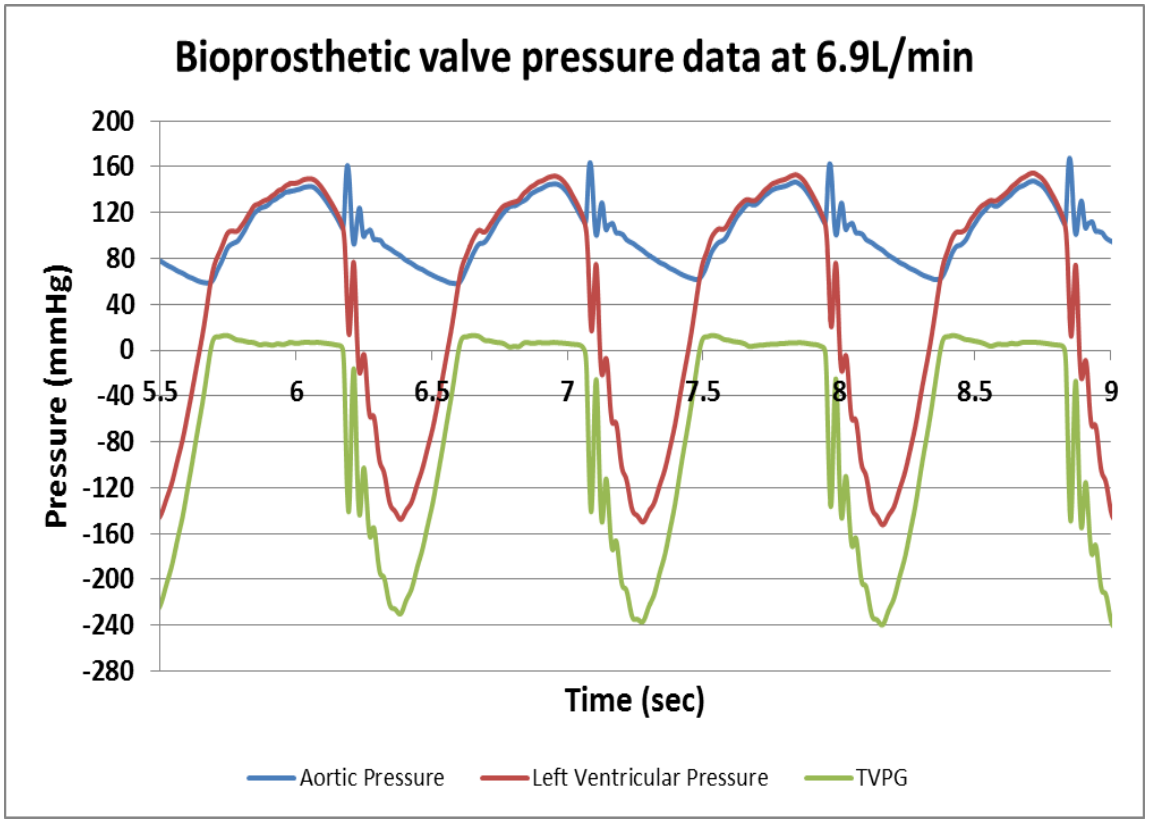

Figure 6.6. A snapshot of pressure data recorded by the SS13L pressure transducers during pulsatile flow hydrodynamic testing of the bioprosthetic valve between 5 to 8 seconds at 6.9L/min. Under this flow rate , the average maximum systolic and diastolic aortic pressure values, n>15 cycles are 143.4mmHg and 62.53 mmHg respectively. Large spikes in aortic pressure wavefroms represents the dicrotic notch.

Typical pressure waveforms generated by polymeric valves are presented below for each of the 4 different flow rates.

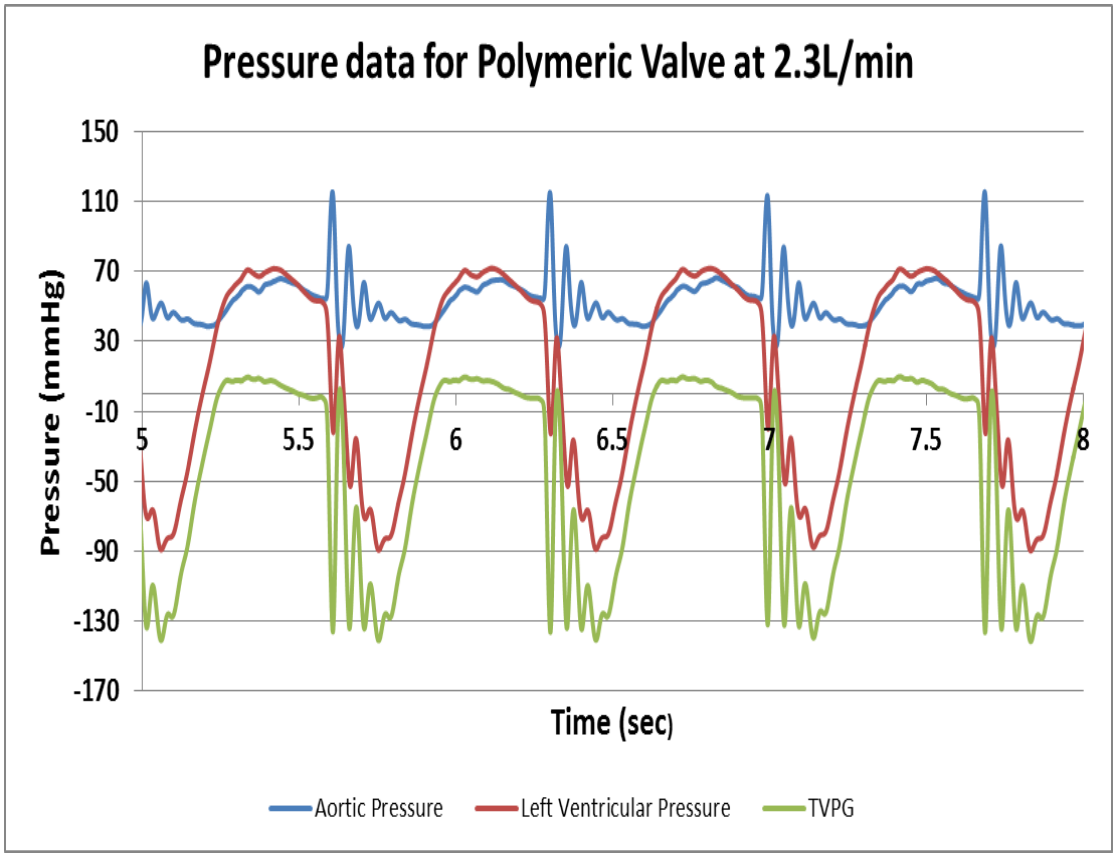

Figure 6.7. A snapshot of pressure data recorded by the SS13L pressure transducers during pulsatile flow hydrodynamic testing of a polymeric valve at 2.3L/min. Under this flow rate , the average systolic and diastolic aortic pressure values, n >15 cycles, are 66.1mmHg and 38.63 mmHg respectively. Large spikes in aortic pressure waveforms represents the dicrotic notch.

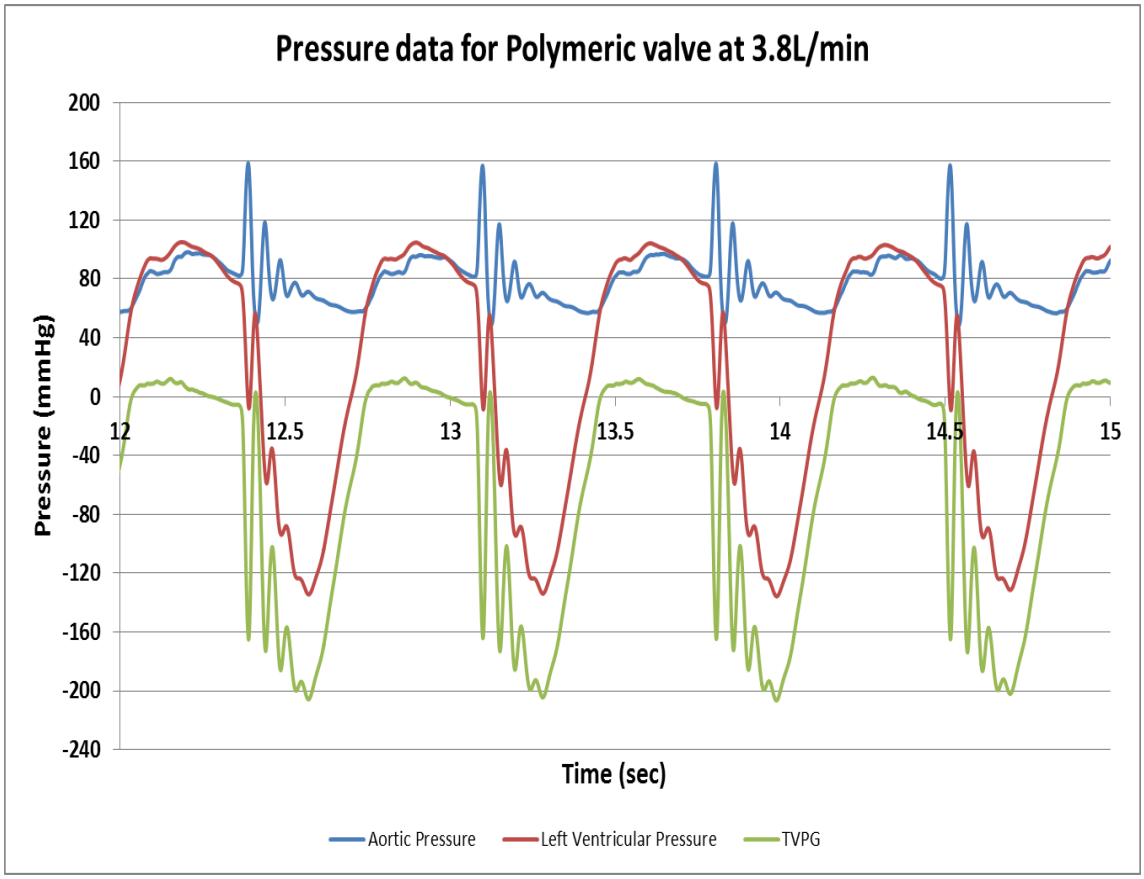

Figure 6.8. A snapshot of pressure data recorded by the SS13L pressure transducers during pulsatile flow hydrodynamic testing of a polymeric valve at 3.8L/min. Under this flow rate , the average systolic and diastolic aortic pressure values, n >15 cycles, are 96.2 mmHg and 55.52 mmHg respectively. Large spikes in aortic pressure waveforms represents the dicrotic notch.

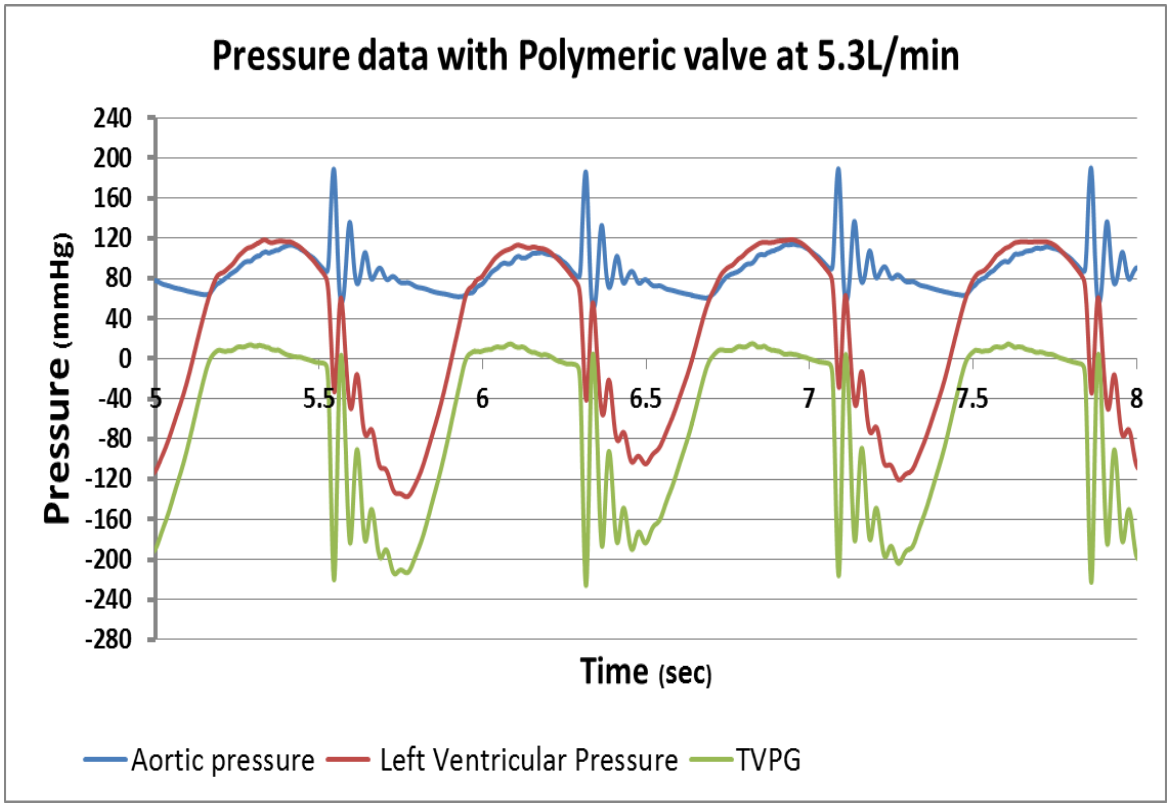

Figure 6.9. A snapshot of pressure data recorded by the SS13L pressure transducers during pulsatile flow hydrodynamic testing of a polymeric valve between 5 to 8 seconds at 5.3L/min. Under this flow rate, the average systolic and diastolic aortic pressure values, n>15 cycles are 112.83 mmHg and 62.5 mmHg respectively. Large spikes in aortic pressure waveforms represents the dichrotic notch.

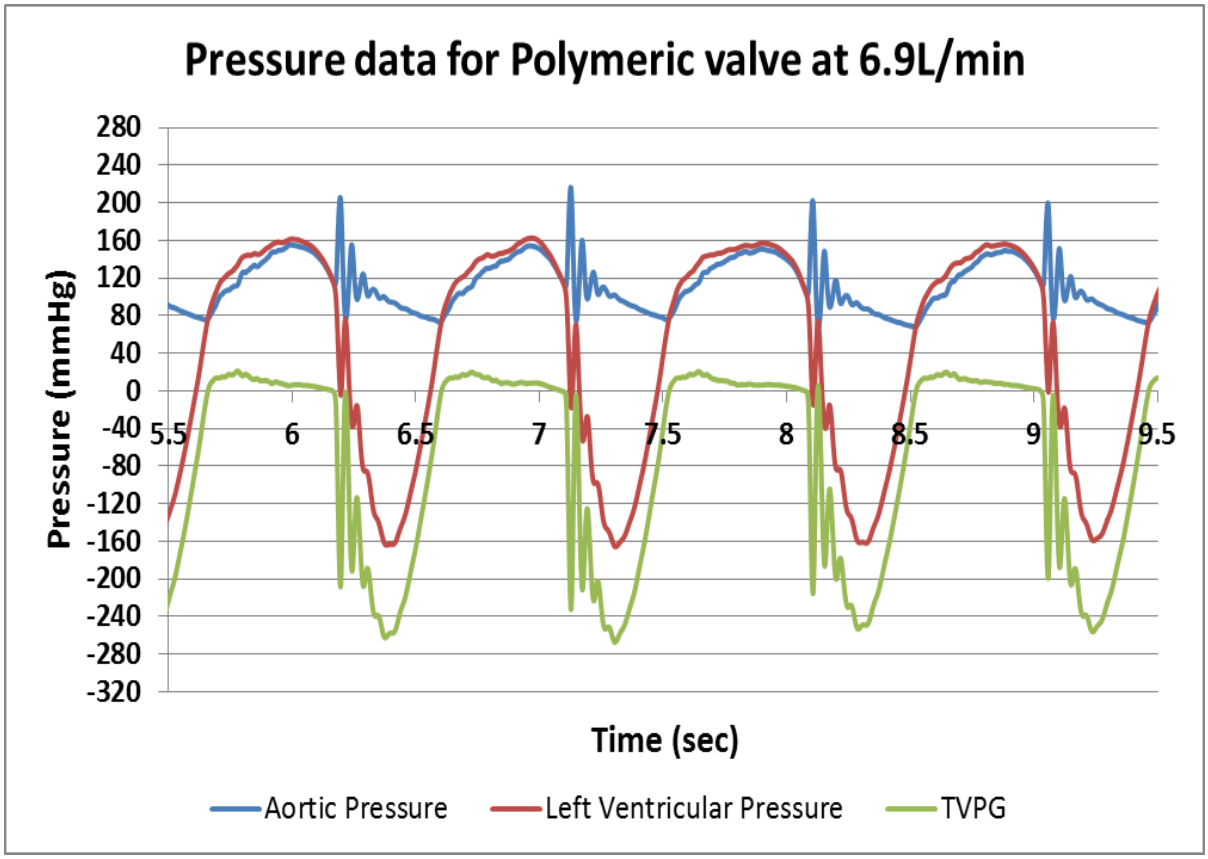

Figure 6.10. A snapshot of pressure data recorded by the SS13L pressure transducers during pulsatile flow hydrodynamic testing of a polymeric valve between 5 to 8 seconds at 6.9L/min. Under this flow rate, the average systolic and diastolic aortic pressure values, n>15 cycles are 149.75 mmHg and 72.85 mmHg respectively. Large spikes in aortic pressure wavefroms represents the dichrotic notch.

The systolic and diastolic values per aortic pressure per cycle were identified using a custom MATLAB script and exported into a Minitab worksheet where descriptive statistics were determined and interval plots were done. Systolic and diastolic pressure values for the 4 polymeric valves and singular Carpentier Edwards SAV 2650 bioprosthetic valve employed for the study are presented below for flow rates between 2-7 L/min. These are presented as interval plot with a 95% confidence interval for mean. One way ANOVA tests were conducted using Minitab with significance level α=0.05. one way ANOVA was selected since we are comparing variance between the means of multiple valves.

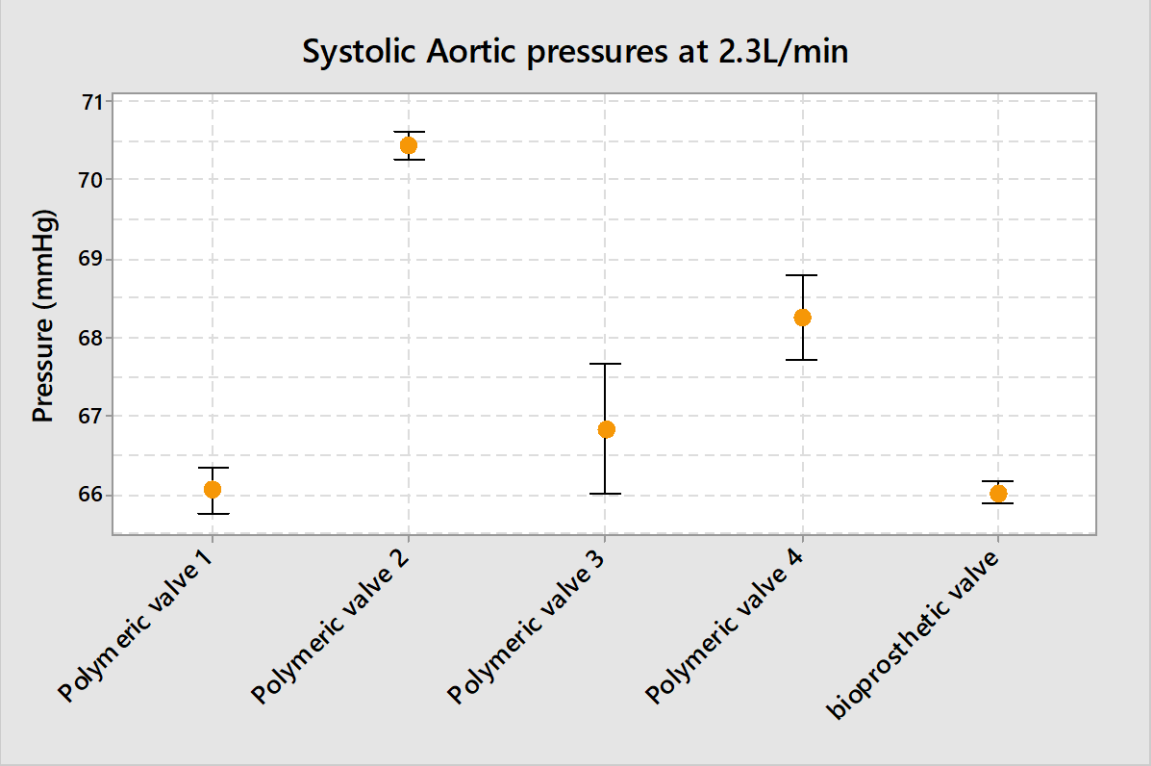

Figure 6.11. Interval plot showing systolic pressures of the 4 polymeric valves and singular bioprosthetic valve under a 2.3 L/min flow rate. Under this flow rate, systolic pressure ranges from (66-71mmHg). Data is presented as mean with standard deviation, with n>15 cycles. One way ANOVA test showed p=0.00 thus suggesting statistical signifcant differnce between the valves.

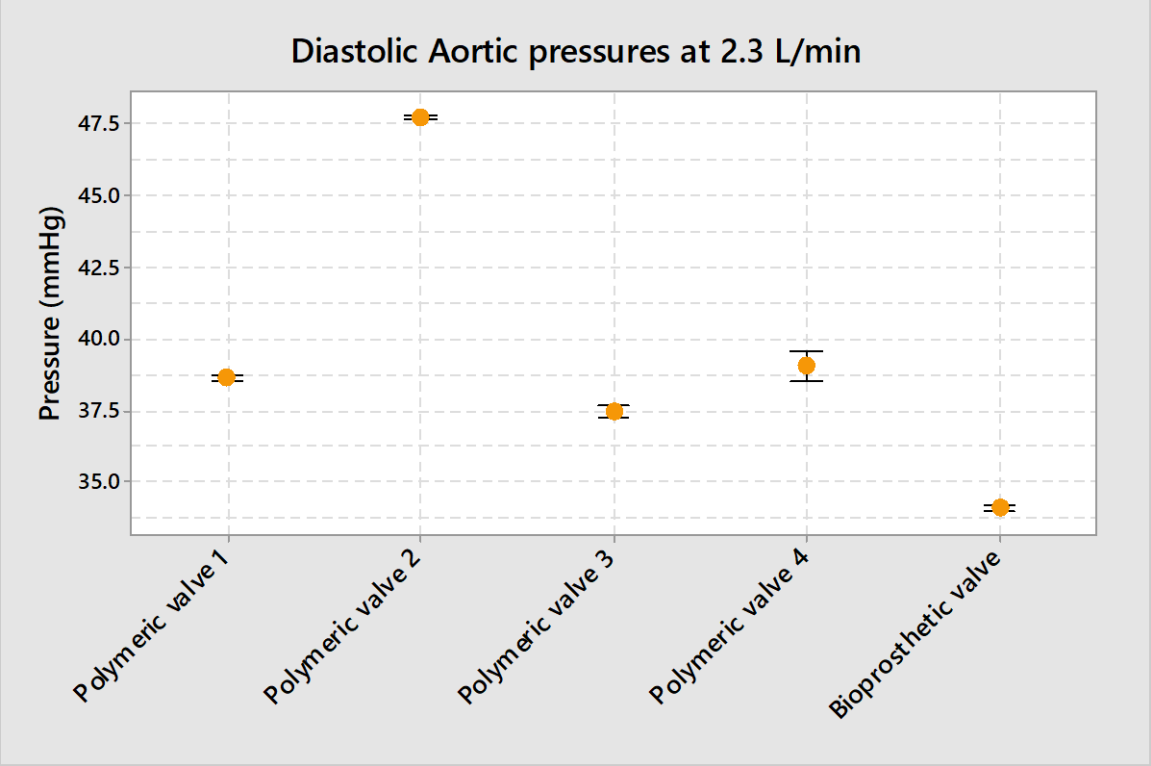

Figure 6.12.Interval plot showing diastolic pressures of the 4 polymeric valves and singular bioprosthetic valve under a 2.3 L/min flow rate. Under this flow rate, systolic pressure ranges from (34-48mmHg). Data is presented as mean with standard deviation, with n>15 cycles. One way ANOVA test showed p=0.00 thus suggesting significant differences .

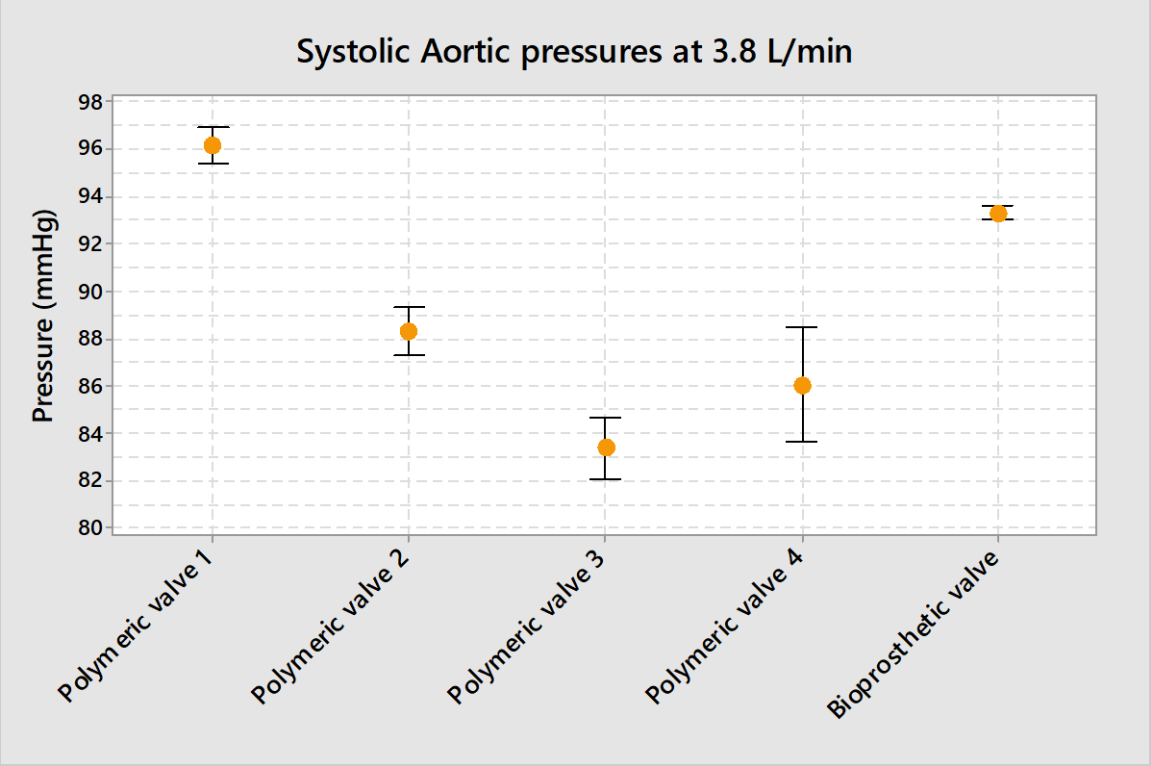

Figure 6.13. Interval plot showing systolic pressures of the 4 polymeric valves and singular bioprosthetic valve under a 3.8 L/min flow rate. Under this flow rate, systolic pressure ranges from (83-97mmHg). Data is presented as mean with standard deviation, with n>15 cycles. One way ANOVA test showed p=0.00 thus suggesting statistically significant differences.

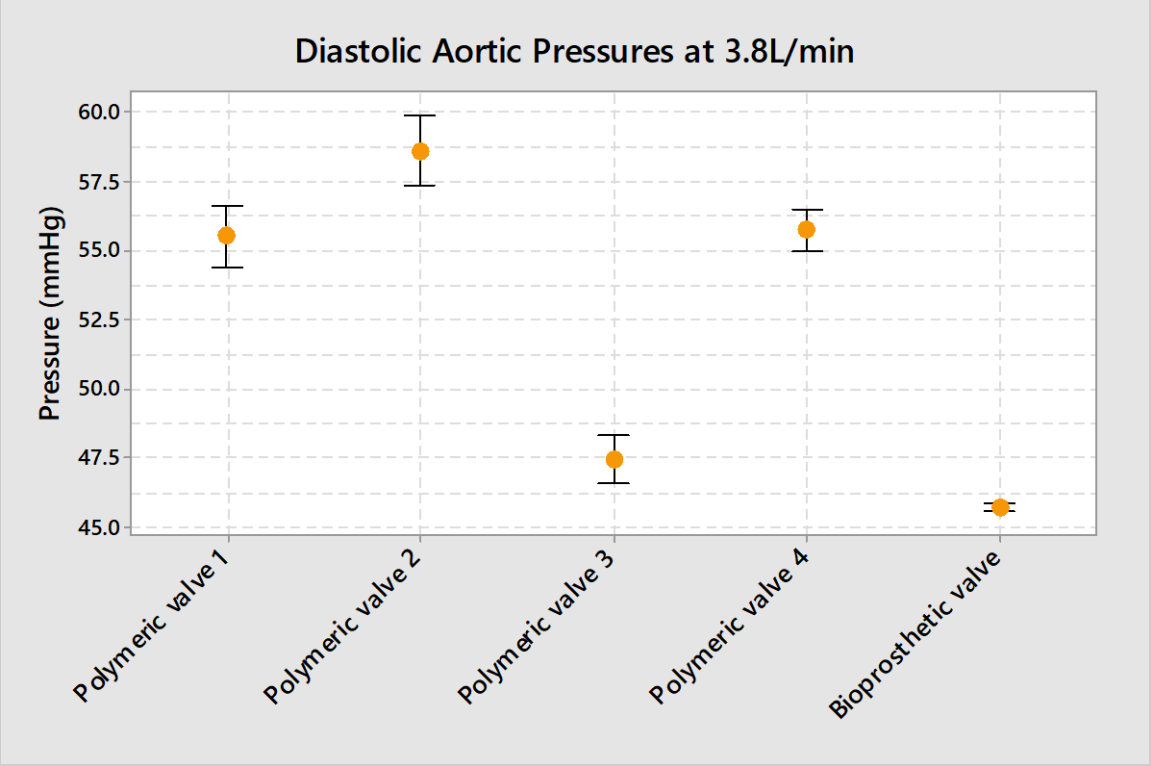

Figure 6.14.Interval plot showing diastolic pressures of the 4 polymeric valves and singular bioprosthetic valve under a 3.8 L/min flow rate. Under this flow rate, systolic pressure ranges from (45-59 mmHg). Data is presented as mean with standard deviation, with n>15 cycles. One way ANOVA test showed p=0.00 thus siggesting statistically significant differences.

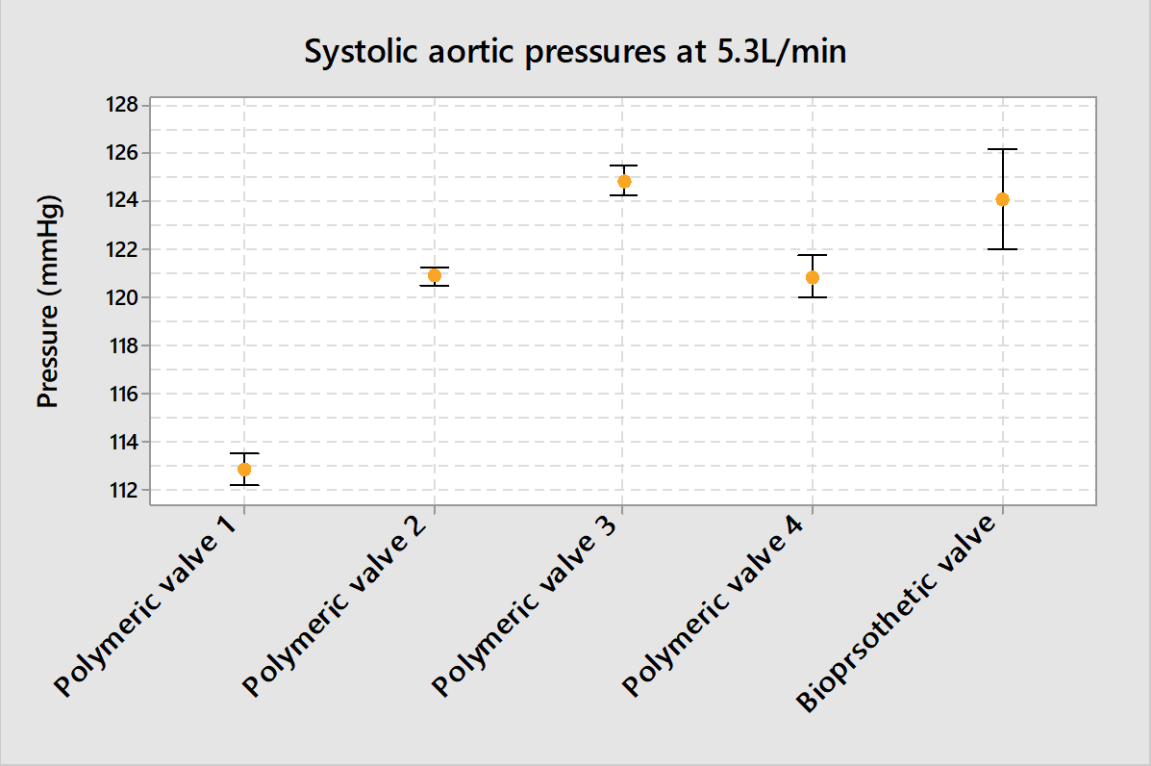

Figure 6.15. Interval plot showing systolic pressures of the 4 polymeric valves and singular bioprosthetic valve under a 5.3 L/min flow rate. Under this flow rate, systolic pressure ranges from (112-125mmHg). Data is presented as mean with standard deviation, with n>15 cycles. One way ANOVA test showed p=0.00 thus suggesting statistically significant differences.

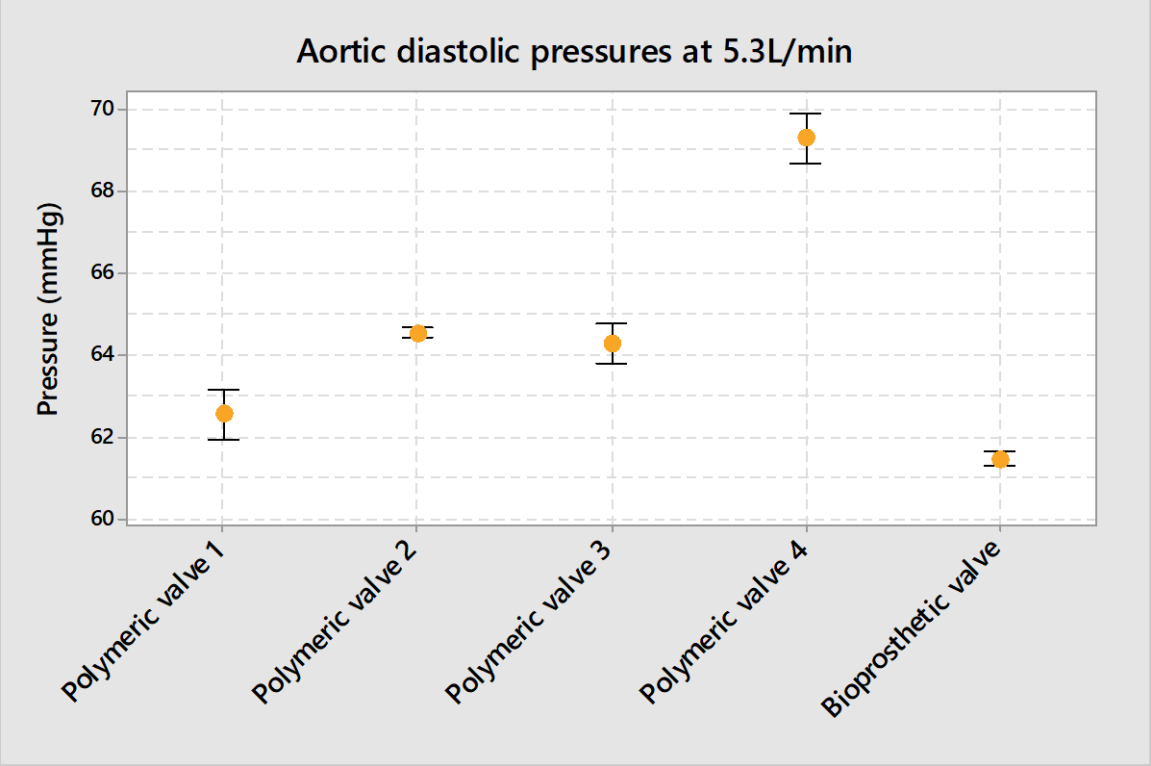

Figure 6.16. Interval plot showing diastolic pressures of the 4 polymeric valves and singular bioprosthetic valve under a 5.3 L/min flow rate. Under this flow rate, diastolic pressure ranges from (61-70 mmHg). Data is presented as mean with standard deviation, with n>15 cycles. One way ANOVA test showed p=0.00 thus suggesting statisitically significant differences.

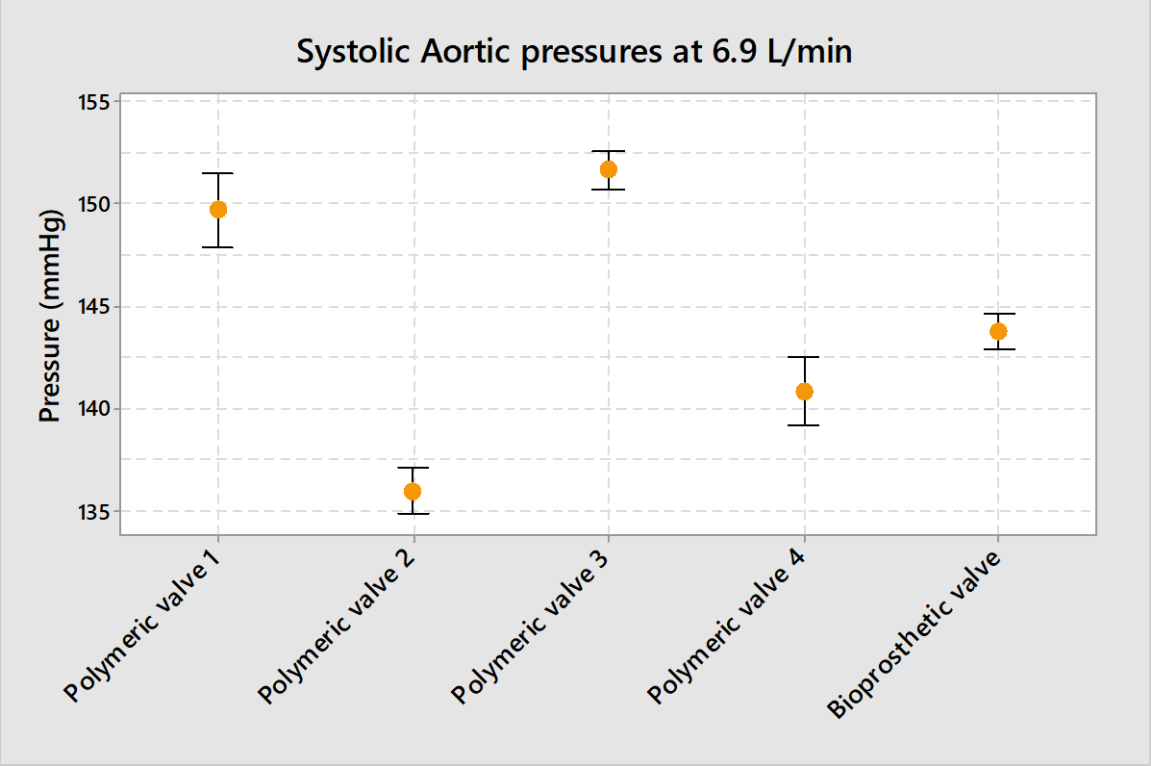

Figure 6.17. Interval plot showing systolic pressures of the 4 polymeric valves and singular bioprosthetic valve under a 6.9 L/min flow rate. Under this flow rate, systolic pressure ranges from (136-150 mmHg). Data is presented as mean with standard deviation, with n>15 cycles. One way ANOVA test showed p=0.00 thus suggesting statisitically significant differences .

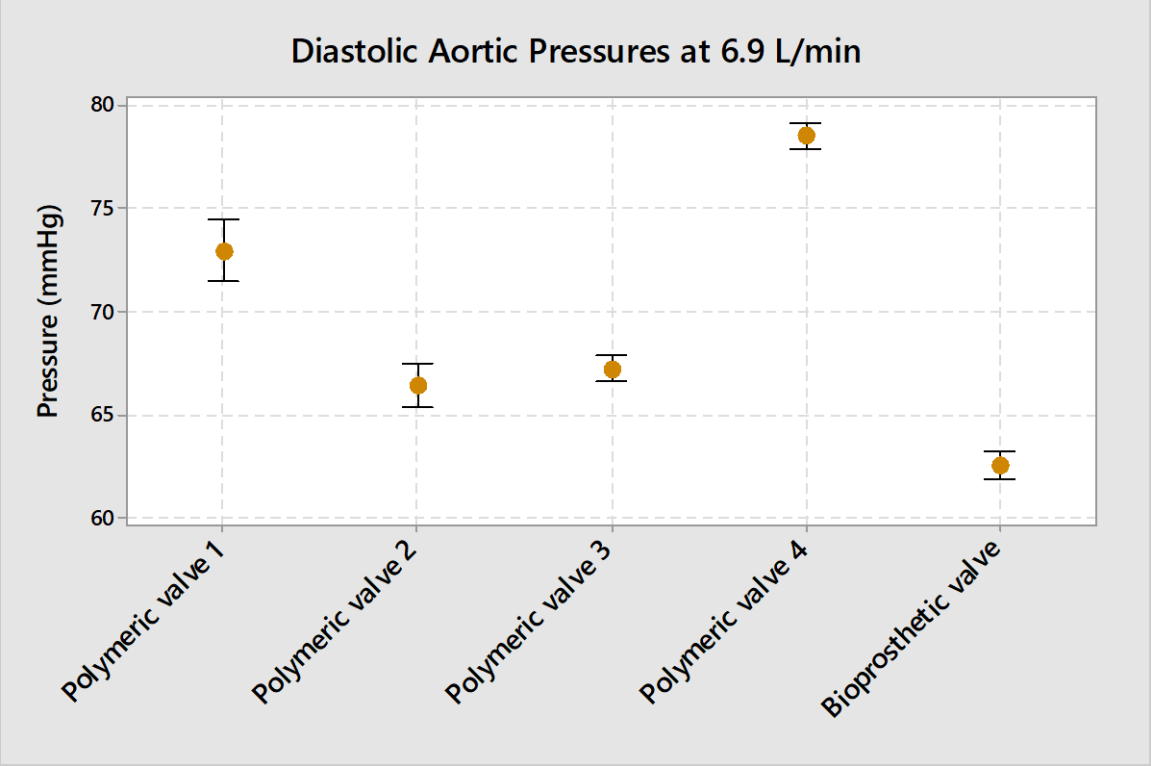

Figure 6.18. Interval plot showing diastolic pressures of the 4 polymeric valves and singular bioprosthetic valve under a 6.9 L/min flow rate. Under this flow rate, systolic pressure ranges from (62-79 mmHg). Data is presented as mean with standard deviation, with n>15 cycles. One way ANOVA test showed p=0.00 thus suggesting statisitically significant differences.

From Figures 6.11 to 6.18, it can be observed that the systolic and diastolic aortic pressure increased with increase in flow rate or cardiac output for all the 4 polymeric valves and singular bioprosthetic valve. one way ANOVA tests conducted to test variablitiiy amongst the means of the valves however revealed significant differences $p<0.05$ under each of the 4 different flow rates employed in the study. Mean pressure values with standard deviation, are displayed in table 6.2

	2.3 L/min		3.8 L/min		5.3 L/min		6.9 L/min		
	SP	**DP**	**SP**	**DP**	**SP**	**DP**	**SP**	**DP**	
PV 1	66.06 ± 0.57	38.63 ± 0.17	96.20 ± 1.69	55.51 ± 2.56	112.83 ± 1.58	62.54 ± 1.16	149.75 ± 4.41	72.34 ± 3.65	
PV 2	70.45 ± 0.36	47.71 ± 0.18	88.34 ± 2.22	58.60 ± 2.90	120.92 ± 0.87	64.53 ± 0.21	136.01 ± 2.75	66.56 ± 2.59	
PV 3	66.84 ± 1.64	37.47 ± 0.41	83.39 ± 2.73	47.46 ± 1.94	124.90 ± 1.52	64.28 ± 1.00	151.69 ± 2.39	67.42 ± 2.90	
PV 4	68.25 ± 1.10	39.04 ± 1.10	86.08 ± 5.08	55.76 ± 1.71	120.88 ± 2.10	69.29 ± 1.22	140.85 ± 4.17	78.23 ± 1.85	
BV	66.03 ± 0.26	34.10 ± 0.24	93.35 ± 0.66	45.75 ± 0.30	124.09 ± 5.00	61.45 ± 0.34	143.81 ± 2.10	62.52 ± 1.46	

Table 6.2. Systolic and diastolic aortic pressure of the polymeric and bioprosthetic valves. Data presented as Mean ± Standard deviation, with n>15 cycles. All values are in mmHg. PV= Polymeric valve, BV=Bioprosthetic valve, SP = Systolic Pressure, DP = Diastolic Pressure

6.3. HYDROYNAMIC TESTING

The 4 polymeric valves and singular Carpentier Edwards bioprosthetic valve were subjected to pulsatile flow testing according to ISO 5840 standards under 4 different flow rates between 2-7L/min. The parameters of interests are the Mean Systolic Pressure Difference (MSPD) and also the Effective Orifice Area (EOA).

6.3.1 MEAN SYSTOLIC PRESSURE DIFFERENCE (MSPD)

The Mean Systolic Pressure Difference for each cycle was calculated by subtracting the aortic pressure wavefrom from the ventricular pressure waveform thus resulting in an

waveform known as the Transvalvular Pressure Gradient. A custom MATLAB script was used to determine the start and end point of the systolic phase by locating the first and last positive value on the TVPG waveform coinciding with the intersection of the aortic and ventricular pressure waveform. These data points over that time range are then averaged and is thus referred to as the Mean Systolic Pressure Difference. The MSPD values of the polymeric and bioprosthetic valves are displayed in the figure below.

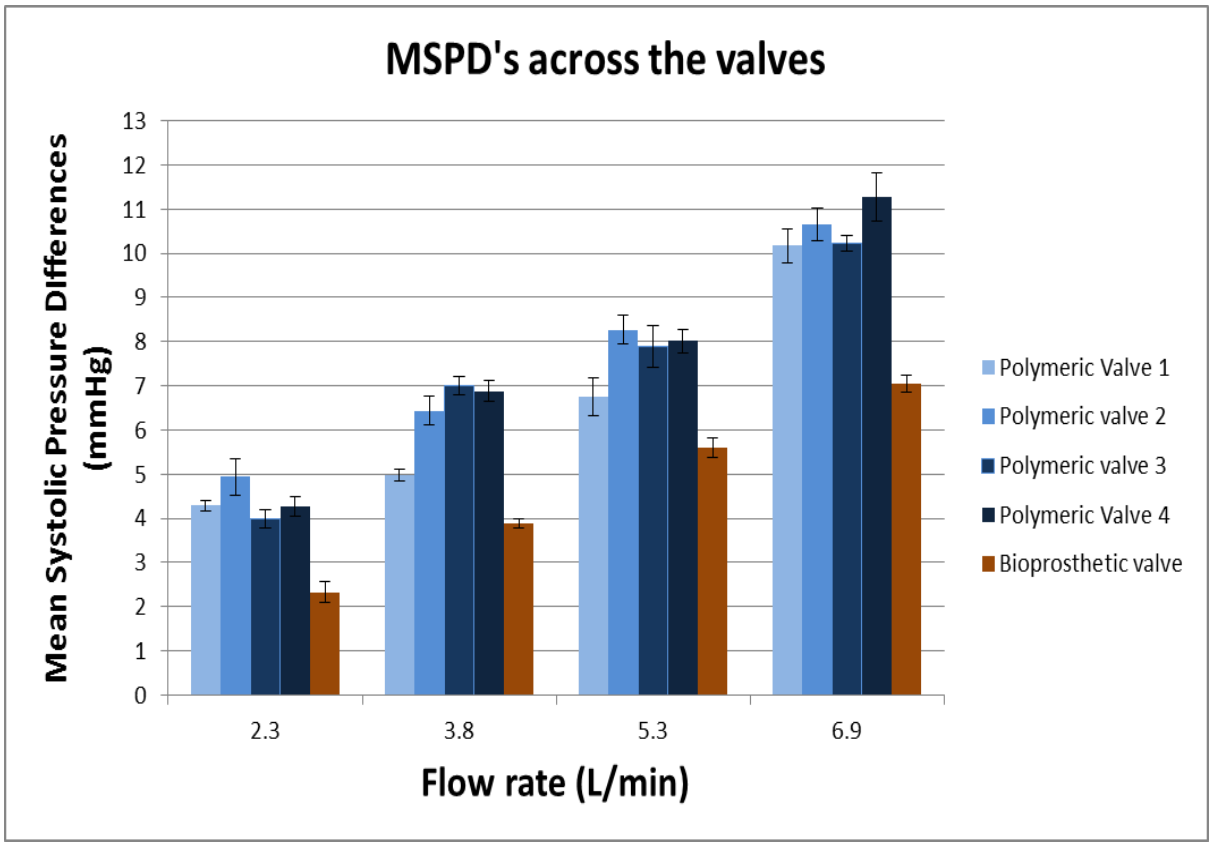

Figure 6.19. Mean Systolic Pressure Difference of the 4 polymeric valves and singular bioprosthetic valve employed during the pulsatile flow hydrodynamic testing.

From figure 6.19, it can be observed that the MSPDs increases with increasing flow rate. All the polymeric valves, at each flow rate, exhibited a higher MSPD relative to the bioprosthetic valve. In order to determine significance of the differences between the MSPDs of the polymeric and bioprosthetic valves, multiple 2 sample t tests were performed. All the

polymeric valves exhibited $p<0.05$ in comparison with the bioprosthetic valve, at each of the 4 flow rates.

Between the 4 polymeric valves however under 2 sample t test, polymeric valves 1 and 4 exhibited insignificant differences at the 2.3 L/min flow rate ($p=0.882$). Polymeric valves 3 and 4 also exhibited insignificant differences ($p=0.332$) under the 5.3 L/min flow rate. Polymeric valves 1 and 3 exhibits insignificant difference under the 6.9L/min flow rate ($p=0.619$). All other instances revealed significant differences between the polymeric valves ($p<0.05$). The reasons for this are still pretty unclear.

6.3.2. EFFECTIVE ORIFIC AREA

The second parameter of interest in the pulsatile flow testing , was the Effective Orifice Area. This is determined using the Gorlin formula, which is quoted as

$$EOA(cm^2) = \frac{CO}{HR \times SEP \times 51.6C \times \sqrt{\Delta P/\rho}}$$

- CO= Cardiac output (ml/min)
- HR= Heart Rate (beats per min) : 75bpm
- SEP= Systolic Ejection Period (s) ,which for our study , is approximated via visual inspection of the aortic pressure waveforms, as 0.37seconds.
- C=Discharge coefficient : 1
- ΔP= Mean Systolic Pressure Difference (mmHg). These are the mean values already displayed in figure 7.17.
- ρ=density (g/cm^3). At 20% glycerol –water solution, ρ ~1.04

The origin and derivation of the Gorlin's formula has already been described in section 5.3.5 of the thesis. The effective orifice areas of the polymeric and bioprosthetic valves are displayed below.

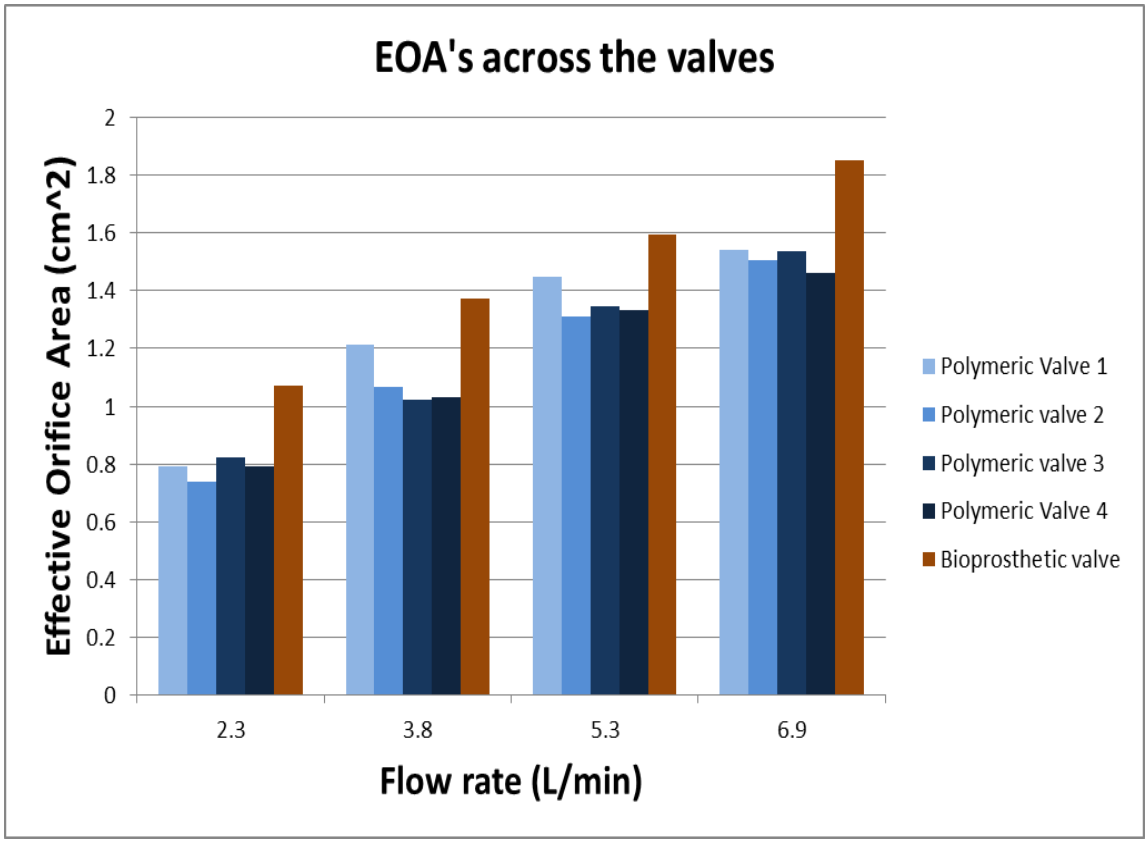

Figure 6.20. The effective orifice areas of the 4 polymeric valves and singular bioprosthetic valves used in the pulsatile flow hydrodynamic testing.

Mathematically, there exists an inverse relationship between MSPD and EOA, according to the Gorlin's formula, thus the bioprosthetic valve exhibits a higher EOA relative to the polymeric valves. The EOAs also increases with increasing flow rate.

6.4. THE EFFECTS OF STENOSIS ON TRANSVALVULAR PRESSURE

In order to investigate the effect valvular stenosis has on the Mean Systolic Pressure Difference of the valves, the polymeric and bioprosthetic valves, were subjected to 4 levels of flow obstruction (stenosis), ie 0% , 25%, 50% and 75% obstruction for each flow rate. The stenosis simulation process has been described in section 5.2.2. A one way ANOVA test was conducted between the valves at each obstruction level and flow rate to test for variability amongst the valves. The results are presented in the figures and tables below. The 0% obstruction level labelled in these figures and tables, simply refers to the non stenotic state at which the hydrodynamic valve testing was conducted prior to stenosis simulation tests.

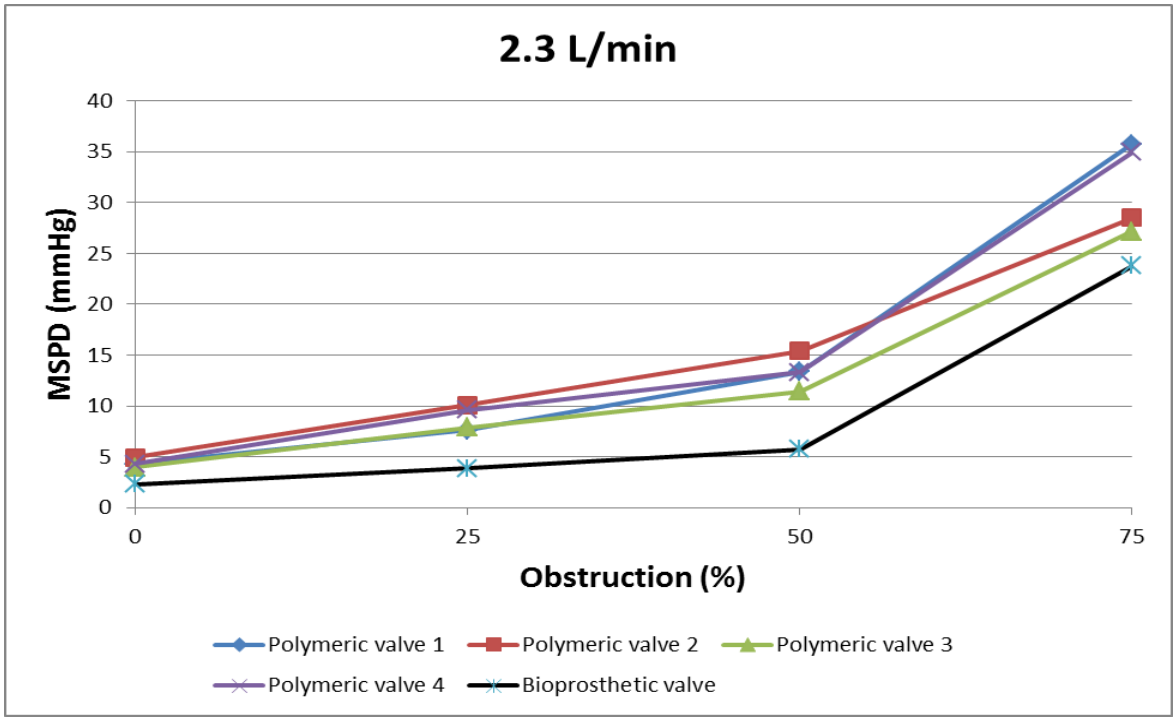

Figure 6.21. Simulated stenosis at 2.3 L/min and its corresponding change in MSPD. Data is presented as mean, with n>15 cycles. One way ANOVA tests revealed statistically significant differences ($p=0.00$) under each of the 4 obstruction conditions ($p<0.05$).

2.3 L/min	0% obstruction	25% obstruction	50% obstruction	75% obstruction
Polymeric valve 1	4.29 ± 0.11	7.60 ± 1.04	13.34 ± 1.28	35.76 ± 0.39
Polymeric valve 2	4.94 ± 0.42	10.11 ± 0.14	15.39 ± 0.14	28.49 ± 1.04
Polymeric valve 3	3.98 ± 0.21	7.91 ± 0.10	11.45 ± 0.47	27.19 ± 1.35
Polymeric valve 4	4.28 ± 0.22	9.61 ± 0.56	13.32 ± 0.93	34.94 ± 0.47
Bioprosthetic valve	2.33 ± 0.24	3.88 ± 0.17	5.75 ± 0.82	23.76 ± 0.55

Table 6.3.Mean Systolic pressure differences at each degree of obstruction, at a flow rate of 2.3L/min. Data is presented as Mean ± Standard deviation. All values are in mmHg.

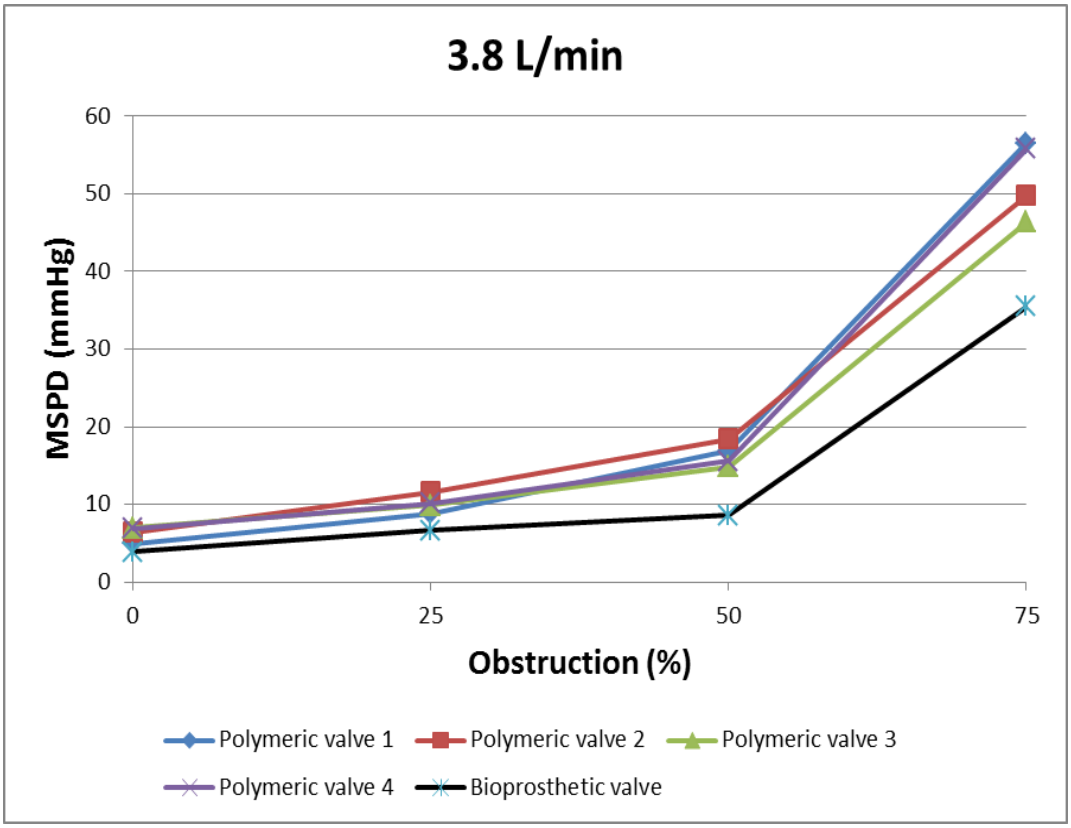

Figure 6.22. Simulated stenosis at 3.8 L/min and its corresponding change in MSPD. Data is presented as mean, with n>15 cycles. One way ANOVA tests revealed statistically significant differences under each obstruction level (p=0.00).

3.8 L/min	0% obstruction	25% obstruction	50% obstruction	75% obstruction
Polymeric valve 1	4.97 ± 0.14	8.82 ± 0.6	16.86 ± 0.39	56.50 ± 4.10
Polymeric valve 2	6.43 ± 0.32	11.56 ± 0.64	18.42 ± 0.36	49.73 ± 0.59
Polymeric valve 3	7.00 ± 0.20	9.91 ± 0.15	14.85 ± 0.13	46.31 ± 0.51
Polymeric valve 4	6.88 ± 0.24	10.17 ± 1.00	15.58 ± 0.76	55.74 ± 4.11
Bioprosthetic valve	3.88 ± 0.10	6.65 ± 0.14	8.61 ± 0.28	35.46 ± 1.30

Table 6.4. Mean Systolic pressure differences at each degree of obstruction, at a flow rate of 3.8 L/min. Data is presented as Mean ± Standard deviation. All values are in mmHg.

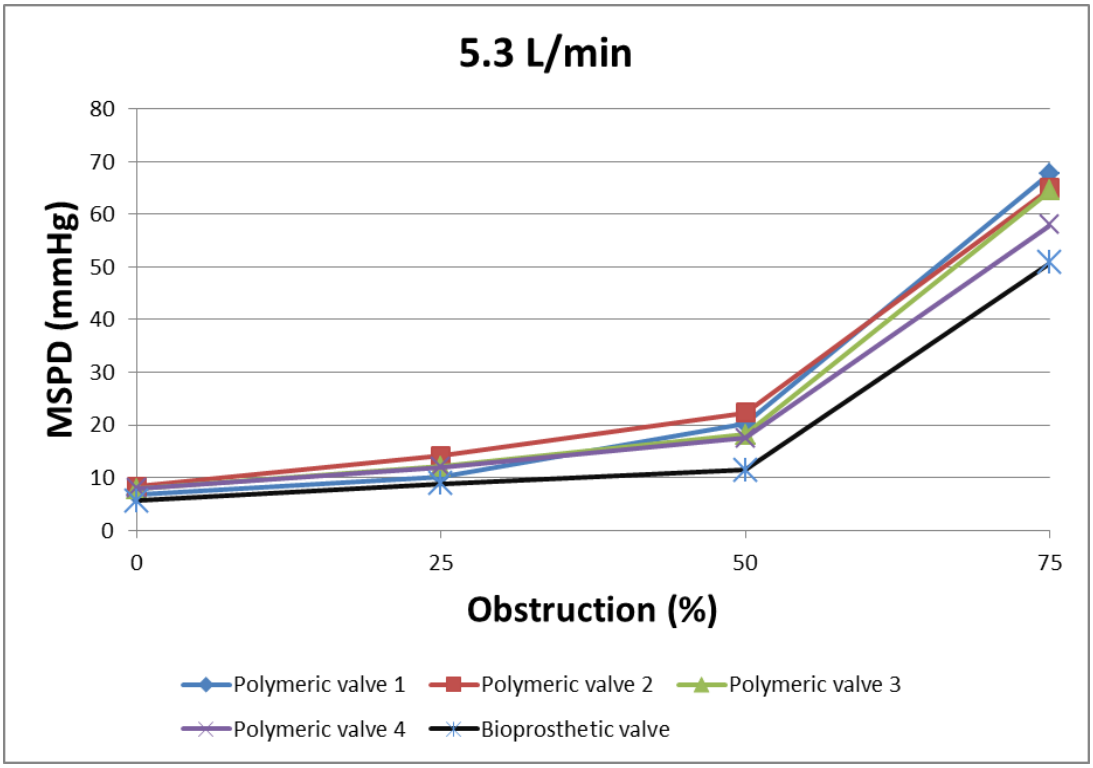

Figure 6.23. Simulated stenosis at 5.3 L/min and its corresponding change in MSPD. Data is presented as mean, with n>15 cycles. One way ANOVA tests revealed statistically significant differences amongst the valves($p=0.00$) under each obstruction level .

5.3 L/min	0% obstruction	25% obstruction	50% obstruction	75% obstruction
Polymeric valve 1	6.76 ± 0.44	10.24 ± 0.49	20.21 ± 0.46	67.80 ± 7.22
Polymeric valve 2	8.27 ± 0.32	14.15 ± 0.18	22.27 ± 0.43	64.97 ± 3.23
Polymeric valve 3	7.89 ± 0.5	12.16 ± 0.23	18.16 ± 0.74	64.50 ± 1.22
Polymeric valve 4	8.02 ± 0.26	12.04 ± 1.33	17.47 ± 1.57	58.04 ± 7.91
Bioprosthetic valve	5.60 ± 0.21	8.87 ± 0.30	11.42 ± 0.21	50.77 ± 1.11

Table 6.5. Mean Systolic pressure differences at each degree of obstruction, at a flow rate of 5.3 L/min. Data is presented as Mean ± Standard deviation. All values are in mmHg.

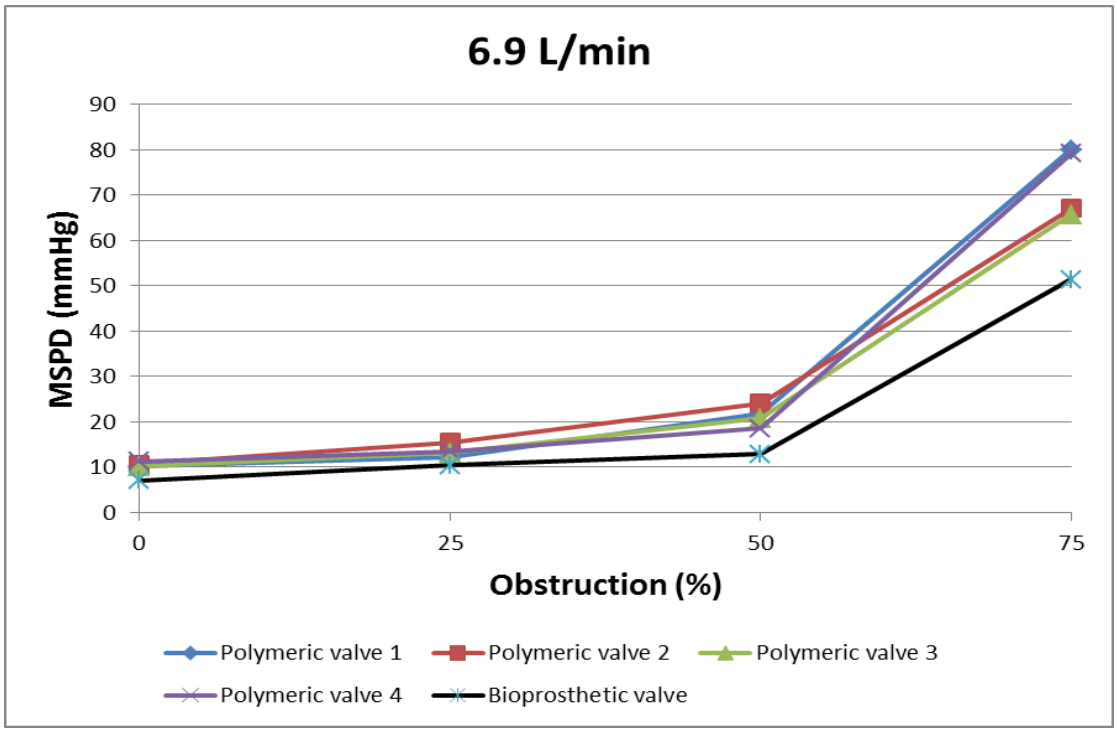

Figure 6.24. Simulated stenosis at 6.9 L/min and its corresponding change in MSPD. Data is presented as mean, with n>15 cycles. One way ANOVA tests revealed statistically significant differences under each obstruction level (p=0.00).

6.9 L/min	0% obstruction	25% obstruction	50% obstruction	75% obstruction
Polymeric valve 1	10.17 ± 0.39	12.14 ± 1.01	21.74 ± 1.11	80.04 ± 3.39
Polymeric valve 2	10.65 ± 0.37	15.42 ± 0.53	24.06 ± 1.44	67.06 ± 3.19
Polymeric valve 3	10.23 ± 0.18	13.09 ± 1.82	20.80 ± 1.23	65.70 ± 1.36
Polymeric valve 4	11.27 ± 0.54	13.54 ± 0.45	18.60 ± 0.47	79.11 ± 3.63
Bioprosthetic valve	7.05 ± 0.19	10.41 ± 0.52	12.93 ± 0.24	51.36 ± 1.68

Table 6.6. Mean Systolic pressure differences at each degree of obstruction, at a flow rate of 6.9 L/min. Data is presented as Mean ± Standard deviation. All values are in mmHg.

From the tables and figures above, it was observed that there exists a clear relationship between obstruction and the Mean Systolic Pressure Difference (MSPD) across the valves. MSPD experienced a slow but steady rise with increasing degree of obstruction, from 0-50% obstruction. However at the 75% obstruction, there was a massive increase in the MSPD experienced amongst all the valves at all flow rates. Secondly , the MSPD's across the polymeric valves were consistently of higher magnitude relative to the bioprosthetic valve.

6.5. INSTRUMENTATION OF THE VALVES

In the quest to develop a valves embedded with sensors to detect changes due to simulated stenosis, 4 polymeric valves were instrumented with strain gauges and subjected to stenosis simulation tests under 4 degrees of valve obstruction in our hydrodynamic tester. The simulation tests for the instrumented valves have already been described in section 6.5.

In these experiments, the variable of interest was difference between the maximum and minimum points per cycle , of the strain gauge data. Determination of peak to peak strain

difference was aided by a custom MATLAB script. Aortic pressure and strain recordings were taken simultaneously to assess the integrity of the strain gauges in replicating the pressure pattern. A sample of strain and pressure waveform data is shown below

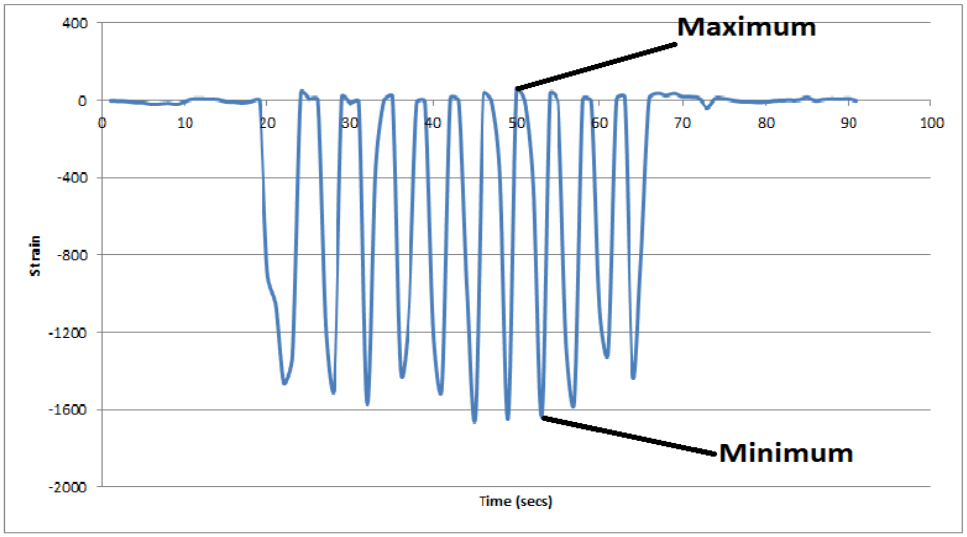

A

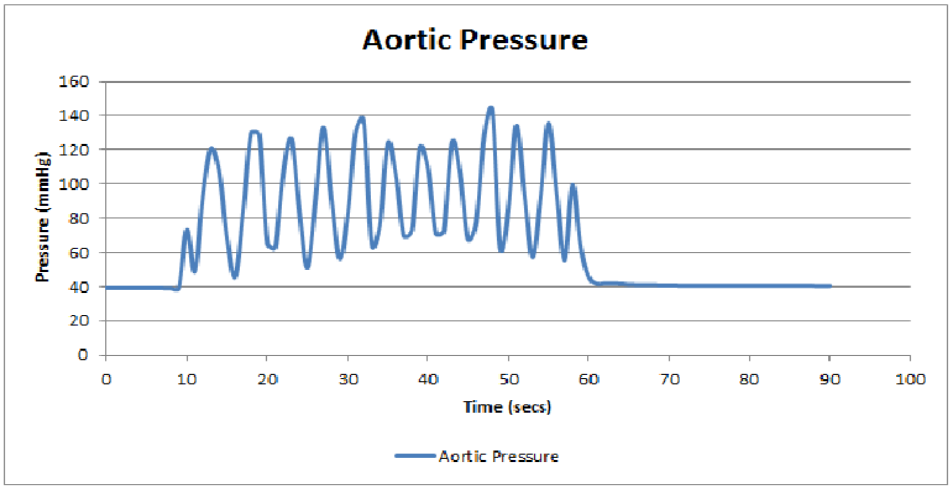

B

Figure 6.25. A-Sample of strain gauge waveform showing maximum and minimum point peaks. B- Aortic pressure waveform. Both A and B were recorded simultaneously at 1 sample per second at a flow rate of 5.3 L/min.

From figure 6.25, it can be observed that the strain pattern, although appears inverted follows closely that of the pressure pattern. This relationship was anticipated under these test conditions.

Results from the stenosis simulation tests which the 4 instrumented valves were subjected to, are presented below for each flow rate.

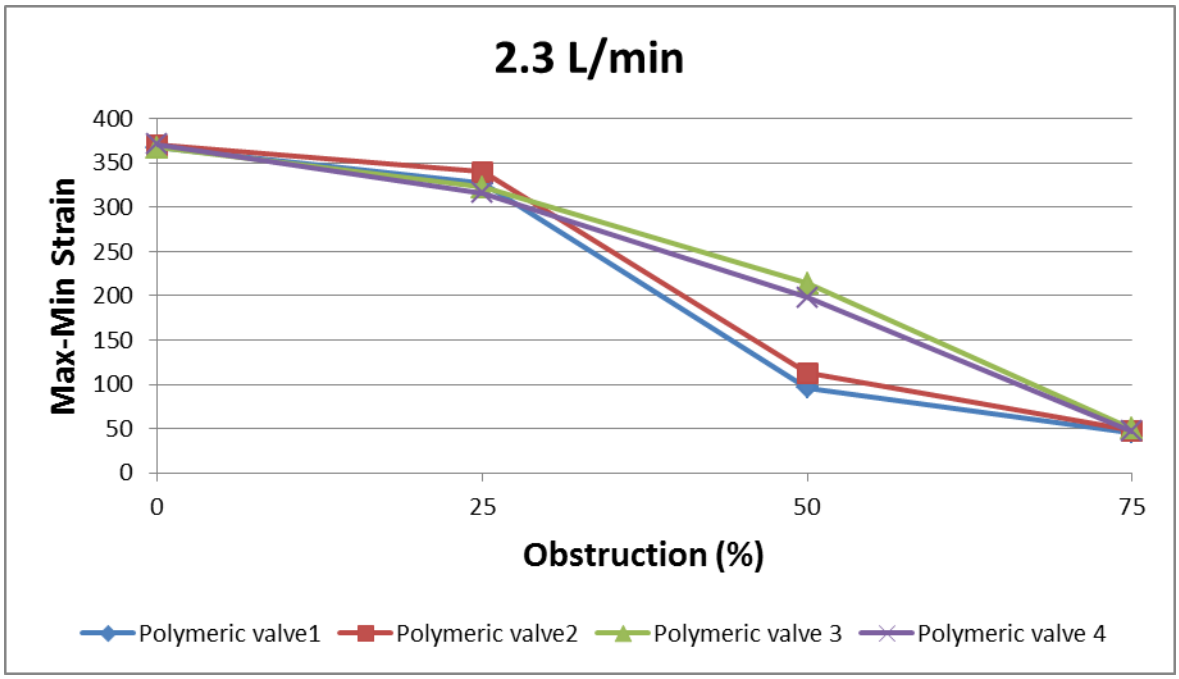

Figure 6.26. Results of stenosis simulation of strain gauged polymeric valves under a flow rate of 2.3 L/min. Data is presented as mean with n=15 cycles. One way ANOVA amongst the valves revealed statistically insignificant differences $p>0.05$ ($p=0.962$, 0.118, 0.402 and 0.79) for the 0%, 25%, 50% and the 75% obstruction conditions.

2.3 L/min	0% obstruction	25% obstruction	50% obstruction	75% obstruction
Polymeric valve 1	367 ± 35.11	326.70± 47.80	95.80 ± 28.5	45.67± 16.91
Polymeric valve 2	370.13± 29.68	339.60 ±39	112.9 ± 41.50	47.53 ± 19.19
Polymeric valve 3	367.27 ± 3.73	322.58± 30.44	214 ± 51.30	50 ± 15.64
Polymeric valve 4	371 ± 40.33	315.60± 37.67	198.1± 209.90	46.57 ± 17.32

Table 6.7. Maximum –Minimum strain difference at each degree of obstruction, at a flow rate of 2.3 L/min. Data is presented as Mean ± Standard deviation. Strain is dimensionless.

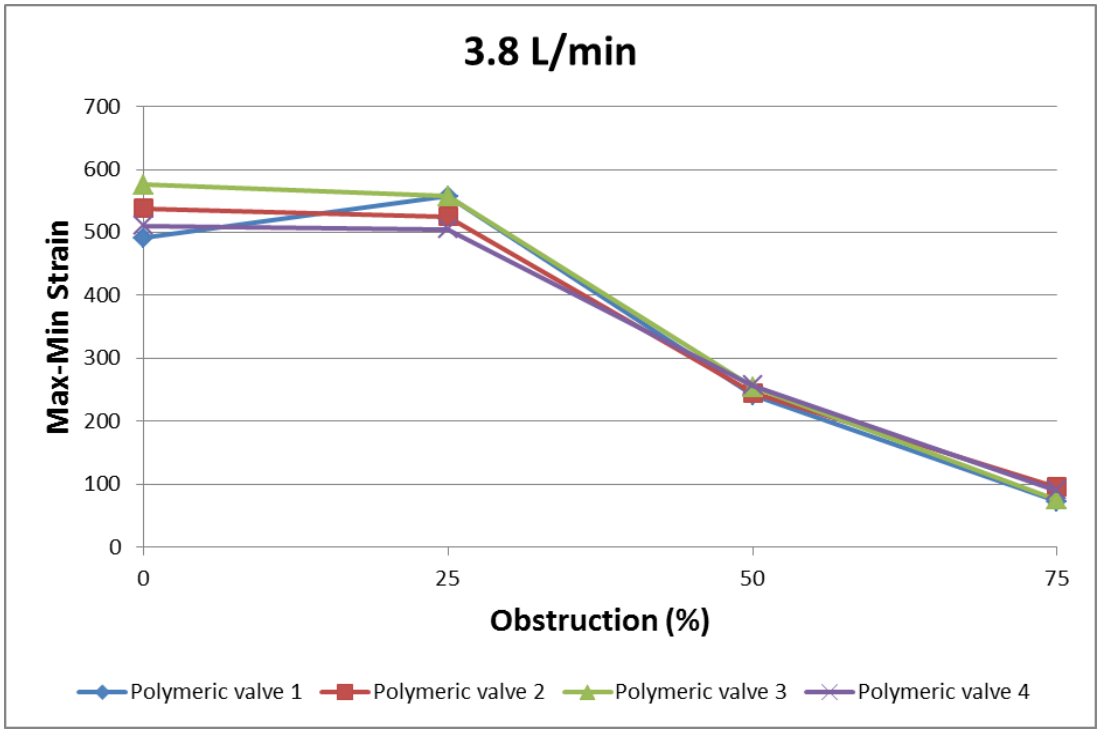

Figure 6.27.Results of stenosis simulation of strain gauged polymeric valves under a flow rate of 3.8 L/min. Data is presented as mean with n=15 cycles. One way ANOVA amongst the valves revealed insignificant difference between the valves $p>0.05$ at the 25% ($p=0.581$) and 50% ($p=0.469$) obstruction condition and $p<0.05$ ($p=0.012$ and $p= 0.045$) in the 0% and 75% obstruction conditions respectively

3.8 L/min	0% obstruction	25% obstruction	50% obstruction	75% obstruction
Polymeric valve 1	491.3 ± 88.6	557± 105	241.2 ± 18.83	72.75± 16.76
Polymeric valve 2	537.7± 72.4	525.37±114.10	245.2 ± 25.87	95.63 ± 19.84
Polymeric valve 3	576 ± 73.8	557.05±102.71	254.13 ±29.94	75.38 ± 21.55
Polymeric valve 4	510.8 ± 65.9	505.45± 95.2	256.90± 43.7	89.38 ± 11.51

Table 6.8. Maximum –Minimum strain difference at each degree of obstruction, at a flow rate of 3.8 L/min. Data is presented as Mean ± Standard deviation, with n=15 cycles. Strain is dimensionless.

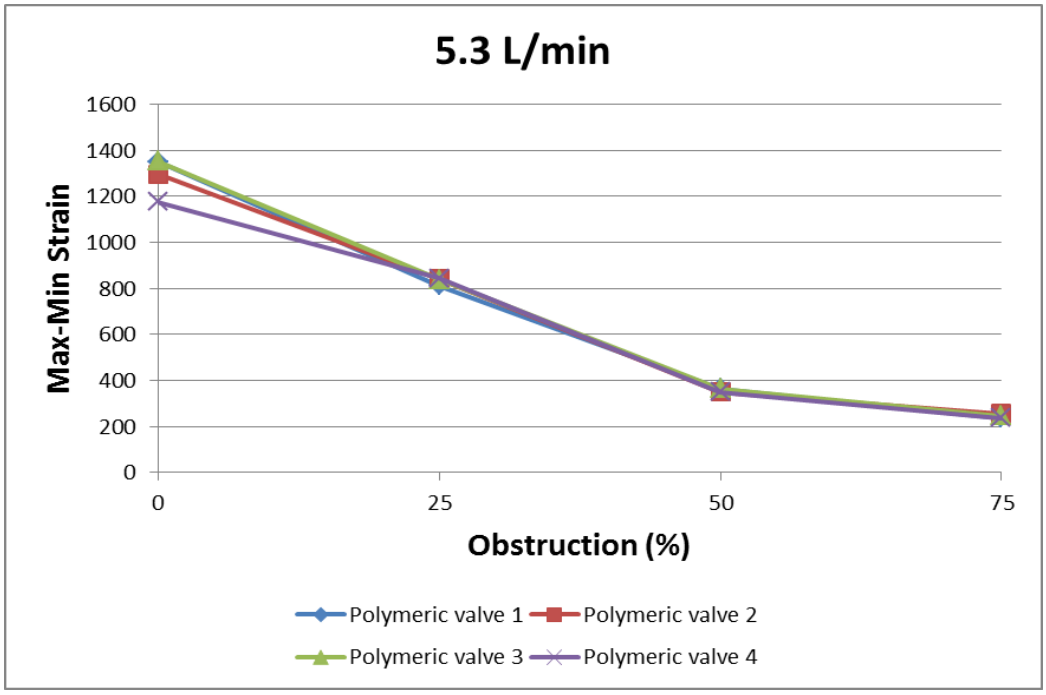

Figure 6.28. Results of stenosis simulation of strain gauged polymeric valves under a flow rate of 5.3 L/min. Data is presented as mean with n=15 cycles. One way ANOVA amongst the valves revealed statistically insignificant differences, $p>0.05$ ($p=0.858,0.784,0.776$) at the 25%, 50% and 75% obstruction conditions respectively and statistically significant difference ($p=0.00$) at the 0% obstruction condition.

5.3 L/min	0% obstruction	25% obstruction	50% obstruction	75% obstruction
Polymeric valve 1	1350.5 ± 304.2	812.3± 95.50	364.46 ±65.26	236.75± 24.08
Polymeric valve 2	1297.1±209.40	842.2±71.70	349.5± 75.1	256 ± 38
Polymeric valve 3	1354.1 ±276.7	838.50±108.2	365 ±49.74	246 ± 46.1
Polymeric valve 4	1177.4 ±173.9	845.20±116.3	350.59± 62.86	238 ± 51.6

Table 6.9. Maximum –Minimum strain difference at each degree of obstruction, at a flow rate of 5.3 L/min. Data is presented as Mean ± Standard deviation, with n=15 cycles. Strain is dimensionless.

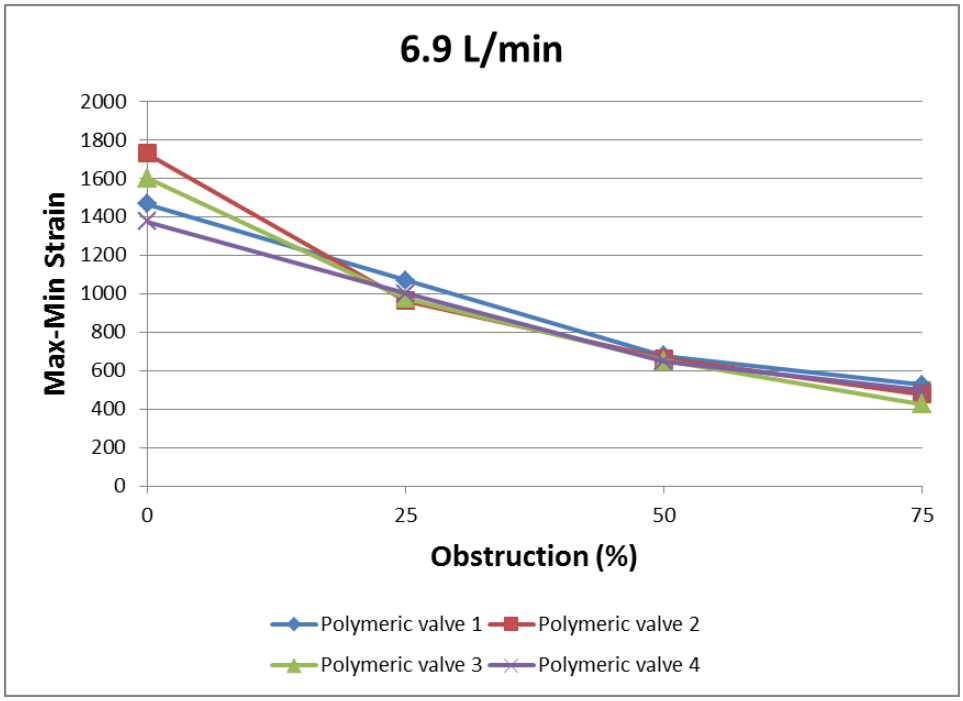

Figure 6.29. Results of stenosis simulation of strain gauged polymeric valves under a flow rate of 6.9 L/min. Data is presented as mean with n=15 cycles. One way ANOVA amongst the valves revealed statistically insignificant differences ie $p>0.05$ ($p=0.531$) at the 50% obstruction condition and statistically significant differences ie $p<0.05$ ($p=0.000$, 0.009, 0.000) in the 0%, 25% and 75% obstruction conditions respectively..

6.9 L/min	0% obstruction	25% obstruction	50% obstruction	75% obstruction
Polymeric valve 1	1468.6 ± 368.7	1068.3± 121.2	677.7 ±78.7	525.6± 27.45
Polymeric valve 2	1729.2±138.7	964.8±102.1	662.4± 71.3	476.5 ± 51.9
Polymeric valve 3	1602.1 ±123.5	976.5±59.8	652.5 ±42.4	425.33 ± 35.93
Polymeric valve 4	1376.3 ±123.1	1001.4±39.7	648.27± 26.14	498.27 ± 26.14

Table 6.10. Maximum –Minimum strain difference at each degree of obstruction, at a flow rate of 6.9 L/min. Data is presented as Mean ± Standard deviation, with n=15 cycles. Strain is dimensionless.

From figures 6.26 to figures 6.29, and tables 6.7 to 6.10, it can be observed that the peak to peak strain difference decreased with increasing obstruction/stenosis. Furthermore increasing the flow rate had an increasing effect on the strain difference.

In order to test the long term reliability of the strain gauges, a singular polymeric valve instrumented with the strain gauge was fabricated and tested in the hydrodynamic tester continuously for 10 hours. This test was conducted at a 5.3 L/min flow rate. The peak to peak strain results were averaged at 30 minute intervals and the results are presented below.

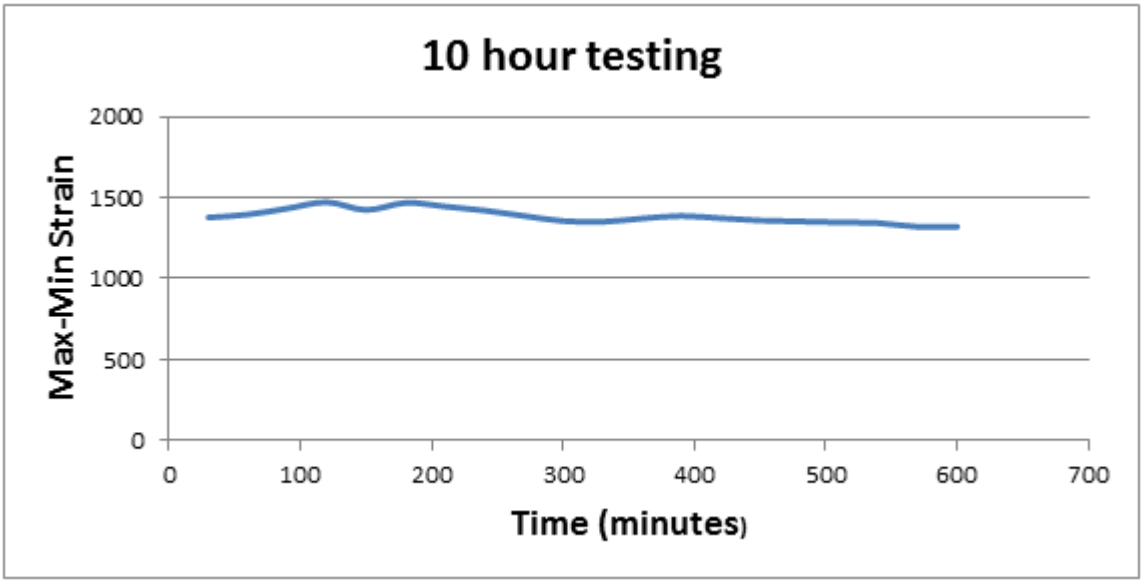

Figure 6.30. Continuous 10 hour testing of a strain gauge instrumented polymeric valve at a 5.3L/min flow rate. Data is presented as mean at 30minute intervals.

.

Time (minutes)	Mean peak to peak strain difference	Standard deviation
30	1378	345
60	1396	363
90	1433.59	404
120	1472	367
150	1424	363
180	1468	369
210	1446	178
240	1421	188
270	1388	354
300	1356	362
330	1351	247
360	1372	262
390	1387	222
420	1373	243
450	1359	250
480	1353	253
510	1348	243
540	1343	215
570	1321	244
600	1321	214

Table 6.11. Peak to peak strain data from continuous 10 hour test. Both mean and standard deviation per every 30 minutes are displayed on the table

From figure 6.30 and table 6.11, it can be observed that there was about a 3.9% drop in peak to peak strain difference from the initial to final 30 minutes. A paired t test conducted revealed $p<0.05$ thus suggesting the drop is statistically significant.

6.6. SUMMARY

In this chapter, we present the results from the custom hydrodynamic tester. Sample aortic and ventricular pressure waveforms are presented at flow rates 2.3, 3.8, 5.3 and 6.9 L/min. Systolic and diastolic aortic pressure values for 4 polymeric valves and one Carpentier Edwards SAV 2650 bioprosthetic heart valve are also presented. Mean Systolic Pressure Difference (MSPD) and Effective Orifice Area (EOA), which were the 2 variables of interests in pulsatile flow hydrodynamic testing are also presented for the 4 polymeric and one bioprosthetic heart valve under 4 flow rates. From these results , it was observed that the polymeric valves exhibited a higher MSPD and lower EOA relative to the bioprosthetic valve. Stenosis simulation tests at four levels of obstruction, (0, 25, 50 and 75%) of the polymeric and bioprosthetic valves are also presented in this chapter. From this , it was observed that the MSPD experiences a slow and steady rise with increasing level of obstruction, however at the 75% obstruction level, a massive increase in MSPD was observed, at all flow rates. 4 polymeric valves , instrumented with strain gauges have been subjected to stenosis simulation tests and the difference between the maximum and minimum strain (peak to peak strain) per cycle was measured and presented in this chapter. From these results, it was observed that the peak to peak strain decreased with increasing valve obstruction. Finally, a continuous 10 hour test was conducted on one instrumented polymeric valve in order to assess the long term reliability of the strain gauges.

CHAPTER 7 DISCUSSION

7.1 MAKING THE VALVES

Fabrication of polymeric heart valves via dipcoating is a common method used mainly due to its simplicity. Major drawbacks however include difficulty in achieving uniform thickness distribution and reproducibility. During the dipcaoting process, the mandrel is turned upside down for the solution to dry. Since the solution flows downwards under gravity, the polymer solution accumulates at the free edge of the valve leaflets, thus causing a higher magnitude of thickness after drying. For our study, we took a cue from Mackay and the valve leaflets where trimmed at the free edge after fabrication, thus getting rid of the thick accumulated dried polymer and creating a more uniform, thickness distribution (Mackay, 1992; Mackay *et al.*, 1996). The difficulty in producing uniform thickness distribution and reproducibility via dipcoating has been experienced and documented by various researchers (Jansen and Reul, 1992; Mackay, 1992; Mackay *et al.*, 1996; Kuan *et al.*, 2011; du Preez *et al.*, 2015; Masheane, du Preez and Combrinck, 2016).

Although a major focus on literature has been on finding an optimum way to achieve leaflet thickness uniformity, KuA1 et al and Clairborne et al have argued that native heart valves themselves do not possess perfect thickness uniformity but rather a thickness distribution that actually aids in their dynamic function. Specifically, the native aortic heart valves tend to have thicker leaflet edges which aids in optimum valve coaptation and also durability (KuA1 *et al.*, 2011;Claiborne, Slepian, *et al.*, 2013). As a result, the focus should be more on creating a reproducible method of manufacturing valve via dipcoating

With this in mind, our primary concern during the fabrication of our polymeric valves was to develop a method that would produce consistent and reproducible results. To do this we had to identify the variables that affect the reproducibility. Mackay and his team identified that factors such as viscosity, evaporation rate of the polymeric solution, ambient temperature, concentration of the solution , the dipping and drying process and the shape of the mould contribute to the thickness distribution and reproducibility (Mackay, 1992). Consistency in the evaporation rate, viscosity and ambient temperature was achieved in our study by placing the mandrel on a hot plate set to a constant heat setting after the dipping process. Dipping of the valves was also done inside a fume cupboard at controlled room temperature. Concentration of the polymer solution is also easily achieved by maintaining a consistent solute to solvent ratio whilst preparing the polymeric solution (full details of the polymer solution preparation are outlined in section 5.1.3). The same mandrel was used in dipcoating all the valves developed in our study, as a result as long as the integrity of the mandrel was not compromised; it no longer becomes a factor affecting reproducibility. With viscosity, evaporation rate, ambient temperature, concentration of solution and shape of the mould being easy to control, the issue of reproducibility then falls almost entirely on the dipping and drying process.

Dipping and drying process

Polymeric valves fabricated via dipcaoting is traditionally done by multiple dipping and drying cycles in a polymeric solution of low concentration till the desired leaflet thickness is achieved (Ghista and Reul, 1977; Russell *et al.*, 1980; Wisman *et al.*, 1982; Jansen *et al.*, 1991; Jansen and Reul, 1992; Knierbein *et al.*, 1992). Multiple dips however exposes the entire procedure to inconsistencies as small changes in the dipping and drying sequence per

cycle are likely to occur. These small changes over multiple dips may serve as a hindrance to reproducibility. Several researchers have tried to minimise the human/operator dependency variable on dip coating by developing mechanical and semi automated dipping mechanism, albeit with varying outcomes (Jansen and Reul, 1992; Knierbein *et al.*, 1992;Masheane, du Preez and Combrinck, 2016).

The desired leaflet thickness is mainly a function of the concentration of the solution and also the amount of consecutive dipping and drying cycles. Mackay et al suggest the desired thickness can equally be achieved by increasing the concentration of the solution and reducing the number of dips and by so doing eliminates the need for multiple dips and its associated disadvantages (Mackay *et al.*, 1996).

During initial experiments in our study, we attempted a single dip in a 60% concentrated polymeric solution as done by Mackay (Mackay, 1992). We however found out that the solution was extremely viscous and didn't allow for a good integrity of dipcoating the mandrel. Various experiments lead to a compromise of 35% w/v concentration with 2 dips as outlined in section 5.1.3. In order to achieve reproducibility, we developed a very stringent and consistent dipcoating protocol which was used throughout the valve manufacturing process.

The mandrel was inverted and clamped to a stand during the dipping process. This was done in order to eliminate movement of the valve during the dipping process. A small circular bubble level was also placed on top of the suspended mandrel to ensure perfect vertical orientation. This allows for the polymer solution to flow down the mandrel in a consistent uniform manner. The polymeric solution was stored in a glass beaker with a neck not much larger in diameter than that of the mandrel with the stent around at the tip. This was to limit lateral movement during dipping. Keeping the mandrel clamped, the container with the

polymeric solution was slowly lifted towards the mandrel till about half the length of the mandrel was coated in the polymeric solution and the container was then lowered. Another variable that was kept as consistent as possible was the time the mandrel was spent on the hot plate as the drying process per dipping cycle took place.

One other thing that occurred at randomly, was the formation of bubbles on the mandrel after dipping. This mostly appeared at the stent/leaflet junction and had to be detected early and manually eliminated before the solution dried. There was no easy remedy realised for this and this made the fabrication process difficult. Formation of the bubbles was something that was also experienced by Mackay (Mackay, 1992).

7.1.1 Comparison of results with literature

The protocol followed during dipcoating, allowed for a more reproducible method of fabricating polymeric valves to be realised. The valves designed in our lab for the study were thicker at the free edges/top of the commissure than the belly. The free edges of the polymeric valves had a mean value of 212um (n=6), whereas the belly had a mean value of 188 (n=6) see figure 7.1. This trend is consistent with results from other reserchers (Mackay, 1992; Mackay *et al.*, 1996; Rahmani, Tzamtzis, Ghanbari, Burriesci and Alexander M Seifalian, 2012; du Preez *et al.*, 2015; Masheane, du Preez and Combrinck, 2016).

The valves designed in our lab had leaflet thicknesses between (177-222um) with a mean thickness of 200um. A comparison with various studies of valves fabricated via dipcoating is presented in the table below.

Mean leaflet thickness (um)	Researchers
100-200	(Rahmani, Tzamtzis, Ghanbari, Burriesci and Alexander M Seifalian, 2012)
60-200	(Bernacca *et al.*, 1997)
48-238	(Bernacca *et al.*, 2002)
100	(Mackay *et al.*, 1996)
80-200	(Daebritz *et al.*, 2004)
100-300	(Daebritz *et al.*, 2003)

Table 7.1. Polymeric valve leaflet thickness of selected literature.

As seen in the table 7.1, common mean thickness of polymeric valve leaflets range from 48-300um. The valves produced in our study all fall well within this range. Studies show that there is an effect of valve thickness on valve durability and hydrodynamic performance with, thicker valves being more durable and thinner valves performing better hydrodynamically. Specifically, Rahmani et al in their study, discovered that thin valves (100um) exhibited superior hydrodynamic performance compared to a control bioprosthetic valve (Rahmani, Tzamtzis, Ghanbari, Burriesci and Alexander M Seifalian, 2012). Mackay et al also demonstrates that valves with thickness between 100-150um exhibit superior hydrodynamic function, however reducing leaflet thickness to less than 100um may have some concerning effects on valve durability (Mackay *et al.*, 1996). Durability testing conducted by Daebritz et al of leaflets with thickness varying from 100-300um showed that these valves were able to undergo 600milion -1 billion cycles respectively (Daebritz *et al.*, 2003). Some researchers also suggest a leaflet thickness of 150um provides the best compromise in terms of durability and hydrodynamic function (Ghista and Reul, 1977; Bernacca *et al.*, 1997; Kuan *et al.*, 2011).

In summary, one of the aims of the present study was to fabricate polymeric heart valves. We have been successful in developing polymeric valves via dipcoating with fairly good reproducibility. This was achieved by 2 successive dips in a 35%w/v polymeric solution, following a stringent dipping and drying cycles. The valves we have developed tend to be thinner in the belly relative to the free edge and were consistent with results from literature. Literature suggests that thinner valves tend to exhibit better hydrodynamic function whereas thicker valves tend to be more durable.

7.2 DESIGNING THE HYDRODYNAMIC TESTER

In the design of the hydrodynamic tester, the main objective is to simulate in so far as possible, the physiological environment of the left side of heart. This means the system has to replicate the magnitude and shape of the ventricular and aortic pressure waveform at a normal cardiac output at rest (see Wiggers diagram, figure 5.9). Looking at sample pressure waveforms at cardiac outputs between 2-7 L/min,(see figures 6.3 to 6.10), a gradual physiological rise in both ventricular and aortic pressure can be observed during the systolic phase. However during valve closure i.e. the dicrotic notch at the start of the diastolic phase, non-physiological oscillations were present in the aortic pressure waveform, after which a slow physiological decline is observed for the rest of the diastolic phase. An ideal physiological ventricular pressure waveform experiences a sharp decline in pressure during the diastolic phase to about 0mmHg. In our hydrodynamic tester however, this sharp decline exceeded in to negative values, which is not physiological. The reason for the non-physiological waveform patterns in the diastolic phase can be attributed primarily to the nature of our pump.

A common practice in the design of hydrodynamic testers (pulse duplicators or mock circulatory loop) is the use of servo motor controlled pumps (Fisher, Jack and Wheatley, 1986; Felipini, 2005; De Paulis *et al.*, 2005; Walker, 2006; Lanzarone, Vismara and Fiore, 2009; Bazan and Ortiz, 2011; Tuzun *et al.*, 2011; Leopaldi *et al.*, 2012; Taylor and Miller, 2012; Claiborne, Sheriff, *et al.*, 2013a; Fortini *et al.*, 2013; Jordaan, 2017). The advantage of servo controlled motors is that they are programmable and can be interfaced with waveform generators. This gives researchers the flexibility to alter the waveform generated by the pump in order to produce as best as possible, the physiological waveform of ventricular pressure.

The pump employed in our study is a gear motor connected to a piston arm and operates in a rocker arm like mechanism (see figure 5.6). This system doesn't allow for programming or interfacing with other control systems thus we are extremely limited in terms of pump waveform modification. This means that essentially the ventricular pressure waveform is determined by the intrinsic pump pressure profile. By connecting this pump to our membrane ventricular chamber, we were successful in creating a smoother sinusoidal ventricular waveform, although we were still plagued by non-physiological negative pressures in diastole. During experimental testing it was discovered that our pump naturally produces a high level of suction during the backward/ diastolic phase. This high suction causes a rapid pressure decline and causes polymeric valves to snap shut at the end of the systolic phase. This forcible contraction of the heart valve during closure causes the non-physiological oscillations experienced in the dicrotic notch of the aortic pressure waveform. The oscillations were also present but in the opposite direction on the ventricular pressure waveform. The sudden change in direction of fluid flow causing these oscillations in pressure waveform is a phenomenon known as "water hammer effect". Water hammer effects were experienced by various researchers who attributed it to the high velocity of the reverse flow of the pump used in the hydrodynamic tester. (Umezu *et al.*, 1986; Knierbein *et al.*, 1992;

Hirai *et al.*, 1998). Similar to our study, these researchers also employed pumps with non-programmable waveforms. The magnitude of the water hammer effect seemed to increase with increase in flow rate (see figures 6.3-10), which is logical as assuming constant area, increasing flow rate will increase velocity as per the equation Q=VA, where Q is the flow rate, V is the velocity and A is the area. Some researchers , such as De Gaetano et al also experienced negative pressure values of approximately -80mmhg at approximately 5L/min even with the use of servo controlled motors. The authors however failed to comment on this in their papers (De Gaetano *et al.*, 2015; DE GAETANO *et al.*, 2015)

Negative pressure values in the ventricular pressure waveforms may also be caused by other factors. Both Gregory and Lanzarone et al in their designs noticed a slight dip in the ventricular pressure during the start of the diastolic period which they attributed to the inertia of the fluid as it leaves the left ventricle. (Gregory, 2009; Lanzarone, Vismara and Fiore, 2009) It is important to mention that both studies utilised pumps with programmable waveform generators. Lanzarone et al actually experienced a negative pressure of approximately -50mmhg during ventricular diastole. De Gaetano et al also experienced negative pressure values of approximately -80mmhg at approximately 5L/min even with the use of servo controlled motors. The authors however failed to comment on this in their papers (De Gaetano *et al.*, 2015; DE GAETANO *et al.*, 2015). With that being said, high negative pressures are not necessarily ideal physiological conditions as it may lead to haemolysis if experienced over a long period of time (Wielogorski, Cross and Nwadike, 1975).

In an effort to mitigate the high suction effect of our pump, we tried to vary the pressure head of the pump and also inserted a custom 3D printed ball and cage valve into the suction line of the pump; however these did not have the desired effect as the waveform. The waveform pattern is intrinsic to the pump and as a result, difficult to modify. From the literature and previous studies, we believe the non physiological oscillations and high negative pressures in

the aortic and ventricular pressure waveforms respectively, could be mitigated with a pump possessing the ability to be easily interfaced with a programmable waveform generator, although this approach did not totally resolve the issues of negative pressures in some of these previous studies (De Gaetano *et al.*, 2015)

Another limitation of our hydrodynamic tester that was encountered during testing was the lack of a convenient disconnection system., Some designs of hydrodynamic testers, incorporate quick disconnect systems that allows researchers to quickly and conveniently isolate various components of the circulatory loop (Walker, 2006). This is particularly useful during the replacement of latex membranes, inserting a new test valve or generally introducing a fresh batch of perfusate. The design of our hydrodynamic tester didn't incorporate such mechanisms and as a result, complete drainage of the system was necessary prior to performing the aforementioned tasks. Although this didn't necessarily affect the results produced by the hydrodynamic tester, having to totally drain the system tends to be an arduous tasks and leads to water spillages.

Even with the limitations of the pump system, we were able to produce a fairly physiological aortic pressure waveform by introducing resistance and compliance into the hydrodynamic tester. We were successful in achieving normotensive peak systolic and diastolic aortic values of 112-125mmHg and 61-70mmHg respectively at a flow rate of 5.3L/min. Furthermore, over the systolic phase, both ventricular and aortic pressure waveforms follow closely that of the Wiggers diagram.

For the purpose of our study, we designed a hydrodynamic tester to perform pulsatile flow testing of the valve under ISO 5840:2009 standards, with parameters of interest being transvalvular pressure gradient and effective orifice area. These parameters are calculated only over the systolic phase as a result the ability of the hydrodynamic tester to simulate

adequate physiological environment during the systolic phase especially, is key. Looking at the results from the hydrodynamic tester, it can be seen that over the systolic phase, pressure tracings follow closely that of the physiological ones thus we are confident of the reliability of our system for the conduction of pulsatile flow hydrodynamic testing to assess transvalvular pressure and valve effective orifice area.

7.3 HYDROYNAMIC TESTING

7.3.1 Transvalvular pressure gradient

Pulsatile flow hydrodynamic testing helps to provide an indication of the fluid dynamic characters of the valves prior to in vivo application. Ideally, a heart valve is supposed to exhibit little to no transvalvular pressure gradient or mean systolic pressure difference (MSPD) i.e. “just a few mmHg” during the systolic phase (Klabunde, 2012b). A low pressure gradient during the systolic phase suggests low obstruction/ resistance to flow as change in pressure can be expressed as a product of flow and resistance.

For our study we tested valves in the aortic position. At baseline physiological conditions of 5.3L/min and 75bpm heart rate, the polymeric valves and bioprosthetic valve exhibit an average MSPD of 7.73 and 5.53mmhg respectively (see figure 6.19). The ISO 5840:2009 standards do not necessarily specific an accepted range of pressure gradient values, however the results from our study have been compared to that from literature at baseline physiological conditions of 4-6L/min. Dea Geateno et al performed pulsatile flow hydrodynamic tests on 2 types of 21mm polymeric valves in the aortic position and reported MSPD values of approximately 5.5 and 12.20 mmHg respectively at 5L/min (De Gaetano *et al.*, 2015). Clairborne et al observed MSPDs of 20.91mmHg with their xSIBS polymer valves at 5.6L/min (Claiborne, Sheriff, *et al.*, 2013b). This is about 2.7 times than the 7.73mmhg experienced in our study thus suggesting superior hydrodynamic function of our valves. Rotman et al reports a MSPD of approximately 16mmHg at 5l/min during their

hydrodynamic testing of 21 mm polymeric TAVI in a Vivitro Pulse duplicator (Rotman, Kovarovic, Chiu, *et al.*, 2019). Pulsatile flow testing of polymeric TAVI valves by Guo et al revealed MSPD of approximately 8.2mmHg at 5.6L/min. In another study, Rahmani et al designed and performed pulsatile flow hydrodynamic testing on POSS-PCU nanocomposite polymeric valves of 21 mm internal diameter and mean leaflet thickness of 100, 150 and 250um. At baseline physiological cardiac output of 5L/min, the researchers report a much lower MSPD between 2-5mmHg (Rahmani, Tzamtzis, Ghanbari, Burriesci and Alexander M. Seifalian, 2012). Burresci et al also reports a pressure difference of 3.2mmHg on their 22mm internal diameter polymeric valves tested at 5L/min (Burriesci, Marincola and Zervides, 2010).

Looking at figure 6.19, the MSPD increases with increasing flow rate and this is consistent with results from literature involving pulsatile flow testing of heart valves (Fisher, Jack and Wheatley, 1986; Mackay *et al.*, 1996; Wheatley *et al.*, 2000; De Paulis *et al.*, 2005; Rahmani, Tzamtzis, Ghanbari, Burriesci and Alexander M. Seifalian, 2012; Claiborne, Sheriff, *et al.*, 2013a; De Gaetano *et al.*, 2015; DE GAETANO *et al.*, 2015; Rotman, Kovarovic, Chiu, *et al.*, 2019;Rahmani *et al.*, 2019). Pressure difference is directly proportional to flow rate according to the equation Pressure difference=Flow *Resistance. Thus assuming resistance to flow is constant, increasing the rate of forward flow affects the pressure difference accordingly.

Comparing the results of our polymeric valves to that of the control Carpenter Edwards SAV 2650 bioprosthetic valve, it can clearly be seen that at all instances of cardiac outputs, the pressure differences where significantly lower in the bioprosthetic ones than that of the polymeric valves $p<0.05$ (5.53mmHg at 5.3L/min) there are a couple of reasons for this.

Firstly is the size difference. The polymeric valves designed in our lab have internal diameters of approximately 22mm. The ideal comparison situation would have been to have a bioprosthetic valve of roughly the same size of the polymeric valve. However the closest we were able to get was a 27mm internal diameter Carpentier Edwards SAV valve. with a valve with a bigger radius, one would expect less resistance to forward flow to be experienced. This can be expressed mathematically with a variation of poisulles law considering laminar flow in a tube i.e. $R \propto \frac{n.L}{r^4}$ ……eq 7.1, where R is the resistance, n is the viscosity, L is the length of the tube, r is the radius of the tube. An increase in the radius, leads to an increase in the geometric orifice area of the valve, will culminate in a reduction of the pressure gradient. Hagen Pouiseulle's law describes the relationship between pressure and area in a flow conduit as $\Delta P \propto \frac{F}{A^2},$ ……eq 7.2 where ΔP is the transvalvular pressure, F is the flow rate and A is the cross sectional area of the conduit, or the valve in this situation.

Marquez et al, in their performance of pulsatile flow hydrodynamic testing of various bioprosthetic valves also discovered a wide range of values for MSPD and an inverse relationship between pressure difference and size (Marquez, Hon and Yoganathan, 2001). The results are presented in the figure below.

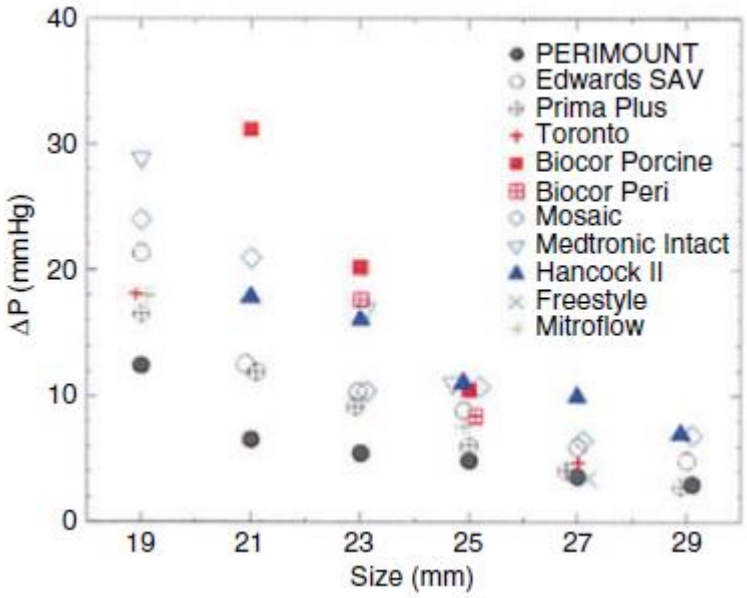

Figure 7.1. Pressure gradient against valve size for various commercially available bioprosthetic valves in the aortic position. Figure taken from (Marquez, Hon and Yoganathan, 2001) in " Heart valves from clinical design to implementation"

Observing figure 7.1, Marquez et al reports a pressure difference of approximately 6mmHg for the 27mm Edwards SAV. The Edwards SAV valve, also known as the Carpentier Edwards SAV valve, is the same model and size used as a control valve for our experiments. During our pulsatile testing, we observed a 5.53 mmHg pressure difference at 5.3 L/min, which is similar to that reported by Marquez et al.

Another reason for the significant difference between the polymeric and bioprosthetic valve in our study, was the flexibility and thinness of the valve stent and valve leaflets respectively. The Carpentier Edwards valve has a noticeably more flexible stent and thinner leaflets in comparison to our polymeric valves. This aids in hydrodynamic function by ensuring the valve opens wide during forward flow thus ensures the valve makes full use of its orifice area with less obstruction to flow.

7.3.2 Effective Orifice Area (EOA)

The ISO 5840:2009 defines the minimum acceptable effective orifice area under baseline physiological cardiac output of 5L/min, as a function of size and also position. For valves tested in the aortic position, minimum performance requirements for effective orifice area is presented below.

size(mm)	19	21	23	25	27	29	31
EOA(cm^2)	≥0.70	≥0.85	≥1.00	≥1.20	≥1.40	≥1.60	≥1.80

Table 7.2. Minimum acceptable requirements of effective orifice area of aortic prosthetic valves. Data taken from ISO 5840:2009

The polymeric valves fabricated in our labs have a 22mm size. Thus the closest to that size in the table 7.2, is either the 21 or 23mm valve size. Since the table above is the minimum requirements, we have decided to compare our valves to that of the 23mm valves with an acceptable EOA of ≥1cm^2 . Looking at figure 6.20, the 4 polymeric heart valves all displayed an EOA >1cm^2 (mean 1.36cm^2) at 5.3 L/min, thus showing our valves exceeds minimum performance requirements. The EOA's increased with increasing flow rate which can be explained mathematically from the Gorlin's equation (see 5.3.5). In fact except for the lowest flow rate of 2.3L/min, EOA's exceeded 1cm^2 for all other instances of simulated cardiac output. There's also an inverse relationship between the systolic pressure difference and EOA experienced in our study, (see figures 6.19 and 6.20) which is in line with the Gorlin's formula.

The EOA of the control Carpentier Edwards bioprosthetic valve was significantly higher than that of the 4 polymeric valves at 5.3L/min i.e. 1.6cm^2. The Gorlin's formula used to calculate EOA is a function of the Mean Systolic Pressure Difference (MSPD) and as a result, whatever influences the pressure difference will ultimately affect the EOA. As earlier

explained, the MSPD of the bioprosthetic valve was lower than that of the polymeric valve due to size difference, stent flexibility and thickness of the leaflets. Thus employing the Gorlin's formula with the MSPD values, a higher EOA was suspected and also realised in our experiments.

The results of our polymeric valves were relatively comparable with some of the commercially available prosthetic heart valves in literature. Some EOAs of commercial valves conducted under pulsatile flow heart valve testing by Yoganathan et al are presented in the table below .

Type	Valve	EOA (cm^2)
Tilting disc	Bjork Shiley Monostrut	2.00, *1.45
	Medtronic Hall	2.26,
Bileaflet	St Jude Medical	2.24, *1.81
	Carbiomedics	2.28, *1.66
	Sorin Bicarbon	2.07, *1.54
Stented bioprosthetic	Hancock Porcine	1.73, *1.31
	Hancock II porcine	1.81, *1.48
	Ionescu-Shiley Standard Pericardial Mosaic Porcine	1.74, * 1.54
	Mitroflow Pericardial	2.12
Non stented bioprsothetic	Medtronic Freestyle Porcine	2.69 *2.17
Polymeric valve	***22mm valve designed for our study***	*****1.36***

Table 7.3. EOA's of selected commercially available prosthetic valves and also the valve designed for this study *=21mm, **=22mm all others are 23mm. The polymeric valve designed for this study is expressed in bold italic font in the last row. Data for commercially available valves taken from (Yoganathan, He and Casey Jones, 2004)

It should be mentioned that pulsatile flow testing can also be conducted to assess other parameters such as valve regurgitation, energy losses and opening and closing times of the

valve with our study being focused on valve obstruction, pulsatile flow testing was done to assess the parameters that indicate obstruction thus we focused on transvalvular pressure gradient and EOA. Based on the results from these parameters, it can be said that the polymeric valves not only met but exceeded the minimum requirements of pulsatile flow testing. The success of the polymeric valves in terms of passing the tests reaffirms the potential of polymeric heart valves as a total heart valve replacement option.

7.4 THE EFFECTS OF OBSTRUCTION ON TRANSVALVULAR PRESSURE

Obstruction of heart valves occur commonly through thrombus and pannus formation in mechanical valves and calcification of bioprosthetic valves. When this happens, it effectively narrows the area of the valve and theoretically causes a high pressure build up upstream of the valve relative to downstream, thus causing an increase in the transvalvular pressure gradient.

For the purpose of our work, we were interested in determining a pattern between increasing obstruction and the transvalvular pressure gradient. Knowing this pattern will allow us to determine the validity of the sensors to be ultimately instrumented into the heart valves. In obstruction simulation studies, researchers such as (Lanning and Shandas, 2003) simulated increasing levels of thrombus formation in mechanical valves by applying increasing layers of silicone rubber to the interior side of the valves. In our study we used obstruction discs that effectively obstruct a % of the valve annulus. This was to provide a more stable and controllable way of systematically increasing the level of obstruction. This is by no means to duplicate the formation of thrombus or pannus formation but rather the pathophysiology and mechanical effects of valve stenosis.

Looking at figure 6.21 to 6.24, it can be observed that the transvalvular pressure rose with increasing flow rate and also increasing obstruction. A graph of obstruction vrs flow rate for each of the 4 polymeric valves is presented below

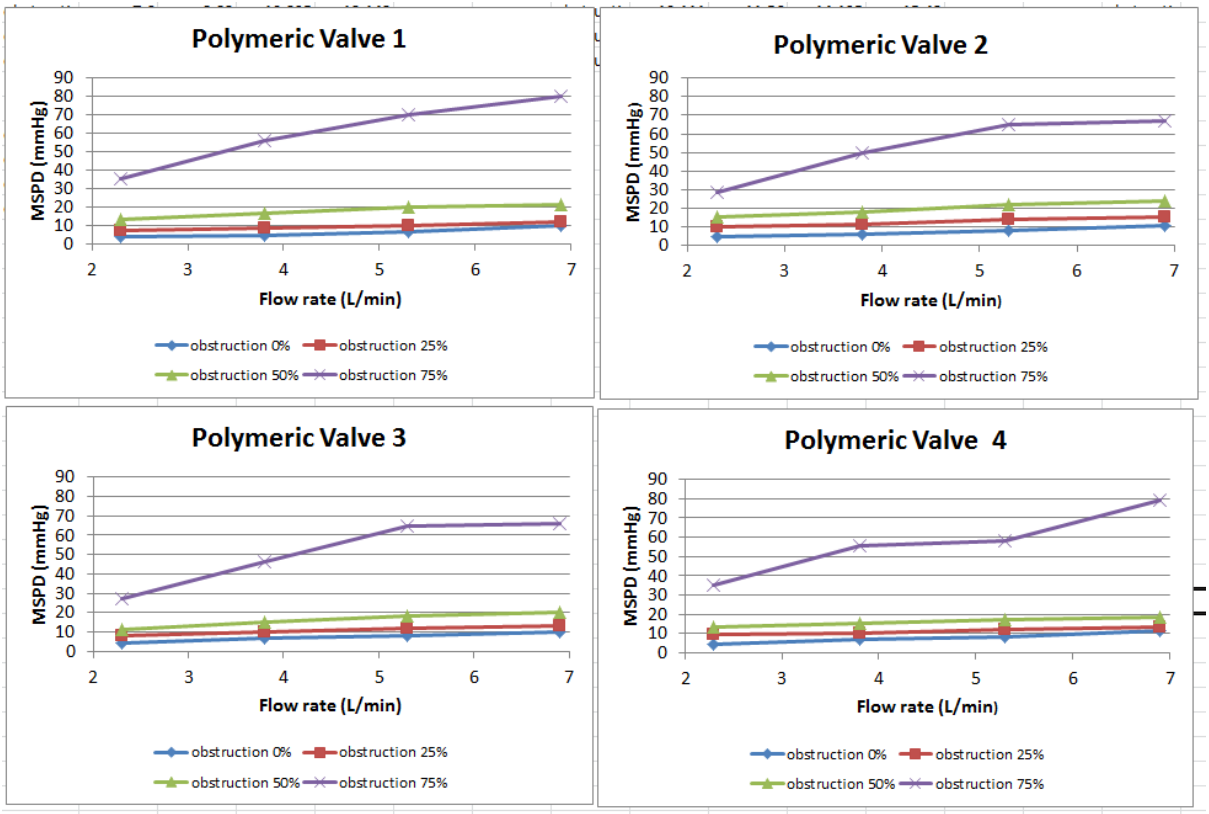

Figure 7.2. Flow rate, obstruction and their corresponding effects on transvalvular pressure gradient for the 4 polymeric valves subjected to obstruction tests.

According to AHA/ACC guidelines, severe Aortic Stenosis (AS) is characterised by MSPD >40mmhg, moderate AS (25-40mmHg) and mild AS (<25mmHg) (Bonow et al., 2006).

Both polymeric and bioprosthetic valve exhibited an exponential like rise in MSPD as obstruction levels were introduced. They began as slow increments from a no obstruction state to a 50% obstruction state, where they suddenly increase as obstruction is increased to 75%. With the exception of the low flow rate of 2.3L/min, no to mild stenosis were experienced from a 0%-50% obstruction state (ie MSPD<25). At 75% obstruction however,

all the polymeric valves experienced severe stenosis (ie MSPD>40mmHg) according to the ACC/AHA classification. Under the same obstruction conditions, 2.3 L/min flow rate displayed low MSPDs with the highest being 31.6mmHg at 75% obstruction condition. Based solely on the cut-offs for stenosis by the ACC/AHA standards, this would have been classified as mild instead of severe stenosis thus leading to the underestimation of the severity of valve stenosis. The findings from this experiment are consistent with a conundrum known as "low flow, low gradient stenosis", which suggests that patients with severe stenosis may present low transvalvular pressure gradients under low flow (Hachicha *et al.*, 2007; Clavel *et al.*, 2008, 2013; Tribouilloy *et al.*, 2009; Dumesnil, Pibarot and Carabello, 2010; Pibarot and Jean G Dumesnil, 2012). In such instances, means of assessing stenosis severity such as valve resistance, stroke work, dobutamine stress test may be employed (Bonow *et al.*, 2006). According to Clavel et al, low flow low gradient stenosis affects about 5-10% of patients with aortic stenosis (Clavel *et al.*, 2008), whereas Hachicha et al suggests it actually affects about 35% of patients with AS (Hachicha *et al.*, 2007).

From the figures 6.21 to 6.24, it can be seen that the relationship between MSPD and obstruction is not linear but rather exponential in nature. According to the Hagen-Poiseulles equation describing flow in a pipe,

$\Delta P = \frac{8\mu LQ}{\pi r^4}$, where μ is dynamic viscosity, L=length of the pipe, Q is the flow rate and r is the radius of the pipe. Now since cross sectional area of a conduit is $A = \pi r^2$, the equation can then be modified as $\Delta P = \frac{8\mu LQ}{A^2}$. Relating this to our experiments, at each flow rate, L, Q,μ are constant thus the equation is further reduced to $\Delta P = K\frac{1}{A^2}$, where K is a constant. Introducing obstruction discs to simulate stenosis, as done in the study, causes a reduction in the radius of the valve annulus and subsequently the area of the flow conduit. The equation $\Delta P = K\frac{1}{A^2}$, is analogous to the function $y = \frac{1}{x^2}$, where ΔP is y, A is x and K is assumed as 1.

Plotting this function with arbitrary x values, with x decreasing, also yields an exponential curve of similar pattern to the ones from our study (see figures 6.21 to 6.24), thus validation our findings.

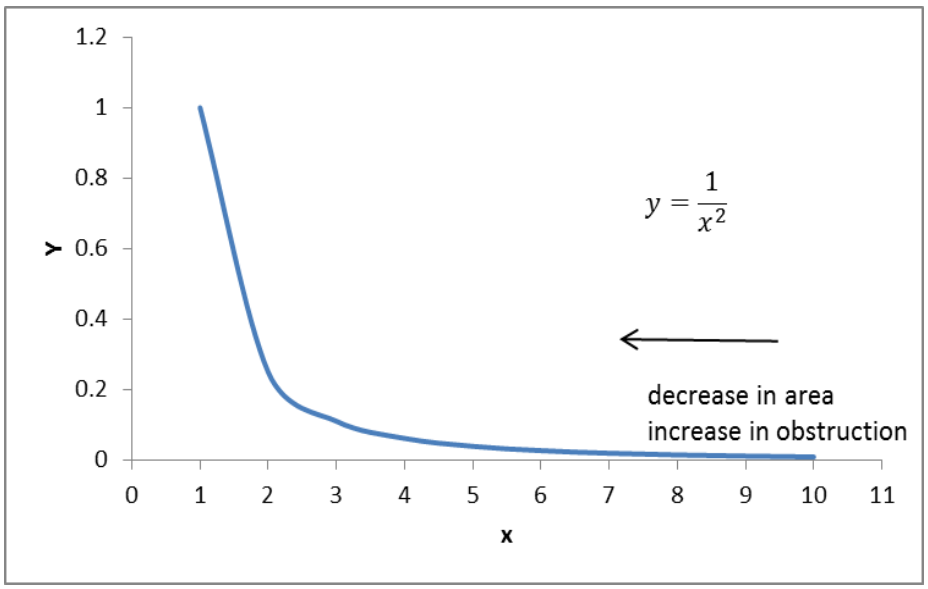

Figure 7.3. Plot of the function y=1/x^2 , with x being arbitrary values of the range 10≥x≥1

The pattern of MSPD with obstruction ie slow and steady rise with a sudden upshot, supports the idea that valve stenosis, which presents as obstruction of the valve, is a slow progressive disease which may not necessarily present very clear symptoms until the situation becomes severe (Iung et al., 2002; Magant et al., 2010).

Comparing the results of the polymeric valve to that of the bioprosthetic valve, it is seen that at all instances of cardiac output and obstruction conditions, the polymeric valves consistently exhibited a higher MSPD as compared to the bioprosthetic ones. This again can be attributed mainly to the difference in diameter of the bioprosthetic valve relative to the polymeric valve. Obstruction was expressed in decrements of 25% of the valve annulus. However since the valve diameters are different, i.e. 27mm for bioprosthetic and 22mm for polymeric valve, 25% increments in obstruction will still result in different diameters as seen

in table 5.1. The effective internal diameter of the bioprosthetic valve will thus be larger than that of the polymeric valve, causing lower MSPDs to be experienced. Similar to the pulsatile flow testing results, the flexibility of the bioprosthetic valve stent and also its thinner leaflets could also be additional causes for the lower pressure differences experienced.

7.5 INSTRUMENTATION OF THE VALVES

The purpose of instrumenting valves with sensors is to investigate its potential as a diagnostic tool for detection of valve obstruction or stenosis. The ability to acquire direct and continuous data from the valve, via the use of the sensors, can go a long way to aid in accurate diagnosis of valve obstruction.

For the purpose of our study, strain gauges were attached to the interior portions of the valve stents and valves were subjected to the obstruction simulation tests. Sections 5.5.2 and 5.5.3 explains the justification of our choice of strain gauges. We were interested to determine changes in peak to peak strain difference on the valve stent during simulated obstruction.

In an ideal unobstructed valve, an increase in pressure in the valve (intervalvular pressure) is expected during systole as the valve opens to accommodate fluid flow. This increase in pressure will theoretically put the interior portion of the valve stent under tension i.e. peak positive strain. Conversely, compression strain (i.e. peak negative strain) is expected in diastole (see figure 6.25) . As a result it is expected that the ability to detect changes in peak to peak strain difference would aid in detecting the obstruction state of the valve.

From looking at the figures 6.26 through to 6.29, it can be observed that the peak to peak strain difference decreases as the obstruction increases. The peak to peak difference also increases as the flow rate is increased. This implies that as the obstruction increases, the

amount of fluid flow and as a result, pressure in the valve decreases. This manifests as a lower magnitude of strain experienced by the walls of the valve stent. Lower tension and compressive strains being experienced from our findings further suggests that opening and closing of the valve is compromised during obstruction, which is similar to the effects of obstruction in vivo. Since pressure of the fluid exerts a strain on the wall of the stent, assessing the peak to peak strain provides an indication of the pressure changes within the valve ie intravalvular pressure.

Looking at the data from the strain gauging the polymeric valves, it can be observed that the peak to peak strain difference was statistically different amongst the 4 instrumented polymeric valves under a 0% obstruction condition at 5.3L/min, a 0% and 75% obstruction condition at 3.8L/min and 0%, 25% 75% obstruction condition at 6.9L/min ($p<0.05$). All other flow rate and obstruction conditions exhibited insignificant differences between the 4 polymeric valves ($p>0.05$). This suggests that the strain gauges exhibit fairly consistent and reliable results with regards to peak to peak strain difference.

The data from the strain gauges is placed in juxtaposition with that from the biopac pressure transducers for comparison

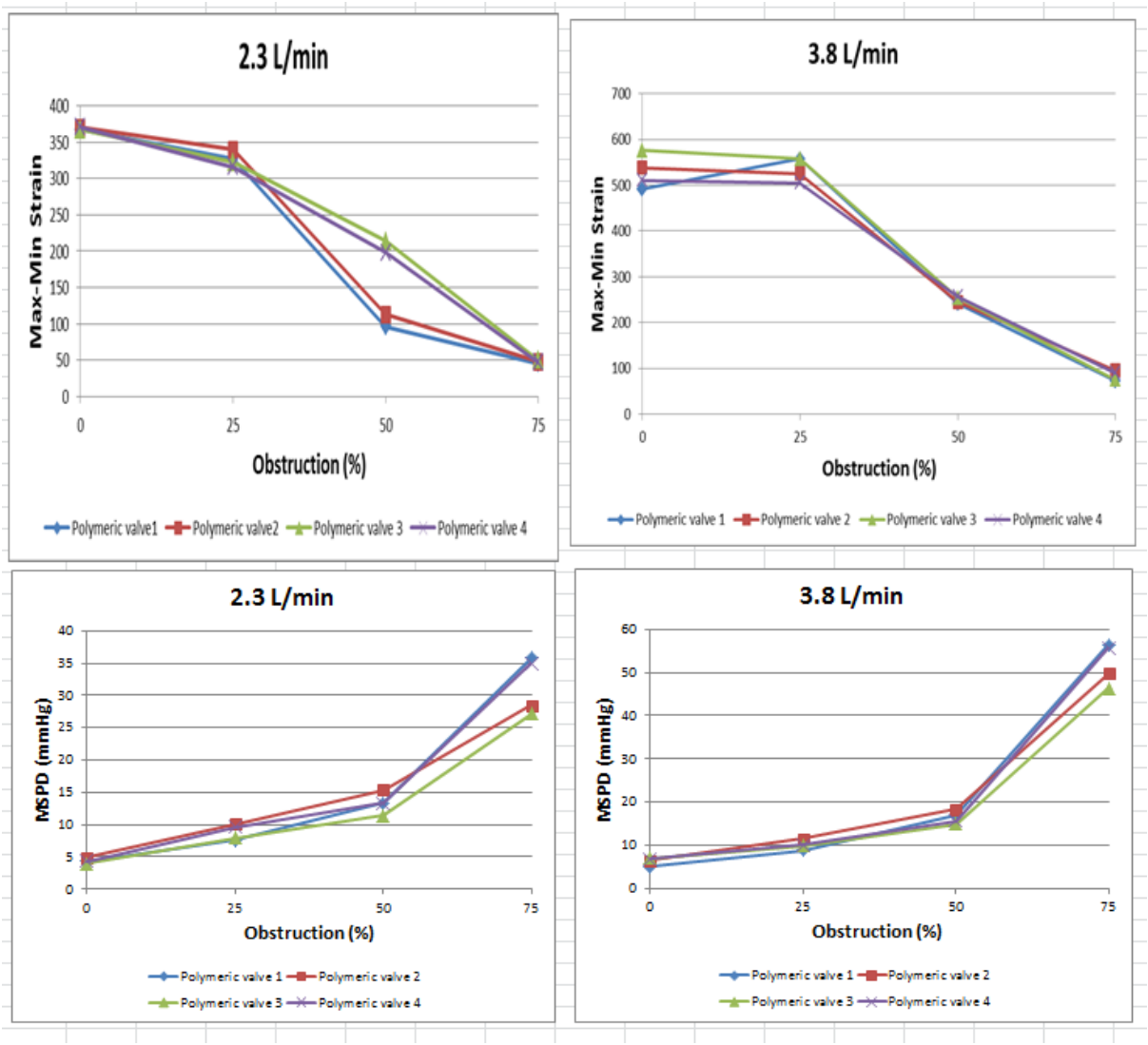

Figure 7.4. Obstruction simulation results of strain gauge and BIOPAC pressure transducers at flow rates of 2.3 and 3.8L/min. top row =strain gauge, bottom row= BIOPAC pressure transducers

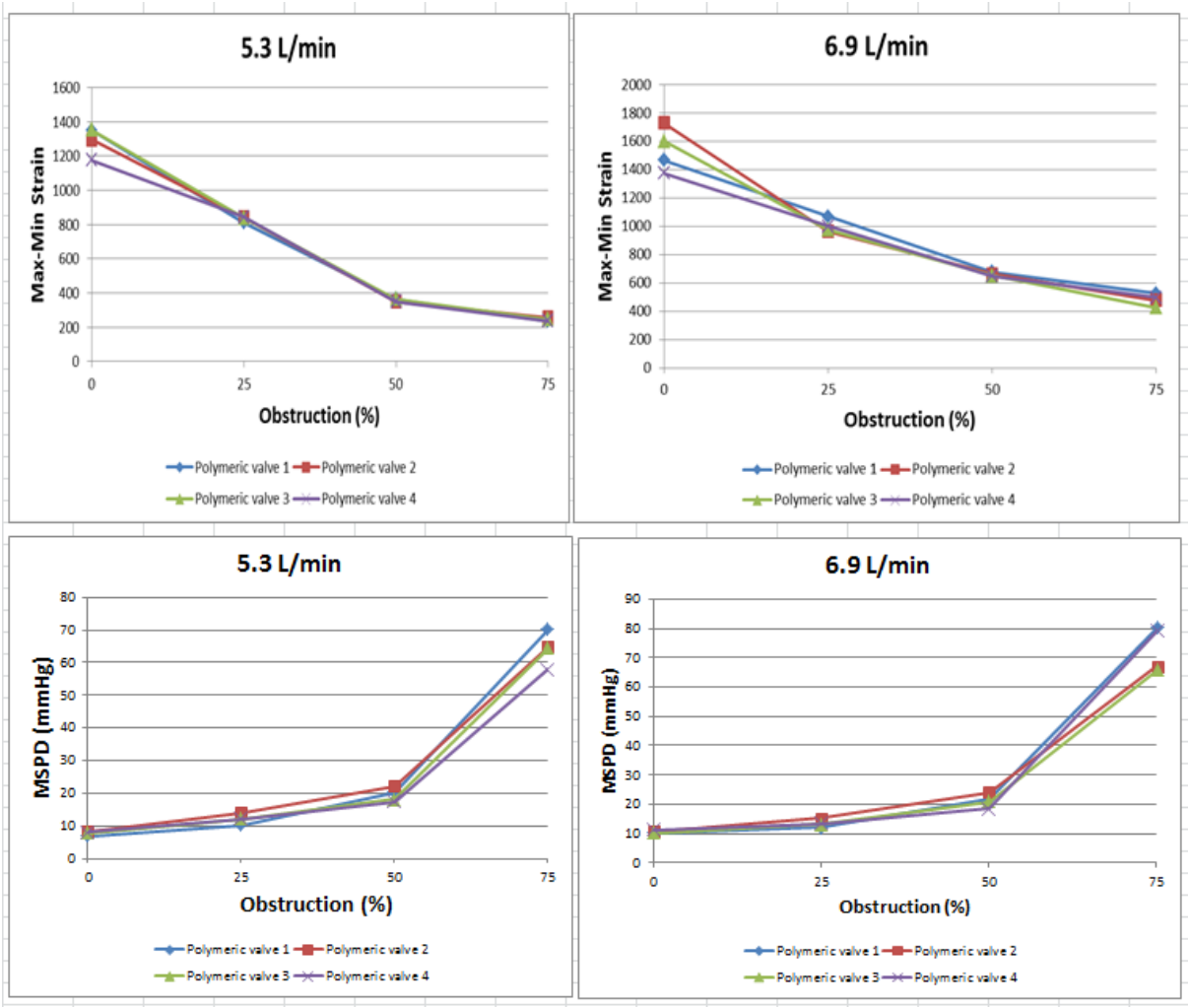

Figure 7.5. . Obstruction simulation results of strain gauge and BIOPAC pressure transducers at flow rates of 5.3L/min and 6.9 L/min. top row =strain gauge, bottom row= BIOPAC pressure transducers.

Visual observation of figures 7.4 and 7.5 shows an inverse relationship between data acquired from the strain gauges and that from the BIOPAC pressure transducers. The MSPD increases with an increase in obstruction whereas the strain difference decreased with an increase in obstruction. This is because, both strain gauges and the BIOPAC pressure transducers were not measuring the same variable. During the obstruction simulation tests with the BIOPAC pressure transducers, 2 pressure transducers were placed in ports upstream and downstream the valve in the aortic position and the difference between the pressures recorded

(TRANSVALVULAR PRESSURE) was calculated. As obstruction is introduced, the ventricular pressure increases relative to the aortic pressure thus causing a higher pressure difference across the valve in the aortic position to be observed. On the other hand, by instrumenting the valves with strain gauges, the parameter that can be practically measured is the strain exerted on the inner walls of the valves stent. This strain exerted is a direct function of the pressure experienced in the valve, as a result as previously mentioned , this method assesses the pressure in the valve i.e. (intravalvular pressure), instead of pressure across the valve. With our method of obstruction simulation, a low volume of fluid flows through the valve under obstruction thus less pressure is exerted on the walls of the stent which is detected as the low peak to peak strain difference by the strain gauges.

Our findings suggest considering flow in a heart valve, the intravalvular pressure has an inverse relationship with transvalvular pressure when the valve annulus is obstructed.

Although strain gauges are employed as components in a lot of implantable pressure sensors, literature on the direct application of strain on heart valves is very limited. Lin et al employed micro strain gauges imbedded in polymeric valve leaflets in order to investigate the strain distribution in the leaflets with the aim of ultimately enhance durability of these leaflets (Lin *et al.*, 2010). Rainer et al also investigated both in vitro and in vivo stress forces on a aortic prosthetic valve using strain gauges (Rainer *et al.*, 1975). Extensive literature search however did not yield much result on the application of strain gauges directly on the stents of polymeric valves. In our study, we faced some challenges which could possibly be related to the unpopularity of strain gauging valve stents. These challenges are highlighted below:

The valve stents were machined from a thermoplastic acetal homopolymer known as Delrin. When a polymer material is subjected to a constant stress, the material doesn’t experience a constant strain but rather an increase in strain with time. This property is known as “creep”

and is more pronounced in plastics than metals (Gerdeen, Lord and Rorrer, 2006). Creep was particularly an issue when we attempted to calibrate the strain gauge as a function of pressure. In our attempt to calibrate we had inserted the strain gauged valve stent in an airtight chamber pressurised to a constant pressure value. However, continual step wise increase in the strain was recorded even under the constant pressure. This increase in strain was however not consistent nor did it possess good repeatability. Additionally, the rate of loading and unloading was very inconsistent with the strain gauges attached to the stent. Essentially, there was no linear or easily identifiable pattern between the strain and pressure under steady state making calibration difficult. Examining the strain gauge data under pulsatile flow, ie pulsatile pressure, however, it was realised that the time occurrence of the maximum and minimum strain coincided with the systolic and diastolic aortic pressures respectively (see figure 6.25) and had fairly good repeatability over a short period of time. This informed our decision to make the difference in the maximum and minimum strain the parameter of interest of the valve instrumentation process.

Another challenge faced was achieving adequate bonding. Strain gauges detect the strain of the surface it is bonded to. As a result for accurate results, the integrity of bonding between the strain gauge and the measuring surface has to be impeccable. The curvature of the interior wall of the valve stent did present a challenge with regards to bonding. We also had to make sure that the strain gauges and adhesives being employed were suitable for bonding on plastic surfaces. During the installation of the strain gauges, there were moments when the strain gauges came off after installation and new gauges had to be installed before testing, which made the process cumbersome. Improper bonding of the strain gauges could also lead to creep and hysteresis like properties in the strain gauge data thus leading to questionable reliability (Enser *et al.*, 2017).

A summary of our findings from strain gauging the valves are listed below:

- Strain experienced on the wall of the polymeric valve stent decreases as the obstruction of the valve annulus is increased. This suggests that in pressure in the valve, (intervalvular pressure) reduces when the valve is obstructed.
- The strain gauges were able to detect these changes in strain during obstruction.
- The pressure in the valve (intervalvular pressure) has an inverse relationship with pressure across the valve (transvalvular pressure) when the valve annulus is obstructed.
- Issues such as creep and inadequate bonding between the strain gauge and its measuring surface could potentially cause inaccuracies in strain detected.

CHAPTER 8 CONCLUSION

This aim of this thesis was to determine if instrumenting heart valves would provide information on the obstruction condition of heart valves. This is the first step to ultimately realise an alternate diagnostic solution that incorporates direct and continuous monitoring of valve function after implantation.

To achieve this aim, we set out a list of specific objectives:

First objective was to manufacture polymeric valves. These valves were developed via dipcoating in a 35% w/v polymeric solution. We also developed a stringent dipping and drying protocol that aided in a relatively reproducible method of developing polymeric valves. Based on the success, we are confident we have been able to 100% meet this objective.

The second objective was to develop a hydrodynamic tester or mock circulatory loop within which the manufactured valves can be tested in. this circulatory loop is to simulate the physiological pressure and flow conditions of the left side of the heart. This was achieved by employing a 2 element windkessel model with compliance and peripheral resistance components. The pressure tracings of both aortic and ventricular pressure were physiological in the systolic phase, however non physiological oscillations were observed during valve closure which was mainly attributed to the high suction effect created by the pump. Based on the results from the tester, we are confident we have been able to achieve 80% of this objective.

The third objective was to perform pulsatile flow hydrodynamic testing of the manufactured polymeric valves . This was to assess the hydrodynamic performance of the valve over the systolic phase with regards to transvalvular pressure gradient and effective orifice area. Hydrodynamic performance was assessed over 4 different flow rates between 2-7L/min. The

results suggests that the all the polymeric valves exceeded the minimum requirements for effective orifice area according to the ISO 5840:2009 standards. We are confident we have been able to achieve 100% of this objective.

The fourth objective was to investigate the effect of obstruction on the transvalular pressure difference over the systolic phase. Four increasing levels of obstruction were simulated under the same flow conditions of hydrodynamic testing. Our findings suggest that the pressure difference began as an initial slow and steady increase with increase in obstruction and then at severe obstruction, there was a sharp increase in pressure difference was detected. With these findings, we are confident we have been able to achieve a 100% of this objective.

The fifth and final objective was to instrument the valves with sensors and investigate their ability to detect obstruction conditions. Strain gauges were attached to the interior walls of the valve stent and obstruction simulation tests were conducted. The strain guage was able to detect maximum tension and maximum compression strain which are indicative of systolic and diastolic pressures respectively. The difference between the maximum and minimum strain was the variable of interest. From the findings , it can be seen that the difference in strain decreased as the obstruction levels were increased, thus suggesting that the sensors are able to detect changes in intravalvular pressure indicative of valve obstruction. Issues such as creep of the polymer stent and bonding inconsistencies however serve as challenges in the use of strain gauges in polymeric valves. Based on these findings, we are confident we have been able to achieve 80% of this objective.

CHAPTER 9. FUTURE WORKS

Future works include:

- Improving upon the design of the hydrodynamic tester to create a more physiological nature of pressure waveform tracings in the hydrodynamic tester. This can be achieved by employing a servo controlled linear actuator pump with a programmable waveform detector. We also would look to make the operation of the hydrodynamic tester more convenient by introducing a quick disconnect system.
- Performing further hydrodynamic and durability testing of the heart valves
- Miniaturisation of the sensor system and also investigating the best way to incorporate telemetry to aid wireless transmission of signals from the sensors.
- In vitro and in vivo testing of valves with the miniaturised sensor system, incorporated with wireless capabilities under obstruction conditions.

REFERENCES

Aguirre-chagala, Y. E., Altuzar-aguilar, V. M., Domínguez-chávez, J. G., Rubio-Cruz, E. F. and Mendoza-Barrera, C. O. (2017) 'Influence of Relative Humidity on The Morphology of Electrospun Polymer Composites', *Der Chemica Sinica*, 8(1), pp. 83–92.

Allen, M., Fonseca, M., White, J., Kroh, J. and Stern, D. (2006) 'High Q Factor Sensor', 1(12), p. 19.

Altaf, K., Ashcroft, I. . and Hague, R. J. . (2011) 'Investigation of the effect of relative humidity on polymers by depth sensing indentation', *Journal of Material Science*, 46(23), pp. 7551–7557.

Amar, A. Ben, Kouki, A. B. and Cao, H. (2015) 'Power approaches for implantable medical devices', *Sensors (Switzerland)*, 15(11), pp. 28889–28914.

Andreucci, M., Faga, T., Serra, R., De Sarro, G. and Michael, A. (2017) 'Update on the renal toxicity of iodinated contrast drugs used in clinical medicine', *Drug, healthcare and patient safety*. Dove Medical Press, 9, pp. 25–37.

Annabi, M., Salaun, E., Cosyns, B., Lancellotti, P. and Pibarot, P. (2018) 'Multimodality Imaging Assessment of Prosthetic Aortic Valve', in Fattouch, K., Lancellotti, P., Vannan, M. A., and Speziale, G. (eds) *Advances in Treatments for Aortic Valve and Root Diseases*. Cham: Springer International Publishing, pp. 95–123.

Attmann, T., Steinseifer, U., Cremer, J. and Lutter, G. (2006) 'Percutaneous valve replacement: a novel low-profile polyurethane valved stent', *European Journal of Cardio-Thoracic Surgery*, 30(2), p. 379.

Awtry, E. and Davidoff, R. (2011) 'Low-flow/low-gradient aortic stenosis', *Circulation*, 124(23), pp. 739–742.

Axisa, F., Jourand, P., Lippens, E., Rymarczyk-Machal, M., De Smet, N., Schacht, E., Vanfleteren, J., Puers, R. and Cornelissen, R. (2009) 'Design and fabrication of a low cost implantable bladder pressure monitor', *Proceedings of the 31st Annual International Conference of the IEEE Engineering in Medicine and Biology Society: Engineering the Future of Biomedicine, EMBC 2009*, pp. 4864–4867.

Bach, D. S., Schmitz, C., Dohmen, G., Aaronson, K. D., Steinseifer, U. and Kleine, P. (2012) 'In vitro assessment of prosthesis type and pressure recovery characteristics: Doppler echocardiography overestimation of bileaflet mechanical and bioprosthetic aortic valve gradients', *The Journal of Thoracic and Cardiovascular Surgery*, 144(2), pp. 453–458.

Bagno, A., Anzil, F., Buselli, R., Pesavento, E., Tarzia, V., Pengo, V., Bottio, T. and Gerosa, G. (2009) 'Bileaflet mechanical heart valve closing sounds: in vitro classification by phonocardiographic analysis', *Journal of Artificial Organs*, 12(3), pp. 172–181.

Bagno, A., Anzil, F., Tarzia, V., Pengo, V., Ruggeri, A. and Gerosa, G. (2009) 'Application of Wavelet Analysis to the Phonocardiographic Signal of Mechanical Heart Valve Closing Sounds', *The International Journal of Artificial Organs*. SAGE Publications, 32(3), pp. 166–172.

Bagno, A., Buselli, R., Anzil, F., Tarzia, V., Pengo, V., Ruggeri, A., Bottio, T. and Gerosa, G. (2008) 'In vitro characterization of bileaflet Mechanical Heart Valves closing sound', in *2008 Computers in Cardiology*, pp. 945–947.

Baldoni, J. A. and Yellen, B. B. (2007) 'Magnetic tracking system: Monitoring heart valve prostheses', *IEEE Transactions on Magnetics*, 43(6), pp. 2430–2432.

Barakat, M. T., Thosani, N. C., Huang, R. J., Choudhary, A., Kochar, R., Kothari, S. and Banerjee, S. (2018) 'Effects of a Brief Educational Program on Optimization of Fluoroscopy

to Minimize Radiation Exposure During Endoscopic Retrograde Cholangiopancreatography', *Clinical Gastroenterology and Hepatology*, 16(4), pp. 550–557.

Barbetseas, J., Nagueh, S. F., Pitsavos, C., Toutouzas, P. K., Qui??ones, M. A. and Zoghbi, W. A. (1998) 'Differentiating thrombus from pannus formation in obstructed mechanical prosthetic valves: An evaluation of clinical, transthoracic and transesophageal echocardiographic parameters', *Journal of the American College of Cardiology*, 32(5), pp. 1410–1417.

Barrat-Boyes, B. . ., Roche, A. . H. G., Brandt, P. W. T., Smith, J. C. and Lowe, J. B. (1969) 'Aortic Homograft Valve Replacement (A Long-Term Follow-Up of an Initial Series of 101 Patients)', *Circulation*, (40), pp. 763–775.

Barroso Freitas-Ferraz, A., Beaudoin, W., Couture, C., Perron, J. and Sénéchal, M. (2019) 'Prosthetic aortic valve thrombosis: To fibrinolyse or not to fibrinolyse? That is the question!', *Echocardiography*. John Wiley & Sons, Ltd (10.1111), 36(4), pp. 787–790.

Bashore, T. (2009) 'Clinical Haemodynamics in Valvular Heart Diseases', in Wang, A. and Bashore, T. (eds) *Valvular Heart Disease*. 1st edn. New York: Humana Press, pp. 93–123.

Bateman, M. G., Quill, J. L., Hill, A. J. and Iaizzo, P. A. (2013) 'Anatomy and Function of the Atrioventricular valves', in A, I. P., Bianco, R. W., Hill, A. J., and St. Louis, J. D. (eds) *Heart Valves From Design to Clinical Implantation*. New York: Springer Science+Business Media, pp. 3–27.

Baumgartner, H. (2009) 'The Challenge of Assessing Heart Valve Prostheses by Doppler Echocardiography', *Journal of the American Society of Echocardiography*. American Society of Echocardiography, 22(4), pp. 394–395.

Baumgartner, H., Hung, J., Bermejo, J., Chambers, J. B., Edvardsen, T., Goldstein, S.,

Lancellotti, P., Lefevre, M., Miller, F. and Otto, C. M. (2017) 'Recommendations on the echocardiographic assessment of aortic valve stenosis: A focused update from the European Association of Cardiovascular Imaging and the American Society of Echocardiography', *European Heart Journal Cardiovascular Imaging*, 18(3), pp. 254–275.

Baumgartner, H., Hung, J., Bermejo, J., Chambers, J. B., Edvardsen, T., Goldstein, S., Lancellotti, P., LeFevre, M., Miller Jr, F. and Otto, C. M. (2016) 'Recommendations on the echocardiographic assessment of aortic valve stenosis: a focused update from the European Association of Cardiovascular Imaging and the American Society of Echocardiography', *European Heart Journal - Cardiovascular Imaging*, 18(3), pp. 254–275.

Baumgartner, H., Schima, H. and Kühn, P. (1993) 'Discrepancies between Doppler and catheter gradients across bileaflet aortic valve prostheses', *American Journal of Cardiology*. Elsevier, 71(13), pp. 1241–1243.

Bazan, O. and Ortiz, J. P. (2011) 'Design and construction of a new pulse duplicator system for in vitro evaluation of prosthetic heart valves - conception of an experimental setup on mitral position', *21st Brazilian Congress of Mechanical Engineering (COBEM 2011)*, p. 9 p.

Bech-Hanssen, O., Caidahl, K., Wallentin, I., Ask, P. and Wranne, B. (2001) 'Assessment of effective orifice area of prosthetic aortic valves with Doppler echocardiography: An in vivo and in vitro study', *The Journal of Thoracic and Cardiovascular Surgery*. Elsevier, 122(2), pp. 287–295.

Bender, J. R. (1992) 'Heart Valve Disease', in *Yale School of Medicine Heart Book*, pp. 167–175.

Berg, G. A., Sonecki, P., Berg, R. B. S. and MacArthur, K. J. D. (2010) 'The Vascutek Elan stentless porcine prosthesis — The Glasgow experience', in Yankah, C. A., Weng, Y., and

Hetzer, R. (eds) *Aortic Root Surgery: The Biological Solution*. Heidelberg: Steinkopff, pp. 396–405.

TEN BERGE, L. (1958) 'A flexible cardiac valve prosthesis; preliminary report on the development of an experimental valvular prosthesis.', *Archivum chirurgicum Neerlandicum*. Netherlands, 10(1), pp. 26–33.

Bernacca, G. M., Connor, B. O., Williams, D. F. and Wheatley, D. J. (2002) 'Hydrodynamic function of polyurethane prosthetic heart valves : influences of Young ' s modulus and leaflet thickness', *Biomaterials*, 23(1), pp. 45–50.

Bernacca, G. M., Mackay, T. G., Gulbransen, M. J., Donn, A. W. and Wheatley, D. J. (1997) 'Polyurethane heart valve durability: effects of leaflet thickness and material.', *The International journal of artificial organs*. United States, 20(6), pp. 327–331.

Bezuidenhout, D., Williams, D. F. and Zilla, P. (2015) 'Polymeric heart valves for surgical implantation, catheter-based technologies and heart assist devices', *Biomaterials*. Elsevier Ltd, 36(January), pp. 6–25.

Blais, C., Pibarot, P., Garcia, D. and Chen, D. (2001) 'Comparison of Valve Resistance With Flow Dependence', *American Journal of Cardiology*, 88(01), pp. 45–52.

Blanchard, S. (2005) 'Anatomy and Physiology', in Bronzino, J., Enderle, J. D., and Blanchard, S. M. (eds) *Introduction to Biomedical Engineering*. 2nd edn. Elsevier Academic Press, pp. 73–126.

Bleiziffer, S., Krane, M., Deutsch, M. A., Elhmidi, Y., Piazza, N., Voss, B. and Lange, R. (2013) 'Which way in? The necessity of multiple approaches to transcatheter valve therapy', *Current cardiology reviews*. 2013/11/. Bentham Science Publishers, 9(4), pp. 268–273.

Bloomfield, P. (2002) ‘Valve disease Choice of heart valve prosthesis’, *Heart (British Cardiac Society)*, 87(6), pp. 583–9.

Bonhoeffer, P., Boudjemline, Y., Saliba, Z., Merckx, J., Aggoun, Y., Bonnet, D., Acar, P., Le Bidois, J., Sidi, D. and Kachaner, J. (2000) ‘Percutaneous replacement of pulmonary valve in a right-ventricle to pulmonary-artery prosthetic conduit with valve dysfunction’, *The Lancet*, 356(9239), pp. 1403–1405.

Bonow, R. O., Carabello, B. A., Chatterjee, K., de Leon Jr, A. C., Faxon, D. P., Freed, M. D., Gaasch, W. H., Lytle, Bruce Whitney, Nishimura, R. A., O’Gara, P. T., O’Rourke, R. A., Otto, C. M., Shah, P. M., Shanewise, J. S., Smith Jr, S. C., Jacobs, A. K., Adams, C. D., Anderson, J. L., Antman, E. M., *et al.* (2006) ‘ACC/AHA 2006 Guidelines for the Management of Patients With Valvular Heart Disease’, *Journal of the American College of Cardiology*, 48(3), pp. e1--e148.

Bourantas, C. V. and Serruys, P. W. (2014) ‘Evolution of transcatheter aortic valve replacement’, *Circulation Research*, 114(6), pp. 1037–1051.

Braunwald, N. S., Cooper, T. and Morrow, A. G. (1960) ‘Complete replacement of the mitral valve. Successful clinical application of a flexible polyurethane prosthesis.’, *The Journal of thoracic and cardiovascular surgery*. United States, 40, pp. 1–11.

Brown, D. (2018) *Physical Principles Of Cardiovascular Function, Vermont Veterinary Cardiology Services*. (Accessed: 8 November 2018).

Burke, A. P. (2013) *Pathology of rheumatic heart disease, Medscape*. (Accessed: 15 October 2015).

Burriesci, G., Marincola, F. C. and Zervides, C. (2010) ‘Design of a novel polymeric heart valve.’, *Journal of medical engineering & technology*, 34(1), pp. 7–22.

Burwash, I. G., Forbes, A. D., Sadahiro, M., Verrier, E. D., Pearlman, A. S., Thomas, R., Kraft, C. and Otto, C. M. (1993) 'Echocardiographic volume flow and stenosis severity measures with changing flow rate in aortic stenosis.', *The American journal of physiology*. United States, 265(5 Pt 2), pp. H1734-43.

Cabell, C. H., Abrutyn, E. and Karchmer, A. W. (2003) 'Cardiology patient page. Bacterial endocarditis: the disease, treatment, and prevention.', *Circulation*, 107(20), pp. e185–e187.

Calvert, J. W. and Lefer, D. J. (2012) 'Overview of Cardiac Muscle Physiology', in Hill, J. A. and Olson, E. N. (eds) *Muscle (Fundamental Biology and Mechanisms of Disease*. Second Edi. Elsevier Inc., pp. 57–66.

Cannon, J. D., Zile, M. R., Crawford, F. A. and Carabello, B. A. (1992) 'Aortic valve resistance as an adjunct to the gorlin formula in assessing the severity of aortic stenosis in symptomatic patients', *Journal of the American College of Cardiology*, 20(7), pp. 1517–1523.

Carapetis, J. R. (2007) 'Rheumatic heart disease in developing countries.', *The New England journal of medicine*, 357(5), pp. 439–441.

Carpentier, A. (1989) 'From valvular xenograft to valvular bioprosthesis: 1965–1970', *The Annals of Thoracic Surgery*, 48(3, Supplement), pp. S73–S74.

Carrel, T. P. (2009) 'Aortic valve and/or aortic root replacement using an aortic homograft.', *Multimedia manual of cardiothoracic surgery*, 2009(626), p. mmcts.2009.003905.

Catanho, M., Sinha, M. and Vijayan, V. (2012) *Model of Aortic Blood Flow Using the Windkessel Effect*.

Cavalcante, J. L., Lalude, O. O., Schoenhagen, P. and Lerakis, S. (2016) 'Cardiovascular

Magnetic Resonance Imaging for Structural and Valvular Heart Disease Interventions', *JACC: Cardiovascular Interventions*, 9(5), pp. 399–425.

Chaikof, E. L. (2007) 'The development of prosthetic heart valves — Lessons in form and function', *New England Journal of Medicine*, 357(14), pp. 1368–1371.

Chambers, J. (2009) 'Valve Substitutes', in Henien, M. Y. (ed.) *Valvular Heart Disease in Clinical Practice*. London: Springe-Verlag London Limited, pp. 241–263.

Chaothawee, L. (2012) 'Diagnostic approach to assessment of valvular heart disease using MRI-Part I: a practical approach for valvular regurgitation', *Heart Asia*. BMJ Publishing Group, 4(1), pp. 38–43.

Chauhan, S., Hasija, S. and Singh, S. P. (2014) 'Paravalvular leak after mitral valve replacement: Advantage of 3D echo', *Annals of Cardiac Anaesthesia*, 17(2), pp. 137–138.

Chen, L. Y., Tee, B. C. K., Chortos, A. L., Schwartz, G., Tse, V., J. Lipomi, D., Wong, H. S. P., McConnell, M. V. and Bao, Z. (2014) 'Continuous wireless pressure monitoring and mapping with ultra-small passive sensors for health monitoring and critical care', *Nature Communications*. Nature Publishing Group, 5, pp. 1–10.

Chen, P., Rodger, D. C., Saati, S., Humayun, M. S. and Tai, Y. (2008) 'Implantable Parylene-Based Wireless Intraocular Pressure Sensor', 17(6), pp. 2008–2011.

Chiang, C.-C., K. Lin, C.-C. and Ju, M.-S. (2007) 'An implantable capacitive pressure sensor for biomedical applications', *Sensors and Actuators A: Physical*, 134(2), pp. 382–388.

Chikwe, J., Filsoufi, F. and Carpentier, A. F. (2010) 'Prosthetic valve selection for middle-aged patients with aortic stenosis', *Nat Rev Cardiol*. Nature Publishing Group, a division of Macmillan Publishers Limited. All Rights Reserved., 7(12), pp. 711–719.

Choudhary, S. K., Talwar, S. and Airan, B. (2016) 'Choice of prosthetic heart valve in a developing country', *Heart Asia*. BMJ Publishing Group, 8(1), pp. 65–72.

Claiborne, T. E., Sheriff, J., Kuetting, M., Steinseifer, U., Slepian, M. J. and Bluestein, D. (2013a) 'In Vitro Evaluation of a Novel Hemodynamically Optimized Trileaflet Polymeric Prosthetic Heart Valve', *Journal of Biomechanical Engineering*. ASME, 135(2), pp. 21021–21028.

Claiborne, T. E., Sheriff, J., Kuetting, M., Steinseifer, U., Slepian, M. J. and Bluestein, D. (2013b) 'In Vitro Evaluation of a Novel Hemodynamically Optimized Trileaflet Polymeric Prosthetic Heart Valve', *Journal of Biomechanical Engineering*, 135(2), p. 021021.

Claiborne, T. E., Slepian, M. J., Hossainy, S. and Bluestein, D. (2013) 'Polymeric trileaflet prosthetic heart valves: evolution and path to clinical reality', *Expert Review of Medical Devices*, 9(6), pp. 577–594.

Clausen, I., Seeberg, T. M., Gheorghe, C. and Prieur, F. (2010) 'Investigations of TiO2as a protective coating on diaphragm-based in vivo sensors', *Proceedings of the 6th International Workshop on Wearable, Micro, and Nano Technologies for Personalized Health: 'Facing Future Healthcare Needs', pHealth 2009*, pp. 21–24.

Clavel, M.-A., Ennezat, P. V., Maréchaux, S., Dumesnil, J. G., Capoulade, R., Hachicha, Z., Mathieu, P., Bellouin, A., Bergeron, S., Meimoun, P., Arsenault, M., Le Tourneau, T., Pasquet, A., Couture, C. and Pibarot, P. (2013) 'Stress Echocardiography to Assess Stenosis Severity and Predict Outcome in Patients With Paradoxical Low-Flow, Low-Gradient Aortic Stenosis and Preserved LVEF', *JACC: Cardiovascular Imaging*, 6(2), pp. 175 LP – 183.

Clavel, M.-A. and Pibarot, P. (2019) 'Functional and Morphological Interplay of the Aortic Valve, the Aortic Root, and the Left Ventricle', in Stanger, O. H., Pepper, J. R., and

Svensson, L. G. (eds) *Surgical Management of Aortic Pathology: Current Fundamentals for the Clinical Management of Aortic Disease*. Vienna: Springer Vienna, pp. 99–114.

Clavel, M., Fuchs, C., Burwash, I. G., Mundigler, G., Dumesnil, J. G., Baumgartner, H., Bergler-klein, J., Beanlands, R. S., Mathieu, P., Magne, J., Pibarot, P. and Stenosis, L. A. (2008) 'Surgery for Valvular Heart Disease Predictors of Outcomes in Low-Flow , Low-Gradient Results of the Multicenter TOPAS Study', *Circulation*, 118(14), pp. 234–242.

Cohen, M. V and Gorlin, R. (1972) 'Modified orifice equation for the calculation of mitral valve area', *American Heart Journal*. Elsevier, 84(6), pp. 839–840.

Costello, J. E., Cecava, N. D., Tucker, J. E. and Bau, J. L. (2013) 'CT Radiation Dose: Current Controversies and Dose Reduction Strategies', *American Journal of Roentgenology*. American Roentgen Ray Society, 201(6), pp. 1283–1290.

Cribier, A., Eltchaninoff, H., Bash, A., Borenstein, N., Tron, C., Bauer, F., Derumeaux, G., Anselme, F., Laborde, F. and Leon, M. B. (2002) 'Percutaneous Transcatheter Implantation of an Aortic Valve Prosthesis for Calcific Aortic Stenosis', *Circulation*. American Heart Association, 106(24), pp. 3006–3008.

Daebritz, S. H., Fausten, B., Hermanns, B., Schroeder, J., Groetzner, J., Autschbach, R. and Messmer, B. J. (2004) 'Introduction of a flexible polymeric heart valve prosthesis with special design for aortic position', *European Journal of Cardio-thoracic Surgery*, 25(6), pp. 946–952.

Daebritz, S. H., Sachweh, J. S., Hermanns, B., Fausten, B., Franke, A., Groetzner, J., Klosterhalfen, B. and Messmer, B. J. (2003) 'Introduction of a Flexible Polymeric Heart Valve Prosthesis With Special Design for Mitral Position', *Circulation*, 108(90101), pp. 134–139.

Dagdeviren, C., Yang, B. D., Su, Y., Tran, P. L., Joe, P., Anderson, E., Xia, J., Doraiswamy, V., Dehdashti, B., Feng, X., Lu, B., Poston, R., Khalpey, Z., Ghaffari, R., Huang, Y., Slepian, M. J. and Rogers, J. A. (2014) 'Conformal piezoelectric energy harvesting and storage from motions of the heart, lung, and diaphragm', *Proceedings of the National Academy of Sciences*, 111(5), pp. 1927–1932.

Dasi, L. P., Simon, H. A., Sucosky, P. and Yoganathan, A. P. (2009) 'Fluid mechanics of artificial heart valves', *Clinical and Experimental Pharmacology and Physiology*, 36(2), pp. 225–237.

Deviri, E., Sareli, P., Wisenbaugh, T. and Cronje, S. L. (1991) 'Obstruction of mechanical heart valve prostheses: Clinical aspects and surgical management', *Journal of the American College of Cardiology*, 17(3), pp. 646–650.

DeWall, R. ., Qasim, N. and Carr, L. (2000) 'Evolution of mechanical heart valves', *The Annals of Thoracic Surgery*, 69(00), pp. 1612–1621.

Dima, C. (2014) 'Mitral Stenosis', *Medscape Drugs and Diseases*.

Dumesnil, J. G., Pibarot, P. and Carabello, B. (2010) 'Paradoxical low flow and / or low gradient severe aortic stenosis despite preserved left ventricular ejection fraction : implications for diagnosis and treatment', *European Heart Journal*, 31(3), pp. 281–289.

Dweck, M. R., Jones, C., Joshi, N. V, Fletcher, A. M., Richardson, H., White, A., Marsden, M., Pessotto, R., Clark, J. C., Wallace, W. A., Salter, D. M., McKillop, G., van Beek, E. J. R., Boon, N. A., Rudd, J. H. F. and Newby, D. E. (2012) 'Assessment of valvular calcification and inflammation by positron emission tomography in patients with aortic stenosis.', *Circulation*. United States, 125(1), pp. 76–86.

Echt, D. S., Cowan, M. W., Riley, R. E. and Brisken, A. F. (2006) 'Feasibility and safety of a

novel technology for pacing without leads', *Heart Rhythm*, 3(10), pp. 1202–1206.

Edler, I. and Lindström, K. (2004) 'The history of echocardiography', *Ultrasound in Medicine and Biology*, 30(12), pp. 1565–1644.

Edmunds, L. H. (1987) 'Thrombotic and Bleeding Complications of Prosthetic Heart Valves', *The Annals of Thoracic Surgery*. The Society of Thoracic Surgeons, 44(4), pp. 430–445.

Edwards, M.-B., Mclean, J., Solomonidis, S., Condon, B. and Gourlay, T. (2015) 'In vitro assessment of the lenz effect on heart valve prostheses at 1.5 T.', *J Magn Reson Imaging*, 41(1), pp. 74–82.

EdwardsLifesciences (2002) 'Carpentier-Edwards Bioprosthesis Aortic Model 2625 and Mitral Model 6625', pp. 1–2.

Elliot, E. C. and Callaghan, J. C. (1958) 'All plastic ventricle-type pump with tricuspid valves.', *Canadian journal of surgery. Journal canadien de chirurgie*. Canada, 1(4), pp. 308–312.

Elmasry, M. (2014) *Role of cinefluoroscopy in prosthetic valve disease, SlideShare:Health and Medicine Category*. (Accessed: 20 May 2019).

Elsner, J. J. and McKeon, B. P. (2017) 'Orthopedic Application of Polycarbonate Urethanes: A Review', *Techniques in Orthopaedics*, 32(3), pp. 132–140.

Enser, H., Sell, J. K., Schatzl-linder, M., Strauß, B., Hilber, W. and Jakoby, B. (2017) 'Hysteresis and Material Effects of Printed Strain Gauges Embedded in Organic Coatings', in *Eurosensors*, pp. 2–5.

European Commission - DG Health and Consumer (2010) 'MEDDEV 2. 4/1 Rev. 9

Classification of medical devices.', *MEDICAL DEVICES: Guidance document*.

Fadel, B. M., Bakarman, H., Bech-Hanssen, O., Pergola, V. and Di Salvo, G. (2014) 'Intermittent entrapment of a prosthetic mitral valve disc: What you see is not what you get', *Circulation*, 129(2), pp. 13–15.

Fagman, E., Perrotta, S., Bech-Hanssen, O., Flinck, A., Lamm, C., Olaison, L. and Svensson, G. (2012) 'ECG-gated computed tomography: a new role for patients with suspected aortic prosthetic valve endocarditis', *European Radiology*, 22(11), pp. 2407–2414.

Faletra, F. F., Ramamurthi, A., Dequarti, M. C., Leo, L. A., Moccetti, T. and Pandian, N. (2014) 'Artifacts in Three-Dimensional Transesophageal Echocardiography', *Journal of the American Society of Echocardiography*, 27(5), pp. 453–462.

Felipini, C. L. (2005) 'ELECTRO-FLUID-DYNAMIC SIMULATOR OF THE CARDIOVASCULAR SYSTEM FOR THE RESEARCH IN ASSISTED CIRCULATION AREA aorta natural', in *18th International Congress of Mechanical Engineering*, p. 7.

Ferguson, J. E. and Redish, D. (2011) 'Wireless communication with implanted medical devices using the conductive properties of the body', *Expert Review of Medical Devices*, 8(4), pp. 427–433.

Fisher, J., Jack, G. R. and Wheatley, D. J. (1986) 'Design of a function test apparatus for prosthetic heart valves. Initial results in the mitral position', *Clinical Physics and Physiological Measurement*, 7(1), pp. 63–73.

Fonseca, M. a, Allen, M. G., Kroh, J. and White, J. (2006) 'Flexible wireless passive pressure sensors for biomedical applications', *Solid State Sensors, Actuators and Microsystems Workshop, Hilton Head Island, SC, USA*, (1), pp. 37–42.

Fortini, S., Querzoli, G., Espa, S., Costantini, M., Sorgini, F., Z, D. P., Annolfo, D. A. and Bisegna, P. (2013) 'Influence on fluid-dynamics of the aortic root morphological modifications induced by Marfan syndrome', in *10TH Internationnal symposium on particle image velocimetry -PIV13*.

Fritzsche, D., Eitz, T., Laczkovics, A., Liebold, A., Knaut, M., Matschke, K., Sagie, A., Mehlhorn, U., Horstkotte, D. and Koerfer, R. (2007) 'Early Detection of Mechanical Valve Dysfunction Using a New Home Monitoring Device', *The Annals of Thoracic Surgery*, 83(2), pp. 542–548.

Fritzsche, D., Eitz, T., Minami, K., Reber, D., Laczkovics, A., Mehlhorn, U., Horstkotte, D. and Korfer, R. (2005) 'Digital frequency analysis of valve sound phenomena in patients after prosthetic valve surgery: its capability as a true home monitoring of valve function.', *The Journal of heart valve disease*. England, 14(5), pp. 657–663.

Fritzsche, D., Schenk, S., Eitz, T., Mantas, J., Horstkotte, D. and Koerfer, R. (2007) 'Patient self-monitoring of prosthetic heart valve function.', *The Journal of heart valve disease*, 16(5), pp. 558–66.

DE GAETANO, F., BAGNOLI, P., ZAFFORA, A., PANDOLFI, A., SERRANI, M., BRUBERT, J., STASIAK, J., MOGGRIDGE, G. D. and COSTANTINO, M. L. (2015) 'a Newly Developed Tri-Leaflet Polymeric Heart Valve Prosthesis', *Journal of Mechanics in Medicine and Biology*, 15(02), p. 1540009.

De Gaetano, F., Serrani, M., Bagnoli, P., Brubert, J., Stasiak, J., Moggridge, G. D. and Costantino, M. L. (2015) 'Fluid dynamic characterization of a polymeric heart valve prototype (Poli-Valve) tested under continuous and pulsatile flow conditions', *The International Journal of Artificial Organs*, 38(11), pp. 600–606.

Gallocher, S. (2007) ‘Durability assessment of polymer trileaflet heart valves’, *FIU Electronic Theses and Dissertations*.

Gallocher, S. L., Aguirre, A. F., Kasyanov, V., Pinchuk, L. and Schoephoerster, R. T. (2006) ‘A novel polymer for potential use in a trileaflet heart valve’, *Journal of Biomedical Materials Research Part B: Applied Biomaterials*. John Wiley & Sons, Ltd, 79B(2), pp. 325–334.

Garbi, M., Chambers, J., Vannan, M. A. and Lancellotti, P. (2015) ‘Valve stress echocardiography: A practical guide for referral, procedure, reporting, and clinical implementation of results from the HAVEC group’, *JACC: Cardiovascular Imaging*, 8(6), pp. 724–736.

Garcia, D., Dumesnil, J. G., Durand, L.-G., Kadem, L. and Pibarot, P. (2003) ‘Discrepancies between catheter and Doppler estimates of valve effective orifice area can be predicted from the pressure recovery phenomenon: practical implications with regard to quantification of aortic stenosis severity.’, *Journal of the American College of Cardiology*. United States, 41(3), pp. 435–442.

Garcia, D. and Kadem, L. (2006) ‘Orifice Area , Effective Orifice Area , or Gorlin Area ?’

Gawlinski, A. (2000) ‘Measuring cardiac output: intermittent bolus thermodilution method.’, *Critical care nurse*, 20(2), pp. 118–120, 122.

Gerdeen, J. C., Lord, H. W. and Rorrer, R. AL (2006) *Engineering Design with Polymers and Composites*. 1st edn. Boca Raton: Taylor and Francis Group.

Ghanbari, H., Viatge, H., Kidane, A. G., Burriesci, G., Tavakoli, M. and Seifalian, A. M. (2009) ‘Polymeric heart valves: new materials, emerging hopes’, *Trends in Biotechnology*, 27(6), pp. 359–367.

Ghista, D. N. and Reul, H. (1977) ‘Optimal prosthetic aortic leaflet valve: Design parametric and longevity analyses: Development of the avcothane-51 leaflet valve based on the optimum design analysis’, *Journal of Biomechanics*, 10(5), pp. 313–324.

Gibari, M. E., Bleis, C. Le, Lirzin, G., Lauzier, B., Ginestar, S., Tissier, J., Latrach, M., Gautier, C. and Li, H. (2017) ‘Thermal drift compensation of piezoresistive implantable blood pressure sensors with low cost analog solutions’, in *2017 29th International Conference on Microelectronics (ICM)*, pp. 1–4.

Ginggen, A., Tardy, Y., Crivelli, R., Bork, T. and Renaud, P. (2008) ‘A telemetric pressure sensor system for biomedical applications’, *Ieee Transactions on Biomedical Engineering*, 55(4), pp. 1374–1381.

Gjesteby, L., Man, B. De, Jin, Y., Paganetti, H., Verburg, J., Giantsoudi, D. and Wang, G. (2016) ‘Metal Artifact Reduction in CT: Where Are We After Four Decades?’, *IEEE Access*, 4, pp. 5826–5849.

Gorlin, R. and Gorlin, S. G. (1951) ‘Hydraulic formula for calculation of the area of the stenotic mitral valve, other cardiac valves, and central circulatory shunts. I’, *American Heart Journal*, 41(1), pp. 1–29.

Gott, V. L., Alejo, D. E. and Cameron, D. E. (2003) ‘Mechanical heart valves: 50 years of evolution’, *The Annals of Thoracic Surgery*, 76(6), pp. S2230–S2239.

Gourlay, T. (1997) *Controlled Pulsatile Architecture in Cardiopulmonary Bypass: In vitro and clinical studies*. University of Strathclyde.

Gregory, S. D. (2009) *Simulation and development of a mock circulation loop with variable compliance*.

Grunkemeier, G. L., Li, H.-H., Naftel, D. C., Starr, A. and Rahimtoola, S. H. (2015) 'Long-term performance of heart valve prostheses', *Current Problems in Cardiology*, 25(2), pp. 78–154.

Gulsin, G. S., Singh, A. and McCann, G. P. (2017) 'Cardiovascular magnetic resonance in the evaluation of heart valve disease', *BMC medical imaging*. BioMed Central, 17(1), p. 67.

Guo, F., Jiao, K., Bai, Y., Guo, J., Chen, Q., Yang, R. and Zhang, X. (2019) 'Novel transcatheter aortic heart valves exhibiting excellent hemodynamic performance and low-fouling property', *Journal of Materials Science & Technology*. The editorial office of Journal of Materials Science & Technology, 35(1), pp. 207–215.

Hachicha, Z., Dumesnil, J. G., Bogaty, P. and Pibarot, P. (2007) 'Paradoxical Low-Flow, Low-Gradient Severe Aortic Stenosis Despite Preserved Ejection Fraction Is Associated With Higher Afterload and Reduced Survival', *Circulation*, 115(22), pp. 2856–2864.

Hakki, A. H., Iskandrian, A. S., Bemis, C. E., Kimbiris, D., Mintz, G. S., Segal, B. L. and Brice, C. (1981) 'A simplified valve formula for the calculation of stenotic cardiac valve areas', *Circulation*, 63(5), pp. 1050–1055.

Hameedullah, I., Ahmed, E. O., Alzoobiy, A. and Elkhateeb, O. (2018) 'Discrepancy between catheter and doppler gradients immediately post transcatheter aortic valve replacement in an underexpanded prosthesis', *Clinical case reports*. John Wiley and Sons Inc., 6(6), pp. 1117–1120.

Hannan, M. A., Abbas, S. M., Samad, S. A. and Hussain, A. (2012) 'Modulation techniques for biomedical implanted devices and their challenges', *Sensors*, 12(1), pp. 297–319.

Hargreaves, B. A., Worters, P. W., Pauly, K. B., Pauly, J. M., Koch, K. M. and Gold, G. E. (2011) 'Metal-induced artifacts in MRI', *AJR. American journal of roentgenology*, 197(3),

pp. 547–555.

Harpster, T. J., Hauvespre, S., Dokmeci, M. R. and Najafi, K. (2002) ‘A passive humidity monitoring system for in situ remote wireless testing of micropackages’, *Journal of Microelectromechanical Systems*, 11(1), pp. 61–67.

Harvey, A., Montezano, A. C. and Touyz, R. M. (2015) ‘Vascular biology of ageing—Implications in hypertension’, *Journal of Molecular and Cellular Cardiology*, 83, pp. 112–121.

Harvey, F. (1996) ‘Evolution of Echocardiography’, *Circulation*. American Heart Association, 93(7), pp. 1321–1327.

Henein, M. (2009) *Valvular Heart Disease in Clinical Practice*. London: Springer.

Hildebrand, D. K. (2003) *DESIGN AND EVALUATION OF A NOVEL PULSATILE BIOREACTOR FOR by*. University Of Pittsburgh.

Hill, G. D., Ginde, S., Rios, R., Frommelt, P. C. and Hill, K. D. (2016) ‘Surgical Valvotomy Versus Balloon Valvuloplasty for Congenital Aortic Valve Stenosis: A Systematic Review and Meta-Analysis.’, *Journal of the American Heart Association*. England, 5(8).

Hinson, J. S., Ehmann, M. R., Fine, D. M., Fishman, E. K., Toerper, M. F., Rothman, R. E. and Klein, E. Y. (2017) ‘Risk of Acute Kidney Injury After Intravenous Contrast Media Administration.’, *Annals of emergency medicine*. United States, 69(5), pp. 577-586.e4.

Hirai, S., Fukunaga, S., Sueshiro, M., Watari, M., Sueda, T. and Matsuura, Y. (1998) ‘Assessment of a new silicone tri-leaflet valve seamlessly assembled with blood chamber for a low-cost ventricular assist device.’, *Hiroshima journal of medical sciences*. Japan, 47(2), pp. 47–55.

Hiratzka, L. F., Kouchoukos, N. T., Grunkemeier, G. L., Miller, D. C., Scully, H. E. and Wechsler, A. S. (1988) 'Outlet strut fracture of the Björk-Shiley 60 ° Convexo-Concave valve: Current information and recommendations for patient care', *Journal of the American College of Cardiology*, 11(5), pp. 1130–1137.

Ho, N. and Desai, M. Y. (2018) *Use of CT in the Assessment of Valvular Function*, *American College of cardiology*. (Accessed: 21 November 2019).

Hoffmann, G., Lutter, G. and Cremer, J. (2008) 'Durability of bioprosthetic cardiac valves.', *Deutsches Arzteblatt international*, 105(8), pp. 143–148.

Horstkotte, D., Piper, C., Niehues, R., Wiemer, M. and Schultheiss, H. P. (1995) 'Late prosthetic valve endocarditis.', *European heart journal*, 16 Suppl B, pp. 39–47.

Huang, Q.-A., Dong, L. and Wang, L.-F. (2016) 'LC Passive Wireless Sensors Toward a Wireless Sensing Platform: Status, Prospects, and Challenges', *Journal of Microelectromechanical Systems*, 25(5), pp. 822–841.

Hubbert, L., Baranowski, J., Delshad, B. and Ahn, H. (2017) 'Left Atrial Pressure Monitoring with an Implantable Wireless Pressure Sensor after Implantation of a Left Ventricular Assist Device', *ASAIO Journal*, 63(5), pp. e60–e65.

Hui, S., Mahmood, F. and Matyal, R. (2018) 'Aortic Valve Area — Technical Communication : Continuity and Gorlin Equations Revisited', *Journal of Cardiothoracic and Vascular Anesthesia*. Elsevier Inc., 000, pp. 1–8.

Hurwitz, S. E., Waxman, D. and Hecht, S. (2009) 'Acute Failure of a St. Jude's Prosthetic Aortic Valve: Large Pannus Formation Masked by a Small Thrombus', *Journal of the American Society of Echocardiography*. Elsevier Inc, 22(9), pp. 1086.e1-1086.e3.

Institute, D. H. and H. (2011) ‘SJM Mechanical Valve Manufacturing’.

Iung, B., Baron, G., Tornos, P., Gohlke-Barwolf, C., Butchart, E. G. and Vahanian, A. (2007) ‘Valvular heart disease in the community: a European experience.’, *Current problems in cardiology*. United States, 32(11), pp. 609–661.

Iung, B., Gohlke-Bärwolf, C., Tornos, P., Tribouilloy, C., Hall, R., Butchart, E. and Vahanian, A. (2002) ‘Recommendations on the management of the asymptomatic patient with valvular heart disease’, *European Heart Journal*, 23(16), pp. 1253–1266.

Jacobs, L. D., Salgo, I. S., Goonewardena, S., Weinert, L., Coon, P., Bardo, D., Gerard, O., Allain, P., Zamorano, J. L., de Isla, L. P., Mor-Avi, V. and Lang, R. M. (2005) ‘Rapid online quantification of left ventricular volume from real-time three-dimensional echocardiographic data’, *European Heart Journal*, 27(4), pp. 460–468.

Jamieson, W. R. E., Lewis, C. T. P., Sakwa, M. P., Cooley, D. A., Kshettry, V. R., Jones, K. W., David, T. E., Sullivan, J. A., Fradet, G. J. and Bach, D. S. (2011) ‘St Jude Medical Epic porcine bioprosthesis: Results of the regulatory evaluation’, *Journal of Thoracic and Cardiovascular Surgery*. The American Association for Thoracic Surgery, 141(6), pp. 1449–1454.

Jansen, J. and Reul, H. (1992) ‘A synthetic three-leaflet valve.’, *Journal of medical engineering & technology*. England, 16(1), pp. 27–33.

Jansen, J., Willeke, S., Reiners, B., Harbott, P., Reul, H. and Rau, G. (1991) ‘New J-3 Flexible-Leaflet Polyurethane Heart Valve Prosthesis with Improved Hydrodynamic Performance’, *The International Journal of Artificial Organs*. SAGE Publications, 14(10), pp. 655–660.

Je, S. S., Sharma, T., Lee, Y., Gill, B. and Zhang, J. X. (2011) ‘A thin-film piezoelectric

PVDF-TrFE based implantable pressure sensor using lithographic patterning', *Proceedings of the IEEE International Conference on Micro Electro Mechanical Systems (MEMS)*, pp. 644–647.

Jiang, G. (2010) 'Design challenges of implantable pressure monitoring system', *Frontiers in Neuroscience*, 4(FEB), pp. 2–5.

Joana, C. and Filsoufi, F. (2013) *Mechanical Valves, The mitralvalve*. (Accessed: 10 February 2016).

Jordaan, C. J. (2017) *The hydrodynamic and coagulation characteristics of a re-engineered mechanical heart valve in an ovine model*. University of the Free State.

Kanjanauthai, S. and Sharma, G. K. (2015) *Mitral Valve Anatomy, Medscape drugs and diseases*. (Accessed: 26 April 2018).

Karuppiah, S., George, G., Chacko, B. and Philip, M. A. (2015) 'Entrapped left atrial pressure monitoring catheter in a prosthetic mitral valve', *Annals of cardiac anaesthesia*. Medknow Publications & Media Pvt Ltd, 18(2), pp. 276–277.

Katz, E. (2014) 'Implanted Biofuel Cells Operating In Vivo', *Implantable Bioelectronics*, 9783527335, pp. 363–379.

Kelley, T. A., Marquez, S. and Popelar, C. F. (2013) 'In vitro testing of heart valve substitutes', in Iaizzo, P. A., Hill, A. J., Bianco, R. W., and St. Louis, J. D. (eds) *Heart Valves From Design to Clinical Implantation*. 1st edn. New York: Springer Science+Business Media, pp. 283–321.

Khanna, V. K. (2016) 'Wireless Communications and Powering of Implants BT - Implantable Medical Electronics: Prosthetics, Drug Delivery, and Health Monitoring', in

Khanna, V. K. (ed.). Cham: Springer International Publishing, pp. 185–207.

Khouzam, R. N. (2007) ‘Cinefluoroscopy as the gold standard for mechanical valve mobility’, *The Canadian journal of cardiology*. Pulsus Group Inc, 23(12), p. 998.

Kim, A., Powell, C. R. and Ziaie, B. (2016) ‘An Universal packaging technique for low-drift implantable pressure sensors’, *Biomedical Microdevices*. Biomedical Microdevices, 18(32), pp. 1–8.

Kim, K. M., Herrera, G. a and Battarbee, H. D. (1999) ‘Role of glutaraldehyde in calcification of porcine aortic valve fibroblasts.’, *The American journal of pathology*, 154(3), pp. 843–852.

Klabunde, R. (2012a) ‘Cardiac Function’, in *Cardiovascular Physiology Concepts*. 2nd edn. Lippincott Williams & Wilkins, pp. 60–92.

Klabunde, R. (2012b) ‘Cardiovascular Integration, Adaptation and Pathophysiology’, in *Cardiovascular Physiology Concepts*. 2nd edn. Philadelphia: Lippincott Williams & Wilkins, pp. 198–234.

Klabunde, R. (2012c) ‘Vascular Function’, in *Cardiovascular Physiology Concepts*. 2nd edn. Philadelphia: Lippincott Williams & Wilkins, pp. 93–123.

Knierbein, B., Rosarius, N., Unger, A., Reul, H. and Rau, G. (1992) ‘CAD-design, stress analysis and in vitro evaluation of three leaflet blood-pump valves’, *Journal of Biomedical Engineering*, 14(4), pp. 275–286.

Kober, G. and Hilgermann, R. (1987) ‘Catheter entrapment in a Bjöurk-Shiley prosthesis in aortic position’, *Catheterization and Cardiovascular Diagnosis*. John Wiley & Sons, Ltd, 13(4), pp. 262–265.

KuA1, Roggenkamp, J., Urban, U., Schmitz-Rode, T. and Steinseifer, U. (2011) ‘Polyurethane heart valves: past, present and future’, *Expert Review of Medical Devices*, 8, p. 227+.

Kuan, Y. H., Lakshmi, P. D., Yoganathan, A. P. and Leo, H. L. (2011) ‘Recent Advances in Polymeric Heart Valves Research’, *International Journal of Biomaterials Reasearch and Engineering (IJBRE)*, 1(2), p. 17.

Kusko, M. C. and Maselli, K. (2015) ‘Introduction to Cardiac Auscultation’, in Taylor, A. J. (ed.) *Learning Cardiac Auscultation: From Essentials to Expert Clinical Interpretation*. London: Springer London, pp. 3–14.

LaHaye, S., Lincoln, J. and Garg, V. (2014) ‘Genetics of Valvular Heart Disease’, *Current cardiology reports*, 16(6), p. 487.

Lancellotti, P., Pibarot, P., Chambers, J., Edvardsen, T., Delgado, V., Dulgheru, R., Pepi, M., Cosyns, B., Dweck, M. R., Garbi, M., Magne, J., Nieman, K., Rosenhek, R., Bernard, A., Lowenstein, J., Vieira, M. L. C., Rabischoffsky, A., Vyhmeister, R. H., Zhou, X., *et al.* (2016) ‘Recommendations for the imaging assessment of prosthetic heart valves: A report from the European Association of Cardiovascular Imaging endorsed by the Chinese Society of Echocardiography, the Inter-American Society of Echocardiography, and the Brazilian ’, *European Heart Journal Cardiovascular Imaging*, 17(6), pp. 589–590.

Lankford, J. (1999) ‘Assuring Heart Valve Reliability’, *SwRI Summer 1999 Technology Today Article*, pp. 7–11.

Lanning, C. and Shandas, R. (2003) ‘Development and validation of implantable sensors for monitoring function of prosthetic heart valves: in vitro studies.’, *Medical & biological engineering & computing*, 41(4), pp. 416–424.

Lanzarone, E., Vismara, R. and Fiore, G. B. (2009) 'A new pulsatile volumetric device with biomorphic valves for the in vitro study of the cardiovascular system', *Artificial Organs*, 33(12), pp. 1048–1062.

Lapum, J. L., Verkuyl, M., Garcia, W., St-Amant, O. and Tan, A. (2018) 'Vital Sign Measurement Across the Lifespan', in *Vital Sign Measurement Across the Lifespan - 1st Canadian edition*. 1st edn. Ontario: eCampusOntario, pp. 127–172.

Le, H. T., Hangiandreou, N., Timmerman, R., Rice, M. J., Smith, W. B., Deitte, L. and Janelle, G. M. (2016) 'Imaging Artifacts in Echocardiography', *Anesthesia & Analgesia*, 122(3), pp. 633–646.

Leopaldi, A. M., Vismara, R., Lemma, M., Valerio, L., Cervo, M., Mangini, A., Contino, M., Redaelli, A., Antona, C. and Fiore, G. B. (2012) 'In vitro hemodynamics and valve imaging in passive beating hearts', *Journal of Biomechanics*. Elsevier, 45(7), pp. 1133–1139.

Li, Z., Zhu, G., Yang, R., Wang, A. C. and Wang, Z. L. (2010) 'Muscle-driven in vivo nanogenerator', *Advanced Materials*, 22(23), pp. 2534–2537.

Lilly, L. S. (1998) *Pathophysiology of Heart Disease*. Baltimore: Williams & Wilkins.

Lin, Y., Su, K.-T., Chen, G.-S. and Liu, J.-S. (2010) 'Fabrication and Characterization of Microscale Sensors for Strain Measurement in Flexible Polymer Heart Valve Leaflet', *Materials and Manufacturing Processes*, 25(4), pp. 243–245.

Lindsey, D. P., McKee, E. L., Hull, M. L. and Howell, S. M. (1998) 'A new technique for transmission of signals from implantable transducers', *IEEE Transactions on Biomedical Engineering*, 45(5), pp. 614–619.

Liu, K. (2013) 'Contribution of Three-Dimensional Transesophageal Echocardiography to

Diagnosis and Management of Thrombosis of a St. Jude Mechanical Prosthesis in the Aortic Valve Position', *American Journal of Cardiology*. Elsevier Inc., 111(2), pp. 301–302.

Lu, B., Chen, Y., Ou, D., Chen, H., Diao, L., Zhang, W., Zheng, J., Ma, W., Sun, L. and Feng, X. (2015) 'Ultra-flexible Piezoelectric Devices Integrated with Heart to Harvest the Biomechanical Energy', *Scientific Reports*. Nature Publishing Group, 5, pp. 1–9.

MacGill, M. (2017) *What should my heart rate be, Medicalnewstoday*. (Accessed: 24 April 2019).

Mackay, T. G. (1992) *Towards a tri-leaflet polyurethane heart valve prosthesis*. University of Strathclyde.

Mackay, T. G., Wheatley, D. J., Bernacca, G. M., Fisher, a. C. and Hindle, C. S. (1996) 'New polyurethane heart valve prosthesis: Design, manufacture and evaluation', *Biomaterials*, 17(19), pp. 1857–1863.

Madell, R. and Cherney, K. (2018) *Blood Pressure Readings Explained, Healthline*. (Accessed: 24 April 2019).

Maganti, K., Rigolin, V. H., Sarano, M. E. and Bonow, R. O. (2010) 'Valvular Heart Disease: Diagnosis and Management', *Mayo Clinic Proceedings*, 85(5), pp. 483–500.

Maleki, H., Shahriari, S., Labrosse, M., Pibarot, P. and Kadem, L. (2014) 'An In Vitro Model of Aortic Stenosis for the Assessment of Transcatheter Aortic Valve Implantation', *Journal of Biomechanical Engineering*, 136(5), p. 54501.

Maleki, M. and Esmaeilzadeh, M. (2012) 'The evolutionary development of echocardiography.', *Iranian journal of medical sciences*, 37(4), pp. 222–32.

Manda, Y. R. and Baradhi, K. M. (2018) *Cardiac Catherisation, risks and complications*.

Statpearls Publishing.

Manji, R. A., Zhu, L. F., Nijjar, N. K., Rayner, D. C., Korbutt, G. S., Churchill, T. A., Rajotte, R. V., Koshal, A. and Ross, D. B. (2006) 'Glutaraldehyde-fixed bioprosthetic heart valve conduits calcify and fail from xenograft rejection', *Circulation*, 114(4), pp. 318–327.

Maraj, R., Jacobs, L. E., Ioli, a and Kotler, M. N. (1998) 'Evaluation of hemolysis in patients with prosthetic heart valves.', *Clinical cardiology*, 21, pp. 387–392.

Marquez, S., Hon, R. T. and Yoganathan, A. P. (2001) 'Comparative hydrodynamic evaluation of bioprosthetic heart valves.', *The Journal of heart valve disease*. England, 10(6), pp. 802–811.

Martin, C. M. (2013) 'Acquired Valve Disease and Processes', in Iaizzo, P. A., Bianco, R. W., Hill, A. J., and St Louis, J. D. (eds) *Heart Valves From Design to Clinical Implantation*. New York: Springer Science+Business Media, pp. 73–81.

Martini, F. H., Nath, J. L. and Bartholomew, E. F. (2018) 'The heart', in Beauparlant, S. (ed.) *Fundamentals of Anatomy and Physiology*. 11th edn. Essex: Pearsons Education Limited, pp. 734–773.

Masheane, L., du Preez, W. . and Combrinck, J. (2016) 'ASSESSMENT OF MANUFACTURABILITY AND PERFORMANCE OF POLYURETHANE HEART VALVES PRODUCED THROUGH A LOCALLY DEVELOPED DIP MOULDING PROCESS', in *17th RAPDASA Annual International Conference*, pp. 1–10.

Mathieu, C., Mikaïl, N., Benali, K. and Iung, B. (2017) 'Characterization of 18 F-Fluorodeoxyglucose Uptake Pattern in Noninfected Prosthetic Heart Valves', *Circulation:Cardiovascular Imaging*, 10(3), pp. 1–9.

Matthews, A. M. (1998) ‘The development of the Starr-Edwards heart valve.’, *Texas Heart Institute journal*, 25(4), pp. 282–293.

Mayet, J. and Hughes, A. (2003) ‘Cardiac and vascular pathophysiology in hypertension’, *Heart*, 89(9), pp. 1104 LP – 1109.

McClelland, R., Dennis, R., Reid, Lola, M., Palsson, B. and Macdonald, J. M. (2005) ‘Tissue Engineering’, in Bronzino, J., Enderle, J. D., and Blanchard, S. M. (eds) *Introduction to Biomedical Engineering*. 2nd edn. Bronzino, Joseph Enderle, John D Blanchard, Susan M, pp. 313–400.

Mezilis, N. E., Salame, M. Y. and Oakley, G. D. G. (1999) ‘Predicting mitral regurgitation following percutaneous mitral valvotomy with the inoue balloon: Comparison of two echocardiographic scoring systems’, *Clinical Cardiology*. John Wiley & Sons, Ltd, 22(7), pp. 453–458.

Miller, N. (2012) ‘Warning! Cardiac cath complications’, *Nursing made Incredibly Easy*, 10(4), pp. 8–10.

Mohan, J. C., Mohan, V., Shukla, M. and Sethi, A. (2017) ‘Significant intra-valvular pressure loss across EPIC SUPRA and perimount magna supra-annular designed aortic bioprostheses in patients with normal aortic size’, *Indian heart journal*. 2016/06/11. Elsevier, 69(1), pp. 87–92.

Montorsi, P., De Bernardi, F., Muratori, M., Cavoretto, D. and Pepi, M. (2000) ‘Role of cine-fluoroscopy, transthoracic, and transesophageal echocardiography in patients with suspected prosthetic heart valve thrombosis’, *The American Journal of Cardiology*, 85(1), pp. 58–64.

Moore, M. A. and Adams, A. K. (2001) ‘Calcification resistance, biostability, and low immunogenic potential of porcine heart valves modified by dye-mediated photooxidation’,

Journal of Biomedical Materials Research, 56(1), pp. 24–30.

Mootanah, R. and Bader, D. (2006) 'Pressure Sensors', in Akay, M. (ed.) *Encyclopedia Biomedical*. 1st edn. New Jersey: John Wiley and Sons, pp. 2837–2852.

Morris, P. E. (1979) 'Retrograde left ventricular catheterization in patients with a Bjork-Shiley valve prosthesis', *American Journal of Cardiology*. Elsevier, 44(3), p. 578.

Mouneimne, K., Garitey, V. and Tanne, D. (2010) 'Testing transcatheter heart valve devices', *European Medical Device Technology*, (March).

Murakawa, K., Kobayashi, M., Nakamura, O. and Kawata, S. (1999) 'A wireless near-infrared energy system for medical implants', *IEEE Engineering in Medicine and Biology Magazine*, 18, pp. 70–72.

Muratori, M., Montorsi, P., Maffessanti, F., Teruzzi, G., Zoghbi, W. A., Gripari, P., Tamborini, G., Ghulam Ali, S., Fusini, L., Fiorentini, C. and Pepi, M. (2013) 'Dysfunction of Bileaflet Aortic Prosthesis: Accuracy of Echocardiography Versus Fluoroscopy', *JACC: Cardiovascular Imaging*, 6(2), pp. 196–205.

Muratori, M., Montorsi, P., Teruzzi, G., Celeste, F., Doria, E., Alamanni, F. and Pepi, M. (2006) 'Feasibility and Diagnostic Accuracy of Quantitative Assessment of Mechanical Prostheses Leaflet Motion by Transthoracic and Transesophageal Echocardiography in Suspected Prosthetic Valve Dysfunction', *The American Journal of Cardiology*, 97(1), pp. 94–100.

Murphy, O. H., Bahmanyar, M. R., Borghi, A., McLeod, C. N., Navaratnarajah, M., Yacoub, M. H. and Toumazou, C. (2013) 'Continuous in vivo blood pressure measurements using a fully implantable wireless SAW sensor', *Biomedical Microdevices*, 15(5), pp. 737–749.

Myerson, S. G. (2012) ‘Heart valve disease: investigation by cardiovascular magnetic resonance’, *Journal of Cardiovascular Magnetic Resonance*, 14(1), p. 7.

Najafi, K. (2007) ‘Packaging of implantable microsystems’, *Proceedings of IEEE Sensors*, pp. 58–63.

Neo, W. T., Pua, U. and Lee, Y. S. (2010) ‘Catheter-induced aortocoronary artery dissection: utility and appearance on CT coronary angiogram’, *Int J Cardiol*, 144, p. 334.

Neuman, M. R. (2000) ‘Physical Measurements’, in Bronzino, J. (ed.) *The Biomedical Engineering Handbook*. 2nd edn. Boca Raton: CRC Press LLC, pp. 871–887.

Nishimura, R. A. and Carabello, B. A. (2012) ‘Hemodynamics in the cardiac catheterization laboratory of the 21st century’, *Circulation*, 125(17), pp. 2138–2150.

Nishimura, R. A., Otto, C. M., Bonow, R. O., Iii, J. P. E., Fleisher, L. A., Jneid, H., Mack, M. J., Mcleod, C. J., Gara, P. T. O., Rigolin, V. H. and Iii, T. M. S. (2017) ‘2017 AHA / ACC Focused Update of the 2014 AHA / ACC Guideline for the Management of Patients With Valvular Heart Disease A Report of the American College of Cardiology / American Heart Association Task Force on Clinical Practice Guidelines’, *Circulation*, 135(25), pp. e1159–e1195.

Nkomo, V. T., Gardin, J. M., Skelton, T. N., Gottdiener, J. S., Scott, C. G. and Enriquez-Sarano, M. (2006) ‘Burden of valvular heart diseases: a population-based study’, *The Lancet*, 368(9540), pp. 1005–1011.

Nobari, S., Mongrain, R., Gaillard, E., Leask, R. and Cartier, R. (2012) ‘Therapeutic vascular compliance change may cause significant variation in coronary perfusion: a numerical study’, *Computational and mathematical methods in medicine*. 2012/03/05. Hindawi Publishing Corporation, 2012, p. 791686.

Olivo, J., Carrara, S., De Micheli, G. and Micheli, G. De (2011) ‘Energy Harvesting and Remote Powering for Implantable Biosensors’, *IEEE Sensors Journal*, 11(7), pp. 1573–1586.

Omar, R. Z., Morton, L. S., Beime, M., Blot, W. J., Lawford, P. V., Hose, R. and Taylor, K. M. (2001) ‘Outlet strut fracture of Björk-Shiley convexo-concave valves: Can valve-manufacturing characteristics explain the risk?’, *Journal of Thoracic and Cardiovascular Surgery*, 121(6), pp. 1143–1149.

Ozkok, S. and Ozkok, A. (2017) ‘Contrast-induced acute kidney injury: A review of practical points’, *World journal of nephrology*. 2017/05/06. Baishideng Publishing Group Inc, 6(3), pp. 86–99.

Padmavati, S. (1978) ‘[Rheumatic fever and rheumatic heart disease in the developing countries].’, *Bulletin of the World Health Organization*, 56(4), pp. 543–550.

Pappano, A. J. and Wier, W. G. (2013a) ‘The arterial system’, in *Cardiovascular Physiology*. 10th edn. Philadelphia: Elsevier Mosby, pp. 135–151.

Pappano, A. J. and Wier, W. G. (2013b) ‘The cardiac pump’, in *Cardiovasuclar Physiology*. 10th edn. Philadelphia: Elsevier Mosby, pp. 55–90.

Parikh, S. A. and O’Gara, P. T. (2009) ‘Medical Therapy of Valvular Heart Disease’, in Wang, A. and Bashore, T. (eds) *Valvular Heart Disease*. New York: Humana Press, pp. 359–375.

Parnell, A. and Swanevelder, J. (2009) ‘High transvalvular pressure gradients on intraoperative transesophageal echocardiography after aortic valve replacement: what does it mean?’, *HSR Proceedings in Intensive Care & Cardiovascular Anesthesia*. EDIMES Edizioni Internazionali Srl, 1(4), pp. 7–18.

Patrick, M. M., Grillot, J. M., Derden, Z. M. and Paul, D. W. (2017) 'Long–term Drifts in Sensitivity Caused by Biofouling of an Amperometric Oxygen Sensor', *Electroanalysis*. John Wiley & Sons, Ltd, 29(4), pp. 998–1005.

De Paulis, R., Schmitz, C., Scaffa, R., Nardi, P., Chiariello, L. and Reul, H. (2005) 'In vitro evaluation of aortic valve prosthesis in a novel valved conduit with pseudosinuses of Valsalva', *Journal of Thoracic and Cardiovascular Surgery*, 130(4), pp. 1016–1021.

Peltz, M. (2013) 'Surgery for Valvular Heart Disease', in Antman, E. M. and Sabatine, M. S. B. T.-C. T. A. C. to B. H. D. (Fourth E. (eds) *Cardiovascular Therapeutics: A Companion to Braunwald's Heart Disease*. 4th edn. Philadelphia: W.B. Saunders, pp. 691–713.

Pibarot, P. and Dumesnil, J. G. (2009) 'Prosthetic Heart Valves: Selection of the Optimal Prosthesis and Long-Term Management', *Circulation*, 119(7), pp. 1034–1048.

Pibarot, P. and Dumesnil, Jean G. (2012) 'Improving assessment of aortic stenosis', *Journal of the American College of Cardiology*. Elsevier Inc., 60(3), pp. 169–180.

Pibarot, P. and Dumesnil, Jean G (2012) 'Low-Flow , Low-Gradient Aortic Stenosis With Normal and Depressed Left Ventricular Ejection Fraction', *JAC*. Elsevier Inc., 60(19), pp. 1845–1853.

Pibarot, P., Sengupta, P. and Chandrashekhar, Y. (2019) 'Imaging Is the Cornerstone of the Management of Aortic Valve Stenosis', *JACC: Cardiovascular Imaging*, 12(1), pp. 220 LP – 223.

Pizzi, M. N., Roque, A., Cuéllar-Calabria, H., Fernández-Hidalgo, N., Ferreira-González, I., González-Alujas, M. T., Igual-Barceló, A., Garcia-Dorado, D., Almirante, B., Castell-Conesa, J., Escobar Amores, M., Tornos, P. and Aguadé-Bruix, S. (2016) '18F-FDG-PET/CTA of Prosthetic Cardiac Valves and Valve-Tube Grafts: Infective Versus

Inflammatory Patterns', *JACC: Cardiovascular Imaging*, 9(10), pp. 1224–1227.

Poon, A. S. Y., O'driscoll, S. and Meng, T. H. (2010) 'Optimal frequency for wireless power transmission into dispersive tissue', *IEEE Transactions on Antennas and Propagation*, 58(5), pp. 1739–1750.

Prabhu, M., Raju, D. and Pauli, H. (2012) 'Transesophageal echocardiography: Instrumentation and system controls', *Annals of Cardiac Anaesthesia*, 15(2), pp. 144–155.

du Preez, W. ., Masheane, L., Combrinck, J. and Booysen, G. (2015) 'Developing a process for manufacturing of a polymer heart valve', in *16th Annual RAPDASA International Conference*.

Price, S. and Gibson, D. (2010) 'Mitral Valve Disease', in Griffiths, M. J. D., Cordinley, J. J., and Price, S. (eds) *Cardiovascular Critical Care*. Blackwell Publishing Limited, pp. 315–329.

Puymirat, E., Chassaing, S., Trinquart, L., Barbey, C., Chaudeurge, A., Bar, O. and Blanchard, D. (2010) 'Hakki's formula for measurement of aortic valve area by magnetic resonance imaging', *American Journal of Cardiology*. Elsevier Inc., 106(2), pp. 249–254.

Rahmani, B., McGregor, C., Byrne, G. and Burriesci, G. (2019) 'A Durable Porcine Pericardial Surgical Bioprosthetic Heart Valve: a Proof of Concept', *Journal of Cardiovascular Translational Research*.

Rahmani, B., Tzamtzis, S., Ghanbari, H., Burriesci, G. and Seifalian, Alexander M. (2012) 'Manufacturing and hydrodynamic assessment of a novel aortic valve made of a new nanocomposite polymer', *Journal of Biomechanics*. Elsevier, 45(7), pp. 1205–1211.

Rahmani, B., Tzamtzis, S., Ghanbari, H., Burriesci, G. and Seifalian, Alexander M (2012)

‘Manufacturing and hydrodynamic assessment of a novel aortic valve made of a new nanocomposite polymer’, *Journal of Biomechanics*. Elsevier, 45(7), pp. 1205–1211.

Rainer, W. G., Christopher, R. A., Golter, L. B., Sadler, T. R. J. and Serkes, K. D. (1975) ‘In vivo strain measurements of a prosthetic aortic valve.’, *The Journal of thoracic and cardiovascular surgery*. United States, 70(4), pp. 732–734.

Ramaraj, R. and Sorrell, V. L. (2008) ‘Degenerative aortic stenosis’, *BMJ (Clinical research ed.)*. BMJ Publishing Group Ltd., 336(7643), pp. 550–555.

Rashtian, M. Y., Stevenson, D. M., Allen, D. T., Yoganathan, A. P., Harrison, E. C., Edmiston, W. A., Faughan, P. and Rahimtoola, S. H. (1986) ‘Flow characteristics of four commonly used mechanical heart valves.’, *The American journal of cardiology*. United States, 58(9), pp. 743–752.

REEDER, G. U. Y. S., CURRIE, P. J., HAGLER, D. J., TAJIK, A. J. and SEWARD, J. B. (1986) ‘Use of Doppler Techniques (Continuous-Wave, Pulsed-Wave, and Color Flow Imaging) in the Noninvasive Hemodynamic Assessment of Congenital Heart Disease’, *Mayo Clinic Proceedings*. Elsevier, 61(9), pp. 725–744.

Rippe, J., Fishbein, M. C., Carabello, B., Angoff, G., Sloss, L., Collins, J. J. and Alpert, J. S. (1980) ‘Primary myxomatous degeneration of cardiac valves. Clinical, pathological, haemodynamic, and echocardiographic profile.’, *British heart journal*, 44(6), pp. 621–9.

Rivero, G., García-Páez, J. M., Alvarez, L., Multigner, M., Valdés, J., Carabias, I., Spottorno, J. and Hernando, A. (2007) ‘Magnetic Sensor for Early Detection of Heart Valve Bioprostheses Failure’, *Sensor Letters*, 5(1), pp. 263–266.

Roberts, J. R., Park, J., Helton, K., Wisniewski, N. and McShane, M. J. (2012) ‘Biofouling of polymer hydrogel materials and its effect on diffusion and enzyme-based luminescent

glucose sensor functional characteristics', *Journal of Diabetes Science and Technology*, 6(6), pp. 1267–1275.

Roberts, W. C. and Ko, J. M. (2009) 'Morphologic Aspects of Valvular Heart Disease', in Wang, A. and Bashore, T. (eds) *Valvular Heart Disease*. New York: Humana Press, pp. 1–37.

Rotman, O. M., Kovarovic, B., Bianchi, M., Slepian, M. J. and Bluestein, D. (2019) 'In Vitro Durability and Stability Testing of a Novel Polymeric Transcatheter Aortic Valve', *ASAIO Journal*, Online Fir.

Rotman, O. M., Kovarovic, B., Chiu, W.-C., Bianchi, M., Marom, G., Slepian, M. J. and Bluestein, D. (2019) 'Novel Polymeric Valve for Transcatheter Aortic Valve Replacement Applications: In Vitro Hemodynamic Study', *Annals of Biomedical Engineering*, 47(1), pp. 113–125.

Rozeik, M. M., Wheatley, D. J. and Gourlay, T. (2014a) 'Percutaneous heart valves; Past, present and future', *Perfusion (United Kingdom)*, 29(5), pp. 397–410.

Rozeik, M. M., Wheatley, D. J. and Gourlay, T. (2014b) 'The aortic valve: Structure, complications and implications for transcatheter aortic valve replacement', *Perfusion (United Kingdom)*, 29(4), pp. 285–300.

Rozeik, M. M., Wheatley, D. J. and Gourlay, T. (2017) 'Investigating the Suitability of Carbon Nanotube Reinforced Polymer in Transcatheter Valve Applications', *Cardiovascular Engineering and Technology*, 8(3), pp. 357–367.

Ruparelia, N. and Prendergast, B. D. (2016) 'Technical aspects of transcatheter aortic valve implantation (TAVI)', *E-journal of Cardiology Practice*, 14(5).

Russell, F. B., Lederman, D. M., Singh, P. I., Cumming, R. D., Morgan, R. A., Levine, F. H., Austen, W. G. and Buckley, M. J. (1980) 'Development of seamless tri-leaflet valves.', *Transactions - American Society for Artificial Internal Organs*. United States, 26, pp. 66–71.

S., G. A., Zhanqing, S., M., S. P., M., K. A., J., S. M., W., L. D., O., A. O., A., R. R., K., B. D. and L., K. D. (1995) 'Assessment of Cardiac Function by Three-dimensional Echocardiography Compared With Conventional Noninvasive Methods', *Circulation*. American Heart Association, 92(4), pp. 842–853.

Saidani, M. and Gijs, M. A. M. (2002) 'Three-dimensional miniaturized power inductors realized in a batch-type hybrid technology', *Journal of Micromechanics and Microengineering*, 12(4), pp. 470–474.

Saikrishnan, N., Kumar, G., Sawaya, F. J., Lerakis, S. and Yoganathan, A. P. (2014) 'Accurate assessment of aortic stenosis: A review of diagnostic modalities and hemodynamics', *Circulation*, 129(2), pp. 244–253.

Salamon, J., Munoz-Mendoza, J., Liebelt, J. J. and Taub, C. C. (2015) 'Mechanical valve obstruction: Review of diagnostic and treatment strategies', *World journal of cardiology*. 2015/12/26. Baishideng Publishing Group Inc, 7(12), pp. 875–881.

Schoenhagen, P., Hausleiter, J., Achenbach, S., Desai, M. Y. and Tuzcu, E. M. (2011) 'Computed tomography in the evaluation for transcatheter aortic valve implantation (TAVI)', *Cardiovascular diagnosis and therapy*. AME Publishing Company, 1(1), pp. 44–56.

Scholtens, A. M., Swart, L. E., Kolste, H. J. Te, Budde, R. P. J., Lam, M. G. E. H. and Verberne, H. J. (2018) 'Standardized uptake values in FDG PET/CT for prosthetic heart valve endocarditis: a call for standardization', *Journal of nuclear cardiology : official publication of the American Society of Nuclear Cardiology*. 2017/06/05. Springer US, 25(6),

pp. 2084–2091.

Shapero, A. and Tai, Y. C. (2018) ‘Parylene-oil-encapsulated low-drift implantable pressure sensors’, in *2018 IEEE Micro Electro Mechanical Systems (MEMS)*, pp. 47–50.

Shiota, T. (2014) ‘Role of modern 3D echocardiography in valvular heart disease’, *The Korean journal of internal medicine*. 2014/10/31. The Korean Association of Internal Medicine, 29(6), pp. 685–702.

Siddiqui, A. (2011) ‘Effects of Vasodilation and Arterial Resistance on Cardiac Output’, *Journal of Clinical & Experimental Cardiology*, 02(11).

Simonato, M. and Dvir, D. (2019) ‘Transcatheter aortic valve replacement in failed surgical valves’, *Heart*, 105(Suppl 2), p. s38 LP-s43.

Singh, S. and Goyal, A. (2007) ‘The origin of echocardiography: a tribute to Inge Edler’, *Texas Heart Institute journal*. Texas Heart Institute, 34(4), pp. 431–438.

Singhal, P., Luk, A. and Butany, J. (2013) ‘Bioprosthetic Heart Valves: Impact of Implantation on Biomaterials’, *ISRN Biomaterials*, 2013, pp. 1–14.

Sinning, J.-M., Werner, N., Nickenig, G. and Grube, E. (2012) ‘Next-generation transcatheter heart valves: current trials in Europe and the USA.’, *Methodist DeBakey cardiovascular journal*, 8(2), pp. 9–12.

Sinning, J. M., Werner, N., Nickenig, G. and Grube, E. (2012) ‘Next-generation transcatheter heart valves: current trials in Europe and the USA.’, *Methodist DeBakey cardiovascular journal*, 8(2), pp. 9–12.

Solan, M. (2016) *Your resting heart rate can reflect your current — and future — health*, *Harvard Health Publishing*. (Accessed: 24 April 2019).

Starling, E. H. and Visscher, M. B. (1927) ‘The regulation of the energy output of the heart’, *The Journal of physiology*, 62(3), pp. 243–261.

Starr, A. (2007) ‘Lasker Clinical Medical Research Award. The artificial heart valve.’, *Nature medicine*, 13(10), pp. 1160–4.

Steinberg, B. (1988) ‘PROSTHETIC VALVE AND MONITORING SYSTEM AND METHOD’, *4,769,032*. USA.

Stern, D. R., Fonseca, M. a, Kroh, J., White, J., Allen, M. G. and O’Brien, D. (2010) ‘Implantable wireless sensor’, *US Patent 7699059*, 2(12).

Stout, K. K. and Verrier, E. D. (2009) ‘Acute valvular regurgitation’, *Circulation*, 119(25), pp. 3232–3241.

Sun, M., Mickle, M., Liang, W., Liu, Q. and Sclabassi, R. J. (2003) ‘Data communication between brain implants and computer’, *IEEE Transactions on Neural Systems and Rehabilitation Engineering*, 11(2), pp. 189–192.

Susin, F. M., Tarzia, V., Bottio, T., Pengo, V., Bagno, A. and Gerosa, G. (2011) ‘In-vitro detection of thrombotic formation on bileaflet mechanical heart valves.’, *The Journal of heart valve disease*. England, 20(4), pp. 378–386.

Takahata, K., Dehennis, A., Wise, K. D. and Gianchandani, Y. B. (no date) ‘STENT AND T W O PRESSURE SENSORS UTILIZING A DUAL-INDUCTOR ANTENNA’, pp. 216–219.

Takahata, K., DeHennis, A., Wise, K. D. and Gianchandani, Y. B. (2004) ‘A wireless microsensor for monitoring flow and pressure in a blood vessel utilizing a dual-inductor antenna stent and two pressure sensors’, in *17th IEEE International Conference on Micro*

Electro Mechanical Systems. Maastricht MEMS 2004 Technical Digest, pp. 216–219.

Tan, E. L., DeRouin, A. J., Pereles, B. D. and Ong, K. G. (2011) 'Design, Fabrication, and Implementation of a Wireless, Passive Implantable Pressure Sensor Based on Magnetic Higher-Order Harmonic Fields', *Biosensors*, 1(4), pp. 134–152.

Tanasie, C., Chandonnet, M., Chin, A., Kokis, A., Ly, H., Perrault, L. P. and Chartrand-Lefebvre, C. (2011) 'Catheter-Induced Aortic Dissection After Invasive Coronary Angiography: Evaluation With MDCT', *American Journal of Roentgenology*. American Roentgen Ray Society, 197(6), pp. 1335–1340.

Tarun, T., Aggarwal, K. and Dohrmann, M. (2019) 'AORTIC DISSECTION DURING CARDIAC CATHETERIZATION', *Journal of the American College of Cardiology*, 73(9 Supplement 1), p. 2538.

Taylor, C. E. and Miller, G. E. (2012) 'Mock Circulatory Loop Compliance Chamber Employing a Novel Real-Time Control Process.', *Journal of medical devices*, 6(4), pp. 450031–450038.

Thakkar, B. V (2014) 'Mitral Valve Prolapse', *Medscape drugs and diseases*.

The surprising dangers of CT scans and X-rays (2015) *Consumer Reports*. (Accessed: 20 May 2019).

Tosoni, S., Tarzia, V., Colli, A., Gerosa, G. and Bagno, A. (2017) 'Phonographic detection of mechanical heart valve thrombosis', *Journal of Artificial Organs*, 20(4), pp. 394–398.

Tribouilloy, C., Lévy, F., Rusinaru, D., Guéret, P., Petit-Eisenmann, H., Baleynaud, S., Jobic, Y., Adams, C., Lelong, B., Pasquet, A., Chauvel, C., Metz, D., Quéré, J.-P. and Monin, J.-L. (2009) 'Outcome After Aortic Valve Replacement for Low-Flow/Low-Gradient Aortic

Stenosis Without Contractile Reserve on Dobutamine Stress Echocardiography', *Journal of the American College of Cardiology*, 53(20), pp. 1865 LP – 1873.

Trochu, J.-N., Kyndt, F., Schott, J.-J., Gueffet, J.-P., Probst, V., Bénichou, B. and Le Marec, H. (2000) 'Clinical characteristics of a familial inherited myxomatous valvular dystrophy mapped to Xq28', *Journal of the American College of Cardiology*, 35(7), pp. 1890–1897.

Turton, E. W. and Ender, J. (2017) 'Role of 3D Echocardiography in Cardiac Surgery: Strengths and Limitations', *Current anesthesiology reports*. 2017/07/21. Springer US, 7(3), pp. 291–298.

Tuzun, E., Rutten, M., Dat, M., Van De Vosse, F., Kadipasaoglu, C. and De Mol, B. (2011) 'Continuous-flow cardiac assistance: Effects on aortic valve function in a mock loop', *Journal of Surgical Research*. Elsevier Inc, 171(2), pp. 443–447.

Ueda, T., Teshima, H., Fukunaga, S., Aoyagi, S. and Tanaka, H. (2012) 'Evaluation of Prosthetic Valve Obstruction on Electrocardiographically Gated Multidetector-Row Computed Tomography', *Circulation Journal*, 77(February).

Umezu, M., Yoshihara, T., Takano, H., Tsuchiya, K. and Akutsu, T. (1986) 'Effects of artificial heart drive conditions on water hammer phenomenon.', *Sot Inst and Contr Eng, Japan 1986:*

Vachiéry, J.-L. and Dewachter, C. (2018) 'Right Heart Catheterization BT - The Interventional Cardiology Training Manual', in Myat, A., Clarke, S., Curzen, N., Windecker, S., and Gurbel, P. A. (eds). Cham: Springer International Publishing, pp. 79–89.

Vahanian, A., Baumgartner, H., Bax, J., Butchart, E., Dion, R., Filippatos, G., Flachskampf, F., Hall, R., Lung, B., Kasprzak, J., Nataf, P., Tornos, P., Torracca, L. and Wenink, A. (2007) 'Guidelines on the management of valvular heart disease: The task force on the management

of valvular heart disease of the European society of cardiology', *European Heart Journal*, 28(2), pp. 230–268.

Valenti, V., Sciarretta, S., Levin, M., Shubayev, L., Edelstein, S., Zia, M. I., Rubattu, S., Volpe, M., Uretsky, S. and Wolff, S. D. (2015) 'An easy and reproducible parameter for the assessment of the pressure gradient in patients with aortic stenosis disease: A magnetic resonance study', *Journal of Cardiology*. Japanese College of Cardiology, 65(5), pp. 369–376.

Vandervoort, P. M., Greenberg, N. L., Powell, K. A., Cosgrove, D. M. and Thomas, J. D. (1995) 'Pressure recovery in bileaflet heart valve prostheses. Localized high velocities and gradients in central and side orifices with implications for Doppler-catheter gradient relation in aortic and mitral position.', *Circulation*. United States, 92(12), pp. 3464–3472.

Vannan, M. A. and Sarkar, K. (2003) 'Assessment of mechanical aortic valve prosthesis by means of Doppler echocardiography: What to measure and why?', *The Journal of thoracic and cardiovascular surgery*, 126(02), pp. 317–320.

Vesely, I. (2003) 'The evolution of bioprosthetic heart valve design and its impact on durability', *Cardiovascular Pathology*, 12(5), pp. 277–286.

Vesey, J. M. and Otto, C. M. (2004) 'Complications of prosthetic heart valves', *Curr.Cardiol.Rep.*, 6, pp. 106–111.

Villafana, M. A. (1996) 'Heart Valve Prosthesis incorporating electronic sensing, monitoring and/or pacing circuitry', *5,487,760*. USA.

Vincent, J.-L. (2008) 'Understanding cardiac output', *Critical Care*. BioMed Central, 12(4), p. 174.

Vongpatanasin, W., Hillis, D. and Lange, R. a. (1996) ‘Characteristics of prosthetic valves’, *The New England journal of medicine*, 335(6), pp. 407–416.

Voskerician, G., Shive, M. S., Shawgo, R. S., Von Recum, H., Anderson, J. M., Cima, M. J. and Langer, R. (2003) ‘Biocompatibility and biofouling of MEMS drug delivery devices’, *Biomaterials*, 24(11), pp. 1959–1967.

Waite, L. and Fine, J. (2007a) ‘Cardiovascular Structure and Function’, in *Applied BioFluid Mechanics*. McGraw- Hill Education, pp. 35–75.

Waite, L. and Fine, J. (2007b) ‘Mechanics of heart valves’, in *Applied BioFluid Mechanics*. McGraw- Hill Education, pp. 165–185.

Walker, A. in V. E. of M. H. V. P. (2006) *In vitro Evaluation of Mechanical Heart Valve Performance Using a Novel Test Chamber in an Automated Mock Circulatory Loop, Biomedical Engineering*. Virginia Commonwealth University.

Walther, T. and Kempfert, J. (2012) ‘Transapical vs. transfemoral aortic valve implantation: Which approach for which patient, from a surgeon’s standpoint’, *Annals of cardiothoracic surgery*. AME Publishing Company, 1(2), pp. 216–219.

Wang, A. and Bashore, T. (2009) *Valvular heart disease., Springerlink*. Humana Press.

Wang, Q., McGoron, A. J., Bianco, R., Kato, Y., Pinchuk, L. and Schoephoerster, R. T. (2010) ‘In-vivo assessment of a novel polymer (SIBS) trileaflet heart valve’, *Journal of Heart Valve Disease*. Department of Biomedical Engineering, Florida International University, Miami, FL, United States: ICR Publishers Ltd, 19(4), pp. 499–505.

Wang, S. S. (2014) ‘Aortic Regurgitation’, *Medscape drugs and diseases*.

Westaby, S., Karp, R. B., Blackstone, E. H. and Bishop, S. P. (1984) ‘Adult human valve

dimensions and their surgical significance', *American Journal of Cardiology*. Elsevier, 53(4), pp. 552–556.

Westerhof, N., Elzinga, G. and Sipkema, P. (1971) 'An artificial arterial system for pumping hearts.', *Journal of applied physiology*, 31(5), pp. 776–81.

Westerhof, N., Lankhaar, J.-W. and Westerhof, B. E. (2009) 'The arterial Windkessel', *Medical & Biological Engineering & Computing*, 47(2), pp. 131–141.

Wheatley, D. J., Raco, L., Bernacca, G. M., Sim, I., Belcher, P. R. and Boyd, J. S. (2000) 'Polyurethane: Material for the next generation of heart valve prostheses?', *European Journal of Cardio-thoracic Surgery*, 17(4), pp. 440–448.

Wielogorski, J. W., Cross, D. E. and Nwadike, E. V. O. (1975) 'The effects of subatmospheric pressure on the haemolysis of blood', *Journal of Biomechanics*, 8(5), pp. 321–325.

Wilkins, G. T., Gillam, L. D., Kritzer, G. L., Levine, R. a, Palacios, I. F. and Weyman, a E. (1986) 'Validation of continuous-wave Doppler echocardiographic measurements of mitral and tricuspid prosthetic valve gradients: a simultaneous Doppler-catheter study.', *Circulation*, 74(4), pp. 786–795.

Wisman, C. B., Pierce, W. S., Donachy, J. H., Pae, W. E., Myers, J. L. and Prophet, G. A. (1982) 'A polyurethane trileaflet cardiac valve prosthesis: in vitro and in vivo studies.', *Transactions - American Society for Artificial Internal Organs*. United States, 28, pp. 164–168.

Wolff, M., Witchitz, S., Chastang, C., Regnier, B. and Vachon, F. (1995) 'Prosthetic valve endocarditis in the ICU: Prognostic factors of overall survival in a series of 122 cases and consequences for treatment decision', *Chest*, 108(3), pp. 688–694.

Wright, G. (1988) ‘The Hydraulic Power Outputs of Pulsatile and Nonpulsatile Cardiopulmonary Bypass Pumps’, *Perfusion*, 3, pp. 251–262.

Wu, V. C.-C. and Takeuchi, M. (2017) ‘Three-Dimensional Echocardiography: Current Status and Real-Life Applications’, *Acta Cardiologica Sinica*. Taiwan Society of Cardiology, 33(2), pp. 107–118.

Wu, Y., Liu, F., Adi, D., Yang, Y.-N., Xie, X., Li, X.-M., Ma, X., Fu, Z.-Y., Huang, Y., Chen, B.-D., Shan, C.-F. and Ma, Y.-T. (2017) ‘Association between carotid atherosclerosis and different subtypes of hypertension in adult populations: A multiethnic study in Xinjiang, China’, *PLOS ONE*. Public Library of Science, 12(2), p. e0171791.

Yin, W., Gallocher, S., Pinchuk, L., Schoephoerster, R. T., Jesty, J. and Bluestein, D. (2005) ‘Flow-induced Platelet Activation in a St. Jude Mechanical Heart Valve, a Trileaflet Polymeric Heart Valve, and a St. Jude Tissue Valve’, *Artificial Organs*. John Wiley & Sons, Ltd (10.1111), 29(10), pp. 826–831.

Yoganathan, A. P., He, Z. and Casey Jones, S. (2004) ‘Fluid mechanics of heart valves.’, *Annual review of biomedical engineering*. United States, 6, pp. 331–362.

Yoganathan, A. P., Lemmon, J. D. and Ellis, J. T. (2000) ‘Heart Valve Dynamics’, in Bronzino, J. D. (ed.) *The Biomedical Engineering Handbook*. 2nd edn. Boca Raton: CRC Press LLC, pp. 505–519.

Yu, L., Kim, B. J. and Meng, E. (2014) ‘Chronically implanted pressure sensors: Challenges and state of the field’, *Sensors (Switzerland)*, 14(11), pp. 20620–20644.

Zacharias, S. K. and Goldstein, J. A. (2015) ‘Aortic Stenosis (Case based Diagnosis and therapy)’, in Abbas, A. E. (ed.) *Aortic Stenosis*. London: Springe-Verlag London Limited, pp. 21–28.

Ben Zekry, S., Sagie, A., Ben-Dor, I., Weisenberg, D. A., Nukrian, H., Battler, A. and Shapira, Y. (2005) 'Initial clinical experience with a hand-held device (Thrombocheck) for the detection of bileaflet prosthetic valve malfunction.', *The Journal of heart valve disease*. England, 14(4), pp. 476–480.

Zhang, D. Y., Lozier, J., Chang, R., Sachdev, V., Chen, M. Y., Audibert, J. L., Horvath, K. a. and Rosing, D. R. (2012) 'Case study and review: Treatment of tricuspid prosthetic valve thrombosis', *International Journal of Cardiology*. Elsevier B.V., 162(1), pp. 14–19.

Zhu, R., Wang, Y., Zhang, Z., Ma, D. and Wang, X. (2016) 'Synthesis of polycarbonate urethane elastomers and effects of the chemical structures on their thermal, mechanical and biocompatibility properties', *Heliyon*. Elsevier Ltd, 2(6).

Zoghbi, W. A., Chambers, J. B., Dumesnil, J. G., Foster, E., Gottdiener, J. S., Grayburn, P. A., Khandheria, B. K., Levine, R. A., Marx, G. R., Miller, F. A., Nakatani, S., Qui??ones, M. A., Rakowski, H., Rodriguez, L. L., Swaminathan, M., Waggoner, A. D., Weissman, N. J. and Zabalgoitia, M. (2009) 'Recommendations for Evaluation of Prosthetic Valves With Echocardiography and Doppler Ultrasound. A Report From the American Society of Echocardiography's Guidelines and Standards Committee and the Task Force on Prosthetic Valves, Developed in Conjunction', *Journal of the American Society of Echocardiography*, 22(9), pp. 975–1014.

APPENDIX

A portion of this thesis was submitted and accepted for oral presentation at the BiomedEng 18 conference held at the Imperial College. A copy of the abstract submitted for the conference is shown below:

The development and hydrodynamic assessment of a trileaflet polyurethane heart valve prosthesis

C. Gambrah[1], T. Gourlay [1]

[1] Graham Hills Building, University of Strathclyde, Glasgow.G11QE

Introduction: Mechanical heart valves, although very durable, tend to exhibit limited bio and haemocompatibility. Bioprosthetic valves, on the other hand, possess good heamodynamic function but limited durability. Polymeric heart valves have the potential of combining the benefits of mechanical and bioprosthetic valves, whiles eliminating their deficiencies. This study aims at the hydrodynamic testing of polyurethane heart valves under pulsatile flow conditions.

Methods: 22mm internal diameter valves were developed via dip coating in a polyurethane solution and left to dry, a process which forms the valve leaflets. A custom pulse duplicator, capable of producing physiological aortic valve pressure waveforms, was designed and manufactured. Pressure tracings were validated using a HANCOCK II bioprosthetic valve. Valves were tested under 4 different flow rates, between 2 to 7L/min according to ISO 5840 pulsatile flow testing conditions. Valve performance was assessed based on Effective Orifice Area, (EOA) and the Transvalvular Pressure Gradient (TPG).

Results & Discussion: Both polymeric valves and HANCOCK II bioprosthetic valve exhibited good physiological aortic pressure waveforms in accordance to ISO 5840 standards, thus showing the adequate performance of the custom designed pulse duplicator. Polymeric valve exhibited a higher transvalvular pressure gradient, as compared to that of the bioprosthetic valve. Bioprosthetic valve exhibited a higher effective orifice area than the polymeric valves however they both meet the required standards of a replacement heart valve.

Conclusion: Results from hydrodynamic testing show the promising nature of polymeric heart valves. Further tests are however necessary to in order to fully assess their potential as an ideal alternative to mechanical and bioprosthetic heart valves.

References:

1. Bezuidenhout D, Williams DF, Zilla, P. *Biomaterials*. 2015; 36: 6–25.
2. De Gaetano, F. et al. *Journal of Mechanics in Medicine and Biology*. 2015; 15: 1540009.
3. Mankad S. *Current Treatment Options in Cardiovascular Medicine*. 2012; 14: 608–21.
4. Taylor CE, Miller GE. *Journal of medical devices*. 2012; 6: 450031–450038.
5. Lanzarone E, Vismara R, Fiore GB. *Artificial Organs*. 2009; 33: 1048–1062.
6. Bonow RO. et al. *Journal of the American College of Cardiology*. 2006; 48: 1-48.
7. De Paulis R. et al.*Journal of Thoracic and Cardiovascular Surgery*. 2005; 130: 1016–1021.
8. Vesey JM, Otto CM. *Curr.Cardiol.Rep.* 2004; 6:106-111.
9. Mackay TG. et al. *Biomaterials* 1996; 17: 1857–1863.
10. Westerhof N, Elzinga G, Sipkema P. *Journal of applied physiology* 1971; 31:776–81.

Acknowledgments: I would like to express my gratitude to the Biomedical Engineering department of the University of Strathclyde, for their immense support. There are no conflicts of interest.